Elucidating events during the lifecycle of Merkel cell polyomavirus

Samuel John Dobson

Submitted in accordance with the requirements for the degree of

Doctor of Philosophy

The University of Leeds

Faculty of Biology Sciences

School of Molecular and Cellular Biology

April 2019

The candidate confirms that the work submitted is his own and that appropriate credit has been given where reference has been made to the work of others.

Acknowledgements

A huge thank you goes to Prof. Adrian Whitehouse for allowing me into the lab for the last three and a half years; your continued support, guidance and patience was key to the success of this project. I would also like to thank Dr. Jamel Mankouri and Dr. Andrew Macdonald for their support and collaboration throughout my entire time as a postgraduate student, as without their contributions I don't believe I would be the scientist I am today. My thanks also go to the Medical Research Council for funding this project.

Thank you not only to the Whitehouse group, but the wider Virology community both past and present for not just support in the lab, but for all of the extracurricular activities, particularly all of the Friday nights – I've never been short of someone to share a pint (or too many) and a conversation with!

This thesis is the culmination of immeasurable sacrifice and support from my family not only over the last few years but throughout my entire education and life. Without the opportunities I have been fortunate to have had, I would never have got anywhere close to this moment. I can never thank you enough for all that you have done, and I dedicate this to you. Finally, to Sammy who has been through all of the ups and downs along the way, thank you for putting up with me and being there with me on this journey!

Abstract

The *Polyomaviridae* are a family of viruses which have several lifecycle requirements that have been poorly studied. However, association of these viruses with disease in an immunocompromised host has been well documented. The 2008 discovery of Merkel cell polyomavirus (MCPyV) as the causative agent in Merkel cell carcinoma (MCC) represented the first link of polyomavirus infection to cancer in humans. Further research identified the requirements of a truncation in the large tumour antigen (LT) and clonal integration of mutated viral genomes into the host genome. Despite truncation of LT being essential to MCPyV-positive MCC, the small tumour antigen (ST) has been implicated as the major oncogene that transforms the host cell and promotes several phenotypes associated with cancer.

Previous publications in the Whitehouse laboratory have identified the requirement of ST in stimulating events that contribute to the highly metastatic nature of virus induced MCC. ST facilitates microtubule destabilisation and filamentation of actin to prime the cellular cytoskeleton for movement, however despite identifying the essential interaction with the protein phosphatase 4 catalytic subunit (PP4C), the molecular mechanisms through which these changes are brought about have not been fully investigated. In Chapter 5, we describe how ST activates the p38 mitogen-activated protein kinase (MAPK) in a manner that is dependent upon PP4C perturbation. Using chemical inhibitors, the activity of p38 is shown to be essential to the ability of ST to induce migratory phenotypes both in naïve cells and MCPyV-positive MCC cell lines. Therefore, we provide evidence of cellular mechanisms dysregulated by MCPyV ST to promote metastatic phenotypes, which may provide novel therapeutic targets to restrict MCC spread and improve patient prognoses.

Intriguingly, MCPyV expresses only one minor capsid protein (VP) that is incorporated into the capsid, whilst the majority of polyomaviruses encode VP2 and VP3 which are both packaged. Early events in the polyomavirus lifecycle are poorly understood in part due to lack of suitable systems. In Chapter 3, we therefore produced new reporter systems, using MCPyV pseudoviruses to study events during entry and trafficking, and in Chapter 4 focus upon the role of ion channels. Comparison with the prototypic SV40 reveals novel requirements of transient-type

Ca^{2+} and K^{+} channels for MCPyV and a conserved broad Ca^{2+} channel dependency for both species. This study highlights clinically available drugs that could potentially be repurposed to restrict diseases that are associated with persistent polyomavirus infections.

Table of contents

List of Tables

List of Figures

Abbreviations

αSNAP	N-ethylmaleimide-sensitive factor attachment protein α
4E-BP1	initiation factor 4E-binding protein 1
ADAM	A disintegrin and metalloproteinase
Agno	Agnoprotein
ALTO	Alternate frame of the LT open reading frame
AP-1	Activator protein 1
APS	Ammonium persulphate
ATF2	cAMP-dependent transcription factor 2
ATP	Adenosine triphosphate
BCA	Bicinchoninic acid
BK_{Ca}	Large conductance calcium channel
BKVAN	BKPyV-associated nephropathy
BLAST	Basic local alignment search tool
BSA	Bovine serum albumin
BUNV	Bunyavirus
Ca^{2+}	Calcium ion
cAMP	Cyclic adenosine monophosphate
CDK	Cyclin-dependent kinase
CDK	Cyclin dependent kinase
CFTR	Cystic fibrosis transmembrane conductance regulator
CK	Cytokeratin
Cl^-	Chloride ion
CLIC	Chloride intracellular-channel

CNS	Central nervous system
CREB	cAMP responsive element binding protein
CREBBP	CREB-binding protein
CST	Cell Signaling Technologies
DAPI	4’,6-diamidino-2-phenylindole
DDR	DNA damage response
DIDS	4,4'-Diisothiocyano-2,2'-stilbenedisulfonic acid
DMEM	Dulbecco's Modified Eagle Medium
DMSO	Dimethyl sulphoxide
DNA	Deoxyribonucleic acid
dsDNA	Double stranded deoxyribonucleic acid
EBOV	Ebola virus
E-cadherin	Epithelial-cadherin
ECL	Enhanced chemiluminescence substrate
ECM	Extracellular matrix
ECR	Early coding region
EDTA	Ethylenediaminetetraacetic acid
EdU	5-ethynyl-2'-deoxyuridine
EGF	Epithelial growth factor
EM	Electron microscopy
EMT	Epithelial-mesenchymal transition
ER	Endoplasmic reticulum
ERAD	Endoplasmic-reticulum-associated protein degradation
ERK	Extracellular-signal regulated kinase

F-actin	Filamentous actin
FBS	Foetal bovine serum
G-actin	Globular actin
GAPDH	Glyceraldehyde 3-phosphate dehydrogenase
GFP	Green fluorescent protein
GPCR	G-protein coupled receptor
HA	Hemagglutinin
HIF-1α	Hypoxia-inducible factor 1α
HNSCC	Head and Neck squamous cell carcinoma
hpt	Hours post transduction
HPyV	Human polyomavirus
HR-AH	Host range and adenovirus helper
HRP	Horseradish peroxidase
IARC	International Agency for Research on Cancer
ICTV	International Committee on Taxonomy of Viruses
IF	Immunofluorescence microscopy
IFN	Interferon
IK_{Ca}	Intermediate conductance calcium channel
IKK	Inhibitor of nuclear factor kappa-B kinase
IKK	Inhibitor of NF-κB
IL-1	Interleukin-1
IU/mL	Infectious units per millilitre
JNK	c-Jun N-terminal kinase
K^+	Potassium ion

K_{2P}	Two-pore Potassium channel
K_{ATP}	ATP-sensitive potassium channel
K_{Ca}	Calcium-activated potassium channel
K_{IR}	Inward rectifier potassium channel
K_V	Voltage-gated potassium channel
LAMP	Lysosomal associated membrane protein
LB	Luria broth
LBA	Luria broth agar
LCR	Late coding Region
LIMK1	LIM domain kinase 1
LSD	Large tumour antigen stabilisation domain
LST-c	Lactoseries tetrasaccharide c
LT	Large tumour antigen
MAP2K	MAPK kinase
MAP3K	MAPK kinase kinase
MAPK	Mitogen-activated protein kinase
MCC	Merkel cell carcinoma
MCPyV	Merkel cell polyomavirus
MEM	Minimum Essential Media
MHC-1	major histocompatibility complex class 1
MK2	Mitogen-Activated Protein Kinase-Activated Protein Kinase 2
MKK	MAPK kinase
MOI	Multiplicity of infection
MSK1	Mitogen- and stress-activated protein kinase 1

MT	Middle tumour antigen
MTS	[3-(4,5-dimethylthiazol-2-yl)-5-(3-carboxymethoxyphenyl)-2-(4-sulfophenyl)-2H-tetrazolium
MuPyV	Murine polyomavirus
MUR	Merkel unique region
Na^+	Sodium ion
NAADP	Nicotinic acid adenine dinucleotide phosphate
NanoLuc	Secreted luciferase reporter
NCCR	Non-coding control region
NEMO	Inhibitor of NF-κB subunit gamma
NF-κB	Nuclear factor kappa B
NLS	Nuclear localisation signal
OBD	Origin binding domain
Ori	Origin of replication
PAGE	Poly acrylamide gel electrophoresis
PAK	p21-activated kinase
PBS	Phosphate-buffered saline
PCR	Polymerase chain reaction
PFA	Paraformaldehyde
PML	Progressive multifocal leukoencephalopathy
POLA	DNA polymerase δ
PP2A	Protein phosphatase 2A
PP4C	Protein phosphatase 4C
pRb	Retinoblastoma protein

PRIM	DNA polymerase α-primase
PsV	Pseudovirus
PyV	Polyomavirus
RLU	Relative luciferase units
RNA	Ribonucleic acid
RNAi	Ribonucleic acid interference
RPA	Replication protein A
SAPK	Stress-activated protein kinase
SDS	Sodium dodecyl sulphate
SK_{Ca}	Small conductance calcium channel
SNARE	Soluble NSF attachment protein
ST	Small tumour antigen
STING	Stimulator of interferon genes
STX	Saxitoxin
SV40	Simian virus 40
TAg	Tumour antigen
TAK1	TGFβ-activated kinase 1
TBS	Tris-buffered saline
TBS-T	TBS containing 0.1% (v/v) Tween-20
TDN	Transdominant negative
TEMED	Tetramethylethylenediamine
TGFβ	Transforming growth factor β
TGN	Trans-Golgi network
tLT	truncated LT

TMD	Transmembrane domain
TNFα	Tumour necrosis factor α
TOP1	Topoisomerase 1
TPC	Two-pore channel
TRAF	TNF receptor associated factors
TRP	Transient receptor potential
TTX	Tetrodotoxin
USP21	Ubiquitin specific peptidase 21
US	United States of America
UV	Ultra-violet
V-ATPase	Vacuolar-type H^+-ATPase
VEGF	Vascular endothelial growth factor
VP	Viral protein
WB	Western blot
WHIM	Warts, Hypogammaglobulinemia, Immunodeficiency, and Myelokathexis
WT	Wild-type

Units

μL	Microlitre
μm	Micrometre
μM	Micromolar
bp	Base pair
g	Gram
kbp	Kilobase pair
kDa	Kilodalton
mg	Milligram
mL	Millilitre
mM	Millimolar
ng	Nanogram
nm	Nanometre
nM	Nanomolar
^{o}C	Degrees Celsius

Symbols

α	Alpha
β	Beta
γ	Gamma
δ	Delta
Δ	Delta/Deletion mutation
κ	Kappa
μ	Micro
n	Nano

Nucleotides

A	Adenosine
C	Cytosine/Cytidine
G	Guanine/Guanosine
T	Thymine/Thymidine
U	Uridine

Amino acids

A	Ala	Alanine
C	Cys	Cysteine
D	Asp	Aspartate
E	Glu	Glutamate
F	Phe	Phenylalanine
G	Gly	Glycine
H	His	Histidine
I	Ile	Isoleucine
K	Lys	Lysine
L	Leu	Leucine
M	Met	Methionine
N	Asn	Asparagine
P	Pro	Proline
Q	Gln	Glutamine
R	Arg	Arginine
S	Ser	Serine
T	Thr	Threonine
V	Val	Valine
W	Trp	Tryptophan
Y	Tyr	Tyrosine

Chapter 1

Introduction

1.1 Polyomaviruses

1.1.1 An introduction to polyomaviruses

The *Polyomaviridae* is a family of small, non-enveloped viruses that package a circular double-stranded DNA (dsDNA) genome of approximately 5 kbp. The family is composed of 4 genera with restricted host range and infect mammals, birds and fish. *Polyomaviridae* infections are generally acquired early in life, persistent and asymptomatic, however for a small number of polyomaviruses potentially life-threatening diseases have been attributed to clinical manifestations in immunocompromised cohorts.

The circular dsDNA genome of polyomaviruses (PyVs) can be split into three distinct regions: the non-coding control region (NCCR) which contains the origin of replication (Ori), the early transcript region which is alternatively spliced to produce the functional tumour antigens and the late transcript region which gives rise to the capsid proteins and, in some instances, additional auxiliary proteins.

Polyomavirus virions are non-enveloped and typically around 45 nm in diameter. The capsid itself is icosahedral and made up of 72 major capsid protein pentamers. Under each pentamer sits a minor capsid protein, which links the capsid to the enclosed genome.

1.1.2 History of polyomaviruses

The accidental discovery of Murine PyV (MuPyV) by Ludwik Gross was first reported in 1953, who noticed the growth of tumours in mice whilst working with mouse leukaemia virus (Gross, 1953; Gross, 1976). The name polyomavirus arose from this observation, with ‘polyoma’ a reference to the virus’s ability to cause many (poly) tumours (oma).

Simian Virus 40 (SV40) was next identified in 1959 as a contaminant of poliovirus vaccines that were cultured in Rhesus monkey renal cells (Hilleman, 1998). The administration of the contaminated Salk poliovirus vaccine to an estimated 100 million people in the US between 1955 and 1963, coupled with evidence that not only could SV40 infect humans but cause tumour formation in experimental animals, led to fears that vast quantities of the population could have been exposed to a

tumour virus. However, more recent epidemiological studies have suggested there has been no increased incidence of cancer caused by SV40, with no conclusive link between administration of the vaccine and increased frequency of disease (Shah, 2007).

The first polyomaviruses to be identified as causative agents of disease in a human host were BKPyV and JCPyV, both independently isolated from urine samples in the early 1970s (Gardner et al., 1971; Hogan et al., 1980). Despite adult seroprevalence of 90% (BKPyV) and 50-80% (JCPyV), progression of disease within healthy individuals is low, with an asymptomatic, latent infection typically observed. However, in the case of an immunocompromised host the outcome of disease can be potentially fatal; with BKPyV a causative agent of renal transplant rejection by polyomavirus associated-nephropathy and haemorrhagic cystitis in bone marrow recipients, and JCPyV a precursor to progressive multifocal leukoencephalopathy (Gardner et al., 1971; Padgett et al., 1971; Siguier et al., 2012).

The third human polyomavirus was not identified until 2007, with the discovery of Karolinska Institute PyV (KIPyV) following technological advances in screening and detection of viral genomes (Allander et al., 2007). Since 2007 however there have been a significant number of further additions to the human polyomavirus family, that currently contains 14 known members, which are summarised in Table 1.1.

Of the recently discovered members of the human polyomavirus family, MCPyV in particular has received much attention due to its association as the first polyomavirus directly linked with tumour formation in a human host (Feng et al., 2008).

Table 1.1: Summary of the known human polyomaviruses. (Decaprio and Garcea, 2013; Mishra et al., 2014; Gheit et al., 2017)

Polyomavirus	Abbreviation	Genus	Source of identification	Year	Known associated diseases
BK	BKPyV	Beta	Urine	1971	Haemorrhagic cystitis and PyV-associated nephropathy
JC	JCPyV	Beta	Brain tissue	1971	Progressive multifocal leukoencephalopathy
Karolinska Institute	KIPyV	Beta	Nasopharyngeal tissue	2007	None
Washington University	WUPyV	Beta	Nasopharyngeal tissue	2007	None
Merkel cell	MCPyV	Alpha	Lesions	2008	Merkel cell carcinoma
Human PyV 6	HPyV6	Alpha	Healthy skin	2010	None
Human PyV 7	HPyV7	Delta	Blood and lung	2010	None
Trichodysplasia spinulosa	TSPyV	Delta	Lesions	2010	Trichodysplasia spinulosa
Human PyV 9	HPyV9	Alpha	Serum and skin	2011	None
Malawi PyV	HPyV10	Delta	Stool and skin	2012	WHIM syndrome
Saint Louis	SLPyV	Delta	Stool and skin warts	2013	None
Human PyV 12	HPyV12	Alpha	Gastrointestinal tract	2013	None
New Jersey	NJPyV	Alpha	Pancreas	2014	None
Lyon IARC PyV	LIPyV	N/A	Skin	2017	None

1.1.3 Classification of polyomaviruses

The International Committee on Taxonomy of Viruses (ICTV) has remodelled the classification of PyVs several times due to the ever-expanding list of known species. The initial *Papovaviridae* genus that previously encompassed both polyomaviruses and papillomaviruses due to comparable structural features, was split into the *Polyomaviridae* and *Papillomaviridae* in 2004 to reflect differences in genomic organisation (Mayo, 2005).

The *Polyomaviridae* was again revised in 2011 in response to a burst of newly discovered PyVs, which gave rise to three separate genera: *Orthopolyomavirus*, *Wukipolyomavirus* and *Avipolyomavirus* (Johne et al., 2011). As the name suggests, the *Avipolyomavirus* genus grouped species of PyVs that infect birds, whilst those that infect mammals were split between the remaining two genera dependent upon sequence divergence of the VP1-coding gene.

In 2016, the ICTV again revisited the classification of PyVs, introducing new taxonomy that is currently in use today (Moens et al., 2017). This led to four genera: *Alphapolyomaviruses*, *Betapolyomaviruses*, *Gammapolyomaviruses* and *Deltapolyomaviruses*. As with previous classifications, avian polyomaviruses were grouped together and are contained within the *Gammapolyomavirus* genus using Avian PyV 1 as the type species. The *Alpha*, *Beta* and *Delta* genera were used to categorise mammalian polyomaviruses based on amino acid sequence similarity between the large tumour antigens (LTs) of different species, with MuPyV, SV40 and HPyV6 used as type species, respectively. There are currently 80 recognised PyVs, with 77 classified into a genus.

1.2 The lifecycle of a polyomavirus

The general lifecycle of PyVs is overall conserved between species, however individual mechanistic variations and requirements likely give rise to altered tropisms. Figure 1.1 shows an overview of a PyV lifecycle. Typically, PyVs bind to the host cell through interactions with glycans, before endocytic internalisation into the endo/lysosomal network (Tsai et al., 2003). The use of PyV capsids containing non-viral reporter vectors, termed pseudovirions, has shown that virions can bind to and

penetrate into a range of cell types, which suggests that tropism is not ultimately dictated by the availability of initial binding residues, although it most likely has some impact (Nakanishi et al., 2008). Following penetration, the virion is then trafficked in an endosome that becomes acidic, promoting proteolytic rearrangement of the capsid before arriving at the endoplasmic reticulum (ER) (Qian et al., 2009). Within the ER further processing occurs before trafficking to the nucleus where the genome is released (Jiang et al., 2009).

A single early transcript is initially synthesised in the nucleus, which is alternatively spliced into transcripts encoding functional tumour antigens (TAgs) (Decaprio and Garcea, 2013). All PyVs encode the large tumour antigen (LT) and small tumour antigen (ST), in addition some PyVs encode additional early proteins. The TAgs are the functional proteins that interact with a range of host cellular proteins to perturb pathways and promote an environment that promotes virus propagation whilst avoiding immune detection.

Upon sufficient production of TAgs, LT with support from ST interactions, forms a helicase that binds to the NCCR and unwinds the genome to initiate genome replication and expression of a late viral transcript (Foster and Simmons, 2010).

The late transcript is alternatively spliced to give rise to a variety of mRNAs that encode proteins which vary between PyV family members. In all PyVs the major viral capsid protein 1 (VP1) and minor viral capsid protein 2 (VP2) are expressed (Schowalter and Buck, 2013). Some PyVs are however capable of producing an additional minor viral capsid protein termed VP3 and/or auxiliary proteins that are not incorporated into the capsid such as VP4 and the viroporin agnoprotein (Daniels et al., 2007; Baez et al., 2017).

Within the nucleus, newly synthesised virus genomes recruit host cell histones in order to form chromatin-like complexes, which interact with capsid proteins to produce infectious progeny (Coca-Prados et al., 1982; Dekeyser et al., 2015). Assembled capsids are either trafficked to the cell membrane where they are released by non-lytic exocytosis or lytic mechanisms (Clayson et al., 1989; Daniels et al., 2007; Evans et al., 2015).

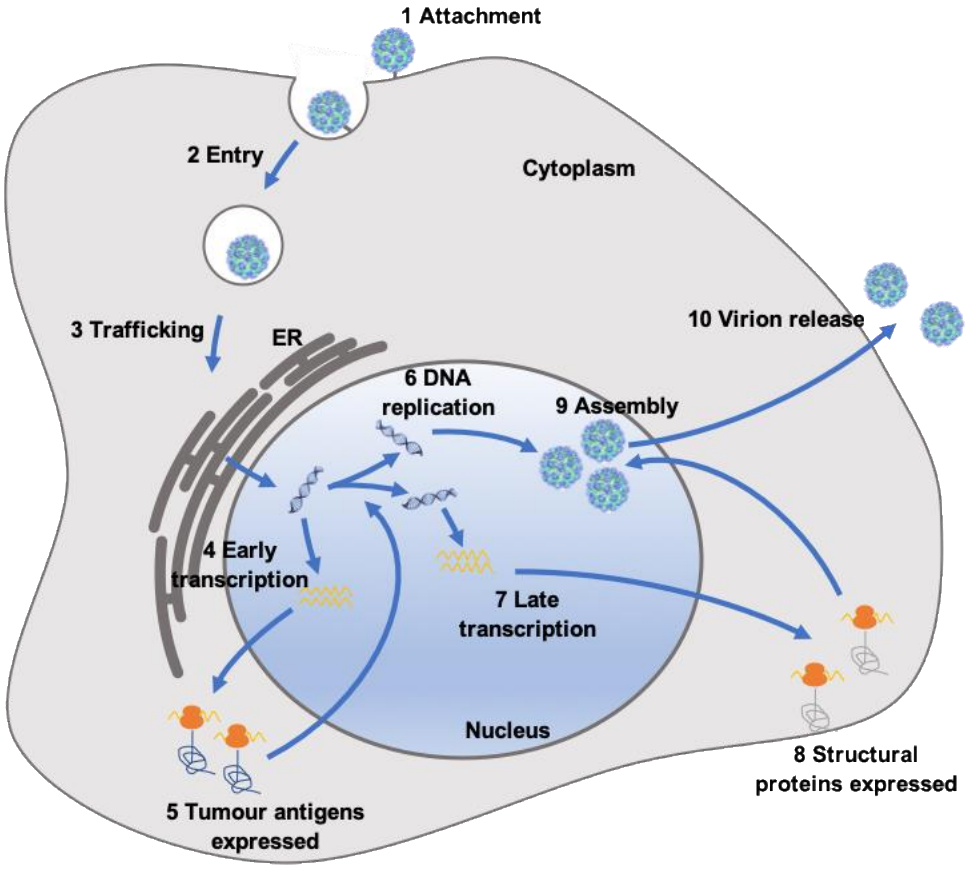

Figure 1.1: Schematic representation the general polyomavirus lifecycle. (1) The polyomavirus enters the cell via endocytosis (2) before trafficking to the nucleus via the endo/lysosomal network and ER (3). Upon entry to the nucleus, transcription of the early tumour antigens is performed (4, 5). DNA replication (6) and transcription of the late structural proteins (7, 8) is then initiated. Virions are then assembled in the nucleus (9) before release from the cell (10).

1.3 Early stages of the polyomavirus lifecycle

1.3.1 Attachment

The initial interaction of PyVs with the host cell varies between species and most likely has some influence upon tropism. The majority of PyVs attach to the cell through VP1 capsomere interaction with sialic acid residues of glycans. MuPyV, BKPyV and JCPyV require sialic acids during entry, as treatment with neuraminidase prevented the ability to agglutinate red blood cells and infect cells (Neu et al., 2009). Similarly SV40 interacts with GM1 gangliosides, however some confusion arose due

to neuraminidase resistance of GM1 and an inability of the virus to agglutinate red blood cells due to narrow specificity (Miller-Podraza et al., 1982; Clayson et al., 1989). SV40 has further been reported to require MHC class I molecules (MHC-1) to permit entry (Norkin, 1999). Reports show that SV40 initially binds to MHC-1 before complexes migrate to lipid rafts (Stang et al., 1997). Following arrival at lipid rafts, MHC-1 is degraded by metalloproteinases before interaction with GM1 gangliosides (Anderson et al., 1998). In contrast, sucrose flotation assays identified that BKPyV utilises GD1b and GT1b receptors for initial binding (Low et al., 2006). JCPyV is an example of a PyV that requires a secondary interaction for entry. Initial binding is to lactoseries tetrasaccharide c (LST-c) which contains a terminal α2,6-linked sialic acid (Neu et al., 2010). Following sialic acid interaction there is a secondary interaction with the serotonin (5-hydroxytryptamine) 2A receptor (5-HT_{2A}R) to permit entry (Elphick et al., 2004; Neu et al., 2010).

A dual entry mechanism is also employed by MCPyV, whereby initial attachment is via a sulphated glycosaminoglycan such as heparan sulphate or chondroitin sulphate, before a secondary interaction with sialylated glycans facilitates entry (Schowalter et al., 2011).

1.3.2 Penetration

Following attachment, PyVs penetrate the cell by endocytosis, however the individual mechanisms can vary. SV40, BKPyV and MCPyV penetrate cells via caveolar- and lipid raft-mediated mechanisms (Gilbert and Benjamin, 2000; Eash et al., 2004; Moriyama et al., 2007; Becker et al., 2019). SV40 and MCPyV were further confirmed to require dynamin, a GTPase that is responsible for endocytosis. JCPyV utilises an alternative clathrin-mediated endocytosis mechanism that requires β-arrestin, with suggestion that this altered phenotype may contribute to its ability to infect cells in the central nervous system (CNS) (Mayberry et al., 2019).

1.3.3 Trafficking to the nucleus

Similarly to all DNA viruses, PyV replication occurs within the nucleus. However, there are several prerequisite stages post-penetration that lead to the priming of the

virion to reveal and release the contained genome so that the host cellular machinery can be utilised for replication.

Following endocytosis, PyVs enter into the endo/lysosomal network (Engel et al., 2011). PyVs such as SV40, MCPyV and BKPyV that are endocytosed by caveolae-mediated mechanisms enter into caveosomes. These are proposed to be endosomes that are coated in caveolin-1 following budding from the plasma membrane although this concept is controversial (Nichols, 2003; Moriyama et al., 2007). JCPyV, on the other hand, is endocytosed in a clathrin-dependent manner and enters directly into early endosomes (Maru et al., 2017).

For SV40, caveolar tyrosine kinases promote trafficking along the cytoskeleton to early endosomes through recruitment of actin and dynamin II in a manner assisted by Rab5 and Arf1 (Mercer et al., 2010; Engel et al., 2011). The SV40 virion is retained in the maturing endosome, with increasing acidity observed as progression into late endosomes and eventually endo/lysosomes continues. During this process it is believed that the virion undergoes rearrangements that make it more susceptible to further processing by cellular proteins (Kuksin and Norkin, 2012a). Throughout these stages the virion maintains an interaction with the initial GM1 receptor used for penetration, which through an unknown mechanism mediates budding of the virion from the endo/lysosome to escape lysosomal enzyme degradation. Virus containing vesicles are then trafficked to the ER independently of the trans-Golgi network (TGN) (Pelkmans et al., 2001; Engel et al., 2011). Within the ER the virion is recognised by the ER associated degradation system (ERAD) as a misfolded protein. In response to identification as misfolded, disulphide bonds that are required for VP1 pentamer stability are reduced by peptide disulphide isomerase and ER protein 57 exposing the previously contained VP2 and VP3 (Schelhaas et al., 2007). The presentation of the hydrophobic N-terminus sequence of VP2 anchors the virion to the membrane of the ER and the partially degraded virion once reduced also interacts with the lumenal chaperone BiP to prevent aggregation (Nishikawa et al., 2001). An essential interaction between glutamic acid residues at position 17 of exposed VP2 with positive charges of the third transmembrane domain of BAP31 and the homologous BAP29 leads to clustering around the virion (Geiger et al., 2011). This in turn creates

a platform through which the partially disassembled virion can pass into the cytoplasm.

Following release from the ER the heavily degraded capsid is further destabilised by changes in physiological conditions, most notably low Ca^{2+} concentrations, and remaining VP1 pentamers are stripped away by cellular chaperones (Li *et al.*, 2003; Kuksin and Norkin, 2012b). This then presents C-terminal nuclear localisation signals (NLSs) located on VP2 and VP3, enabling an interaction with α/β importins for translocation into the nucleus via the nuclear pore (Clever et al., 1993; Yamada and Kasamatsu, 1993; Nakanishi et al., 2002; Nakanishi et al., 2007).

The trafficking events of BKPyV are less studied than that of SV40. Given that entry mechanisms are conserved, it is unsurprising that inhibitor studies support comparable requirements to that of SV40, although it should be noted that the body of work relating to post penetration events in the lifecycle of BKPyV is much smaller (Bennett et al., 2012).

MCPyV also enters the cell by caveolar-mediated endocytosis and Becker *et al.* observed similar requirements to that of SV40 and BKPyV during trafficking (Becker et al., 2019). Interestingly, electron microscopy data in this study did however suggest that MCPyV virions may potentially acquire a lipid-membrane coat whilst in endosomal compartments. How or why coating occurred was not investigated, however suggestions were made that this is potentially to avoid immune detection or simply an unknown aspect or variance from prototypic PyV infection.

As previously stated, the entry of JCPyV differs to SV40, BKPyV and MCPyV in that endocytosis is clathrin dependent. As is the norm with clathrin-mediated endocytosis, following penetration in clathrin-coated pits, JCPyV localises to Rab5-positive early endosomes (Querbes et al., 2004). However, during trafficking JCPyV does not appear to follow the canonical Rab5-endocytic route. At later time points the virus fails to localise to Rab7-positive vesicles, which would be the natural progression into the endo/lysosomal network, but instead localises to cholera toxin B, a routine marker of caveolar/lipid raft-mediated endocytosis (Querbes et al., 2006). Many of the requirements elucidated for JCPyV from this point correlate with

those previously described for SV40, BKPyV and MCPyV suggesting that post-penetration, PyVs have comparable requirements for trafficking through the endo/lysosomal network, ER and nuclear entry (Ferenczy et al., 2012; Bennett et al., 2012; Toscano and de Haan, 2018; Becker et al., 2019).

1.4 The prototypic polyomavirus genome

The circular genome of PyVs is made up of dsDNA and despite some slight variation between species is approximately 5 kbp in size. The genomic organisation and structure of PyV genomes is overall comparable and a schematic representation of the prototypic SV40 genome is shown in Figure 1.2. The genome has a bipartite composition with the early and late coding regions (ECR and LCR, respectively) encoded on opposing DNA strands (Cantalupo et al., 2017). The 5' ends of both the early and late coding regions are separated by the NCCR, which contains the origin of replication required to drive sequential gene expression.

Following infection and trafficking to the nucleus, transcription of the ECR is initiated by RNA polymerase II, producing a single mRNA that is subsequently alternatively spliced to generate mRNAs that encode the TAgs (Spurgeon and Lambert, 2013). All PyVs express LT and ST, which are responsible for priming the cell for replication and production of viral progeny. Some PyVs, namely MCPyV, SLPyV and MuPyV, also encode additional early proteins that are alternatively spliced such as 57 kT, 229T and middle TAg (MT), respectively (Shuda et al., 2008; Lim et al., 2013). There is however no current evidence of an equivalent to MuPyV MT encoded by other mammalian PyVs that has unique functionality (Zhou et al., 2011).

Later during infection there is a switch in transcription, initiated by TAgs binding into and unwinding the NCCR, leading to expression of the LCR transcript alongside replication of the DNA genome. Arguably the largest variation between genome organisation and expression profiles of PyVs relates to late proteins. All PyVs have conserved expression of the structural VP1 and VP2 which appear to be the minimum requirement for a PyV to infect a cell, however beyond this, there can be many different compositions.

The prototypic SV40 produces the greatest number of proteins, with four 'VPs' and the additional auxiliary agnoprotein (Vilchez and Butel, 2004). BKPyV and JCPyV both encode three VPs and agnoprotein, but do not express the non-structural VP4 (Ferenczy et al., 2012; Panou et al., 2018). At the more simple end of the spectrum lies MCPyV, which is a member of a clade of PyVs that only express VP1 and VP2 from the LCR (Schowalter and Buck, 2013).

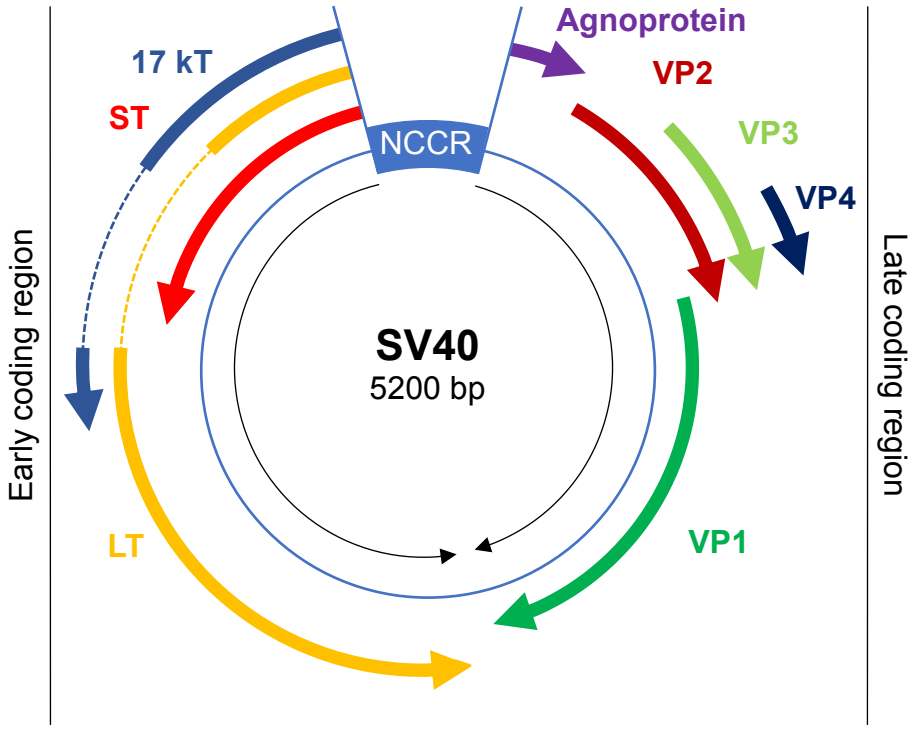

Figure 1.2: Schematic representation of the SV40 genome. Shown is representation of the SV40 genome containing the non-coding control region (NCCR); the early proteins LT, ST and 17 kT; and the late proteins VP1, VP2, VP3, VP4 and agnoprotein.

1.4.1 The genomic organisation of MCPyV

The genome of MCPyV diverges quite significantly from the prototypic SV40. Through comparison of the genomic maps of SV40 (Figure 1.2) and MCPyV (Figure 1.3) it can be noted that MCPyV encodes additional early, and fewer late proteins. Information regarding 57 kT is sparse, with knowledge that it shares interactions comparable to expressed domains of ST and LT, however it is not believed to have

additional functionality in a manner equivalent to MuPyV MT (Spurgeon and Lambert, 2013). Another early protein is ALTO (Alternate frame of the Large T Open reading frame), which currently has no known function and is instead considered to be an early example of viral evolution (Carter et al., 2013).

The LCR of MCPyV is more restricted in comparison to that of SV40, as only VP1 and VP2 are expressed. The genome does not encode an agnoprotein or VP4. There is a reading frame that is consistent with VP3, however the highly conserved N-terminal Met-Ala-Leu motif required for translation is lacking, leading to loss of expression (Schowalter and Buck, 2013).

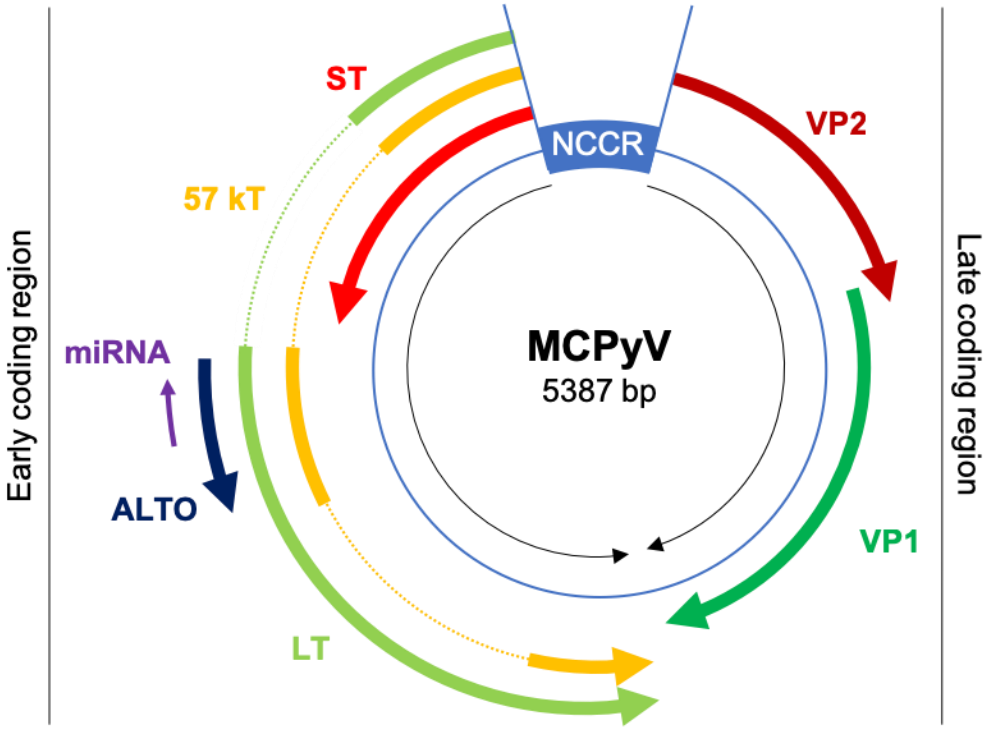

Figure 1.3: Schematic representation of the MCPyV genome. Shown is the non-coding control region (NCCR); the early proteins LT, ST, 57 kT and ALTO (alternate frame of the LT open reading frame); and late proteins VP1 and VP2. The location of the MCPyV precursor miRNA is also shown. Genome mapping is based upon the MCV^{Syn} genome.

1.5 Polyomavirus early proteins

The expression of LT and ST is ubiquitous amongst PyVs and both are essential for manipulation of the host cell, to avoid apoptosis, create an environment that is favourable for viral replication and orchestrate the sequential steps of the lifecycle (Stakaityte et al., 2014). As previously described, TAgs are produced from one transcript through alternative splicing and proteins in addition to LT and ST are produced by some PyVs. An overview of the MCPyV ECR and protein variants is shown in Figure 1.4. Both LT and ST share the first 75-80 amino acids at the N-terminus encoded by the first exon (Decaprio and Garcea, 2013). ST mRNA is produced by read-through of the first splice donor site into a unique region that is bypassed by LT. A stop codon within the ST unique region, coupled with use of the LT splice acceptor leads to production of ST mRNA transcripts. MCPyV is an example of a PyV that encodes an additional early protein, which is termed 57 kT. This protein shares common features with LT, however additional splicing leads to the loss of a large portion of residues towards the C-terminus.

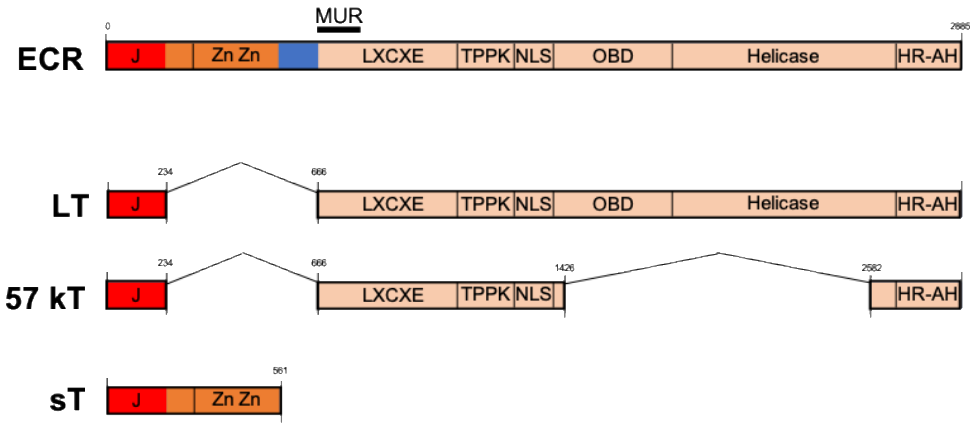

Figure 1.4: Mapping of the MCPyV tumour antigens to highlight major known binding regions and splice sites. The regions of the MCPyV ECR responsible for functional activity are shown in the context of the full gene alongside the LT, ST and 57 kT proteins that are expressed following alternative splicing. Abbreviations annotated upon the schematic represent the DnaJ domain (J), retinoblastoma-associated binding domain (LXCXE), threonine-proline-proline-lysine motif (TPPK), nuclear localisation signal (NLS), origin binding domain (OBD), helicase/ATPase domain (helicase), host range and adenovirus helper function (HR-AH) and Merkel unique region (MUR).

1.5.1 The large tumour antigen

LT is a complex, multi-functional protein that has a range of activities within the cell. The ability of the protein to dysregulate the cell cycle to promote transformation led to a body of early work in SV40, however many of the functions remain conserved between species and are applicable in the context of HPyVs (Van Ghelue et al., 2012; An et al., 2012). To this extent, PyV LTs share a wide range of common features including the DnaJ domain, origin-binding domain, zinc-binding domain and helicase/ATPase domain, the location of which are highlighted in Figure 1.4. The ability of LT to dysregulate several aspects of the host cell lifecycle to promote viral replication is due to interaction with endogenous proteins, some of which are summarised in Figure 1.5.

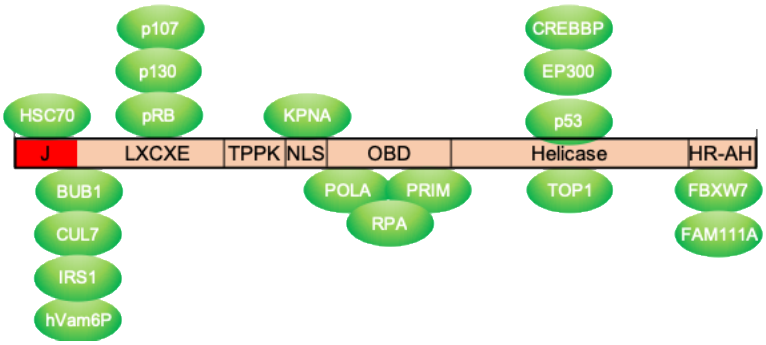

Figure 1.5: LT interactions with cellular proteins required to promote the viral lifecycle. Highlighted are important protein interactions in the lifecycle of PyVs. Interaction of hVam6P is unique to MCPyV which cannot bind BUB1.

1.5.1.1 DnaJ domain

The DnaJ domain of LT, which is also shared with ST, is responsible for binding to the cellular chaperone and transcriptional repressor heat shock chaperone 70 (HSC70). The DnaJ domain is essential for cellular transformation and viral replication in a range of PyVs (Berjanskii et al., 2000; Whalen et al., 2005; Kwun et al., 2009; An et al., 2012). In addition to promoting viral replication, LT binding of HSC70 activates the chaperone's ATPase activity, leading to the dissociation of pRb from its complex with E2F (Sheng et al., 1997; Harris et al., 1998). In the case of the HPyVs BKPyV, JCPyV and MCPyV the DnaJ domain also contains a pentapeptide CR1 LXXLL motif,

which is proposed to assist in pRb/E2F disruption in a manner comparable to adenovirus E1A (Yaciuk et al., 1991; Sheng et al., 1997; Spurgeon and Lambert, 2013).

1.5.1.2 Retinoblastoma binding domain

The retinoblastoma-associated protein (pRb) binding site (LXCXE) cooperates with the DnaJ domain to perturb pRb/E2F interactions to promote cell cycle progression (Stubdal et al., 1997). Following HSC70-mediated pRb/E2F disruption, the LXCXE domain binds to the tumour suppressor pRb as well as the Rb related proteins p130 and p107. In turn this releases the transcription factor E2F to promote progression into S-phase (Figure 1.6) (Weinberg, 1995).

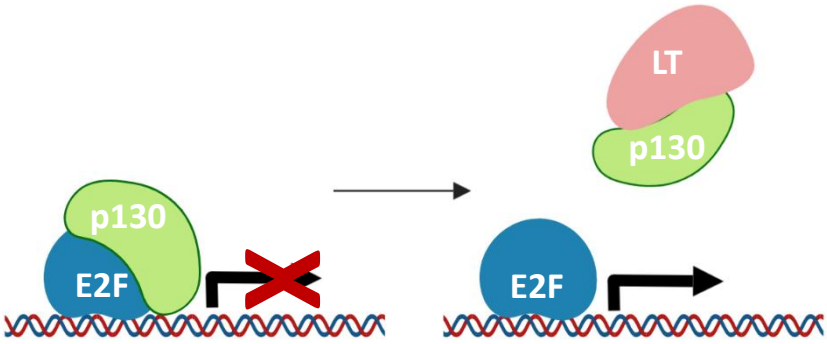

Figure 1.6: Schematic representation of LT disruption of the Rb/E2F complex. LT destabilises p130 interaction with the transcription factor E2F before binding the former and sequestering its activity as a repressor of E2F. E2F can then initiate transcription of genes associated with cell cycle progression.

The majority of PyV LTs can also interact with Bub1 via a WXXWW motif that is conserved between species and located between the DnaJ domain and pRb binding motif (Cotsiki et al., 2004). Bub1 is a serine-threonine protein kinase that acts as a mitotic checkpoint; however, it is believed that binding by LT leads to chromosomal instability. Given that MCPyV is the only HPyV that is currently known to cause cancer in humans and that chromosomal instability is a hallmark of cancer, it is intriguing that the Bub1-binding motif is not present in the genome of MCPyV (Baez et al., 2017; Vargas-Rondón et al., 2018). Instead, MCPyV contains the MCPyV TAg unique region (MUR), which sequesters hVam6P (Vps39-like protein) into the

nucleus (Liu et al., 2011). This disrupts lysosomal clustering and is suggested to potentially contribute to egress of virions.

The ability of SV40 LT to induce immortalisation and transformation of rodent cell lines was shown to require residues 69-83, which interact with Cullin 7 (CUL7) (Kasper et al., 2005). CUL7 acts as a scaffold to organise an E3 ubiquitin ligase composed of FBXW8, Skp1 and the ROC1 RING finger protein (Hartmann et al., 2014). Interaction of LT with CUL7 therefore prevents ligase activity responsible for insulin receptor substrate 1 (IRS1) degradation, promoting downstream signalling pathways that include phosphatidylinositol-3 kinase/protein kinase B (PI3K/Akt) and extracellular signal-related kinase (ERK) mitogen-activated pathway kinase (MAPK) (Hartmann et al., 2014).

Despite latency being commonplace for viruses to avoid immune detection and await host conditions that are more suitable to propagation such as immunosuppression, little is known about how small DNA viruses facilitate long-term persistence. However, MCPyV LT contains several phosphorylation sites that are constitutively recognised by the cellular SCF E3 ubiquitin ligases FBXW7, Skp2 and βTrCP to facilitate degradation of LT (Kwun et al., 2017). In particular alanine mutation of S220 and S239 led to increased LT stabilisation, a phenotype that could also be induced through knock down of any of the ligases.

1.5.1.3 TPPK domain

The TPPK domain is a classic cdc2/CDK1 consensus sequence found in MCPyV LT (T299) and SV40 LT (T124). Studies that prevented phosphorylation of these residues identified that phosphorylation was essential for viral Ori interaction, further highlighting the requirement of LT for initiation of viral replication (Diaz et al., 2014).

1.5.1.4 Origin binding domain

The Ori of PyVs contains a central palindrome consisting of four 5'-GAGGC-3' repeats which interacts with LT (Dean and Hurwitz, 1991; Bochkareva et al., 2006). The origin binding domain of LT is largely composed of positively-charged residues that interact with the negatively-charged viral DNA. Specific residues important for this interaction are K331 and R380 for MCPyV LT binding and R154 and R2024 for SV40 (Bochkareva et al., 2006; Harrison et al., 2011).

1.5.1.5 Helicase domain

In order for PyVs to initiate replication, the genome firstly needs to be unwound prior to recruitment of the cellular DNA polymerase α-primase (PRIM), replication protein A (RPA) and DNA polymerase δ (POLA) to the origin binding domain (Sowd and Fanning, 2012). This is achieved through the binding of two LT hexamers that opposingly twist to reveal the genome. Following initiation the two hexamers then move apart to permit bidirectional DNA replication (Yardimci et al., 2012). Recruitment of topoisomerase 1 (TOP1) is also essential to viral propagation, with interactions required to relieve stress ahead of the replication fork prior to initiation of replication (Khopde and Simmons, 2008; Mahon et al., 2009; Nukuzuma et al., 2016).

The majority of PyVs bind p53 through the opposing surface of the helicase domain to prevent gene expression in response to DNA damage (Lilyestrom et al., 2006). However, this is not the case for MCPyV LT, which despite being able to significantly reduce p53 transcription activity was shown to not directly interact with the protein (Borchert et al., 2014). In addition to p53, SV40 LT also interacts with the transcriptional co-activators CREB-binding protein (CREBBP) and histone acetyltransferase p300 (EP300) (Poulin et al., 2004). This study identified that acetylation of LT was dependent upon binding of p53 as well as CREBBP suggesting this may provide a regulatory mechanism for binding to additional cellular factors. The study further noted that both BKPyV and JCPyV displayed conserved acetylation and that this may therefore be a requirement of several PyVs (Poulin et al., 2004).

1.5.1.6 Host range and adenovirus helper domain

The roles of the host range and adenovirus helper (HR-AH) domain have only been characterised in the context of SV40. Additionally HPyVs, with the exception of BKPyV and JCPyV, do not possess the same length or homology of the final C-terminal domain suggesting that the interactions may be specific to SV40 or that HPyVs compensate through alternative interactions (Decaprio and Garcea, 2013). The requirement of the SV40 LT C-terminus in determination of host range has been known for several years, however it was not until more recently that interaction with FAM111A, a poorly characterised protein with known involvement during DNA

replication, was identified as the essential requirement (Pipas, 1985; Fine et al., 2012). The study by Fine *et al*. showed that loss of FAM111A interaction led to a loss of viral replication, host range restriction and loss of helper functions in promotion of adenovirus replication in monkey cell lineages. Subsequent depletion of FAM111A led to recovery of viral phenotypes associated with full length LT, highlighting the necessity of this interaction to expand the host range of SV40. A more recent study has suggested that FAM111A, which normally localises to the nucleoli in a cell cycle dependent manner, is recruited by LT to replication centres to promote DNA replication (Tarnita et al., 2018).

The C-terminus of SV40 LT, when phosphorylated at T701, also acts as a phosphodegron decoy for the cullin RING ligase substrate adaptor FBXW7 (Welcker and Clurman, 2005). This interaction interferes with FBXW7 mediated degradation of G1-S specific cyclin E1 and MYC to promote cellular growth and proliferation.

1.5.2 The small tumour antigen

All PyVs express ST alongside LT. This small protein of approximately 17 kDa retains the DnaJ domain and functionality relative to LT, which has been previously described. However, by reading through the LT splice junction of mRNA, ST possesses a unique carboxy-terminus (Shuda et al., 2011). A schematic representation of ST and its cellular interacting partners is shown in Figure 1.7.

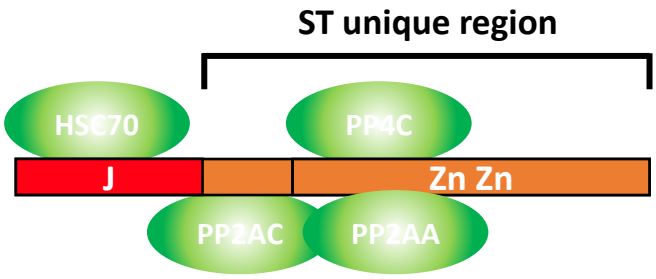

Figure 1.7: Schematic representation of a Polyomavirus ST and known interacting partners. A general overview of a PyV ST. The protein is composed of two domains, the DnaJ domain, which is conserved with LT and the unique zinc finger domain (Zn Zn). Shown are known interacting partners. ST interaction with PP4C has to date only been shown for MCPyV.

The unique region of ST contains two zinc fingers that interact with protein phosphatases to manipulate several cellular events. Several PyVs have been shown to bind with subunits of the major cellular serine/threonine protein phosphatase 2A (PP2A) (Chen et al., 2007; Uhn et al., 2007; Bollag et al., 2010; Kwun et al., 2015). MCPyV ST has further been shown to interact with the protein phosphatase 4 catalytic subunit (PP4C) and regulatory subunit 1 (PP4R1) (Griffiths et al., 2013; Stakaitytė et al., 2017; Abdul-Sada et al., 2017).

1.5.2.1 ST-mediated LT stabilisation

MCPyV ST stabilises and in turn increases the amount of LT within the cell (Kwun et al., 2013; Dye et al., 2019). There is conflicting evidence as to how this is brought about. Kwun *et al*. identified that LT is targeted for proteasomal degradation by SCF E3 ligase FBXW7, however binding of the ligase by ST in the LT stabilisation domain (LSD), which spans residues 91-95 on the opposite molecular face to which PP2A interacts, prevents LT degradation. ST binding further stabilises other cellular proteins such as c-Myc and cyclin E that would otherwise be degraded by FBXW7 to promote transformation. Dye *et al.* confirmed that ST increased the quantity of LT within the cell via the LSD, however found no evidence to support ST interaction with FBXW7. It was therefore suggested that ST interaction with ubiquitin ligases were not required, however no alternative hypothesis was presented.

1.5.2.2 ST interaction with PP2A

Within a cell, regulation of nearly one third of proteins is performed through differential phosphorylation, which in turn controls a vast array of biological functions (Seshacharyulu et al., 2013). PP2A forms a heterotrimeric holoenzyme composed of the horseshoe-shaped scaffold protein (subunit A), a catalytic protein (subunit C) and a regulatory protein (subunit B) (Cho and Xu, 2007). Subunits A and C both have two different isoforms that may be incorporated into the holoenzyme, whilst the regulatory B subunit is more variable, with four different classes made up in total of 16 different isoforms. The four B subunit classes are termed B (PR55), B’ (B56/PR61), B’’ (PR72) and B’’’ (PR93/PR110). Whilst subunit C and A/C dimer may have limited activity, specificity of PP2A is predominantly regulated by the variable N-terminus of different B subunits that make up heterotrimeric complexes (Janssens

and Goris, 2001). Interaction of PyV STs with subunit A isoforms varies. SV40 ST only interacts with PP2A Aα, whereas MuPyV and MCPyV interacts with both PP2A Aα and Aβ (Zhou et al., 2003; Stakaitytė et al., 2017).

PP2A is normally associated with regulating several cellular processes including cell cycle progression and apoptosis through dephosphorylation of signalling proteins such as Akt, p53, c-Myc and β-catenin and as such is considered a tumour suppressor (Baez et al., 2017). It is therefore unsurprising that PP2A dysregulation is associated with a progression of cancer (Ruvolo, 2016).

ST is able to alter substrate specificity of PP2A through competitive binding of subunit A/C dimers, which displaces and prevents the binding of the regulatory B subunit (Figure 1.8) (Pallas et al., 1990; Pallas et al., 1992). This interaction inhibits dephosphorylation of a range of proteins which subsequently leads to continuous activation of pathways related to cellular transformation (Baez et al., 2017). ST-PP2A interaction prevents the dephosphorylation of the CDK inhibitor p27 leading to its degradation and transition from G1-S phase of the cell cycle. S-phase entry is further promoted through expression of cyclin A/CDK2 and cyclin E/CDK2 (Schüchner and Wintersberger, 1999; Skoczylas et al., 2005). The ability of SV40 ST-PP2A binding to transform the host cell has been further described, as CDK2 activation and induction of DNA synthesis mediated by ST-PP2A was sufficient to transform human fibroblasts (Sotillo et al., 2008).

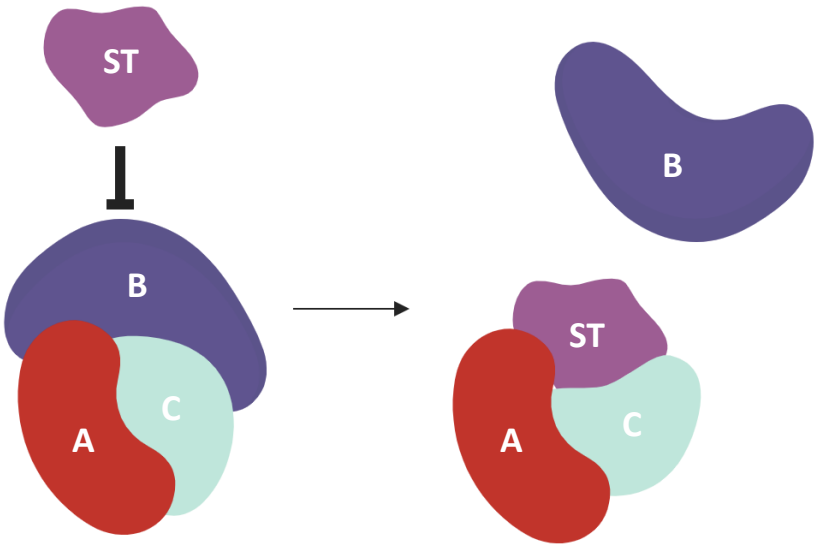

Figure 1.8: Schematic representation of the competitive binding of ST to PP2A. ST acts as a competitive inhibitor of PP2A subunit B, preventing binding to the A/C dimer.

SV40 ST interaction with PP2A has also been shown to activate ERK signalling to upregulate cyclin D1, which in turn enhances proliferation through phosphorylation of pRb to release E2F (Frost et al., 1994). TSPyV ST also phosphorylates ERK and c-Jun via a mechanism dependent upon MEK1/2, although confirmation of PP2A interaction was not performed (Wu et al., 2016).

Increased c-Myc stabilisation is associated with a loss of PP2A-mediated phospho-degradation which further enhances tumorigenesis due to subsequent increased expression of telomerase and cyclin D1 (Klucky and Wintersberger, 2007; Kwun et al., 2013).

1.5.2.3 Interaction of ST with protein phosphatase 4 subunits

SV40 ST upregulates antiapoptotic targets of nuclear factor kappa B (NF-κB) signalling (Sablina and Hahn, 2008). However, the mechanisms behind ST-mediated NF-κB manipulation have only been deciphered in relation to MCPyV ST. ST-mediated inhibition of NF-κB signalling prevents anti-viral responses and promotes expression of pro-inflammatory cytokines through the formation of a complex with PP4C and PP4R1 (Abdul-Sada et al., 2017). The ST-PP4 complex modulates NF-κB signalling through an interaction with the NF-κB essential modulator (NEMO) adaptor protein, inhibiting IκB kinase α (IKKα)/IKKβ-mediated phosphorylation (Griffiths et al., 2013). This restricts translocation of the NF-κB heterodimer to the nucleus preventing transcriptional activity associated with the innate immune response.

MCPyV interaction with PP4C promotes a range of phenotypes that are associated with increased cellular migration and motility. MCPyV ST interaction with PP4C leads to dephosphorylation of stathmin, which in turn prevents acetylation of tubulin and destabilisation of microtubules (Knight et al., 2015). PP4C manipulation by MCPyV ST also leads to alterations in the actin cytoskeleton, promoting actin filamentation and filopodia formation to enhance motility (Stakaitytė et al., 2017). Although the mechanism responsible was not fully elucidated, PP4C-mediated dephosphorylation of β_1 integrin and subsequent activation of the Rho family GTPases cdc42 and RhoA was identified as essential requirements.

1.5.2.4 Protein phosphatase independent ST activities

Whilst most activities associated with PyV STs are mediated through manipulation of protein phosphatases, there is also evidence that some pathways are independently activated.

MCPyV ST can induce cellular proliferation through hyperphosphorylation of initiation factor 4E-binding protein 1 (4E-BP1) and cap-dependent translation, via a mechanism that is independent of upstream mTOR pathway activation and PP2A interaction (Shuda et al., 2011). Activity of 4E-BP1 was shown to be indispensable for ST-mediated anchorage- and contact-independent growth, transformation and serum free proliferation of rodent fibroblasts.

Expression of the cellular sheddases A disintegrin and metalloproteinase (ADAM) 10 and 17 is also induced by MCPyV ST, which act to break down cell-cell junctions to promote cell dissociation, which is an essential step for initiation of metastasis (Figure 1.9) (Nwogu et al., 2018).

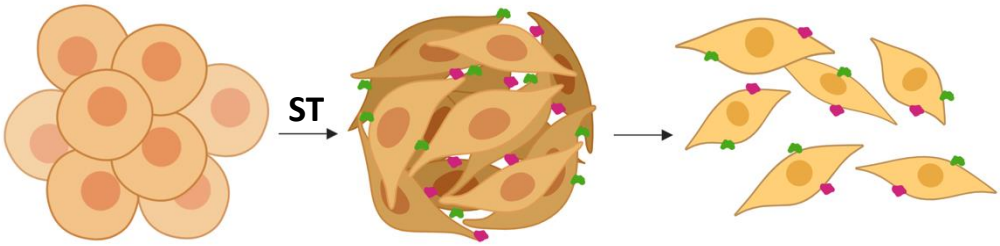

Figure 1.9: Schematic representation of ST-mediated dissociation induced by ADAM 10 and ADAM 17 expression. ST induces ADAM 10 and ADAM 17 expression on the cell surface which disrupts cell-cell junctions enhancing cellular dissociation.

1.5.3 Species-specific additional early proteins

In addition to LT and ST, some PyVs encode extra early proteins. To date however, MuPyV MT is the only protein that has unique functionality in respect to cellular transformation.

MT is the essential oncogene of MuPyV-induced tumour formation and is capable of inducing tumours in certain animal models independent of other TAgs (Treisman et

al., 1981). The protein contains the full-length ST, however through splicing has a unique C-terminus that includes a membrane anchor that can tether the protein to the cell membrane and intracellular membranes (Fluck and Schaffhausen, 2009). The transforming ability of MT is attributed to several interactions. Similarly to PyV STs, MT interacts with PP2A, which results in displacement of the regulatory B subunit. MT also possesses a tyrosine-phosphorylated motif that can interact with the phosphotyrosineinteraction/phosphotyrosinebinding domain of Shc to enhance transformation, with overexpression of Shc sufficient to block transformation (Blaikie et al., 1997). MT induced cellular transformation is also dependent upon the activity of the p110α isoform of phosphatidylinositol 3-kinase (Utermark et al., 2007). MuPyV also expresses tinyT, which is terminated prior to the LT splice site, maintaining DnaJ activity (Riley et al., 1997).

MCPyV encodes two additional proteins termed 57 kT and ALTO, which are shown in Figure 1.3. 57 kT is produced through additional splicing of LT, resulting in the loss of the majority of the helicase and OBD (Kwun et al., 2009). ALTO is produced through gene overprinting (Carter et al., 2013). Although ALTO is evolutionary related to MuPyV MT, it has no influence upon the viral lifecycle and is considered to represent an example of viral evolution.

SV40 expresses 17 kT, a protein that shares the initial exon with LT but through removal of a 746 bp intron and frame shifting contains four unique C-terminal amino acids (Comerford et al., 2012).

BKPyV expresses truncated TAg (truncT), which is produced in a similar manner to SV40 17 kT in that a second intron leads to additional C-terminal amino acids (Abend et al., 2009).

JCPyV encodes three additional TAgs termed T'165, T'136 and T'135 which again share a conserved sequence with LT but an additional intron leads to differential C-terminal amino acids (Trowbridge and Frisque, 1995).

A protein termed 229T was also identified in SLPyV, however no studies have been performed to determine whether this has any influence during the viral lifecycle (Lim et al., 2013).

1.6 Polyomavirus microRNAs

RNA interference (RNAi), through non-coding RNAs, plays an important role in many host processes. The enzymatic and regulatory functions of these molecules, coupled with a role in defence against viral infection, make these short (about 22 nucleotide) RNAs important targets for many viruses in order to avoid detection within infected host cells. miRNAs have been identified in all studied metazoan and although their functions are poorly characterised, a role in animal development and physiology has been proposed (Ambros, 2004). miRNAs specifically regulate gene expression and are initially transcribed as an imperfect hairpin structure that is around 70 nucleotides in length. Processing by Dicer produces the mature miRNA, which can posttranscriptionally regulate gene expression through binding of 3'-untranslated regions (3'-UTRs) (Doench et al., 2003).

PyVs are known to encode one microRNA (miRNA) on the late strand that interacts with early mRNAs through binding the LT sequence (Imperiale, 2014). The miRNA of MCPyV and MuPyV recognises the 5' region of the second LT exon, the complementary region of MCPyV is highlighted in Figure 1.3. The miRNA encoded by SV40, BKPyV and JCPyV in contrast is complementary to the 3' end of LT. There is currently little known about the functions of PyV miRNAs within the cell, but binding to LT mRNA leads to degradation, restricting the ability of the virus to replicate (Seo et al., 2009). MCPyV miRNA-M1 has been implicated in immune evasion through modulation of SP100, which prevents CXCL8 secretion and subsequent viral identification by neutrophils (Akhbari et al., 2018).

1.7 Late stages of the polyomavirus lifecycle

1.7.1 Genome replication

Genome replication has been identified as a block to replication in non-permissive cells and is a major contributor to limited host range (Ferenczy et al., 2012).

As had been previously described, LT is essential for viral replication through formation of a double hexamer at the NCCR and recruitment of a range of host cellular factors. ST plays an auxiliary role to stabilise LT and enhance replication.

Binding of LT to the NCCR represses the early promoter and interaction with transcription-enhancing factor 1 (TEF1) prevents suppression of the late promoter to permit the initiation of viral replication in a bidirectional manner (Berger et al., 1996). Components of the DNA damage response (DDR) colocalise to viral replication centres and are required to promote replication (Tsang et al., 2014). Newly synthesised viral DNA then recruits host cellular histones to form the minichromosome that is subsequently packaged into the virion (Tan, 1977).

1.7.2 Late protein expression and capsid assembly

The production of the late transcript that codes for the structural 'VPs' and any auxiliary proteins begins following initiation of DNA replication (Cubitt, 2006). Following translation, the structural proteins traffic into the nucleus due to the NLS region of the VPs which is also purported to be essential during initial infection. The ability of VPs to translocate across the nuclear membrane does however vary between species and ultimately is dependent upon the presence of an NLS. All SV40 VPs contain an NLS and are therefore able to shuttle into the nucleus independently (Ishii et al., 1994). Mutational analysis further showed that mutation to the NLS of VP1 or VP2/3 did not perturb nuclear localisation when co-expressed, indicating that pentamer and minor capsid interaction occurs within the cytoplasm prior to nuclear import. JCPyV VP1 does not contain an NLS and therefore requires an interaction with VP2/3 to enter the nucleus and in contrast MuPyV VP2/3 requires the NLS-containing VP1 (Forstová et al., 1993; Shishido-Hara et al., 2000).

VP1 pentamers that make up the capsid share almost identical conformations, with C-terminal alteration in the 'arms' that reach out and insert into the cores of neighbouring pentamers to stabilise the capsid (Liddington et al., 1991; Stehle and Harrison, 1997). In the case of BKPyV, interpentameric interactions are further stabilised through incorporation of Ca^{2+} ions which facilitate correct assembly (Li et al., 2003).

The minor capsids proteins VP2 and VP3 (if expressed) share a common C-terminus, whilst a longer N-terminus of VP2 gives rise to a difference in size between the proteins. One minor capsid protein binds to the axial cavity of each VP1 pentamer through a common C-terminus hydrophobic interaction (Chen et al., 1998). The

minor capsid proteins also contain a DNA binding domain which links the viral minichromosome to the capsid. The additional N-terminal region of VP2 contains a myristoylation site which, when mutated, reduces the efficiency of infection (Krauzewicz et al., 1990).

1.7.3 Late auxiliary proteins

Several PyVs including SV40, BKPyV and JCPyV express agnoproteins (agno), which are encoded 5' of the VPs, display a highly conserved sequence and have been implicated in a range of functions to enhance the efficiency of viral production (Royle et al., 2015).

JCPyV agno is a viroporin that localises to the ER to dysregulate Ca^{2+} homeostasis (Suzuki et al., 2010). This has been suggested to generate Ca^{2+} ions that are incorporated into the viral capsid and disrupt the plasma membrane to facilitate viral egress. BKPyV that lacks agno is still able to form complete capsids that are retained within the cell, suggesting that the requirement of Ca^{2+} dysregulation is to facilitate release (Panou et al., 2018). Interaction of BKPyV agno with α-soluble *N*-ethylmaleimide sensitive fusion attachment protein (αSNAP), a component of the SNARE complex, could also facilitate release via a non-lytic mechanism of endocytosis.

JCPyV agno also interacts with heterochromatin protein 1, causing its dissociation from lamin B receptors to destabilise the nuclear envelope to assist exit from the nucleus (Okada et al., 2005).

SV40 also expresses the non-structural VP4 protein, which has been suggested to act as a viroporin to disrupt membranes and facilitate lytic release of progeny (Raghava et al., 2011). An alternative study however suggested that VP4 had no role in the release of SV40 (Henriksen et al., 2016).

1.7.4 Polyomavirus egress

The mechanisms by which PyVs are released from the cell remain poorly characterised and, in the case of VP4, controversial. Studies have shown, as highlighted previously, that agno is required for the release of some PyVs, but for other viruses that do not express auxiliary proteins, there is likely another unknown

mechanism to compensate. BKPyV requires anion homeostasis to facilitate non-lytic release from cells (Evans et al., 2015). This study further suggested that virions were trapped within LAMP-1 coated, acidic compartments, consistent with release through the endo/lysosomal network.

1.8 Viruses and cancer

The dynamic transformation of healthy tissue into a neoplastic state is determined by a complex series of events leading to the manipulation of several intracellular and extracellular functions to enhance cancerous phenotypes. It is suggested that four to six fundamental modifications in cell physiology, known as the hallmarks of cancer (summarised in Figure 1.10), lead to the ability of cancerous cells to replicate uncontrollably. The mechanistic strategy of individual tumours may however vary (Rubin, 1994; Hanahan and Weinberg, 2000). Entry of a cell into a maintainable neoplastic state relies upon evasion of apoptosis, self-sufficiency in growth signals, insensitivity to anti-growth signals, tissue invasion and metastasis, limitless replicative potential and sustained angiogenesis. In most if not all cases of cancer, fulfilment of the listed criteria is deemed essential for progression of disease, which given the complexity of required changes infers why the development of malignant neoplasms remains uncommon within the general human population.

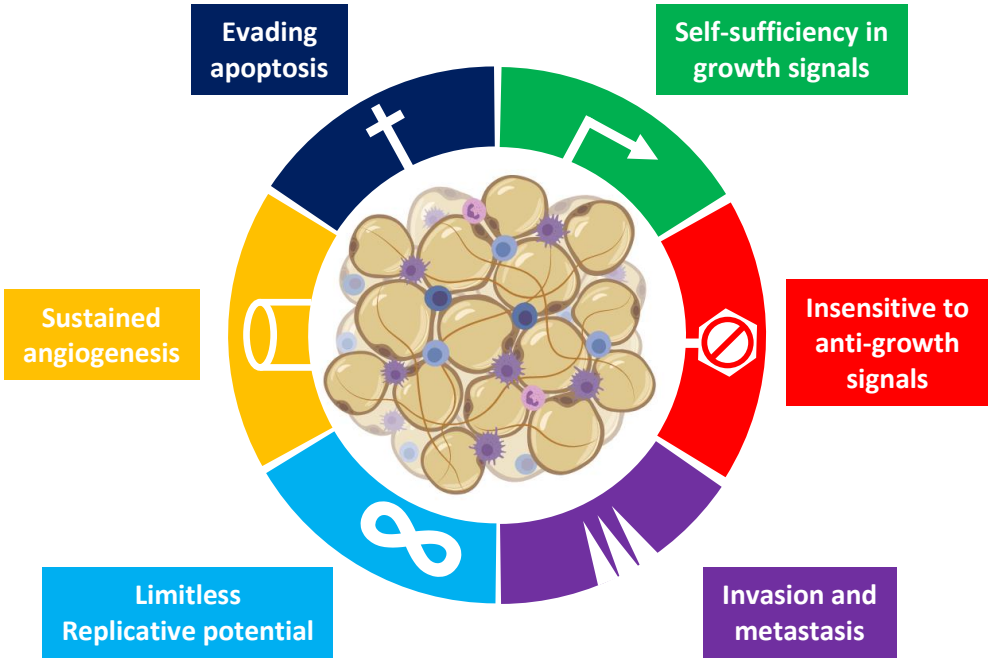

Figure 1.10: Schematic representation of the six fundamental hallmarks of cancer. Sustained growth of the tumour microenvironment requires the dysregulation of at least six cellular processes. Cells through mutation and/or pathogenic intervention are capable of evading apoptosis, self-sufficiency in growth signals, insensitivity to anti-growth signals and limitless replication. Stromal cells react to the tumour microenvironment by causing inflammation, which in turn facilitates sustained angiogenesis which provides the microenvironment with sufficient nutrients and oxygen for growth, and metastasis is initiated through degradation of the extracellular matrix and promotion of anchorage-independent growth. Adapted from Hanahan and Weinberg, 2000.

Due to the similarities between the hallmarks of cancer and the host systems that are hijacked by pathogens, it is not surprising that viral infection is attributed to 15-20% of the global cancer burden (Liao, 2006; Parkin, 2006). Both DNA and RNA tumour viruses have been implicated as causative agents of cancer in humans. However, the minimal number of cases relative to the number of infected individuals, coupled with requirement of additional events such as immunosuppression, somatic mutations, genetic predisposition or exposure to carcinogens highlights the inefficiency of progression from viral infection to cancer development (Liao, 2006). Tumour viruses are typically capable of establishing a persistent infection within the

infected host, with expression of oncogenes leading to the immortalisation and transformation of the infected cell, priming it for virus replication and preventing apoptosis (Carrillo-Infante et al., 2007).

To date there are seven viruses that have been associated with cancer formation and progression, which are summarised in Table 1.2 (Brechot et al., 1980; Dupin et al., 2000; Schiffman et al., 2007; Klein et al., 2007; Boxus and Willems, 2009; Lei et al., 2010; Kaae et al., 2010; Peitsch, 2015; Moens et al., 2015).

Table 1.2: A summary of the seven viruses that are implicated in human cancers. The classification of virus is in accordance with the Baltimore virus classification system.

Virus	Abbreviation	Genus and classification	Year of discovery	Associated diseases
Hepatitis C	HCV	Hepaciviridae IV ((+)ssRNA)	1989	Some hepatocellular carcinomas and lymphomas
T-lymphotropic virus type 1	HTLV-I	Retroviridae VI (ssRNA)	1980	Adult T-cell leukaemia
Hepatitis B	HBV	Hepadnaviridae VII (ss+dsDNA)	1965	Some hepatocellular carcinomas
Epstein-Barr	EBV	Herpesviridae I (dsDNA)	1964	Burkitt's lymphoma, nasopharyngeal carcinoma
Human papillomaviruses 16 and 18	HPV16/18	Papillomaviridae I (dsDNA)	1983/4	Cervical, penile and head and neck cancers
Kaposi's sarcoma herpesvirus	KSHV	Herpesviridae I (dsDNA)	1994	Kaposi's sarcoma and primary effusion lymphoma
Merkel cell polyomavirus	MCPyV	Polyomaviridae I (dsDNA)	2008	Merkel cell carcinoma

1.8.1 Merkel cells and Merkel cell carcinoma

Merkel cells were first identified in 1875 by Friedrich Sigmund Merkel. They are found around hair follicles, certain mucosal tissues and in their largest quantities in touch-sensitive basal layers of the epidermis (Figure 1.11) (Spurgeon and Lambert, 2013). They are specialised sensory receptor cells of epithelial origin that are important for recognition and neural relay of somatosensory stimuli relating to a light touch (Morrison et al., 2009).

MCC (Figure 1.12) is a rare but aggressive neoplasm that typically affects white, elderly and/or immunocompromised patients, who often have a history of sun-exposure related diseases. The significant features of MCC are summarised by the acronym AEIOU: asymptomatic, expanding rapidly, immune suppression, older than 50 years, and ultraviolet exposed site on a person with fair skin (Heath et al., 2008). Due to a lack of distinguishing lesion features and challenging diagnosis, MCC is often not identified early in development with detection in localised lymph nodes a common staging procedure (Gupta et al., 2006; Lemos et al., 2010). Immunohistochemistry is commonly required in addition to clinical examination, with cytokeratin (CK) 20 a positive marker utilised alongside others including CK8, CK18, CK19 and huntingtin-interacting protein (HIP1) (Drusio et al., 2019). MCC may be CK20 negative (<10% of cases), which is usually attributed to high mutational burden in virus negative tumours and may complicate diagnosis. In the case that MCC is diagnosed, lymph node biopsies may be performed to identify the staging of disease.

The incidence of MCC is believed to be around 50-fold lower than that of melanoma, with 0.6, 1.6 and 0.3 incidences per 100,000 people in the United States, Queensland (Australia) and Sweden, respectively, and average onset of disease in the age range of 75-80 years (Youlden et al., 2014; Zaar et al., 2016; Drusio et al., 2019). In England the incidence rate has increased from 0.1 to 0.2 per 100,000 people between 1999 and 2008 (Schadendorf et al., 2017).

With no current specific treatment for MCC and poor prognosis for patients with advanced carcinomas, there is a need to better identify the causative agents of disease so that therapeutic targets can be identified (Schrama et al., 2012; Lim et al.,

2012). In particular, a correlation between metastasis and lowered survival rate has been identified. Table 1.3 describes the current staging system for patients with MCC. A review of an MCC database identified that the 5-year disease-specific survival rate was 64% (Allen et al., 2005). The stage of cancer progression was also found to be of significance to prognosis with 5-year survival based upon disease stage found to be: stage I, 81%; stage II, 67%; stage III, 52%; stage IV, 11%. One study concluded that between 1986 and 2011 the mortality rate of MCC has risen by more than 333% in the United States, however the contribution of better diagnostics should not be discounted (Fitzgerald et al., 2015).

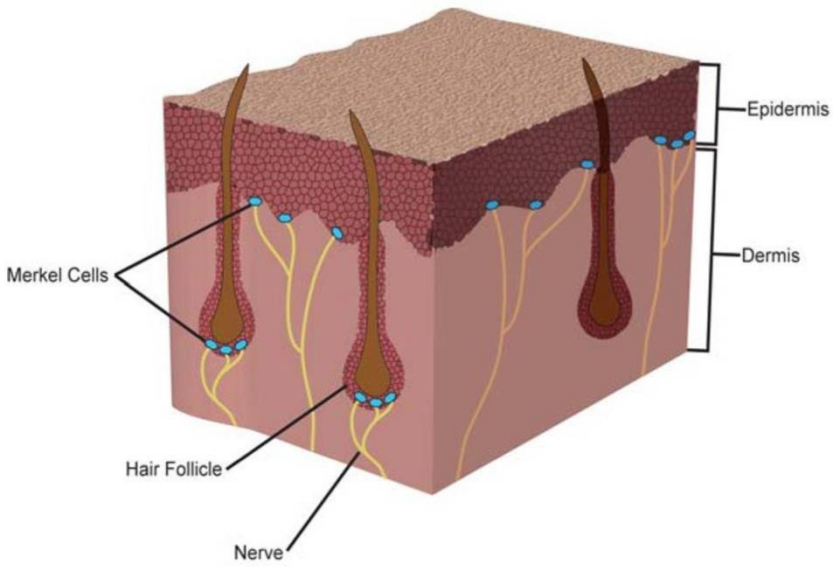

Figure 1.11:Diagrammatic representation of Merkel cell location within skin. Merkel cells (shown in blue), which are located in the basal layer of the epidermis at the terminal of nerves and the bulge region of hair follicles. Taken from Spurgeon and Lambert 2013.

Figure 1.12: Clinical example of MCC. MCC typically progresses in sun exposed areas of the skin. The images show MCCs that have developed on the eyelid (A), hand (B) and forearm (C). Adapted from Heath *et al.* 2008.

Table 1.3: Staging system for patients with MCC.

Stage	Primary tumour ≤ 2 cm	Region lymph node detection	Distant metastatic disease
I	No	Negative	No
II	Yes	Negative	No
III	Any	Positive	No
IV	Any	Any	Yes

1.8.2 Treatment of MCC

Following identification of MCC, wide local excision of the primary tumour is the standard of care (Lebbe et al., 2015; Bichakjian et al., 2018). However, surgery is not always a feasible solution given the typically advanced age of patients and risks associated with extensive surgery under general anaesthetic, coupled with the functional and cosmetic consequences of tissue removal in sun-exposed regions such as the face and neck. In cases where surgery is plausible, any positive lymph nodes would also be removed. Following surgery daily wide-field adjuvant radiotherapy of the primary tumour site and, where applicable, draining lymph node basin is commonly performed for a period of 4-5 weeks post-surgery.

Immunotherapy targeting the immune blockade checkpoint between programmed cell death protein 1 (PD1) and its ligand (PDL1) to activate immune responses against MCC has recently showed promising results (Giraldo et al., 2018; Miller et al., 2018; Del Marmol and Lebbé, 2019). Treatment with the anti-PD1 antibody pembrolizumab led to a response in 56% of patients with advanced-stage MCC which led to progression-free survival of 67%, which was compared with chemotherapy progression-free survival of 24% (Iyer et al., 2016; Nghiem et al., 2016; Nghiem et al., 2017). Avelumab, an antibody targeting PDL1 also showed similar results, with 82% of patients maintaining initial responses (Kaufman et al., 2016).

1.8.3 MCPyV and Merkel cell carcinoma

MCPyV has been attributed to the causation of MCC due to the detection of clonally integrated viral DNA in 80-95% of patients, suggesting that the disease may be of an infectious origin (Feng et al., 2008). The identification of MCPyV relied on a novel method termed digital transcriptome subtraction. RNA extracted from tumours was reverse transcribed, before sequencing of the resulting cDNA. Following subtraction of human transcripts, novel sequences were aligned using a BLAST homology search to identify polyomavirus-like sequences.

With MCC being extremely rare within the population and clonal integration not solely responsible for the onset of disease, it is not surprising that MCC induced by MCPyV infection requires a secondary event. Through comparison of MCC tissues with healthy tissues infected with MCPyV, it was discovered that mutations in the ECR were always evident (Shuda et al., 2008). These mutations result in the insertion of a premature stop codon, leading to truncations of LT. Therefore, for the development of MCPyV-induced MCC, it was assumed that a two-step process occurred; firstly, MCPyV has to become integrated into the host genome before subsequent mutations that are beneficial to transformation, but detrimental to the completion of the viral lifecycle occur.

A more recent publication has provided evidence to the contrary of this hypothesis in that MCPyV mutation precedes integration events, summarised in Figure 1.13 (Schrama et al., 2019). This study identified that the viral genomes integrated into several MCPyV-positive MCC cell lines were concatemers containing the same genome mutation. It is therefore suggested that mutation occurs in the presence of full-length LT which can initiate rolling circle replication of a mutated genome. This concatemer then becomes integrated into the host genome and following WT LT depletion, expression of truncated LT (tLT) and ST leads to tumour formation.

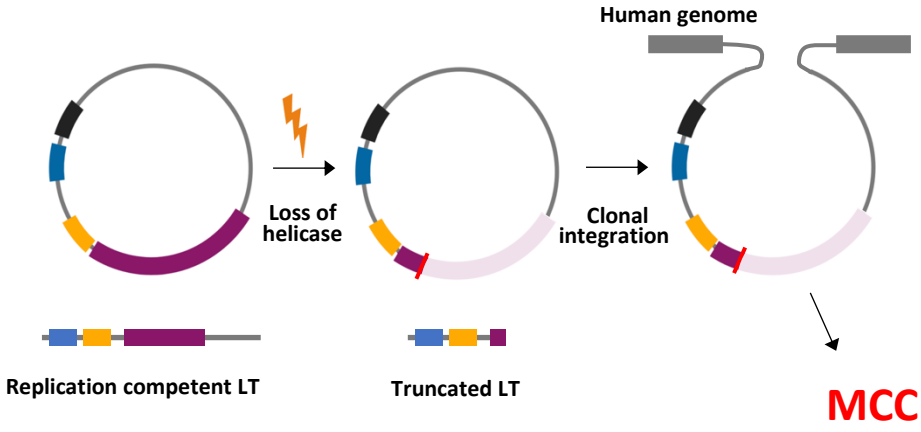

Figure 1.13: Schematic representation of the sequential mutation and clonal integration of MCPyV genomes that leads to MCC. UV-mediated mutagenesis of replication competent viral genome leads to truncation of LT and loss of the helicase domain. The replication incompetent virus then integrates into the host genome where continuous TAg expression leads to MCC.

1.8.4 Truncated large tumour antigen

Genomic sequence analysis of MCPyV positive MCCs identified mutations leading to premature stop codons within LT are present within the clonally integrated viral genome (Shuda et al., 2008; Spurgeon and Lambert, 2013). Previous studies have shown that the subsequent truncated LT (tLT) proteins are still able to bind with pRb but lack the helicase activity of the C-terminus that is necessary for viral DNA replication. The fact that truncations of LT in MCPyV positive MCCs all appear downstream of the LXCXE motif, with upstream functions preserved, suggest that the N-terminal domains are essential in the transformation of healthy tissue into a neoplastic state. Direct comparisons of MCPyV LT, 57 kT and tLT identified that tLT is more effective at promoting growth of human and mouse fibroblasts (Cheng et al., 2013). Biochemical analysis has also found that while neither tLT nor LT are capable of binding p53 directly, the latter is able to reduce p53-dependent transcription in reporter assays (Borchert et al., 2014). Furthermore, tLT is expressed at a higher level than the full length equivalent, possessing a greater affinity for Rb binding.

Phosphorylation at Serine 816 of LT has also been shown to arrest cell growth and induce cellular apoptosis (Li et al., 2015). This could therefore provide further evidence to support the hypothesis that tLT is directly responsible for MCPyV-induced MCC, as truncated proteins lack the required phosphorylation site for induction of apoptosis.

In rare cases, tLT can also lose the NLS that spans amino acids 277-280 (Nakamura et al., 2010). This infers that the NLS is not necessarily required for the progression of disease. However the interaction with hVam6p is always preserved (Liu et al., 2011). LT interacts with and translocates hVam6p from the cytoplasm into the nucleus disrupting lysosomal clustering. Interestingly, in the case of tLT that lack the NLS, localisation to hVam6p still occurs, suggesting that translocation is not required in the early stages of the MCPyV lifecycle. As such, the hijacking of lysosomes may be implicated in endocytosis and virion egress, a process that is not associated with MCC.

1.9 Ion channels

Membrane proteins account for approximately 30% of the total proteome, 50% of which comprise ion channel subunits (Yu et al., 2005). Pore-forming ion channels are transmembrane proteins through which inorganic ions selectively pass down electrochemical gradients at rates faster than diffusion (10^{6-8} ions/second), that is independent of metabolic energy. Over 400 putative ion channels are now thought Membrane proteins account for approximately 30% of the total proteome, 50% of which comprise ion channel subunits (Yu et al., 2005). Pore-forming ion channels are transmembrane proteins through which inorganic ions selectively pass down electrochemical gradients at rates faster than diffusion (10^{6-8} ions/second), that is independent of metabolic energy. Over 400 putative ion channels are now thought to be expressed in mammals (O'Connell et al., 2002; Alberts et al., 2003; Bagal et al., 2013; Wu et al., 2016). Ion channels are present at membranes and intracellular organelles in nearly all animals, plants and bacterium, as ionic homeostasis is responsible for a wide array of physiological activities (PASSANO, 1963; Booth, 2003; Ward et al., 2009). The functionality of ion channels is well documented in excitable

cells where they shape action potentials through gating (activating) the flow of ions. However, channels also play a role in non-excitable cells where they regulate numerous basic cellular processes, including cell proliferation, differentiation and apoptosis (Prevarskaya et al., 2010; Bates, 2015).

Channels consist of a number of transmembrane and pore domain subunits that create a central pore and selectivity filter. They are categorised by the stimulus that gates them, the number of transmembrane domains (TMDs), or the specific ion it conducts. Examples of stimuli that activate channels and their mechanisms are highlighted in Figure 1.14. The selectivity filter is the most narrow point of the pore that selects which ions are conducted, with K^+ channels for example having 10,000-fold greater selectivity for K^+ ions that Na^{2+} ions due to the signature TVGTG selectivity filter sequence (Alberts et al., 2003). Cl^- channels comprise channels that may permit anion conductance (Jentsch et al., 2002).

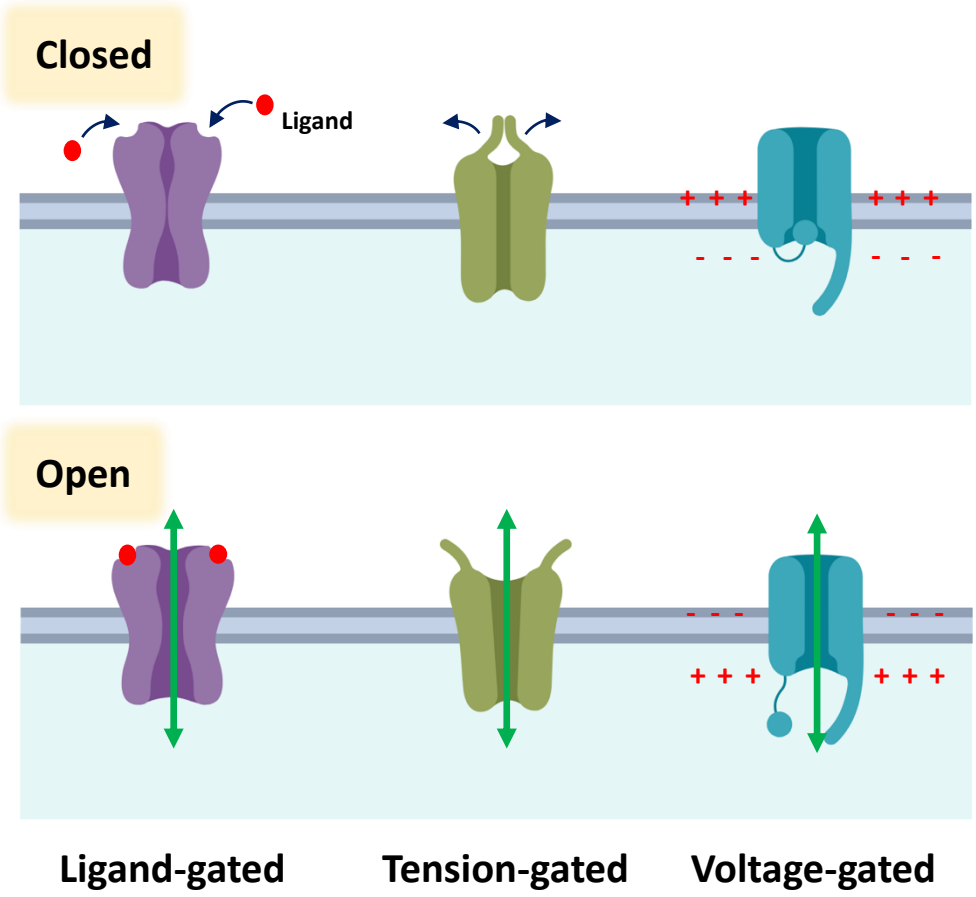

Figure 1.14: Schematic representation of ligand-, tension- and voltage-gated channel activation in response to stimuli. The interaction of a ligand with the ion channel it gates leads to opening of the channel and passage of ions. Tension-gated (or mechanosensitive) channels are activated in response to environmental changes such as increased tension or stretching of the cell. Voltage-gated channels are activated by changes in membrane potential to permit rapid ionic flow and cellular depolarisation. Red balls depict ligands interacting with ligand-gated ion channels to facilitate opening of the pore.

1.9.1 K^+ channels

K^+ ion channels are the most diverse class of membrane proteins expressed within the cell (Grizel et al., 2014). There are four classes of K^+ ion channel that are ubiquitously expressed across nearly all kingdoms of life: (1) voltage-gated (K_V) (six TMDs); (2) inwardly rectifying (K_{IR}) (two TMDs); (3) tandem pore domain (K_{2P}) (four TMDs) channels and (4) Ca^{2+}-activated K^+ channels (K_{Ca}) (6 TMDs) (Zhong et al., 2013; Kuang et al., 2015). K^+ channel classifications are summarised in Figure 1.15.

K^+ channels, with the exception of K_{2p} channels, are composed of four monomers that each contain one pore-forming domain (Kuang et al., 2015). The carbonyl oxygens of threonine residues in the selectivity sequence (TVGYG) provide oxygen layers to which four K^+ ions interact. The arrangement of oxygen around the ion mimics hydrated K^+, resulting in low transfer energy and near diffusion rate conduction. Interaction of K^+ ions within the filter stabilises the pore providing specificity for K^+ over other positively charged ions.

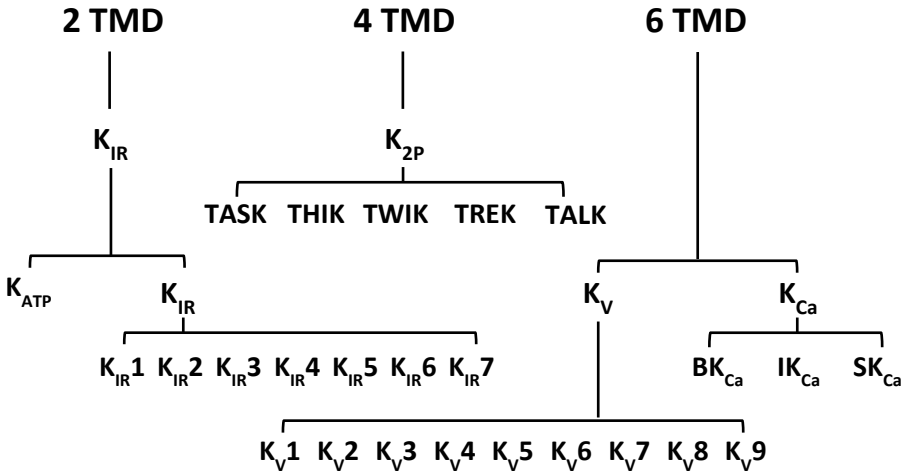

Figure 1.15: Classification of K^+ channels. Adapted from Zhong *et al.*, 2013.

1.9.1.1 K_V channels

K_V channels are gated by voltage sensors that respond to depolarisation of the cell to repolarise the membrane potential (O'Connell et al., 2002). When inactive, the pore is shielded by closing of the selectivity filter (C-type inactivation), closing of the intracellular entrance (S6 gated) or S6 gate blocking by the N-terminus (N-type inactivation) (Yellen, 2002). In excitable cells K_V channels repolarise the cell after action potential firing, in non-excitable cells K_V channels mediate an array of cellular functions including cell volume regulation, acidification and apoptosis.

1.9.1.2 K_{IR} channels

K_{IR} channels in contrast to other channel types facilitate the movement of K^+ ions at membrane voltages negative to the K^+ equilibrium and therefore inwardly. This is achieved not through channel activity but channel blockage (Nichols and Lopatin, 1997). Within the cell Mg^{2+} ions and polyamines block K_{IR} pores in a voltage-dependent manner to restrict the leakage of K^+ ions out of the cell and promote inward conduction.

Kir channels are grouped into seven subfamilies that are classified into four functional groups: classical K_{IR} channels ($K_{IR}2.x$) which are constitutively active, G-protein K_{IR} channels ($K_{IR}3.x$) that are regulated by G-protein coupled receptors, ATP-sensitive channels ($K_{IR}6.x$) which are linked to cellular metabolism and K^+ transport channels ($K_{IR}1.x$, $K_{IR}4.x$, $K_{IR}5.x$ and $K_{IR}7.x$) (Hibino et al., 2010).

1.9.1.3 K_{2p} channels

K_{2p} channels are unique when compared to most K^+ channels as the transmembrane subunit contains two pore loops that structurally resemble two inward rectifier α subunits and form dimers in the membrane. Another unique feature is that they are not voltage-gated, instead responding to stimuli including pH, membrane stretch, polyunsaturated fatty acids and heat to slowly leak K^+ outwardly to regulate resting potential (Piechotta et al., 2011; Braun, 2012). An extracellular cap structure protrudes from TM1 helix and covers the pore to prevent vertical ion efflux and this restricts blockage of the channel with peptide toxins and some small molecule inhibitors.

1.9.1.4 K_{Ca} channels

K_{Ca} channels are activated by Ca^{2+}. Three K_{Ca} subfamilies exist that are divided on the concentration of Ca^{2+} required for activation termed large conductance (BK_{Ca}), intermediate conductance (IK_{Ca}) and small conductance (SK_{Ca}) (Guéguinou et al., 2014). BK_{Ca} channels are activated by membrane depolarisation, whilst IK_{Ca} and SK_{Ca} channels are activated by Ca^{2+} and are independent of voltage.

1.9.2 Ca^{2+} channels

Ca^{2+} channels are predominantly voltage-gated and act as second messengers to a range of downstream signalling pathways associated with muscle contraction, gene transcription, hormone secretion, neurotransmitter release, cell cycle regulation, and apoptosis (Berridge et al., 1998; Tyson and Snutch, 2013).

The pore of voltage-gated Ca^{2+} channels is formed by an α_1 subunit of which 10 isoforms are expressed in the mammalian genome (Dolphin, 2016). Long-lasting (L-type, $Ca_V1.1$-1.4, high-voltage activated) and transient (T-type, Ca_V3, low voltage activated) are widely distributed, whilst purkinje, neural and residual (P/Q-, N- and R-type channels, respectively, $Ca_V2.1$-2.3) are located in the brain and nervous system.

Ligand-gated Ca^{2+} channels include IP_3 receptor channels, ryanodine receptor channels and the NAADP-activated two-pore channels (TPCs) (Zhu et al., 2010).

1.9.3 Na^+ channels

Na^+ channels are associated with the propagation of action potentials in excitable cells, and in non-excitable cells regulate proliferation, migration, differentiation, phagocytosis and endosomal acidification (Catterall, 2000; Roger et al., 2015). Following depolarisation, Na^+ channels are inactivated in milliseconds to ensure unidirectional propagation of action potentials. To date nine functional Na_V isoforms have been identified. However as the channels have similar activities and high degree of amino acid conservation between α subunits there has been difficulty in distinguishing individual function (Catterall, 2000; Yu and Catterall, 2003). Treatment with tetrodotoxin (TTX) and saxitoxin (STX) has revealed differences between some isoforms, with single amino-acid variation in the pore region conferring differential resistance to inhibition (Satin et al., 1992; Sivilotti et al., 1997). The principal cardiac isoform $Na_V1.5$ is 200-fold less sensitive to TTX following mutagenesis of a Phe residue is to Cys. The corresponding residue in $Na_V1.8$ and $Na_V1.9$ is Ser and these isoforms display even greater resistance to TTX treatment.

1.9.4 Cl^- channels

Cl^- channels are a poorly understood family of ion channels that transport anions in a process that is less specific than cation channels. As such these, channels transport a range of ions including Cl^-, HCO_3^-, I^-, and NO_3^-; and have roles in the excitation of excitable cells, cell volume regulation, cell motility, the acidification of endosomes, cell cycle regulation and apoptosis (Anon, 2009; Stakaityte et al., 2018). Cl^- channels are grouped into: Cl^- intracellular-channels (CLIC), cystic fibrosis transmembrane conductance regulator (CFTR), cAMP-, Ca^{2+}-, stretch-, swelling-, and voltage-activated channels (Baumgarten et al., 2005; Suzuki et al., 2006). The structure of Cl^- channel types varies as they may possess between 1 and 12 transmembrane segments.

1.10 Endosomal ion channels

The endo/lysosomal network consists of a series of intracellular organelles that dynamically interconvert as cargo is trafficked into and out of the cell (Hu et al., 2015). There is a long-standing acceptance that the acidification of maturing endosomes and lysosomes is due to the flux of H^+, which whilst true, only reflects a part of the dynamic ionic flux that regulates pH within these compartments. There is an emerging field that identifies ions including K^+, Na^+, Ca^{2+}, and Cl^- in altering pH across the endo/lysosomal network that are summarised in Figure 1.16.

Vacuolar-type H^+-ATPase (V-ATPase) activity is essential for proton translocation into endosomes, however this action alone would quickly lead to self-limiting electrochemical gradients preventing further acidification. To bypass this issue significant flux in the concentration of various ions (summarised in Figure 1.16B) create an environment whereby the H^+ equilibrium is shifted to permit further translocation and lowering of intracompartmental pH (Hara-Chikuma et al., 2005; Steinberg et al., 2010; Scott and Gruenberg, 2011).

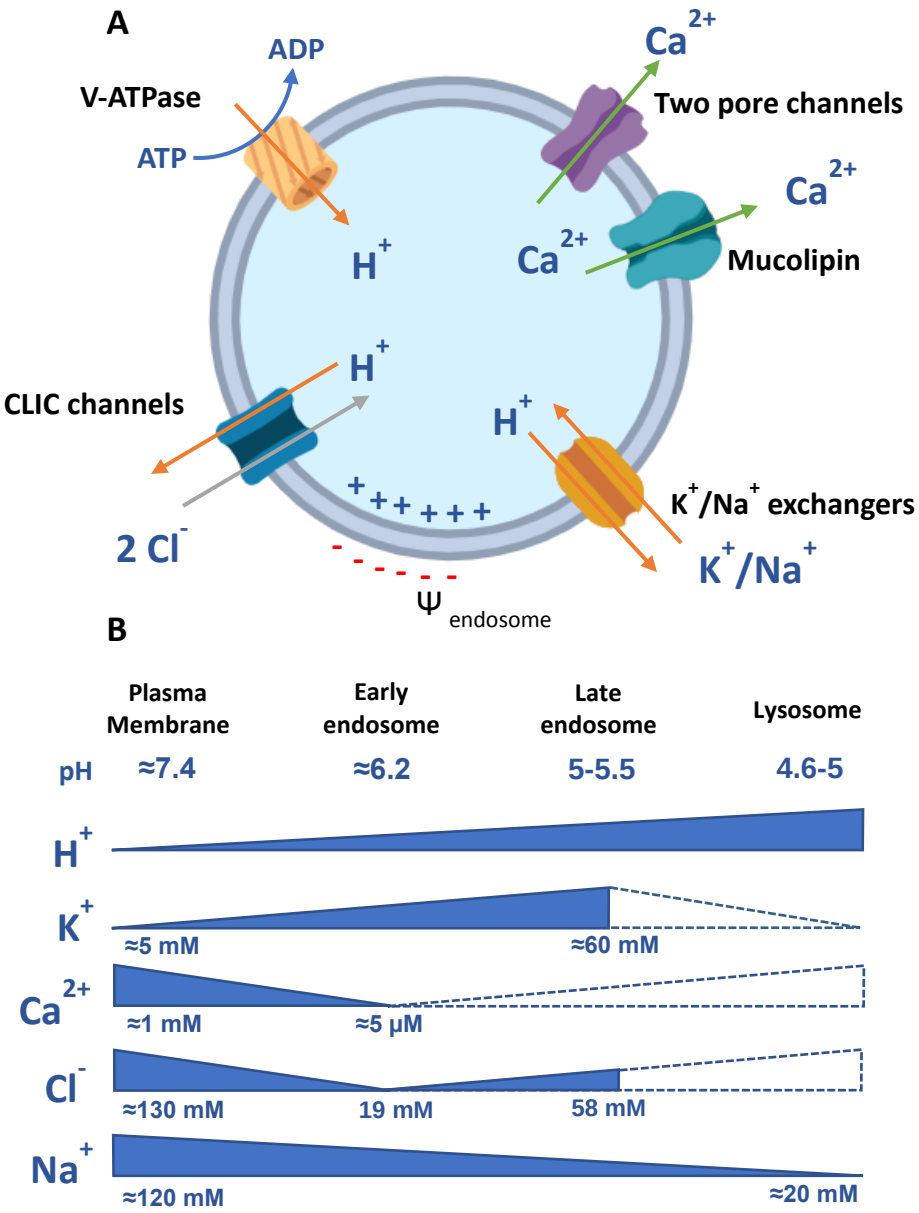

Figure 1.16: Schematic representation of ionic flux in vesicles trafficking through the endo/lysosomal network. (A) Representation of endo/lysosomal channels that regulate a range of functions including pH. (B) Representation of ionic concentration and pH across early endosomes, late endosomes and lysosomes. Solid colour represents known changes whilst dashed lines represent hypothesised flux. Adapted from Scott and Gruenberg, 2011.

Endosomal Ca^{2+} flux is mediated by mucolipins and TPCs. There are three mucolipins (TRPML1, TRPML2 and TRPML3) which are members of the transient receptor potential (TRP) superfamily and are primarily located to late endosomes and lysosomes (Cheng et al., 2010). The role of TRPMLs is poorly understood, however they are believed to leak Ca^{2+} to prevent lysosomes from becoming too acidic and regulate trafficking and fusion. More recently TPC1 and TPC2 have been identified to have endo/lysosomal functionality (Wang et al., 2012; Cang et al., 2013; Cang et al., 2014). The role of TPCs in acidification is somewhat controversial and unclear, however activity in response to the second messenger nicotinic acid adenine dinucleotide phosphate (NAADP) is required for fusion to membranes including the ER and release of Ca^{2+} from endo/lysosomal stores (Galione et al., 2009; Sakurai et al., 2015; Grimm et al., 2017).

Endo/lysosomal membranes also contain a range of proton exchangers with CLICs, Na^+-proton exchangers (NPEs) and K^+-proton exchangers (KPEs) all able to shift equilibrium and regulate pH by transporting Cl^-, Na^+, and K^+ into endosomes at the expense of H^+, respectively (Scott and Gruenberg, 2011).

1.11 Ion channels and disease

Given that ion channels are ubiquitously expressed across all cells and are involved in a range of developmental and cellular functions, their association with human disease, termed channelopathies is unsurprising (Kasianowicz, 2012).

The dysregulation of ion channels, the activity of which are essential for correct neuronal signalling, have been linked with a range of neurological disorders including Alzheimer's, Parkinson's, epilepsy and neuropathic pain (Lemoine et al., 2012).

Channelopathies are not restricted to excitable cells, with cystic fibrosis a well-studied example. The single amino acid ΔF508 deletion in the chloride-sensitive CFTR channel prevents channel folding, impairing transepithelial transport and mucus fluidity, that in turn leads to chronic mucus obstruction, neutrophilic inflammation and respiratory infection (Mall and Hartl, 2014). Hypoglycaemia in infants due to the improper trafficking of ATP-sensitive K^+-selective channel, and hypertension due to

abnormal Na^+ channel turnover are just two further examples (Eaton et al., 2006; Martin et al., 2013).

Due to their association with a wide range of diseases, drugs that modulate channels have been well documented in therapeutic treatment. L-type Ca^{2+} channel inhibitors, including verapamil and nifedipine were clinically approved for the treatment of hypertension in the late 1970s/early 1980s (Bagal et al., 2013). Further examples are the Na^+ channel inhibitors lidocaine, which is used as a local anaesthetic since 1949, and phenytoin and retigabine in the treatment of epilepsy since 1953 and 2011, respectively. More recently conotoxins, which are small peptide channel inhibitors produced by cone snails, have been identified as potential therapeutics in the treatment of a several conditions including chronic pain, stroke, schizophrenia, epilepsy, and neuromuscular disorders (Layer and McIntosh, 2006). Ziconotide is a clinically available example of a synthetically produced conotoxin that has analgesic properties through selective targeting of N-type Ca^{2+} channels in the spinal cord to interrupt pain signalling (McGivern, 2007).

1.12 Ion channel manipulation by viruses

Given the vast array of cellular processes that are regulated by ion channels, it is unsurprising that viruses manipulate and/or mimic channel function to favour their replicative cycle.

1.12.1 Viroporins

Viroporins are small (<120 residue) hydrophobic proteins that adopt transmembrane oligomeric structures, mimicking the functions of ion channels to regulate ionic homeostasis and manipulate pathways relating to autophagy, trafficking, inflammation, transformation, cell survival, and virus assembly and release (Royle et al., 2015). Viroporins are encoded by a wide range of viruses that typically contain RNA genomes including poliovirus (2B), HCV (p7), human immunodeficiency virus 1 (HIV-1) (Vpu) and Influenza A virus (M2); whilst in humans the dsDNA viruses BKPyV and JCPyV encode agnoproteins, whilst HPV-16 encodes E5 (Scott and Griffin, 2015). The role of PyV agnoproteins has previously been described (The production of the late transcript that codes for the structural ‘VPs’ and any auxiliary proteins begins

following initiation of DNA replication (Cubitt, 2006). Following translation, the structural proteins traffic into the nucleus due to the NLS region of the VPs which is also purported to be essential during initial infection. The ability of VPs to translocate across the nuclear membrane does however vary between species and ultimately is dependent upon the presence of an NLS. All SV40 VPs contain an NLS and are therefore able to shuttle into the nucleus independently (Ishii *et al.*, 1994). Mutational analysis further showed that mutation to the NLS of VP1 or VP2/3 did not perturb nuclear localisation when co-expressed, indicating that pentamer and minor capsid interaction occurs within the cytoplasm prior to nuclear import. JCPyV VP1 does not contain an NLS and therefore requires an interaction with VP2/3 to enter the nucleus and in contrast MuPyV VP2/3 requires the NLS-containing VP1 (Forstová *et al.*, 1993; Shishido-Hara *et al.*, 2000).

VP1 pentamers that make up the capsid share almost identical conformations, with C-terminal alteration in the 'arms' that reach out and insert into the cores of neighbouring pentamers to stabilise the capsid (Liddington *et al.*, 1991; Stehle and Harrison, 1997). In the case of BKPyV, interpentameric interactions are further stabilised through incorporation of Ca2+ ions which facilitate correct assembly (Li *et al.*, 2003).

The minor capsids proteins VP2 and VP3 (if expressed) share a common C-terminus, whilst a longer N-terminus of VP2 gives rise to a difference in size between the proteins. One minor capsid protein binds to the axial cavity of each VP1 pentamer through a common C-terminus hydrophobic interaction (Chen et al., 1998). The minor capsid proteins also contain a DNA binding domain which links the viral minichromosome to the capsid. The additional N-terminal region of VP2 contains a myristoylation site which, when mutated, reduces the efficiency of infection (Krauzewicz et *al.,* 1990).

Late auxiliary proteins).

1.12.2 Viral persistence

In addition to its viroporin p7, HCV non-structural protein 5A (NS5A) inhibits liver expressed $K_V2.1$. Channel inhibition enhances viral persistence and survival by

preventing reactive oxygen-species-mediated p38 phosphorylation of $K_V2.1$ at Ser800, that would reduce intracellular K^+ to trigger caspase-mediated apoptosis (Mankouri et al., 2009; Norris et al., 2012). The flux of anions facilitated by CLIC channels (CLIC-1, CLIC-5 and CLIC-7) are essential for HCV lifecycle progression, with inhibition or genetic depletion of these channels leading to loss of viral replication (Igloi et al., 2015).

HIV-1 negative regulatory factor (Nef) and the surface subunit of the envelope protein gp120 have been shown to affect K^+ channel activity to regulate virion release (Choi et al., 2008; Herrmann et al., 2010). Gp120 interacts with the K_V channel brain-specific ether-a-go-go-like channel 1 (BEC1) to repress its activity and inhibit virion release. In contrast, Nef indirectly modulates K^+ channel activity to enhance replication and cell death in a manner that may compensate for the regulatory roles of other viral proteins including gp120.

MCPyV-positive MCC is known to be highly metastatic due to ST-mediated migratory phenotypes. ST enhances the expression of CLIC1 and CLIC4 to promote anion flux, with depletion of the channels resulting in reduced motility and invasiveness of ST expressing cells (Stakaityte et al., 2018).

1.12.3 Viral trafficking

The entry stages of the Filoviruses Ebola virus (EBOV) and Marburg virus require Ca^{2+} channel activity (Gehring et al., 2014; Hover et al., 2017). During EBOV entry, virus-containing endosomes fuse with the ER and the inhibition of TPC1 and TPC2 is sufficient to prevent docking and virion release from the endosomal network (Sakurai et al., 2015). This study identified that the Ca^{2+} channel inhibitors verapamil and tetrandrine restricted the ability of EBOV to traffic through the endosomal network. RNAi-mediated knock-out of TPC1 and TPC2 showed that these channels were required to facilitate docking of endosomes to the ER and by blocking this process entry could not be achieved (Figure 1.17A).

Several members of the *Bunyaviridae* have been shown to require K_{2P} channel activity during trafficking through the endosomal network and it has further been shown that increased intra-endosomal K^+ concentrations are essential during

Bunyavirus (BUNV) entry (Figure 1.17B) (Hover et al., 2016; Hover et al., 2018). HIV requires K_{IR} channels, in particular G-protein-regulated channels, ATP-sensitive-channels (K_{ATP+}), and $K_{IR}1.1$ inhibition was shown to restrict entry and to inhibit virus production and release (Dubey et al., 2019). In both cases, results indicated that membrane depolarisation was required to favour viral lifecycle progression.

Entry of herpes simplex virus 1 (HSV1) can be inhibited through Cl^- channel blockage (Zheng et al., 2014). Manipulation of anion homeostasis has also been implicated in the non-lytic release of BKPyV (Evans et al., 2015). Treatment with the anion exchange inhibitor DIDS led to accumulation of virions within LAMP-1 positive lysosomes, suggesting that that virion release requires anion flux.

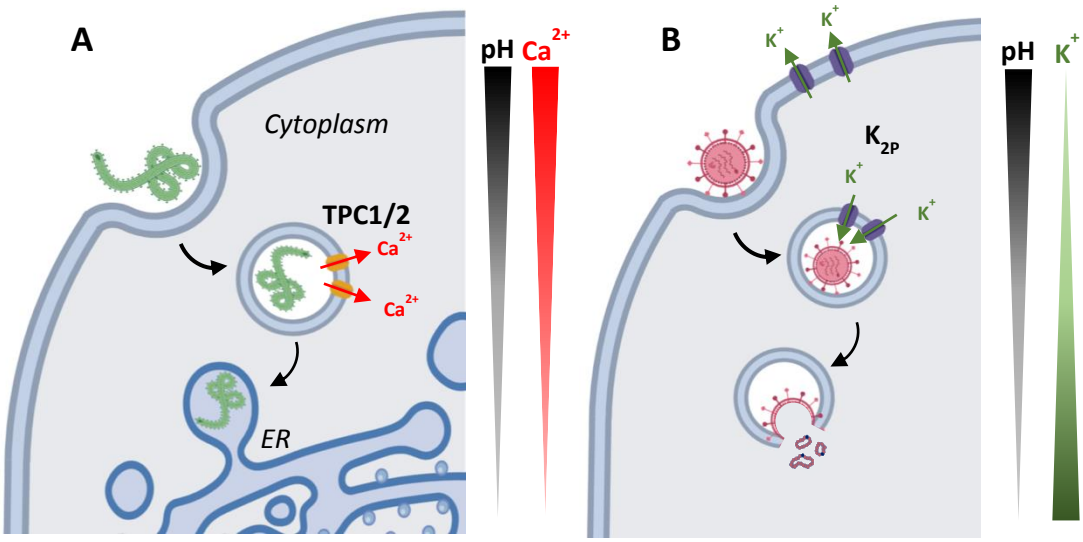

Figure 1.17: Predicted entry mechanisms of EBOV (A) and BUNV (B). (A) Following entry via macropinocytosis, EBOV traffics through the endosomal network. Within late endosomes NAADP-mediated activation of TPC1 and TPC2 releases Ca^{2+} to facilitate fusion with the ER. (B) Following entry, BUNV traffics through the endosomal network where increasing acidity and K^+ concentration cause structural changes in the viral glycoproteins to facilitate release of ribonucleoproteins. Adapted from Hover *et al.*, 2017.

1.13 Mitogen-activated protein kinases

The mitogen-activated protein kinases (MAPKs) are a highly conserved class of serine/threonine protein kinases that form a complex signalling network in all eukaryotic cells (Figure 1.18). Extracellular stimuli that activate MAPKs may include UV exposure, growth factors, proinflammatory cytokines, osmotic shock and heat shock, which ultimately regulate cellular functions including cell differentiation, movement, proliferation and death (Schaeffer and Weber, 1999).

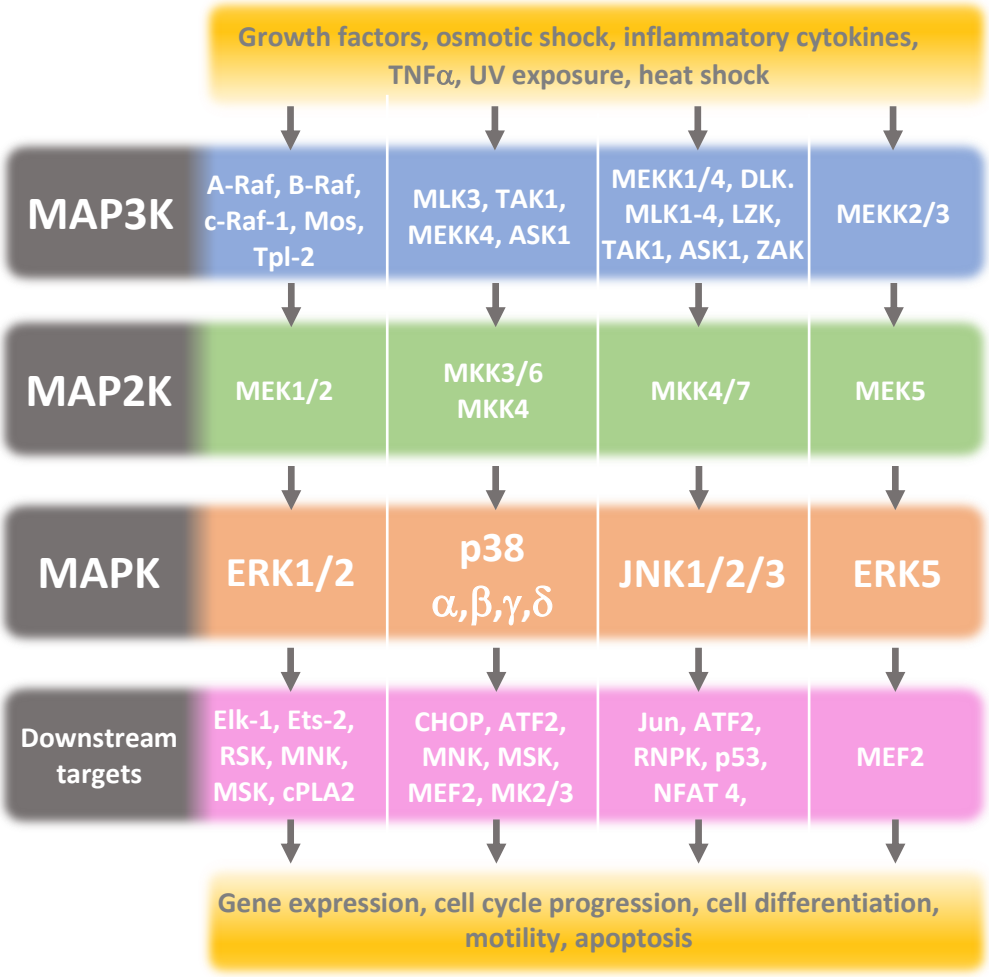

Figure 1.18: Overview of the four MAPK signalling cascades: ERK1/2, p38, JNK and ERK5. A range of stimuli activate MAP3Ks which in turn activate their MAPK cascade. A range of phenotypic outcomes may result, dependent upon the pathways that are activated.

The canonical activity of MAPKs relies upon a three-tiered cascade whereby the downstream kinase serves as a substrate for the upstream activator, with MAPK kinase kinase (MAP3K, MEKK) phosphorylation and activation of a MAPK kinase (MKK, MEK, MAP2K) which in turn phosphorylates and activates the MAPK, with each step amplifying the signal. The active MAPK is then able to translocate into the nucleus to phosphorylate and modify the activity of downstream targets which may include kinases, transcription factors, cytoplasmic enzymes, phospholipids and structural proteins (Chang and Karin, 2001; Yang et al., 2003; Yoon and Seger, 2006).

MAPK signalling is not a straight forward cascade, with several MAP3Ks able to phosphorylate each of the MKKs which may engage in cross-talk to activate more than one MAPK (Chang and Karin, 2001). Scaffold proteins and distinct docking interactions ensure that signal specificity is maintained and downstream cellular responses are regulated (Whitmarsh and Davis, 1998; Van Drogen and Peter, 2002; Tanoue and Nishida, 2003; Morrison and Davis, 2003; Raman et al., 2007).

There are four distinct MAPK pathways within mammalian cells: extracellular signal-regulated kinases (ERK) 1/2, c-Jun NH_2-terminal kinases (JNK) 1/2/3, p38 and ERK5 which is also termed big MAPK-1 (BMK1). Activation of these kinases requires phosphorylation of threonine and tyrosine residues in the activation loop T-X-Y motif, where X represents a glutamic acid in ERKs, a proline in JNKs and a glycine in p38 (Widmann et al., 1999). Dual phosphorylation of the activation loop leads to conformational reorganisation to relieve steric hinderance of the active site and permit substrate interactions.

1.13.1 p38 MAPK

The p38 MAPK pathway is predominantly associated with response to stress, however it can also have roles in immune response, survival, differentiation and invasion and metastasis (Cuadrado and Nebreda, 2010; Barrantes and Nebreda, 2012). p38 (p38α, MAPK14) was named following its identification as a 38 kDa protein and subsequent studies have identified three additional genes that express isoforms with approximately 60% identical amino acid sequence, termed p38β (MAPK11), p38γ (MAPK12, stress-activated protein kinase (SAPK) 3, ERK6) and p38δ

(MAPK12, SAPK4) (Mertens et al., 1996; Jiang et al., 1996; Goedert et al., 1997). An overview of the p38 pathway is described in Figure 1.19.

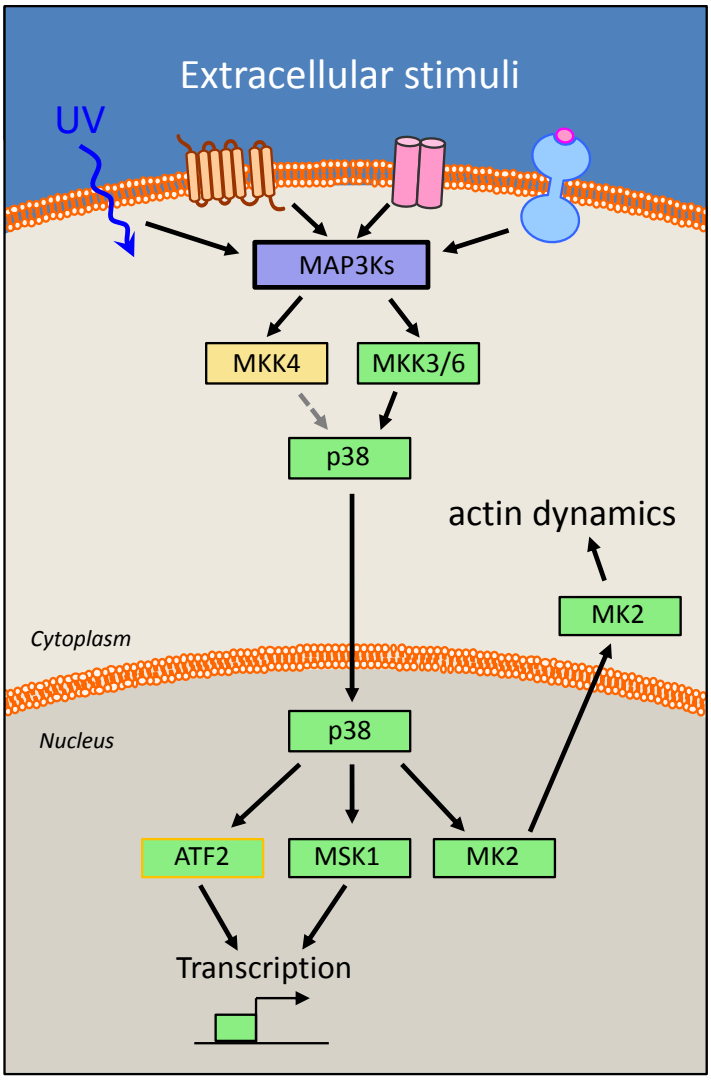

Figure 1.19: Overview of the p38 MAPK pathway. In response to stimuli MAP3Ks are phosphorylated and activated, which in turn phosphorylate and activate MAP2Ks, with either canonical p38 signalling via MKK3/6 or non-canonical signalling via MKK4, phosphorylating and activating p38. p38 then translocates into the nucleus where it phosphorylates and activates a range of targets. For simplicity only the transcription factors ATF2 and MSK1, alongside the kinase MK2 are shown. Following activation, MK2 translocates into the cytoplasm where it can regulate a range of activities including HSP27-mediated actin remodelling and mRNA stabilisation.

p38α is ubiquitously and highly expressed in most cell types, whereas other isoforms are expressed in a tissue specific manner: p38β in the brain, p38γ in skeletal muscle and p38δ in endocrine glands (Cuadrado and Nebreda, 2010). Whilst MAPKs generally have overlapping functionality and targets, there are examples whereby an individual p38 isoform is more efficient in activating a downstream target, such as p38α activation of MAPK activated protein kinase 2 (MK2, MAPKAPK2) (Sudo et al., 2005).

The p38 pathway may be activated by a wide range of environmental stimuli including oxidative stress, inflammatory cytokines, UV irradiation, hypoxia, ischemia, interleukin 1 (IL-1) and tumour necrosis factor α (TNFα) (Cargnello and Roux, 2011). Recruitment of TNF receptor associated factors (TRAFs) by TNFα and IL-1 stimulate MAP3K to activate p38 isoforms. G-protein coupled receptors (GPCRs) and the Rho GTPase family members Rac and cdc42 may also activate p38-related pathways (Bagrodia et al., 1995; Goldsmith and Dhanasekaran, 2007). These stimuli may activate a plethora of MAP3Ks, including MEKK1-3, MLK2/3, ASK1, Tpl2, TAK1 and TAO1/2 (Cuadrado and Nebreda, 2010). It is often the case that stimuli that activate p38 will have a similar effect upon the JNK pathway.

There are three MKKs that are capable of activating the p38 pathway. MKK3 and MKK6 are the canonical and highly specific activators of p38 isoforms, with the former able to activate all four isoforms and the latter able to activate all but p38β; additionally JNK-associated MKK4 can also phosphorylate p38α (Doza et al., 1995; Enslen et al., 1998; Alonso et al., 2000; Brancho et al., 2003).

p38 effects a plethora of proteins localised both in the cytoplasm and the nucleus. In the cytoplasm p38 may phosphorylate cPLA2, MNK1/2 MK2/3, HuR, Bax and Tau, whilst in the nucleus phosphorylation of ATF1/2/6, MEF2, Elk-1, GADD153, Ets1 and MSK1/2 may occur giving rise to a range of different cell fates and phenotypic alterations (Cuadrado and Nebreda, 2010).

1.13.2 p38-association with metastasis

Metastasis is the general term used to summarise the multistage spread of a primary tumour to other tissues and is estimated to be responsible for 90% of all cancer-

associated deaths (Norman, 1952). Mechanistically metastasis is poorly understood, however the process can be defined by several discrete steps: the loss of cell adhesion, gain of cellular motility and invasion of localised tissue which are summarised as epithelial-mesenchymal transition (EMT), degradation of the extracellular matrix (ECM) and entrance into the vascular and lymphatic systems, survival during circulation and colonisation of distant secondary sites (Lambert et al., 2017; Chitty et al., 2018). Following colonisation tumour cells often undergo metastatic latency, where the cells become dormant for a period of months or years, facilitating immune evasion prior to resumed proliferation via unknown mechanisms (Malladi et al., 2016; Pollard, 2016).

It is proposed that tumour cells interact with the surrounding environment, immune cells and secreted signalling molecules including transforming growth factor β (TGFβ), vascular endothelial growth factor (VEGF), TNFα and cytokines such as IL-6 to promote several processes associated with the metastatic cascade (Joyce and Pollard, 2009). Given that the p38 MAPK pathways respond to such stimuli, it is plausible that p38 activity may contribute to metastatic processes.

1.13.3 EMT

The ability of a cell to undergo EMT relies upon the upregulation of a range of different genes, most notably Snail, Slug, Twist and Zeb1 which repress E-cadherin (Thiery, 2002; Kalluri and Weinberg, 2009; Nieto et al., 2016). p38-mediated phosphorylation of Twist at Ser68 stabilises the protein and enhances its ability to induce EMT and invasiveness, whilst p38 activation has also been linked with Snail expression (Hipp et al., 2010; Hong et al., 2011). TGFβ and epidermal growth factor (EGF) mediated activation of p38 led to metastatic progression of breast cancer cells, with the former enhancing lung metastasis (Parvani et al., 2011). p38α can activate hypoxia-inducible factor 1α (HIF-1α) through stabilisation of the α-subunit to promote growth factors and cytokines such as VEGF and TGFβ, in addition to EMT-associated transcription factors Snail and Twist (Emerling et al., 2005; López-Nouoa and Nieto, 2009). Inhibition or RNAi depletion of p38 in head and neck squamous cell carcinoma (HNSCC) led to upregulation of E-cadherin and decreased Snail

transcripts, further highlighting the role of p38 in promoting EMT markers (Lin et al., 2016)

Whilst most evidence supports the role of p38 in EMT it is however not absolute, with evidence that p38α activation may promote E-cadherin expression and suppress TGFβ-activated kinase 1 (TAK1, MAP3K7) phosphorylation restricting EMT in human peritoneal mesothelial cells. This suggests that p38 may have a cell type specific effect upon progression (Strippoli et al., 2010).

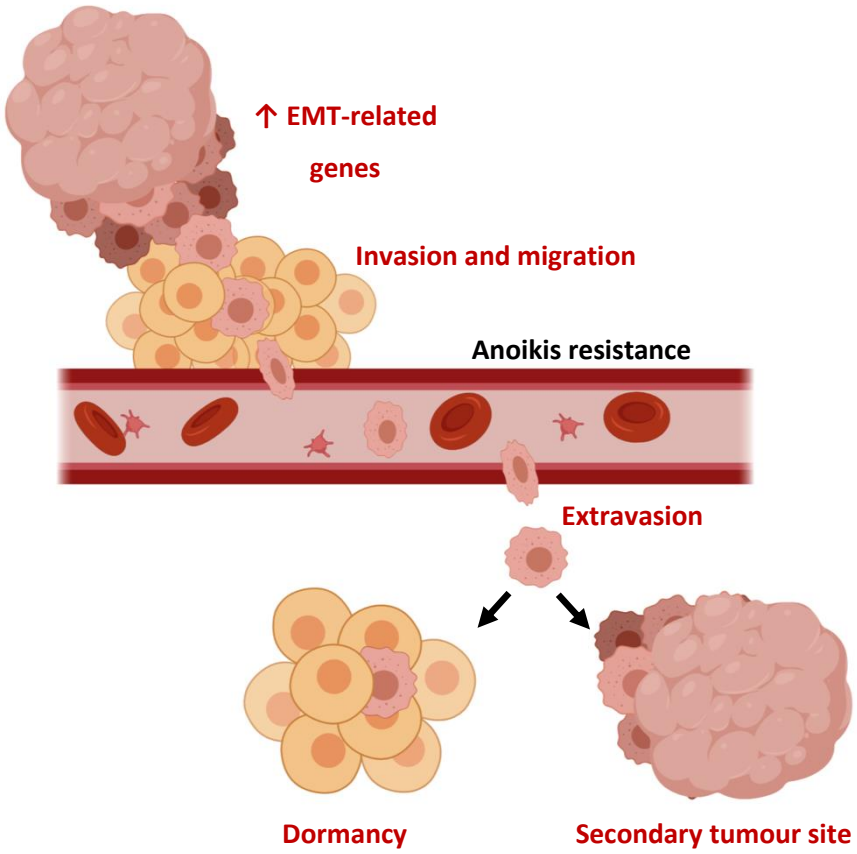

Figure 1.20: Reported roles of p38 in metastasis. p38 activity leads to the upregulation and stabilisation of several proteins that are associated with EMT, which facilitate invasion and migration. p38 is inhibited during circulation to avoid anoikis, before activation to promote extravasation. Dormancy and progression of secondary tumours have both been associated with p38 activity. Stages that require activated p38 are highlighted in red, whilst stages requiring inactivation of p38 are in black. Adapted from del Barco Barrantes and Nebreda, 2012.

1.13.4 Enhanced migration and invasion

The ability of a cancerous cell to migrate and invade distant tissues requires remodelling of the cytoskeleton and secretion of proteins to degrade the ECM.

The dynamic and rapid polymerisation of globular monomeric actin (G-actin) into a filamentous form (F-actin) initiates morphological changes within the cell, priming it for migration (Figure 1.21) (Gardel et al., 2010). Subsequent actin filaments can then form into lamellipodia, filopodia or stress fibres dependent on the presence of actin-associated proteins which either enhance or perturb filament bundling (Yamaguchi and Condeelis, 2007; Mattila and Lappalainen, 2008). Lamellipodia spread over a large area in a quasi-two-dimensional actin mesh, whilst filopodia contain bundled filaments that form antennae-like protrusions from the lamellipodia that push forward the leading edge of the cell. In a motile cell, filaments may bundle together to form stress fibres that become polarised towards the leading edge, with retrograde recycling of trailing edge actin to drive migration (Snider and Omary, 2014). Activated p38α phosphorylates MK2 which in turn phosphorylates HSP27, initiating loss of F-actin cap binding and polymerisation of filaments (Laferrière et al., 2001; Xu et al., 2006). p38 also activates LIM domain kinase 1 (LIMK1), which in turn phosphorylates cofilin to initiate actin polymerisation at the leading edge and supports contractility through depolymerisation and recycling of F-actin at the trailing edge (Kobayashi et al., 2006; Bravo-Cordero et al., 2013).

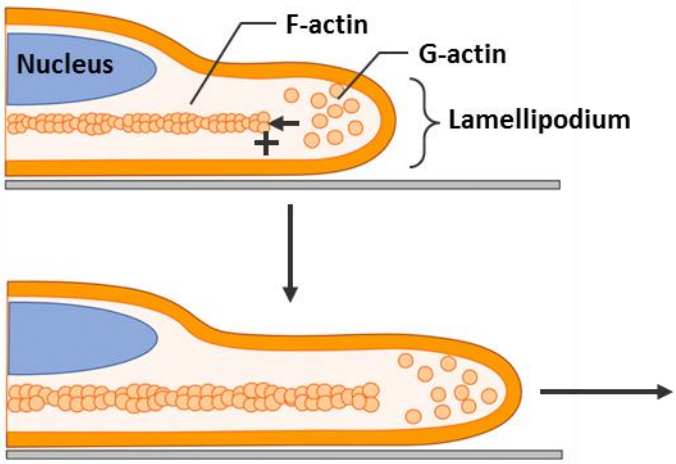

Figure 1.21: Schematic representation of actin rearrangements to drive cellular motility. G-actin is polymerised to form F-actin and drive morphological changes in the actin cytoskeleton. Actin filaments move the leading edge of the cell forward through formation of lamellipodium, filopodium and stress fibres.

The ability of tumour cells to degrade the ECM and invade secondary sites is also essential for metastasis. These processes are mediated by secretion of matrix metalloproteinases (MMPs), for example ADAMs (Deryugina and Quigley, 2006; Mochizuki and Okada, 2007). P38α activity is essential for expression of MMP1, MMP2, MMP9 and MMP13 in a range of cancers including bladder, breast, liver, skin keratinocytes and prostate to promote tumorigenesis (Johansson et al., 2000; Xu et al., 2006; Hsieh et al., 2010; Kumar et al., 2010; Park et al., 2011). Expression of MMP1 and MMP13 in HNSCC progression is regulated by p38δ; and p38γ is required in cooperation with c-Jun to facilitate K-Ras mediated MMP9 expression and breast cancer metastasis (Junttila et al., 2007; Meng et al., 2011).

1.13.5 Viral manipulation of p38 MAPK

MAPKs are responsible for altering a wide range of cellular processes and it is therefore unsurprising that a wide range of viruses manipulate these signalling cascades to promote several aspects of the viral lifecycle. HCV non-structural protein 3 (NS3) enhances hepatocellular carcinoma invasion through an ERK/p38/NF-κB signalling cascade leading to increased expression of MMP9 and cyclooxygenase-2 (Figure 1.22A) (Lu et al., 2015). Encephalomyocarditis virus (ECMV) activates p38 to

enhance translation of viral RNAs, HSV1-mediated inhibition of the innate immune central adaptor stimulator of interferon genes (STING) requires ubiquitin specific peptidase 21 (USP21) phosphorylation by p38 (Figure 1.22B), and Reovirus activates p38 via Ras to dictate host cell permissiveness (Figure 1.22C) (Hirasawa et al., 2003; Norman et al., 2004; Chen et al., 2017). Swine influenza virus activates p38 to enhance inflammation, with mouse model data indicating that inhibition of p38 is sufficient to restrict inflammatory responses and acute lung injury (Wei et al., 2014).

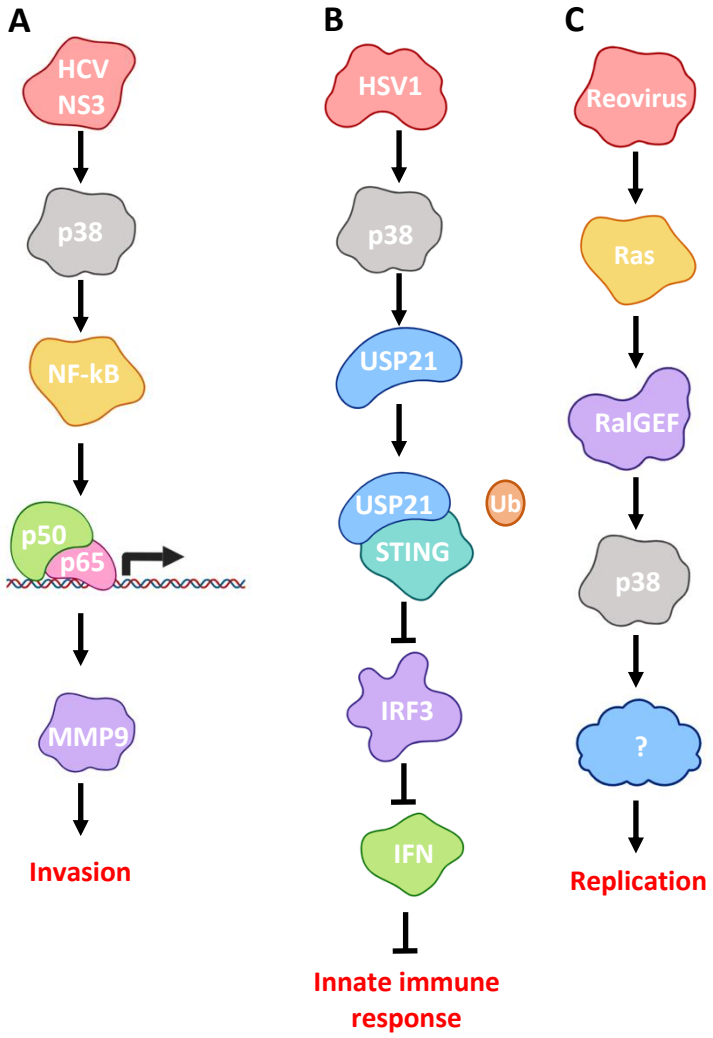

Figure 1.22: Schematic representation of p38 pathway activation by HCV NS3 (A), HSV-1 (B) and reovirus (C). (A) HCV NS3 activates NF-κB via p38 resulting in expression of MPP9 which contributes to invasion. (B) HSV1 activates USP21 via p38. USP21 interacts with and deubiquitinates STING preventing IRF3-mediated IFN expression and subsequent activation of the innate immune system. (C) Reovirus activates Ras which activates the guanine nucleotide-exchange factors (GEFs) for the small G protein Ral (RalGEFs) which in turn activate p38. p38 activity facilitates reovirus replication most likely through another protein intermediate.

1.14 Thesis aims

This thesis describes investigation into two different aspects of the polyomavirus lifecycle, with a focus upon MCPyV.

Following internalisation, trafficking events during PyV entry are poorly defined. Although pseudovirus assays have previously been described, they have seldom been used to study trafficking events, which is in part due to laborious and difficult detection that is synonymous with studying early PyV events (Buck and Thompson, 2007; Schowalter et al., 2012; Gee et al., 2013). We therefore considered novel approaches to quantification using GFP reporter vectors coupled with Incucyte imaging and analysis. SV40, which structurally differs from MCPyV in that two minor viral capsid proteins can be incorporated into the capsid compared with the VP3-less MCPyV, is the most studied of the PyVs. As such, infection studies using SV40 are well documented, but similar to MCPyV end-point analysis has been somewhat restrictive to deciphering early events. Chapter 3 describes the optimisation of MCPyV pseudovirus (PsV) production using reporter vectors and how they can be coupled with automated fluorescence detection and fluorescence microscopy to study trafficking events. A novel, rapid method for the quantification of SV40 infected cells using immunofluorescent detection of SV40 LT coupled with automated Incucyte imaging and analysis is also described.

PyVs are known to traffic through the endosomal network to the ER, before release into the cytoplasm and transport to the nucleus (Kuksin and Norkin, 2012a; Kuksin and Norkin, 2012b; Becker et al., 2019). The requirement of acidification to initiate proteolytic rearrangements of the capsid whilst within endosomes is well established, however the mechanisms that are responsible for acidification had not been investigated. There is an emerging field that identifies the essential role of ion channels to translocate ions to facilitate continued compartment acidification (Scott and Gruenberg, 2011). Using a panel of ion channel inhibitors, the requirement of channel activity during entry of MCPyV and SV40 was therefore investigated using the systems of detection and quantification previously described, leading to identification that Ca^{2+} channel activity is required for efficient entry of both MCPyV and SV40. A novel requirement of T-type Ca^{2+} channels during MCPyV infection was

further characterised. Ion channel targeting is a long-established method in the treatment in a range of diseases and as such there are a wide array of clinically available drugs that may be utilised. By identifying conserved requirements between different polyomavirus species there is the potential that a common inhibitor may be found to treat a range of polyomavirus infection associated diseases.

MCPyV ST, like other PyV STs, is known to interact with cellular protein phosphatases, namely PP2A and PP4 (Kwun et al., 2015; Abdul-Sada et al., 2017). Despite this knowledge and the known link to of protein phosphatases with dephosphorylation, there had been little investigation as to whether kinases were important. It was therefore proposed that through the use of phospho-kinase arrays, cellular kinases that were differentially activated following the expression of ST could be identified and any interesting hits could be further investigated. Building upon previous publications from the Whitehouse laboratory that showed MCPyV ST induces the expression of ADAM10 and ADAM17, induces microtubule destabilisation and stimulates actin rearrangements to enhance filopodia formation via Rho-GTPase activity, particular focus was placed upon signalling pathways that could potentially dysregulate and enhance migratory phenotypes. Results show that the p38 MAPK pathway is activated by ST in a manner independent of extracellular stimuli to enhance migratory phenotypes. Inhibition of p38 using chemical inhibitors is shown to be sufficient to restrict ST-induced wound healing and MCPyV-positive MCC cell line migration during transwell assays. Aligned with previous results, it is identified that PP4C is essential for the phosphorylation and activation of p38 and therefore further highlights the essential nature of ST interactions with protein phosphatases to enhance oncogenic phenotypes.

In summary, these findings highlight the importance of ion channels and p38 signalling pathways in MCPyV infection and tumorigenesis. Importantly, they provide new avenues for potential drug targets to restrict MCC progression and the wide range of diseases associated with polyomavirus-induced diseases.

Chapter 2

Materials and Methods

2.1 Laboratory consumables

2.1.1 Chemicals and solvents

All chemicals and solvents were purchased from Sigma-Aldrich® Fischer Scientific® and Melford Laboratories Ltd. Unless otherwise stated. Where applicable reagents were sterilised using a 0.22 μm filter or by autoclaving (121 ^{o}C, 30 mins, 15 psi). Water for general laboratory experiments was deionised using an ELGA PURELAB ultra machine (ELGA). Water for DNA experiments was ultrapurified using a Milli-Q® water purification system (Merck). Nuclease-free water (New England Biolabs) was used for PCR and cloning.

2.1.2 Chemical inhibitors

The active p38α/β inhibitor SB202190, non-active structural analogue SB202474 and MEK1/2 (indirect ERK1/2) inhibitor U0126 were purchased from Cambridge Bioscience and resuspended in DMSO.

Inhibitors targeting ion channels and trafficking are summarised in Table 2.1 with abbreviations, solvent and manufacturers shown. The target of each inhibitor is also described.

Table 2.1: Ion channel inhibitors used during experiments.

Compound	Abbreviation	Solvent	Target	Additional inhibitory information
Verapamil hydrochloride	Ver	H_2O	Ca^{2+}	L- and T-type channels
Nifedipine	Nif	DMSO	Ca^{2+}	L-type channels
Nitrendipine	Nit	DMSO	Ca^{2+}	L-type channels
5-Nitro-2-(3-phenylpropylamino)benzoic Acid	NPPB	DMSO	Cl-	Broad spectrum
Tetraethyl ammonium	TEA	H_2O	K^+	Broad spectrum, K^+ ion mimic
4-aminopyridine	4AP	H_2O	K^+	Non-selective voltage gated (Kv) channels
Quinine hydrochloride dihydrate	Qn	H_2O	K^+	Non-specific channel inhibitor with unknown mechanism of action
Potassium chloride	KCl	H_2O	K^+	Imbalances ion gradients
Potassium sulphate	K_2SO_4	H_2O	K^+	Imbalances ion gradients
Procainamide hydrochloride	Pro	H_2O	Na^+	Broad spectrum – Class IA antiarrhythmic
Ammonium chloride	NH_4Cl	H_2O	Trafficking	Prevents endosomal acidification
2-[(4-Bromophenyl)methylene]-N-(2,6-dimethylphenyl)-hydrazinecarboxamide	EGA	DMSO	Trafficking	Clustering of acidified late endosomes and lysosomes
Barium chloride	$BaCl_2$	H_2O	K^+	K_{IR} channels
Ruthenium red	RR	H_2O	Ca^{2+}/K^+	K_{2P} channels
Margatoxin	Mgtx	H_2O	K^+	Specific $K_V1.3$ inhibitor
Mibefradil HCl	Mib	DMSO	Ca^{2+}	T-type channels
Flunarizine	Flun	DMSO	Ca^{2+}	T-type channels

2.1.3 Antibodies

Antibodies used in Western blotting and immunofluorescence microscopy are described in Table 2.2. The 2T2 hybridoma used to detect MCPyV LT/ST was a kind gift from Dr Christopher Buck (NIH, Bethesda, USA) and hybridoma medium was diluted as described. The (pAb)108 hybridoma used to detect SV40 LT/ST was a kind gift from Daniel DiMaio (Yale Cancer Centre, Connecticut, USA) and hybridoma medium was diluted as described. Purified MCPyV VP1 (clone 9B2) antibody was a kind gift from Patrick Moore and Yuan Chang (University of Pittsburgh, Pennsylvania, USA).

Species specific secondary HRP-conjugated antibodies for use in Western blotting were purchased from Cell Signaling Technologies (CST) (Rabbit, catalogue number 7074, used diluted 1:2,000) or Agilent (Mouse, catalogue number P044701-2, used diluted 1:5,000). Species specific secondary Alexa Fluor-conjugated antibodies for use in confocal microscopy were purchased from Life Technologies and used diluted 1:500.

Table 2.2: Primary antibodies used for Western blotting and immunofluorescence microscopy. Specific phosphorylation sites for each antibody are shown in brackets in the target column. Antibody dilutions are shown in brackets under the usage column. R and M denote the antibody species which are rabbit and mouse, respectively.

Target	Species	Usage	Company	Product code
Flag tag	R	WB (1:5,000)	Sigma	F7425
GAPDH	M	WB (1:10,000)	Abcam	8245
HA tag	R	WB (1:10,000)	Sigma	H9658
LAMP2	M	IF (1:50)	Santa Cruz	Sc-18822
MCPyV LT/ST	M	WB (1:5)	Gift	2T2
MK2	R	WB (1:1000)	CST	3042
P-ATF2 (T71)	R	WB (1:1000)	CST	5112
P-ERK (T202/Y204)	R	WB (1:2,000)	CST	4370
P-MK2 (S257)	R	WB (1:1000)	CST	3041
P-MKK3/6 (S189)/(S207)	R	WB (1:1000)	CST	12280
P-MKK4 (S257)	R	WB (1:1000)	CST	4514
P-MSK1 (T581)	R	WB (1:1000)	CST	9595
P-p38 (T180/Y182)	R	WB (1:1,000)	CST	4511
p38	R	WB (1:1,000)	CST	9212
SV40 LT/ST	M	IF (1:200)	Gift	(pAb)108
MCPyV VP1	M	WB (1:1,000)	Gift	9B2

2.1.4 Plasmids

pcDNA6 MCV sTco was a gift from Patrick Moore (Addgene plasmid # 40201 ; http://n2t.net/addgene:40201 ; RRID:Addgene_40201). pcsNUC, pwM, pwM2m and ph2m were kind gifts from Dr Christopher Buck. ST-eGFP was created by Dave Griffiths in the Whitehouse laboratory using cDNA extracted from an MCPyV-positive MCC tumour. pEGFP-C1 and pEGFP-N1 were available within the laboratory. The ST-eGFP mutants R7A, Δ100-103, R102A and F103A were produced by Hussein Abdul-Sada in the laboratory of Dr Andrew Macdonald, University of Leeds.

2.2 General methods

2.2.1 Nucleic acid concentration determination

The concentration of DNA and RNA samples was performed using a NanoDrop™ 2000 (Thermo Scientific™) by calculation of absorbance at 260 nm. The ratio of absorbance at 260 nm and 280 nm was used to confirm the purity of samples with a ratio of >1.8 and >2.0 deemed acceptable for DNA and RNA, respectively.

2.2.2 Significance value calculation

Significance values (p values) were calculated using GraphPad Prism 7 software. Analysis was performed using an unpaired parametric t test. P values are represented upon graphs using a star system (*), whereby *= ≤0.05, **= ≤0.005, ***= ≤0.0005 and ****= ≤0.00005.

2.2.3 Production of schematics

Schematics were produced using BioRender and Motifolio Biology Bundle in Microsoft PowerPoint.

2.3 Bacterial cell culture

2.3.1 Growth medium and agar plates

Premixed Luria Broth (Miller's LB Broth Base) was purchased from Invitrogen™ and used as recommended by dissolving 25 g/L in deionised water before autoclaving. LB as described was used for all antibiotics with the exception of zeocin, which due to inactivity at high salt concentration, required a low salt LB medium containing 10 g/L tryptone soya broth, 5 g/L yeast extract and 5 g/L NaCl. For the production of LB agar (LBA) plates, 3% (w/v) agar was added to the Luria Broth mix before autoclaving.

2.3.2 Transforming competent *E. coli* cells for DNA expression

Plasmids were transformed into DH5α competent *E. coli* for bulking of DNA stocks. 50 ng of plasmid or 5 µl of a ligation mixture was added to 50 µl of DH5α cells before incubation on ice for 30 mins. Cells were then heat shocked at 42 ^{o}C for 30 seconds before a further 5 mins on ice. 950 µl of LB media was added to the cells before a 1 hour outgrowth period at 37 ^{o}C with shaking. 20 µl and 200 µl fractions were then

spread onto LBA plates made up with appropriate antibiotic for selection, before overnight incubation at 37 ^{o}C. The next day, colonies were picked and added to 10 ml of LB media containing appropriate antibiotic, before overnight incubation at 37 ^{o}C with shaking. 500 µl of culture was added to 500 µl of 50% glycerol and stored at -80 ^{o}C. To ensure successful transformation, Sanger sequencing was performed following DNA extraction.

2.3.3 Bacterial DNA extraction and purification

DNA was extracted and purified from bacterial culture using kits purchased from QIAGEN as per manufacturer recommendations. For small scale DNA extraction from 10 ml of culture the QIAGEN Plasmid Mini Kit was used, whilst for greater quantities of DNA extraction the QIAGEN Plasmid Midi Kit was used with 100 ml of bacterial culture.

2.4 Mammalian cell culture

2.4.1 Cell culture medium and supplements

Unless specified, all cell culture medium and supplements were purchased from Gibco™ (Life Technologies™). Unless otherwise stated, 10% (v/v) foetal bovine serum (FBS) was added to all medium. Complete medium was stored at 4 ^{o}C and equilibrated at 37 ^{o}C before use.

Dulbecco's modified eagle's medium (DMEM) was supplemented with high glucose (4,500 mg/L) and L-glutamine (580 mg/L).

Roswell Park Memorial Institute 1640 medium (RPMI) was supplemented with 300 mg/L L-glutamine, 10% (v/v) FBS and 50 U/mL penicillin and streptomycin (pen/strep).

Opti-MEM® reduced serum media (Opti-MEM) was used during transfection as the medium in which DNA and transfection reagents were initially incubated to allow complex formation before addition to cells grown in appropriate complete medium.

1X Dulbecco's phosphate buffered saline (PBS) without Ca^{2+} or Mg^{2+} was purchased from Lonza and used for washing of cells before trypsinisation or lysis.

Passaging of cells was performed using trypsin. 10X (2.5% (w/v)) trypsin was aliquoted and stored at -20 ^{o}C. 1X trypsin (0.25% (w/v)) was made up using PBS and stored at 4 ^{o}C. 1X trypsin was equilibrated to 37 ^{o}C before use.

2.4.2 Cell lines and maintenance

Human embryonic kidney 293 (HEK293) cells are a foetal kidney cell line, which was originally immortalised through transformation with sheared Adenovirus 5 DNA. HEK293 cells were purchased from Thermo Scientific™ and maintained in DMEM supplemented with 100 μg/mL zeocin.

HEK293TT (293TT) cells were a kind gift from Christopher Buck (NIH, Bethesda, USA). This cell line expresses high levels of both SV40 ST and LT, is derived from the 293T cell line and is comparable to the commercially available HEK293 FT cell line sold by Thermo Scientific™. This cell line was generated to aid pseudovirus production using plasmids containing an SV40 promoter. 293T cells contain clonally integrated SV40 genome, but typically express very low levels of LT due to splicing bias that favours ST production. Therefore, stable introduction of a second plasmid that solely expresses SV40 LT leads to a high level of SV40 ST and LT expression. This in turn facilitates high expression of plasmid DNA that is transfected into 293TT cells. 293TT cells were maintained in DMEM containing 250 μg/mL Hygromycin B (Invitrogen™).

For experimentation using HEK293 and 293TT cell lines, unless otherwise stated, plates were pre-treated with poly-L-lysine to facilitate adherence. Wells were coated with Poly-L-lysine and washed twice with PBS before seeding of cells.

Vero cells are an African green monkey kidney epithelial cell line that is continuous and aneuploidy. Vero cells were a kind gift from Andrew Macdonald (University of Leeds) and maintained in DMEM supplemented with 50 U/mL penicillin and streptomycin (pen/strep).

WaGa, PeTa, MKL-2 and MS-1 cell lines are all MCPyV-positive MCC cell lines that were a kind gift from James Boyne (University of Bradford) and originally provided by Adam Grundhoff (Heinrich Pette Institute, Leibniz Institute for Experimental Virology, Germany). MCC13 cells are a MCPyV-negative cell line that was purchased

from Sigma-Aldrich®. All MCC lines were grown in RPMI containing 50 μg/mL pen/strep.

With the exception of cell lineages grown in pen/strep, antibiotic selection was removed prior to experimentation with appropriate medium supplemented with only 10% (v/v) FBS used throughout.

2.4.3 Cryogenic storage and recovery of cell lines

Cell lines were frozen in appropriate medium supplemented with 10% (v/v) DMSO to prevent ice crystal formation. $1X10^6$ cells were suspended in 1 mL of freeze-down medium and aspirated into cryotubes. Cryotubes were stored in cryogenic freezing containers for 48 hours, whereby the temperature was steadily reduced at a rate of 1 ^oC/minute. Cryotubes were transferred to liquid nitrogen for long term storage.

Cell lines were raised rapidly through addition of cryotubes from liquid nitrogen to a water bath at a temperature of 37 ^oC. Once thawed, cells were pelleted by centrifugation at 300 *g* for 3 minutes before resuspension in appropriate medium that was pre-warmed to 37 ^oC. Cells were then aspirated into T75 flasks and left for 48 hours to recover and adhere before medium was replaced to remove any dead cells. Cells were passaged for a minimum of 1 week before used for experimentation.

2.4.4 Cell line passaging

Passaging of adherent cell lines was performed by trypsin protease cleavage and dissociation of cells. Growth medium was removed from cells before a wash with PBS to remove residual medium. Cells were then incubated at 37 ^oC in 1X trypsin PBS solution until cells had dissociated. Detached cells were then resuspended in appropriate medium before seeding into vessels for continued passaging or experimentation as required.

MCPyV-positive MCC cell lines do not adhere and therefore grow in suspension. Growth medium in which MCPyV-positive MCC cell lines were growing was transferred into a Falcon tube before pelleting of cells through centrifugation at 300 *g* for 3 minutes. WaGa and PeTa cells were resuspended in growth medium and seeded as required. MKL-2 and MS-1 cell lines tended to adhere together in clumps

and therefore following pelleting cells were washed with PBS and briefly trypsinised to dissociate cells prior to seeding.

2.4.5 Cytotoxicity assay

To evaluate potential cytotoxicity induced by addition of chemical inhibitors during cell-based experimentation the CellTiter 96® AQ_{ueous} One Solution Cell Proliferation Assay was performed. This colorimetric assay relies upon the bioreduction of the tetrazolium compound 3-(4,5-dimethylthiazol-2-yl)-5-(3-carboxymethoxyphenyl)-2-(4-sulfophenyl)-2H-tetrazolium (MTS) to formazan which can be detected by measuring absorbance at 490 nm and is directly proportional to the number of living cells.

$5X10^4$ HEK293 cells were seeded into 96 well plates in 100 μL of growth medium and left overnight to settle. The next day growth medium was removed and replaced with a range of drug dilutions as appropriate in 100 μL fresh medium. Cells were then incubated for a period of time relative to intended experimentation, with addition of 20 μL of MTS reagent for the final hour. Plates were briefly vortexed to ensure produced formazan compound was evenly distributed and absorbance at 490 nm determined using a microplate reader. Untreated cells were used as a positive control against which viability was determined based upon untreated cells representing a 100% viable sample. Medium only wells were used as a negative control to account for background fluorescence and subtracted from each reading. All conditions were evaluated using triplicate experimental repeats.

2.4.6 Transfection of mammalian cell lines

Transfection of HEK293 and 293TT cell lines was performed using Lipofectamine® 2000 (Thermo Scientific™). Described is the protocol used for transfection of a 6 well plate. All concentrations were adjusted for different sized plates based on surface area. 2 μg DNA was mixed by brief vortexing in 100 μl of Opti-MEM. 6 μl of Lipofectamine® 200 was added directly to the DNA mix, before brief vortexing and a 20 minute incubation to allow complexes to form. DNA complexes were then added directly to cells without changing the growth medium. Cells were incubated for 6

hours with complexes before the medium was replaced with fresh DMEM prewarmed to 37^{o}C.

2.4.7 Harvesting of cells for lysis

For experimentation with evaluation by Western blotting cells were washed with PBS before lysis using Leeds lysis buffer consisting of 25 mM glycerol phosphate, 20 mM Tris, 150 mM NaCl, 1 mM EDTA, 1% (v/v) Triton X-100, 10% (v/v) glycerol, 50 mM sodium fluoride and 5 mM sodium pyrophosphate which was adjusted to pH 7.4 using HCl. Roche cOmplete™ protease inhibitor cocktail (Sigma-Aldrich™) and phosphatase inhibitor cocktail set II (Sigma-Aldrich™) were added at the recommended concentration to inhibit cellular proteases and phosphatases, respectively. Cells were scraped into lysis buffer and resuspended by vigorous pipetting to ensure homogenisation. Samples were incubated on ice for 30 minutes before sonication 30 seconds on/off three times to shear cellular DNA. Cells were returned to ice for a further 30 minutes before centrifugation at 12,000 *g* for 10 minutes at 4 ^{o}C to pellet insoluble material. Supernatant was aspirated and stored at -20^{o}C.

2.4.8 Protein standardisation

Protein standardisation was performed using the bicinchoninic acid (BCA) assay (Thermo Scientific™) as per manufacturer specifications. The BCA assay permits quantification of total protein concentration through colorimetric detection of Cu^{1+} following reduction by protein in an alkaline medium.

10 μl of protein sample was incubated with 100 μl of working reagent for 30 minutes to 1 hour at room temperature in a 96 well plate reading absorbance at 562 nm using a microplate reader. All samples were set up in duplicate. BSA standards at concentrations ranging from 25 μg/mL to 2,000 μg/mL made up in lysis buffer were used to create a calibration curve against which protein sample concentration was determined.

2.4.9 Sodium dodecyl sulphate polyacrylamide gel electrophoresis

Sodium dodecyl sulphate polyacrylamide gel electrophoresis (SDS-PAGE) separates proteins by electrophoresis using a discontinuous polyacrylamide gels as a support

medium, with SDS present to denature and solubilise proteins and create a negative net charge leading to migration under electrophoretic conditions. The Bio-Rad Mini-PROTEAN Tetra Cell system was used for all SDS-PAGE applications.

SDS-PAGE gels were made in house using a final percentage of acrylamide appropriate for the protein of interest and ranged from 8-15%. 30% (w/v) acrylamide concentrate with an acylamide:bis-acrylamide ratio of 37.5:1 was purchased from Severn Biotech Ltd®. Stocks and dilution of reagents for stacking and resolving solutions to make two SDS-PAGE gels are shown in Table 2.3 and

Table 2.4, respectively.

Table 2.3: Recipe to make stacking solution for two SDS-PAGE gels.

Component	Stock	Volume	Final concentration
Tris-HCl pH 6.8	1 M	250 μL	62.5 mM
Water	N/A	3 mL	N/A
Acrylamide	30% (w/v)	660 μL	5%
SDS	10% (w/v)	80 μL	0.1%
APS	10% (w/v)	80 μL	0.1%
TEMED	N/A	20 μL	0.5%
Total volume		**10 mL**	

Table 2.4: Recipe to make resolving solution for two SDS-PAGE gels. *Volume of water and 30% acrylamide were adjusted dependent upon the final acrylamide % required, with water used to make the solution up to 10 mL total volume.

Component	Stock	Volume	Final concentration
Tris-HCl pH 8.8	1.5 M	3.75 mL	375 mM
Water	N/A	3.75-6.9 mL*	N/A
Acrylamide	30% (w/v)	4.05-7.5 mL*	8-15%
SDS	10% (w/v)	100 μL	0.1%
APS	10% (w/v)	100 μL	0.1%
TEMED	N/A	25 μL	0.25%
Total volume		**2 mL**	

SDS-PAGE gels were run at 180 V until samples were approaching the end of the gel as indicated by the bromophenol blue indicator loaded into each well. Precision Plus Protein™ Dual Color Standard (Bio-Rad) was loaded onto each gel as a reference of migration and consisted of proteins of known molecular weight from 10-250 kDa.

2.4.10 Protein loading dye

Protein samples that were resolved by SDS-PAGE were diluted 1:1 with 2X loading dye prior to loading onto gels. 2X protein loading dye was composed of 100 mM Tris-HCl pH 6.8, 2% (w/v) SDS, 20% (v/v) glycerol, 0.1% (w/v) bromophenol blue and 5% (v/v) β-mercaptoethanol.

2.4.11 Western blotting

To identify specific proteins from whole cell lysates Western blotting was performed.

Following separation of protein samples by SDS-PAGE, proteins were transferred onto Amersham 0.45 μm nitrocellulose (GE Healthcare) using a Trans-Blot® Turbo™ Transfer System (Bio-Rad). SDS-PAGE gel and nitrocellulose were sandwiched between extra thick blotting paper (Bio-Rad) that were pre-soaked in Bjerrum Shafer-Nielsen buffer. A 10X Bjerrum Shafer-Nielsen buffer stock was made with 250 mM Tris and 1.92 M glycine, with a pH of ~9.2 which was not corrected. When required, 10X buffer was diluted to 1X (25 mM Tris and 192 mM glycine) with water and addition of 20% (v/v) methanol. The pre-set Bio-Rad transfer protocol was followed, with 25 V for 30 minutes applied.

Following protein transfer, nitrocellulose membranes were blocked for 1 hour at room temperature in Tris-buffered saline with 0.1% (v/v) Tween-20 (TBS-T) containing 5% non-fat milk (Marvel). TBS was made as a 10X stock consisting of 500 mM Tris and 1.5 M NaCl and was pH adjusted to 7.6 using concentrated HCl. 1X working TBS-T consisted of 50 mM Tris, 150 mM NaCl and 0.1% (v/v) Tween-20.

Primary antibody was diluted in TBS-T containing either 5% (w/v) non-fat milk or 5% (w/v) BSA as per manufacturer guidelines. If TBS-T containing 5% (w/v) BSA was used, membranes were washed 3 times with TBS-T prior to addition of primary antibody solution. Primary antibody was incubated with the membrane for 1 hour at room temperature or at 4 ^{o}C overnight. Membranes were then washed 3 times

with TBS-T before incubation with a primary species-specific HRP-conjugated secondary antibody made up in TBS-T containing 5% (w/v) non-fat milk for 1 hour at room temperature.

Following secondary antibody incubation cells were washed 3 times with TBS-T before application of ECL Western Blotting Substrate (Promega). Chemiluminescent signal was detected by exposure of Amersham Hyperfilm ECL (GE Healthcare) to the membrane for an appropriate period of time.

All membranes were probed for GAPDH to confirm equal loading and in the case of phosphoproteins, total protein expression may have been determined. In the event of a membrane been probed multiple times for proteins of a similar molecular weight, it was required for stripping of the membrane to remove previous antibodies. This was achieved using Restore Western Blot Stripping Buffer (Merck Millipore) following manufacturer guidelines. Membranes were washed once with TBS-T before application of new primary antibody solution and Western blotting protocol was followed as previously described.

2.4.12 Human Phospho-MAPK array

The Phospho-MAPK array was purchased from R&D Systems (catalogue #ARY002B) and experimentation was performed as per manufacturer guidelines. Briefly, $5x10^5$ HEK 293 cells were plated into a 6-well plate and incubated overnight. The next day cells were transfected with ST-GFP or GFP as a control and fresh growth medium was added after 6 hours. Following a further 18 hour incubation serum free medium was added for 22 hours before a 2 hour serum boost using growth medium containing 10% FBS (v/v). Cells were then lysed using the provided buffer and a BCA assay performed to confirm equal loading. Differences in concentration were corrected using lysis buffer. The manufacturer provided protocol was then followed to immobilise and detect phospho-MAPKs using Amersham Hyperfilm with a range of exposure periods. Quantification was performed by densitometry using ImageJ.

2.4.13 Silver staining

To identify the presence of VLPs in fractions following ultracentrifugation and determine purity silver staining of SDS-PAGE separated samples was performed.

SDS-PAGE was performed as previously described, however due to assay sensitivity the protein standard ladder was used 100-fold more dilute than recommended.

All steps described were performed at room temperature with gentle agitation. Solution recipes to make 100 mL used during the silver staining protocol are described in Table 2.5.

Table 2.5: Solution recipes for use in silver staining of SDS-PAGE resolved protein samples.

Solution	Contents
A	50% (v/v) ethanol, 10% (v/v) acetic acid
B	5% (v/v) ethanol, 1% (v/v) acetic acid
C	0.2 g sodium thiosulphate
D	10 mL solution C
E	0.2 g silver nitrate, 75 μL formaldehyde
F	6 g sodium carbonate, 50 μl formaldehyde, 0.2 mL solution C
G	5% (v/v) acetic acid

Following separation of protein samples by SDS-PAGE the gel was fixed by incubation in a solution A for 30 minutes. The gel was then incubated in a solution B for 15 minutes before 3 5-minute washes with deionised water. Solution D was then added for 1-2 minutes before 3 30-second washes with deionised water. The gel was then incubated in a solution E for 20 minutes before 3 20-second washes. The gel was developed in solution F until protein bands were visible before the reaction was stopped with incubation in solution G until effervescing yielded. The gel was stored in deionised water and imaged using a G:BOX XX9.

2.4.14 Fixation of cells

Cells to be used for immunofluorescence microscopy (IF) were washed once with PBS before incubation with ice-cold 4% (w/v) paraformaldehyde (PFA) for 15 minutes. Cells were then washed 3 times with PBS before storage at 4^{o}C. 4% (w/v) PFA was

produced through addition of 10 g PFA powder to 200 mL of boiling water in a fume hood. Once cooled, 25 mL 10X PBS was added and the solution made up to 250 mL using deionised water and stored at 4^{o}C.

2.4.15 Immunofluorescence staining

Following fixation with PFA, samples were prepared for IF through permeabilization with 0.1% (v/v) Triton X-100 in PBS for 15 minutes. Samples were then washed 2 times with PBS before blocking using 1% (w/v) BSA in PBS (termed PBS blocking buffer (PBB)) for an hour at 37 ^{o}C or overnight at 4 ^{o}C. Primary antibody was diluted appropriately in PBB and incubated on cells for 1 hour at 37 ^{o}C. Cells were then washed 3 times with PBS before addition of species-specific Alexa Fluor conjugated secondary antibody, diluted 1 in 500 in PBB, for 1 hour at room temperature. Cells were then washed 3 times with PBS. Following staining of cells mounted upon coverslips, VECTASHIELD Antifade Mounting Medium containing DAPI (Vector Labs) was added prior to mounting upon slides. For IF performed in plate-based assays, PBS was added to cells prior to imaging.

2.4.16 MCPyV pseudovirus production and purification

MCPyV pseudovirus (PsV) production and purification was performed following a publicly available revised protocol (https://home.ccr.cancer.gov/Lco/production.asp) and has been previously utilised for production of PyV and HPV PsVs.

MCPyV PsVs were produced using either GFP or NanoLuc reporter vectors. For high-throughput screening using inhibitors PsVs packaging a GFP reporter were used. For production of PsVs to visualise intracellular localisation NanoLuc (secreted luciferase) reporter vectors labelled with EdU were used.

All steps following transfection were performed using low-retention microcentrifuge tubes and low-retention filter tips.

To produce MCPyV PsVs 7X10^{6} 293TT cells were seeded into a T75 flask 16 hours to transfection. The next day, 18 μg reporter vector, 15 μg pwM2m (VP1 and VP2 dual vector) and 3 μg ph2m (VP2 only vector) were mixed into 1 mL of opti-MEM and incubated for 5 minutes. 85 μL Lipofectamine 2000 was also mixed into 1 mL of opti-

MEM and incubated for 5 minutes before combination with DNA mix. Transfection mixtures were incubated for 20 minutes to allow complexes to form before addition to 293TT cells.

For production of EdU labelled PsVs, growth medium was replaced after 6 hours with fresh growth medium containing 50 μM EdU. For production of GFP vector-containing PsVs, growth medium was changed the next morning. Cells were incubated for a total period of 48 hours post transfection before harvest.

Supernatants were removed from the cells and adhered cells dissociated by trypsinisation. Growth medium was used to inactivate trypsin and collected cells were added to the supernatant. Flasks were washed with 2 mL of growth medium to collect any residual cells and added to harvested cells and supernatant. Cells were then pelleted by centrifugation at 300 *g* for 5 minutes are room temperature. Supernatant was aspirated and cells resuspended by agitation in residual fluid. Cells were transferred to a 1.5 mL microcentrifuge tube and pelleted (300 *g*, 5 minutes, room temperature) to remove residual fluid. Cell pellets were resuspended in 1.5X pellet volumes PBS containing 9.5 mM $MgCl_2$ and pen/strep. Following resuspension $1/20^{th}$ volume 10% (v/v) Triton X-100, $1/1{,}000^{th}$ volume RNase Cocktail™ Enzyme Mix (Ambion) and $1/40^{th}$ volume 1 M ammonium sulphate, pH 9.0, were added and mixed by agitation. Microcentrifuge tubes were then incubated in a 37 ^{o}C water bath for 20-24 hours to allow maturation of PsVs.

The next day PsVs were extracted from the matured lysate mix. All centrifugation steps performed at 5,000 *g* for 5 minutes at room temperature and all supernatants were combined and retained. Following removal from the water bath, lysates were chilled on ice before centrifugation to clarify the lysate. Pelleted material was washed with 2X pellet volumes PBS and centrifugation followed by a wash with 1X pellet volume PBS and centrifugation 1X pellet volume PBS was then added before freeze thawing on dry ice and centrifugation. A final wash was performed using 1X PBS containing 0.8 M NaCl before centrifugation.

Pooled supernatants were then loading onto a 27-33-39% opti-Prep (iodixanol) cushion gradient made up in PBS containing 0.8 M NaCl in 5 mL UltraClear

ultracentrifuge tubes (Beckmann-Coulter) suitable for use in SW55 Ti ultracentrifuge buckets (Beckmann-Coulter). Ultracentrifugation was then performed at 50,000 rpm (303,000 *g*) for 3.5 hours at 16 ^{o}C. A medium acceleration speed and slowest brake setting (above coast) were used to avoid mixing of the gradient during acceleration/deceleration.

Fractions were then collected initially by puncturing of the underside of the tube, however due to highly variable flow rates fraction by withdrawal from the top of the tube downwards was the preferred method. Two 1.5 mL initial fractions were taken before subsequent 340 μL fractions until all gradient had been aspirated. Fractions were run by SDS-PAGE before Western blotting and silver staining to confirm successful purification PsVs and also purity, respectively. BSA standards were also used for silver staining so that the mass of VP1 could be calculated. Fractions were also used in reporter assays using 293TT cells to ensure that viable PsVs were produced.

For confirmation of viable GFP reporter PsVs, 293TT were transduced for 2 hours before addition of fresh growth medium. Cells were then imaged using an Incucyte ZOOM System (Essen Bioscience) 72 hours post transduction to determine the number of GFP positive cells.

For confirmation of viable NanoLuc, EdU-labelled PsVs 293TT cells were transduced for 2 hours before addition of fresh growth medium. Cells were incubated for 96 hours before removal of growth medium. Growth medium was then tested using the NanoGlo® Luciferase Assay System (Promega) to detect secreted luciferase according to manufacturer guidelines, with slight modification which is described. 25 μL of growth medium was added in triplicate into wells of a white, opaque 96-well plate. Working substrate containing NanoLuc substrate diluted 1:50 in NanoLuc buffer was made up fresh at the time of use. Due to high sensitivity and detection, working substrate was further diluted 1:8 using 10 μL of working substrate and 70 μL PBS. This mix was then injected into wells using a FLUOstar OPTIMA microplate reader (BMG Labtech) and luminescence was detected. The provided FLUOstar OPTIMA software was then used to quantify luminescence and exported to Microsoft Excel for analysis.

2.4.17 MCPyV PsV GFP reporter assay

PsV assays that used GFP for quantification were performed using $5X10^4$ 293TT cells seeded into wells of a poly-L-lysine treated 24 well plate 16 hours before addition of PsVs. If required, pre-treatment with chemical inhibitors was performed for 1 hour. 10 μg VP1 equivalent of PsVs was pre-mixed in 300 μL of growth medium (containing chemical inhibitor if required) and added to wells for 2 hour with gentle shaking every 30 minutes. Fresh growth medium was then added for and cells were incubated for 72 hours before detection of GFP positive cells using an Incucyte ZOOM System. Analysis was performed using pre-set parameters to quantify the number of GFP positive cells. Phase confluence was also determined to ensure that cells treated with chemical inhibitors continued to proliferate relative to untreated cells.

2.4.18 EdU-labelled MCPyV PsV reporter assays

EdU labelled PsVs contained a NanoLuc reporter to confirm viability. This vector was preferred to GFP to ensure that there would be no potential of background fluorescence during microscopy.

293TT cells were seeded into 24-well plates onto 12 mm coverslips that had been pre-treated with poly-L-lysine 16 hours before transduction. Cells were transduced with 50 μg VP1 equivalent of PsVs with pre-treatment and addition of chemical inhibitors as required. Cells were fixed 48 hours post transduction using PFA as previously described. Detection of EdU was performed using the Click-iT™ Plus EdU Alexa Fluor™ 488 Imaging Kit (Life Technologies) according to manufacturer guidelines. Briefly, following fixation cells were washed 2 times using 3% (w/v) BSA in PBS. 0.5% (v/v) Triton X-100 was added before incubation at room temperature for 20 minutes before 2 further washes using 3% BSA (w/v) in PBS. Complete Click-iT® Plus reaction cocktail was added for 30 minutes with gentle rocking protected from light. Cells were then washed with 3% (w/v) BSA in PBS before mounting onto coverslips or performing immunofluorescence staining as previously described.

2.4.19 SV40 production

A stock of SV40, kindly provided by Michelle Antoni (Macdonald group), was used to propagate virions. Vero cells were seeded into T175 flasks so that they were 50-60%

confluent at the time of infection. $1.5X10^6$ infectious units were incubated on the cells for 2 hours with gentle rocking every 30 minutes before addition of fresh growth medium. Cells were incubated for 7 days before the supernatant containing virions was harvested. The supernatant was flash frozen in a dry ice bath containing isopropanol and stored at -80^{o}C.

2.4.20 Quantification of SV40 titre

Quantification of SV40 titre was calculated by Incucyte ZOOM system analysis of cells stained using an SV40 T antigen specific antibody.

$5X10^3$ Vero cells were plated into wells of a 96-well plate 16 hours before infection. Growth medium containing SV40 virions was flash-frozen and then defrosted to mimic storage conditions before supernatant was diluted 1:5 using fresh growth medium. The 1:5 diluted stock was then serially diluted 2-fold to produce a dilution series. 100 μL of diluted samples was added to wells and incubated for 2 hours with gentle rocking every 30 minutes. Fresh growth medium was then added before a further 22-hour incubation. Cells were then fixed using PFA and immunostained using a T antigen specific antibody and species-specific Alexa Fluor 488 secondary antibody. Four images of each well were then taken using the Incucyte ZOOM system and analysed to determine the number of T antigen positive cells in each well for each dilution. Dilution factors were then reversed to determine the total IU/mL for each dilution. The data was then plotted on a graph to identify a plateau indicative of IU/mL and multiplicity of infection (MOI). Each dilution was performed in triplicate so that error bars could identify hypervariability at higher dilution factors caused by amplification of slight changes in positive counts. Samples with visible hypervariability were discounted from analysis.

2.4.21 SV40 infection assays

$5x10^3$ Vero cells were seeded into wells of a 96-well plate 16 hours prior to experimentation. If required cells were pre-treated with chemical inhibitors for 1 hour. SV40 virions were diluted in growth medium (containing chemical inhibitors if applicable) to achieve an MOI of 1 relative to initial seeding and incubated on cells for 2 hours with gentle rocking every 30 minutes. Fresh growth medium was then

added before a further 22-hour incubation. 24 hours after initial infection cells were fixed and stained, before imaging and analysis using an Incucyte ZOOM System as previously described. Chemical inhibitor effects were calculated through comparison to an untreated control which was arbitrarily used to represent 100% infection.

2.4.22 Scratch assays

Scratch assays were performed using an ST-inducible cell line that was under the control of a tetracycline promoter, termed i293-ST cells, in poly-L-lysine 24-well plates (Knight et al., 2015). $5X10^5$ cells were seeded into each well and incubated until 90% confluent. Expression of ST was induced through addition of 2 μg/mL doxycycline hyclate, along with chemical inhibitors if appropriate. Cells were incubated for a further 24 hours to permit ST expression and cell confluency to reach 100%. Scratches were then performed using a 50 μL Clip Tip (Thermo Scientific) and wells were washed 1X using PBS to remove non-adhered cells before addition of fresh growth medium. Images were taken at 1, 24 and 48 hours post scratch using an EVOS FL Auto 2 Imaging System (Invitrogen), before images were processed using ImageJ to determine wound closure.

2.4.23 Transwell migration assays

Transwell migration assays were performed using a CytoSelect 24-well Haptotaxis Assay as per manufacturer guidelines. The assay was performed using the MCPyV-positive MCC cell line PeTa.

Briefly, $1x10^6$ cells/mL were resuspended in serum depleted (0.5% v/v FBS) medium containing drug as appropriate and incubated for 24 hours. Cytoselect plate membranes were rehydrated by incubating serum depleted medium in the upper chamber for 1-hour. Medium was removed and 300 μL medium containing cells added to the upper chamber. 500 μL of serum enriched (20% v/v FBS) growth medium was added to each lower chamber before incubation for 48-hours. Cells in each chamber were resuspended by pipetting and aliquots mixed with trypan blue before quantification of cell number using a Countess II FL Automated Counter. The percentage of migrated cells for each condition was calculated and before comparison to an untreated control.

Chapter 3

Creating systems to study polyomaviruses

3.1 Introduction

Comparable with many other polyomaviruses, the lifecycle of MCPyV is poorly understood. Assumptions are made that the virus will follow similar pathways to the prototypic and more widely studied SV40. Binding of MCPyV to its cellular receptor has been characterised, however requirements post-attachment had not been investigated at the time that this study began (Schowalter et al., 2011; Neu et al., 2012). More recently Becker *et al.* have identified several aspects of MCPyV trafficking and host cellular mechanisms that are required during the early stages of infection (Becker et al., 2019).

Many polyomaviruses bind cell surface sialic acid residues that are associated with glycolipids or glycoproteins, in contrast sialylated glycans are not required for MCPyV attachment (Schowalter et al., 2011). Instead, attachment is dependent upon heparan sulphate interactions, before a secondary interaction with a sialylated cofactor permits entry into the cell. Given that attachment is different to other studied polyomaviruses, it therefore suggests that MCPyV may not follow canonical polyomavirus routes of infection and there may be differences in other aspects of the lifecycle.

It has been demonstrated that MCPyV enters the cell by caveolar/lipid raft mediated endocytosis and that following penetration, virions traffic to the ER via the endosomal network (Becker et al., 2019). Similar to other polyomaviruses, acidification of endosomes and a functional redox environment are required whilst virus-containing endosomes are trafficked via microtubular transport to the ER.

A significant issue challenging the ability to study MCPyV infection is that there are no easily reproducible systems to study the viral lifecycle. Despite recent identification of dermal fibroblasts as a potential cell population that permit the full replication of MCPyV, these cells require substantial manipulation using enzymes, growth factors and chemical inhibitors to promote both infection and replication (Liu et al., 2016). Given that MCPyV has been detected in a range of different tissues and is continuously shed from skin of a large cohort of healthy individuals, it may be that dermal fibroblasts represent only one of many permissive cell types. Further to this,

MCPyV has only been identified as a contributing factor in MCC development, which suggests that further factors such as clonal integration and UV exposure are required for MCPyV to promote oncogenesis. Moreover, the inability to culture Merkel cells has further hindered attempts to conclusively identify connections between infection and disease.

Previous studies have relied upon HEK293 cell-based infection methods, however due to inefficiencies/absence of replication, the ability to detect aspects of the viral lifecycle following native virion infection has remained difficult and provided little insight. We therefore considered an approach using MCPyV PsVs containing reporter vectors to identify viral requirements of the host cell during entry and trafficking.

In order to evaluate several aspects of the virus lifecycle two systems were developed so that penetration, trafficking and subcellular localisation could be assessed. Firstly, an assay that utilised a GFP reporter and end-point Incucyte analysis was developed so that high-throughput drug screening could be performed, secondly a reporter that incorporated EdU was produced enabling penetration and subcellular localisation to be determined by click chemistry. To compare MCPyV requirements to SV40, an immunofluorescent Incucyte assay was also developed to determine infection. This also led to the production of a novel, rapid method to determine infectious titre of SV40 stocks.

3.2 Method of PsV production

Previous studies using MCPyV PsVs are limited, however recent publications have shown that a method for production of HPV PsVs can be adapted to a range of polyomaviruses (Buck and Thompson, 2007; Pastrana et al., 2009; Schowalter et al., 2011).

The production of MCPyV PsVs is a multi-step process that is summarised in Figure 3.1. Following transfection and incubation of 293TT cells for 48 hours, cells were incubated overnight in the presence of detergent to lyse cells and permit capsids to form before purification. Whilst this is in essence simple, there are many small differences that can severely compromise the quality and quantity of viable PsVs in

a preparation. It was therefore required that several rounds of optimisation were performed to create a reproducible system that yielded high quantities of PsVs.

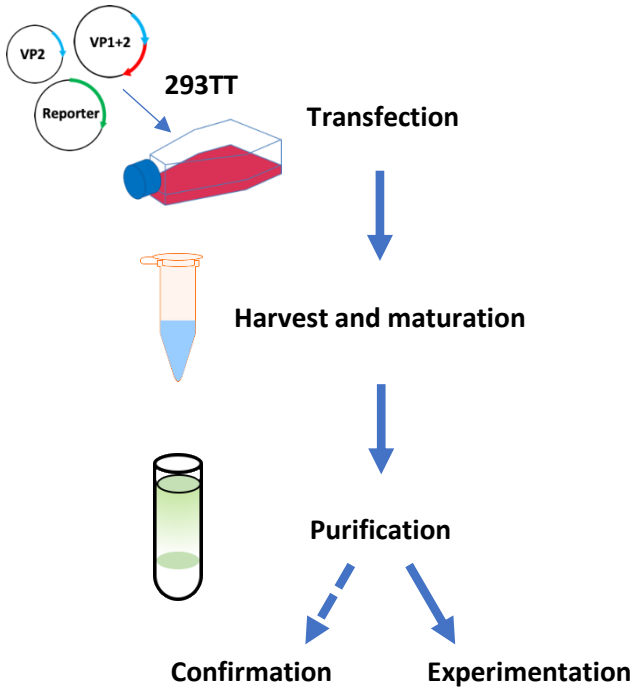

Figure 3.1: Schematic representation of MCPyV PsV production. 293TT cells were transfected with VP1/VP2 and VP2 expressing constructs along with the desired reporter vector. Cells were harvested after 48 hours and matured before purification using an iodixanol cushion gradient. Successful production of viable PsVs was confirmed before use in follow on experiments.

3.3 Expression of MCPyV capsid proteins

It has been previously shown that the amount of VP2 expression can directly impact PsVs, with lower expression correlating with lower transduction efficiencies (Schowalter and Buck, 2013). Whilst a VP2 expression vector was available and used, it was investigated whether the use of a vector that dually expressed VP1 and VP2 would compromise VP1 expression alone. 293TT cells were transfected with constructs that solely expressed VP1 (pwM) or dually VP1/ VP2 (pwM2m) (Figure 3.2). Results showed that transfection with the dual expression vector had no impact

upon the expression of VP1 and this was therefore taken forward into PsV production alongside the VP2 expression vector to ensure a surplus of VP2 was present.

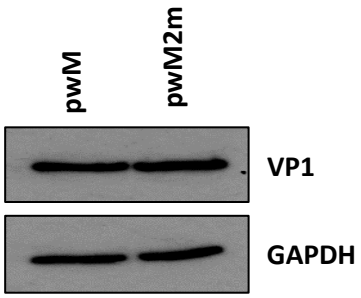

Figure 3.2: The use of a dual VP1/VP2 expression vector does not impact upon the amount of VP1 expressed. 293TT cells were transfected with VP1 only pwM or dual VP1/VP2 expressing pwM2m constructs for 48 hours before lysis. Western blotting was performed to evaluate the quantity of VP1 produced from each construct with GAPDH used as a loading control.

3.4 Confirming production of PsVs

To identify the successful production and purification of PsVs following iodixanol cushion ultracentrifugation and fractionation a range of methods could be used.

To evaluate fractions that potentially contained PsVs, silver staining of fractions was initially performed. Figure 3.3 showed the bulk of cellular proteins were detected in fractions 1-3 which represented the 'top' of the tube and proteins that were unable to enter the iodixanol cushion. As fractions proceeded further down the tube, less host cellular debris could be detected. In fractions 8-10 (predominantly 9) a protein band was more prominent at approximately 50 kDa which corresponded to the molecular weight of VP1. Whilst this band was distinct, there were also other bands present suggesting that there may have been contaminating proteins.

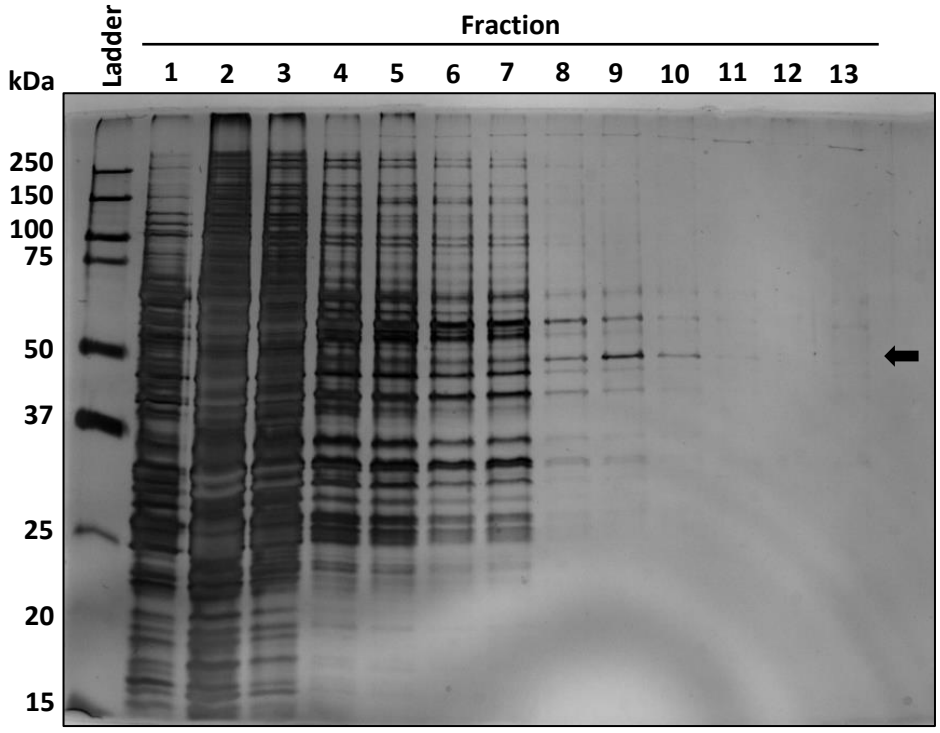

Figure 3.3: Evaluation of fractions following iodixanol purification of a MCPyV PsV preparation. Following ultracentrifugation, fractions were separated by SDS-PAGE before silver staining to visualise resolved proteins. The black arrow indicates the predicted mass of MCPyV VP1.

Due to the detection of potential contaminants, negative stain electron microscopy was performed to visualise peak fractions. Imaging revealed that capsids had been successfully produced and purified, as indicated by the presence of spherical virion-like structures of approximately 45 nm in size (Figure 3.4). As indicated from the silver stain, contaminants were also identified surrounding the purified capsids. It was not clear whether these contaminants were aggregated proteins or partially encapsidated chromosomal DNA, however given that these may have been detrimental to the transducibility of PsVs, slight variations in the method of fractionation were performed in an attempt to produce stocks with improved purity.

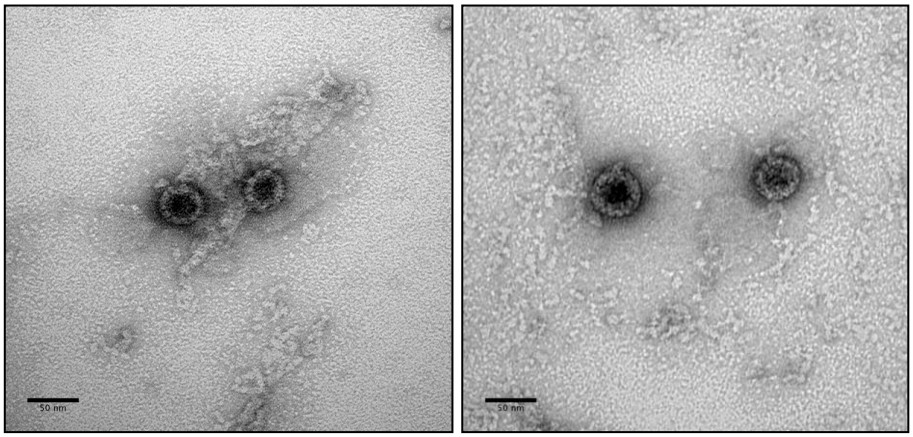

Figure 3.4: Negative stain electron microscopy of PsV preparation. Following ultracentrifugation of MCPyV PsV, the peak fraction was imaged by uranyl acetate negative stain electron microscopy. Scale bar 50 nm. Preparation of grids and electron microscopy was kindly performed by Daniel Hurdiss.

3.5 Optimised purification of PsVs

Previously published protocols for the purification of PsVs relied upon puncturing the bottom of the ultracentrifuge tube with a needle and then collecting equivalent fractions based on the number of drops. An issue with this method was that due to variations in flow rates, there was difficulty in collecting equal fractions. By having to move the tube around quickly between collection tubes there was also the possibility of unintentionally mixing the remaining contents of the gradient leading to more dispersed contaminants and PsVs.

To avoid potential detrimental effects upon the purity of fractions collected caused by this method, fractionation from the top of the tube to the bottom using aspiration with a pipette was performed. Results showed that this method yielded preparations of high purity (Figure 3.5A). Due to knowledge that capsids would migrate through the initial iodixanol cushion, two larger initial fractions (1 and 2) were taken to remove cellular supernatant, before smaller fractions were collected. In comparison to Figure 3.3, this method yielded PsVs of higher purity with no obvious contaminants observed by silver staining in the peak fraction (fraction 7).

To further confirm that the observed band was indeed VP1, Western blotting of the fractions was performed. Figure 3.5B showed that detection of VP1 correlated with the silver stained gel, with VP1 detected predominantly in fraction 7and to a lesser extent in fractions 5, 6 and 8. Detection of GAPDH also confirmed that cellular proteins did not enter the iodixanol cushion, with signal predominantly in fraction 2 which also correlated with the results obtained by silver staining.

Negative stain electron microscopy was performed on peak fractions to identify whether any contamination was present. Results supported the silver stain and Western blot data, showing spherical virions with considerably reduced background contaminants (Figure 3.6) compared with previous preparations (Figure 3.4).

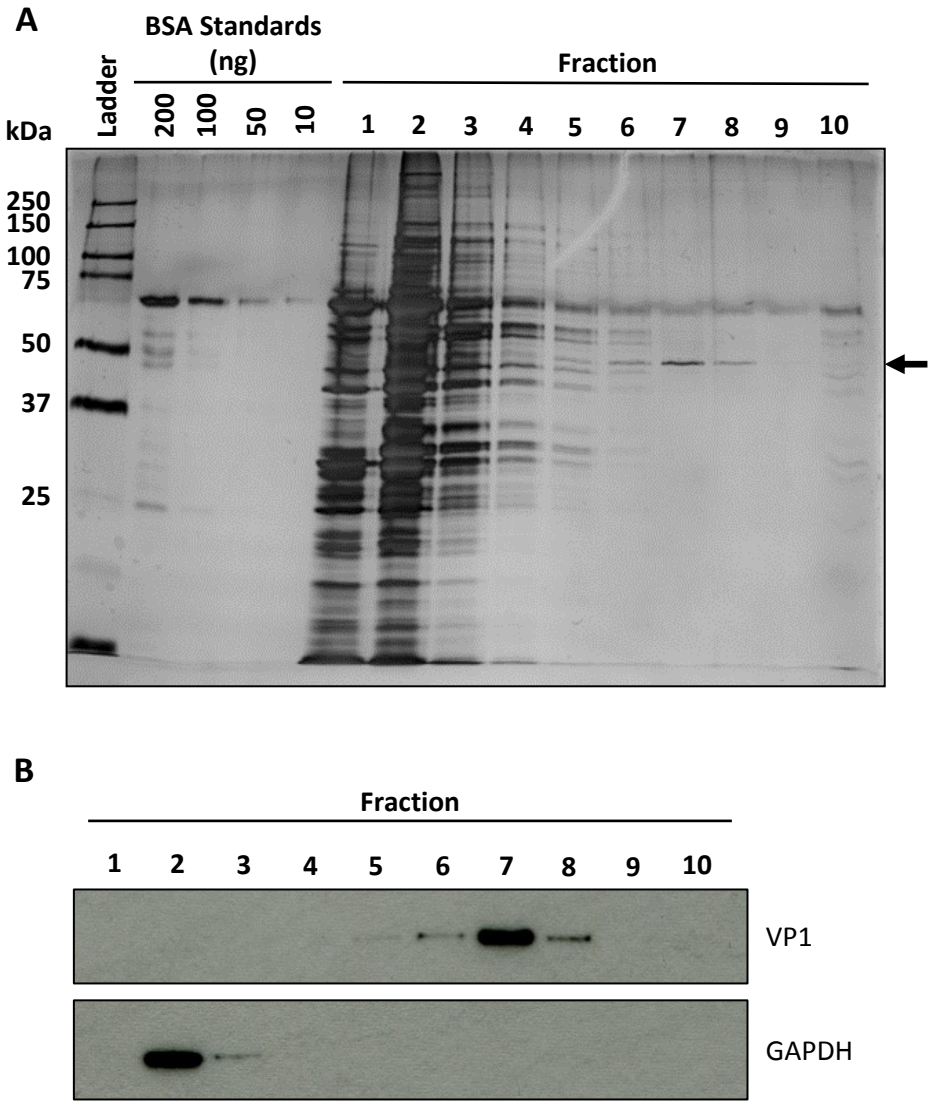

Figure 3.5: Revised purification of MCPyV PsV visualised by silver staining and Western blot. Visualisation of MCPyV fractions by silver stain (A) and Western blotting (B) following ultracentrifugation. (A) fractions were resolved by SDS-PAGE before silver staining to determine purity and quantify the total mass of VP1 by comparison to a BSA standard curve produced using known concentrations that were resolved on the same gel. Black arrow indicates the predicted molecular weight of MCPyV VP1. (B) Western blotting for MCPyV VP1 to confirm that the viral protein was detected in peak fractions. Western blotting for GAPDH was performed to investigate the migration of cellular proteins.

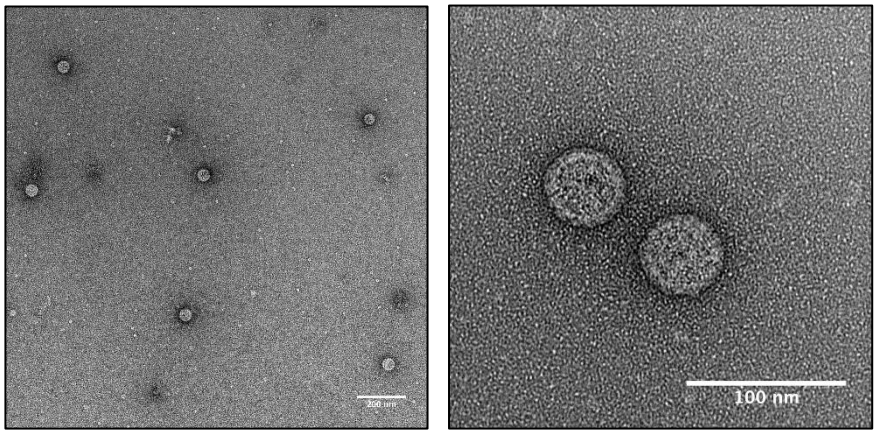

Figure 3.6: Negative stain electron microscopy of fractionation-optimised PsV preparations. Following ultracentrifugation of MCPyV PsV, the peak fraction was imaged by uranyl acetate negative stain electron microscopy. Scale bar 200 and 100 nm for left and right micrographs, respectively. Preparation of grids and electron microscopy was kindly performed by Joseph Snowden.

3.6 GFP PsV analysis using the Incucyte

Previous studies have identified cell lines that are permissive to transduction through the use of MCPyV PsVs packaging a GFP reporter, with quantification by flow cytometry to determine the number of GFP-positive cells (Schowalter and Buck, 2013). Given that 293TT cells are one of a handful of cell lines known to be permissive to transduction, this cell line was considered for further experiments. A caveat to the use of 293TT cells is that they poorly adhere to tissue culture plastic and will readily dissociate into growth medium, particularly at higher confluency. To counter this, plates were treated with poly-L-lysine to promote attachment, although this in turn created an issue whereby there was great difficulty in detaching cells for fixation and further analysis by flow cytometry.

We therefore tested an alternative method of analysis using an Incucyte ZOOM instrument (Incucyte). An Incucyte is an automated microscope that will image tissue culture plates using defined bright field (phase), green fluorescence and red fluorescence parameters. The Incucyte is also housed in a 37 ^{o}C, 5% CO_2 incubator so that time-course experiments using live cells may be performed. In comparison to other microscopy techniques which require manual counting, the Incucyte

incorporates an analysis suite that will autonomously evaluate samples using the same predefined processing definition across all samples, removing any potential human bias.

To validate that GFP PsVs were viable, purified fractions were used to transduce 293TT cells before incubation for 72 hours, correlating with the end-point used in previous publications. After incubation, cells were imaged using the Incucyte to measure cell confluence and detect GFP positive cells (Figure 3.7). Results clearly showed that PsVs were viable as GFP was detected in a large population of cells. Comparison between untransduced and transduced samples showed no change in confluence, which suggested that the presence of iodixanol did not affect cell growth.

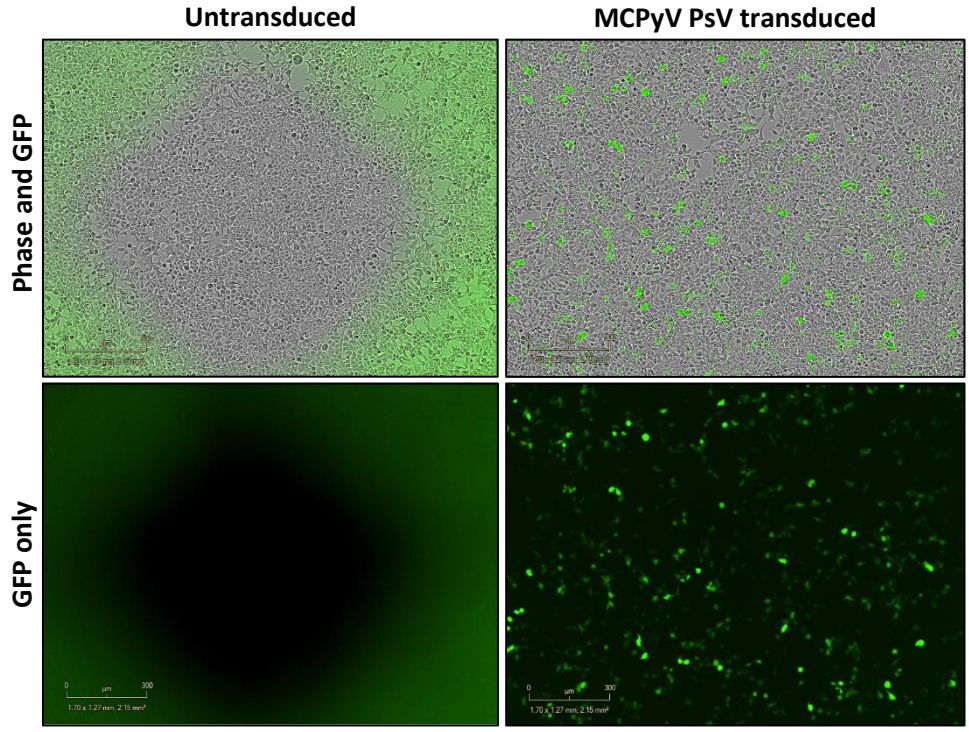

Figure 3.7: Transduction of 293TT cells using MCPyV PsVs. 293TT cells were incubated with MCPyV PsVs for 2 hours before replacement with fresh growth medium. After 72 hours, plates were added to an Incucyte for imaging of phase (brightfield) and green fluorescence.

Following confirmation that PsVs were viable, we explored the possibility of whether an earlier time point could be used in future experiments given that planned used of inhibitors may have led to increased cytotoxicity with longer incubations. 293TT cells were transduced as previously described and plates added to the Incucyte 24 hours post transduction for imaging. Results showed that there was no observed detection of GFP at 24 hours, with only a small proportion of cells GFP positive at 48 hours (Figure 3.8). Imaging at 72 hours post transduction revealed a much higher proportion of GFP positive cells. This confirmed that it was not feasible to use an end point before 72 hours and this time-point was taken forward for future experiments.

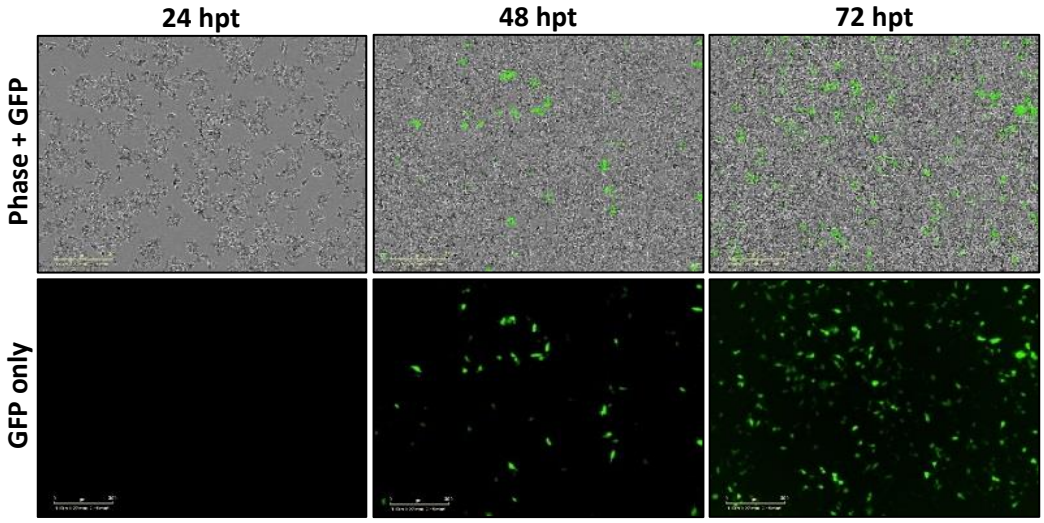

Figure 3.8: MCPyV PsV time course to evaluate optimal assay end point. 293TT cells were incubated with MCPyV PsVs for 2 hours before addition of fresh growth medium. The same region of wells were imaged using an Incucyte at 24, 48 and 72 hours post transduction for phase and green fluorescence.

3.7 Analysis using EdU labelled PsVs

In order to evaluate MCPyV penetration, trafficking and subcellular localisation a second PsV system that utilised an EdU labelled reporter DNA was produced. This system is comparable to more traditional BrdU labelling approaches, however due to the bulky size of antibodies that are required to detect BrdU this was not suitable for detection of encapsidated DNA as the antibody would be unable to penetrate the fully formed capsid to access and bind to the incorporated BrdU. In contrast to BrdU, detection of the thymidine analogue EdU relies upon click chemistry, where an Alexa Fluor dye is conjugated to an azide linker. This is much smaller than an antibody based equivalent, allowing penetration of the capsid to access and react with the alkyne containing EdU via a copper catalysed covalent 'click' reaction.

To remove any potential background fluorescence that may be attributed to GFP expression, a NanoLuc reporter was used rather than the previously described GFP reporter, however the method of PsV production was otherwise unaltered. NanoLuc reporters encode a luciferase that is secreted from the cells, unlike a traditional luciferase which requires cell lysis. Therefore, confirmation that viable PsVs were produced was performed using a luciferase assay with growth medium taken from the wells for analysis by a luciferase reporter assay. Due to the slow speed at which MCPyV PsVs enter and traffic through the cell, coupled with not only the requirement of expression but also secretion, a later time point of 96 hours post transduction was used for evaluation. Results showed that fraction 5 produced the highest amount of luminescence, which correlated with Western blot analysis on the fractions showing peak MCPyV VP1 detection (Figure 3.9). This confirmed that viable PsVs were produced.

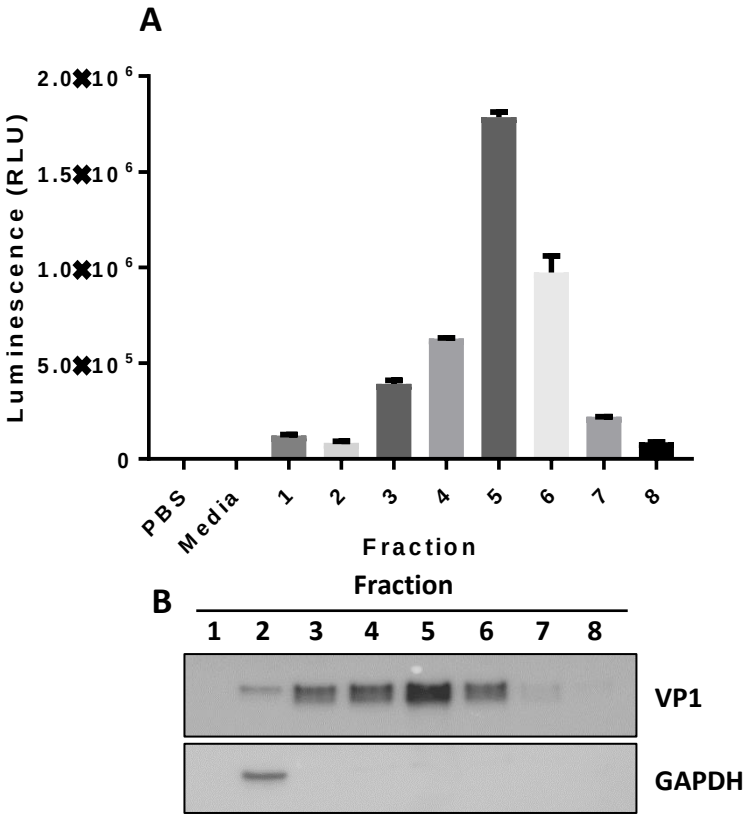

Figure 3.9: Determining viable EdU labelled MCPyV PsV production and purification of peak fractions. Following ultracentrifugation, EdU-labelled, NanoLuc expressing MCPyV PsVs were fractionated before quantification of luciferase activity (A) and quantity of MCPyV VP1 in each fraction (B). (A) 293TT cells were incubated with MCPyV PsVs for 2 hours before replacement with fresh growth medium. Following 96 hours of incubation medium was taken and luciferase activity determined by NanoLuc luciferase reporter assay. (B) fractions were resolved by SDS-PAGE before Western blotting for MCPyV VP1 to determine the presence of viral protein in each fraction. GAPDH was used as a control for cellular protein.

As further confirmation of PsV production, negative stain electron microscopy was performed on the peak fraction 5 (Figure 3.10). This showed that PsVs were formed and that the sample was of high purity. To confirm that virion structure resembled that of a polyomavirus, approximately 300 particles were picked for 2D and 3D class averaging, yielding a structure with a resolution of 23 angstroms. Whilst little information can be revealed with such low resolution, this analysis showed MCPyV PsVs retained the correct composition in relation to the pentameric VP1 heads

present upon the surface of the capsid in comparison to other previously resolved polyomaviruses. Unfortunately, given the low resolution it was not possible to elucidate any information regarding VP2 below the pentamers.

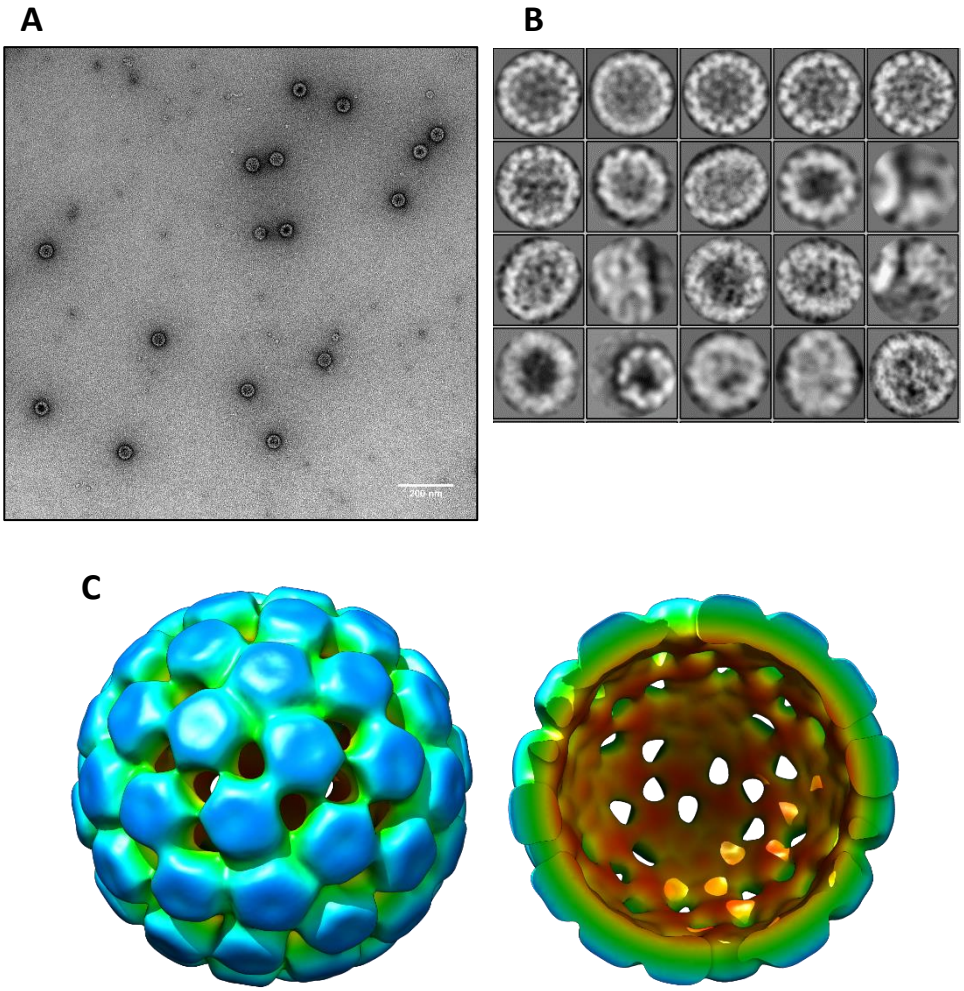

Figure 3.10: Confirmation of EdU labelled MCPyV PsVs production by negative stain electron microscopy (A), with 2D (B) and 3D (C) class averaging. EdU-labelled MCPyV PsVs were imaged by uranyl acetate negative stain electron microscopy to confirm the production and purity of PsVs. Approximately 300 virus particles were picked for 2D and 3D class averaging, yielding a structure of approximately 23 angstroms (B and C). The resulting structure was colour coded to show radial distance from a centre point. Data was kindly collected and analysed by Joseph Snowden.

3.8 Confirmation of EdU incorporation into encapsidated DNA

Whilst the NanoLuc reporter assay and EM confirmed that viable PsVs were produced, it did not however provide evidence as to whether EdU had been successfully incorporated into packaged DNA. To determine this, PsV stocks were serially diluted and 10-40 ng VP1 equivalent mass was added to wells for 48 hours before fixation. A click reaction was then performed to covalently attach Alexa Fluor 488 conjugated dye to EdU before visualisation by confocal microscopy (Figure 3.11). The mock control showed little if any signal, confirming that the click reaction did not lead to the detection of a non-specific signal. Increasing the mass of PsVs incubated with cells correlated with an increase in the number of puncta within cells, consistent with more labelled PsVs leading to increased detection.

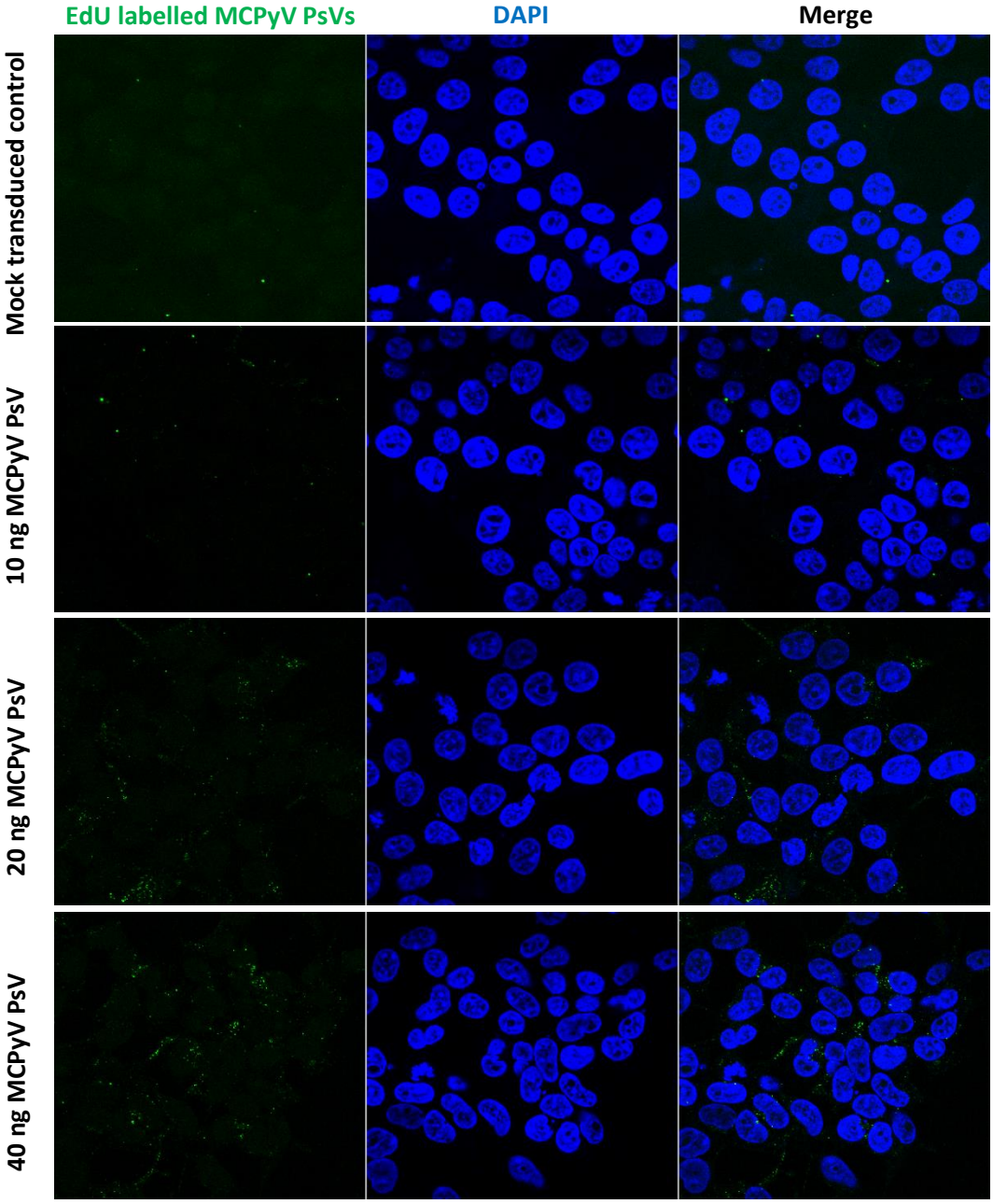

Figure 3.11: Detection of EdU labelled MCPyV PsVs at a range of concentrations to confirm successful integration of EdU into PsVs. MCPyV PsVs were diluted in growth medium to the desired concentration before addition to 293TT cells grown on coverslips. Following a 48-hour incubation cells were fixed, and a click reaction performed to label EdU with Alexa Fluor 488. Coverslips were mounted using mounting medium containing DAPI and imaged using a Zeiss LSM880 upright confocal microscope using pre-set filters for each fluorophore.

To further confirm that the reaction was specific, it was determined that the fluorescence observed was due to EdU detection within cells and not due to background artefacts. In addition to detection of Alexa Fluor 488 labelled EdU, brightfield imaging was also performed to visualise the outline of cells. Results showed that the detection of EdU was specifically within the boundaries of the cell (Figure 3.12). This suggested that only PsVs that had bound to or penetrated the cell were detected and that there was no background signal produced by the click reaction.

Together the data presented in Figure 3.11 and Figure 3.12 confirmed that NanoLuc reporter-containing MCPyV PsVs incorporated EdU which could be detected by click chemistry to investigate penetration, trafficking and subcellular localisation of PsVs.

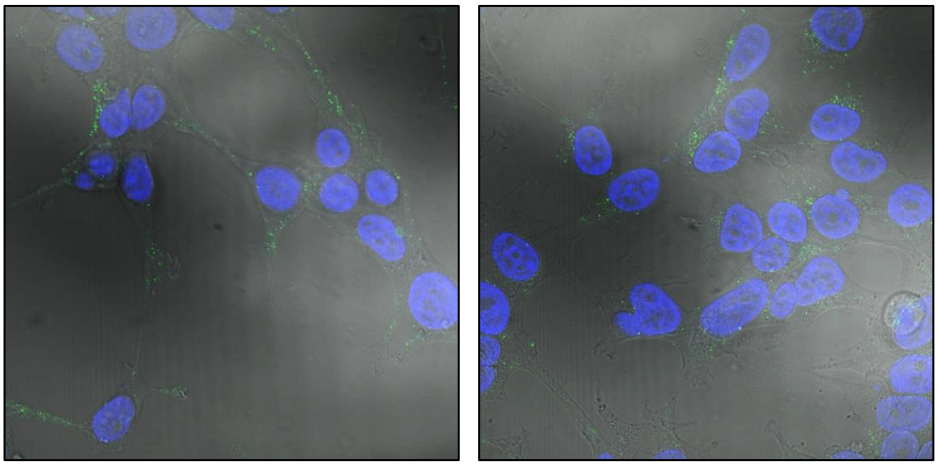

Figure 3.12: Confirmation that EdU labelled MCPyV PsVs are detected within cells. MCPyV PsVs were added to 293TT cells grown on coverslips. Following a 48-hour incubation cells were fixed, and a click reaction performed to label EdU with Alexa Fluor 488. Coverslips were mounted using mounting medium containing DAPI and imaged using a Zeiss LSM880 upright confocal microscope using pre-set filters for each fluorophore. Brightfield imaging was used to visualise the cell cytoplasm.

3.9 Development of a high-throughput SV40 infection system

Similar to MCPyV and other polyomaviruses, there are limited high-throughput assays available for drug screening following SV40 infection. Current methods of detection typically rely upon Western blotting, however a recent example utilises flow cytometry which shortened assays to 48 hours. Although in both cases these assays are laborious, time consuming and given inefficiencies in cell loss during washes and lysis require large amounts of reagents.

Previous unpublished data obtained in the Macdonald group (University of Leeds) had successfully adapted an HCV protocol that used immunofluorescent staining coupled with Incucyte analysis to determine virus titre of BKPyV stocks, which has more recently been utilised to determine SV40 titre. This protocol used immunofluorescent detection of the late structural protein VP1 in cells following fixation. VP1 was chosen to visualise BKPyV infected cells due to an inability to detect early viral proteins following infection.

Given the premise that the aim was to investigate early events in the lifecycle of polyomaviruses, VP1 did not represent an ideal target for evaluation as this could also encompass other aspects of the virus lifecycle, such as the switch between early and late expression and DNA replication. We therefore decided to explore whether it would be possible to use immunofluorescent staining to perform SV40 infection studies using a T antigen antibody.

Vero cells were infected with SV40 for 2 hours before addition of fresh growth medium and fixation after a 24-hour incubation. Following immunostaining using LT antibody and an Alexa Fluor 488 conjugated secondary antibody, wells were imaged using an EVOS FL Auto 2 imaging System. Given that the antibody had not been previously validated, a range of dilutions were tested. Across the dilution series used no visible loss of detection was observed, shown in Figure 3.13 is the lowest concentration of antibody tested (diluted 1:200). In comparison, the mock infected cells were incubated with antibody at the highest concentration used (diluted 1:20) but showed no sign of staining. This confirmed that immunostaining for SV40 LT was a viable option for detection and that a 96 well plate format could be used. This

enabled the volume of reagents and the time taken to complete an experiment to be significantly reduced compared to other previously utilised methods.

Following validation that the LT antibody could be used for immunostaining infected cells, it was next determined whether Incucyte imaging could be performed. Fixed and stained plates were therefore imaged using the Incucyte (Figure 3.14). Results showed that SV40 LT immunostaining was successfully detected by Incucyte imaging and therefore confirmed that similarly to the previously described system for MCPyV, Incucyte analysis was a viable system for evaluation of SV40 infection.

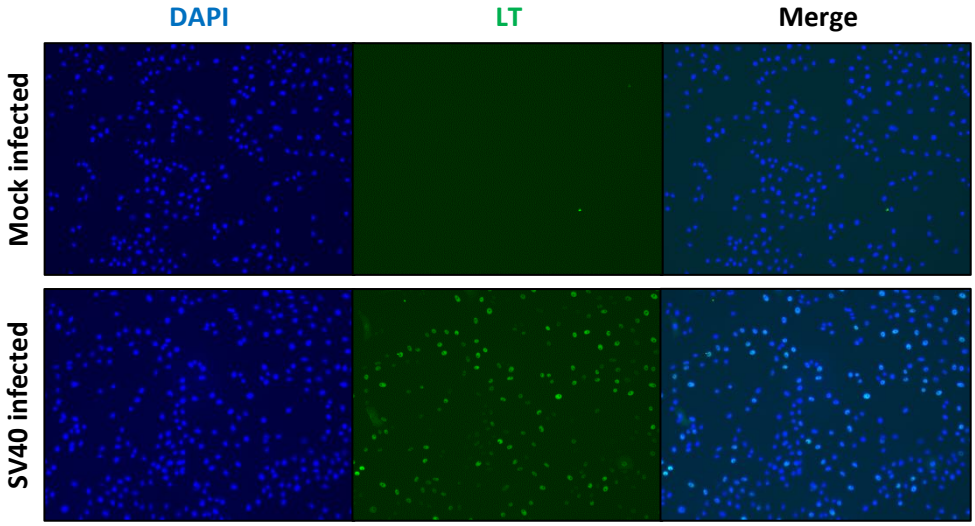

Figure 3.13: Evaluation of SV40 LT staining following infection of Vero cells. Vero cells seeded into 96 well plates were infected with SV40 for 2 hours at a MOI of 1. Fresh growth medium was added, and cells fixed after 24 hours. Following permeabilization and blocking, SV40 LT antibody and a species-specific Alexa Fluor 488 secondary antibody were sequentially used to stain LT. During washes following secondary antibody incubation, DAPI in PBS was incubated with cells to stain nucleic acid. Cells were imaged using an EVOS FL Auto 2 Imaging System.

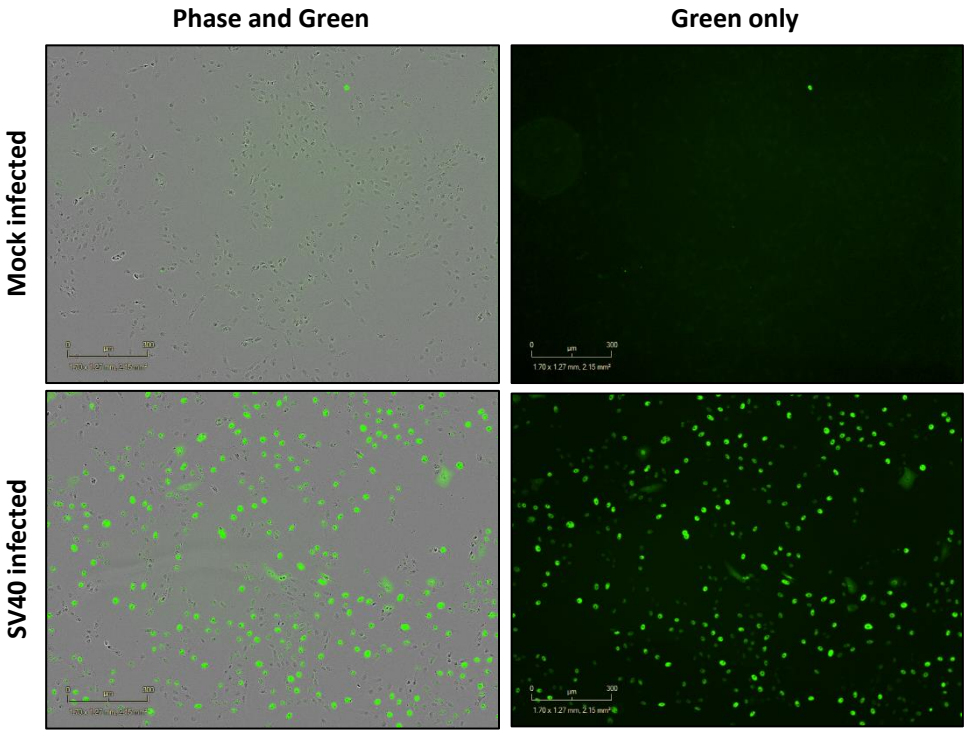

Figure 3.14: Evaluation of SV40 LT staining of infected Vero cells by Incucyte analysis. Vero cells seeded into 96 well plates were infected with SV40 for 2 hours at a MOI of 1. Fresh growth medium was added with cells fixed after 24 hours. Following permeabilization and blocking, SV40 LT antibody and a species-specific Alexa Fluor 488 secondary antibody were sequentially used to stain LT. The plate was added to an Incucyte before detection of phase and green fluorescence was performed using predefined settings.

3.10 A novel system for SV40 stock titre determination

Following confirmation that Incucyte analysis was a viable method for determining infection, we explored the possibility of utilising this method for quantification of SV40 virus stock titre. Stock titre is typically determined by hemagglutination assay, qPCR or plaque assay, which all have disadvantages. A hemagglutination assay whilst relatively quick, does not provide information regarding how many capsids are viable. Due to polyomaviruses readily encapsidating host genomic DNA in addition to viral genomes alongside 'empty' capsids, there is the potential of varied and false titres. In contrast a plaque assay provides a more accurate measure of viable virions at the expense of time, with assays typically taking at least 2 weeks for the formation of small yet visible plaques.

We therefore tested whether a previously published method of HCV quantification could be adapted to SV40. A stock of SV40 provided by the Macdonald laboratory (University of Leeds) with a titre of approximately $7.5x10^5$ infectious units/mL (IU/mL) was 2-fold serially diluted before incubation with Vero cells for 2 hours in 96 well plates. Fresh growth medium was then added before fixation 24 hours post infection. Cells were permeabilised and stained using a LT specific antibody before secondary detection using a species-specific antibody conjugated to Alexa Fluor 488. The immunostained plate was then imaged using an Incucyte with four images taken per well. Representative images of the serial dilution are shown in Figure 3.15. As expected, the mock infected cells showed no detection of fluorescence. Evaluation by eye revealed that there was little change in the number of positive cells in dilutions 1:5 to 1:40, suggesting that at lower dilutions the system was saturated. For higher dilutions, from 1:80 downwards, there was a step-wise reduction in the number of positive cells as would be expected. Values for triplicate wells at each dilution were determined using the Incucyte analysis software (Figure 3.16A). Values determined by the Incucyte showed that low dilutions produced raw reads around $1x10^4$ LT positive cells/well, which given initial seeding of $5x10^3$ Vero cells and an approximate doubling time of 24 hours in cell culture, is consistent with most cells been infected and saturation of the system. For 1:40 dilutions onwards there is a steady sigmoidal decrease in the number of SV40 positive cells, with dilutions of 1:2560 and higher showing detection near to that of the negative mock.

In order to determine IU/mL reciprocal values were calculated by reversal of dilution factors (Figure 3.16B). Following reversal of dilution factors there was an initial linear positive phase, indicative of system saturation. Highlighted in green is the plateau that is representative of IU/mL. The plateau represents the region whereby the system is not saturated but before hypervariability induced by disproportional amplification of small variables in infected cell count (shown in red). To calculate IU/mL from the plateau, an average between all values was found. The example presented yielded a calculate $7.48x10^5$ IU/mL which is directly comparable to the provided $7.5x10^5$ IU/mL stock. This therefore demonstrated that the system was a viable and accurate method for determination of SV40 virus titre, whilst also using

less reagents and reducing incubation periods compared with other potential methods.

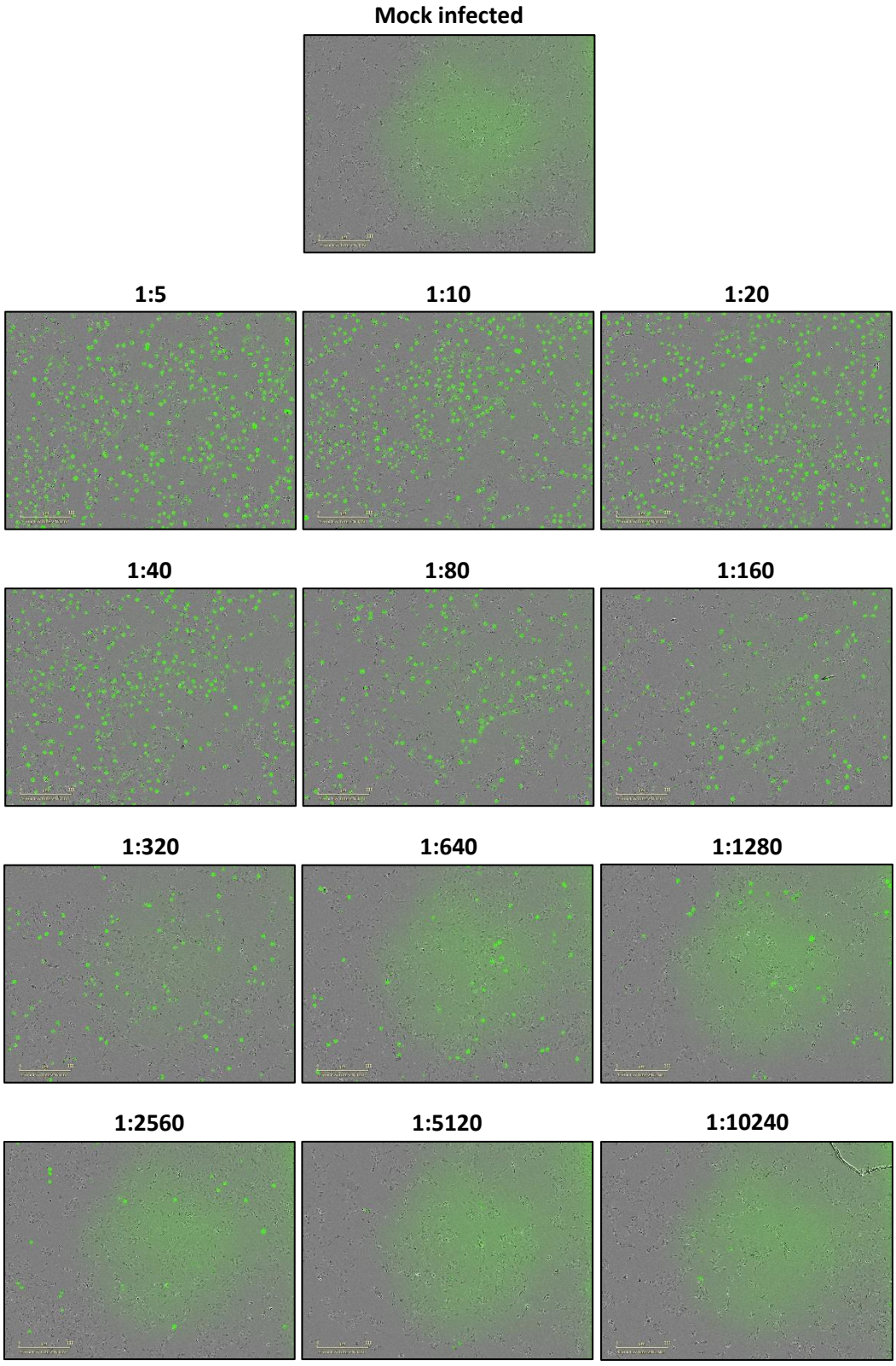

Figure 3.15: Incucyte imaging of Vero cells infected with serially diluted SV40. Vero cells plated into 96 well plates were incubated with serially diluted virus stocks for 2 hours before the addition of fresh growth medium before fixation after 24 hours. Following permeabilization and blocking, SV40 LT antibody and a species-specific Alexa Fluor 488 secondary antibody were sequentially used to stain LT. Plates were then imaged for phase and green fluorescence using an Incucyte, with four images taken of each well. Each dilution was performed in triplicate, with representative images shown.

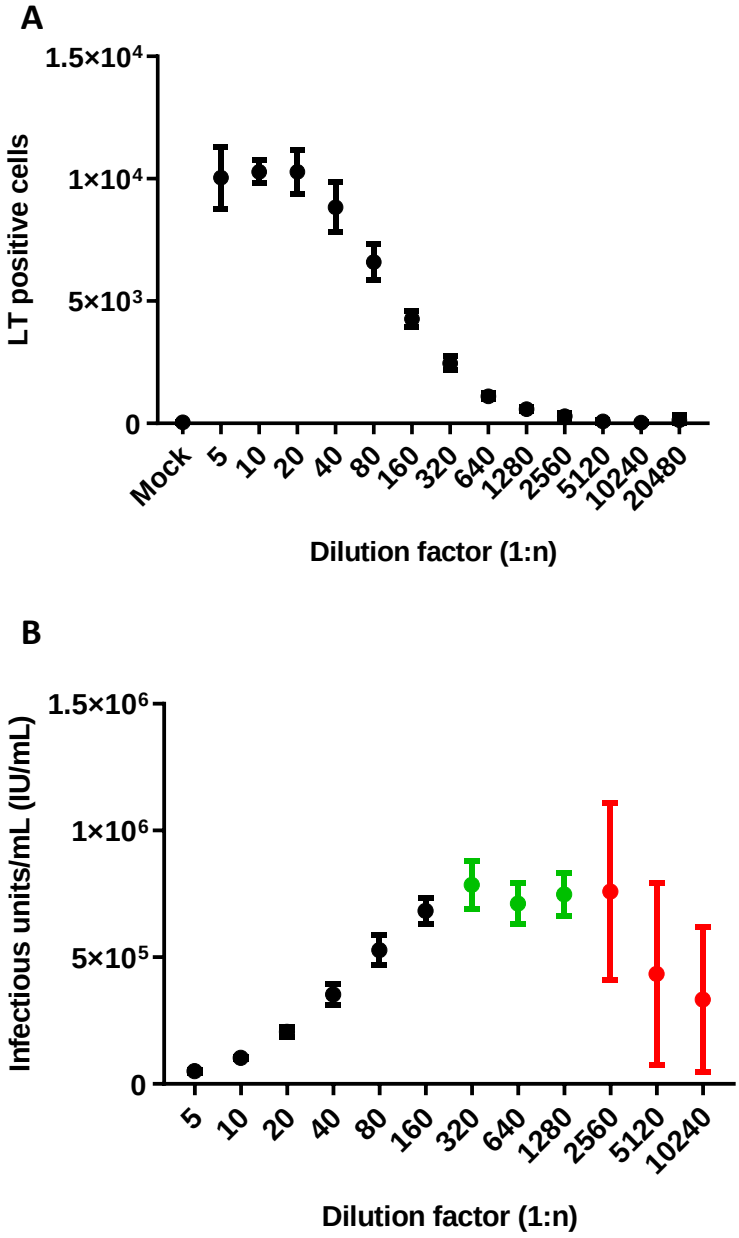

Figure 3.16: Quantification of SV40 stock titre using Incucyte detection and analysis. Following imaging of wells using an Incucyte, a predefine processing definition was used to calculate the number of SV40 LT positive cells in each well (A). IU/mL was then calculated by reversing dilution factors (B). Green data points represent the plateau used to calculated IU/mL. Red data points are indicative of hypervariability following slight fluctuation in positive cells which are amplified following reversal of dilution factors.

3.11 Discussion

The poor characterisation of events during the lifecycle of MCPyV is due to several reasons, but predominantly due to a lack of systems available to study the virus. Until recently there were no efficient methods to determine aspects of the viral lifecycle. Despite the identification of human dermal fibroblasts enabling complete replication, this system requires challenging conditions that are not easily reproducible (Liu et al., 2016). To evaluate early events including attachment and entry, PsVs have therefore been utilised as initial infection itself does not appear to be the limiting factor during the viral lifecycle, with several cell types permissive to initial infection (Pastrana et al., 2009). An added benefit of using alternative cell lines is the ability to move away from primary cell culture, which whilst an essential aspect of cellular biology, is less well suited to high-throughput experimentation due to increased sensitivity and requirements in comparison to easily cultured and more robust transformed cell lines. Given that infection can be achieved in other transformed cell lines, this suggests that initiation of transcription and/or translation is most likely inefficient in primary cells and presents a key mediator of cellular tropism. The use of PsVs however bypasses this issue through packaging of reporter vectors that utilise more efficient promoters, permitting the evaluation of early lifecycle events in more proficient systems. Whilst previous methods to produce MCPyV PsVs have been well documented, use had until recently been limited to binding and initial entry, with subsequent events broadly encompassed by trafficking to the nucleus yet to be elucidated.

Although the literature provided somewhat detailed protocols for production of PsVs, several areas still required optimisation. Subtle alterations to the production and purification of MCPyV PsVs led to enhanced yield and in particular significant improvement in the purity of stocks. Initial purification attempts resulted in large amounts of contaminants, which were assumed to be aggregated protein or large fragments of partially encapsidated DNA. Through increasing the centripetal force applied during ultracentrifugation, better sample purity was achieved. Given that there was increased detection by silver staining in the final fractions, it was believed that the higher forces permitted larger aggregates to pass further through the

gradient whilst PsVs were unable to penetrate the lower cushion. Purity was further confirmed by electron microscopy, which showed that contamination was removed by increased centripetal force.

An issue facing the use of PsVs in high-throughput assays was the ease at which experimentation could be performed. Previously, GFP reporter constructs were used alongside flow cytometry to determine the number of infected cells, which was both time consuming and wasteful with reagents given that processing would require larger starting cell numbers. A method of live cell detection using an Incucyte was therefore successfully adopted. This system reduced the size and cost associated with each sample and also meant that a greater number of samples could be simultaneously processed, whilst maintaining unbiased analysis through automated computational quantification.

To visualise the location of PsVs an alternative system that utilised EdU-labelled PsVs was produced. EdU was used to label genomic content rather than the more tradition BrdU due to the method of detection. BrdU relies upon antibody detection methods, which for most applications is straight forward and follows standard immunostaining protocols. However, an issue arises when DNA is encapsidated inside a virion as the bulky antibodies used for detection cannot penetrate formed capsid shells. In contrast, EdU reactions require a much smaller molecule conjugated to a fluorescent probe which can be covalently attached by click chemistry. The size of the molecule is crucial, as this is small enough to pass through the small holes between VP1 pentamers that make up the virus capsid in order to label the contained vector and visualise subcellular localisation.

In addition to methods described for the detection of MCPyV, a novel high-throughput protocol to determine virus titre and in experimentation using SV40 is described.

Determination of SV40 titre is typically performed by plaque assay, which given the speed of viral propagation generally requires several weeks of incubation before sufficient plaque formation. In contrast, the described method used a 96-well plate format and an incubation of only 24 hours before fixation and immunofluorescent detection of SV40 T antigen positive cells. Coupled with Incucyte detection, which

negates the requirement of manual counting, this had led to a novel method of detection that is significantly quicker than tradition alternatives whilst maintaining comparable accuracy.

The use of immunostaining and Incucyte analysis has also permitted the development of a high-throughput screening method to evaluate inhibitor effects upon early lifecycle events. Typically, Western blotting to determine whether T antigens are expressed has been used to investigate changes in infection. This method provides reasonable information regarding the total amount of T antigen, but it fails to indicate whether less cells are infected or if replication is impeded, therefore immunostaining and manual cell counting is performed to determine which aspect of the early viral lifecycle is affected. Whilst Incucyte analysis could also provide information regarding fluorescence intensity which would be indicative of total protein present, in this instance it was optimised in a binary manner whereby the number of infected cells was calculated to determine how many cells are virus positive. This could permit high-throughput screening of inhibitor effects during SV40 infection in a 96-well plate format.

In summary this chapter described the optimisation of MCPyV PsV production and how existing protocols were adapted to permit high-throughput assays to determine the effects of inhibitors upon early stages of the viral lifecycle. In addition, a novel and rapid method for the quantification of SV40 viral titre was developed, which can be further utilised for inhibitor screening. The described procedures were taken forward for use in experiments to determine polyomavirus host cell requirements during entry and trafficking, which are described in Chapter 4.

Chapter 4

Ion channels and polyomavirus infection, novel therapeutic targets?

4.1 Introduction

The mechanisms by which polyomaviruses infect the host are mostly shrouded in uncertainty. This is in part due to lack of appropriate systems but also limited studies have been performed to elucidate these early events. Given that many diseases associated with polyomaviruses are generally due to persistent infections that lead to severe degradation of tissues, it is surprising that host factors required for infection of naïve cells have not been better studied. Restriction of infection could be a viable option for therapeutic intervention and ultimately prevention of disease progression.

SV40 is the most widely studied of the *Polyomaviridae* and the assumption is often made that other family members will follow similar routes of infection. However, SV40 and MCPyV represent arguably one of the most variable compositions of the polyomavirus family. Despite the principally similar composition of polyomavirus genomes, the encoding of an additional early protein for MCPyV (57 kT) and three additional late proteins for SV40 (agnoprotein, VP3 and VP4) there is the potential that variable entry mechanisms are required (Stakaityte et al., 2014; Moens et al., 2017). Whilst agnoprotein and VP4 are not incorporated into the capsid and are most likely required to assist viral egress, a major difference between MCPyV and many other polyomaviruses, including SV40, is that there is no expression of a second minor capsid protein (Schowalter and Buck, 2013). The additional minor capsid protein present in VP3-containing virions is believed to facilitate secondary interactions and loss of either VP2 or VP3 leads to perturbation of JCPyV infection (Nelson et al., 2015). In contrast, given that MCPyV infects the host without a secondary minor capsid protein suggests that this is dispensable, although it has been proposed that the presence of a larger VP1 could compensate for this loss.

Differences in capsid composition could however mean differences in infection mechanisms. This is highlighted by the observed differential cellular attachment and penetration between polyomaviruses which likely contributes to varied tropisms (Norkin, 1999; Decaprio and Garcea, 2013). However, events following attachment and penetration have been less well studied and there is the potential that these differences could equate to more substantial variation in infection requirements

within the host during stages, such as trafficking and genome release. It has been well established that polyomaviruses traffic through the endo/lysosomal network and it is believed that acidification is required for initiation of capsid rearrangement and destabilisation facilitating genome release. The mechanisms by which acidification occurs is currently unclear, however there is an emerging field that identifies ion flux to be important and these alterations are regulated by host cell ion channels.

Specific requirements of ion channels during the lifecycle of polyomaviruses have previously been characterised (Evans et al., 2015; Stakaityte et al., 2018). Within the Whitehouse group, CLIC channels have been shown to be important for MCPyV ST enhanced cellular motility and Evans *et al.* identified the importance of anion homeostasis during non-lytic virion release of BKPyV. To date however, no studies have investigated the potential role of ion channels during early events of polyomavirus infection, despite identification of requirements for other viral families. For example, K^+ ions are required for acidification events during initial Bunyamwera infection and two pore Ca^{2+} channel inhibition severely restricts Ebola infection (Sakurai et al., 2015; Hover et al., 2016; Hover et al., 2018).

Using systems described in Chapter 3, we investigated whether MCPyV required acidification of the endo/lysosomal network similarly to other polyomaviruses. The requirement of ion channels during transduction of MCPyV and infection of SV40 was characterised, with identification of K^+ ion channels as a novel requirement during MCPyV entry. It was confirmed that the clinically available Ca^{2+} channel inhibitor verapamil could restrict both MCPyV and SV40 and that the T-type Ca^{2+} inhibitors mibefradil and flunarizine ablated MCPyV entry. Therefore, Ca^{2+} channel inhibitors potentially represent candidate targets to restrict polyomaviruses that cause disease through a persistent, continuous infection that cause tissue degradation, particularly in an immunocompromised host.

4.2 MCPyV PsVs appear to localise to vesicular structures

During development of the previously described EdU system to visualise MCPyV PsVs within cells, it was noted that the PsVs appeared to localise in vesicular structures.

To validate these observations, 293TT cells were incubated with PsVs for 48 hours before fixation and a click reaction performed to visualise PsVs. Consistent with previous observations it was confirmed that the click reaction was highly specific and that PsVs appeared to localise in spherical structures within cells (Figure 4.1).

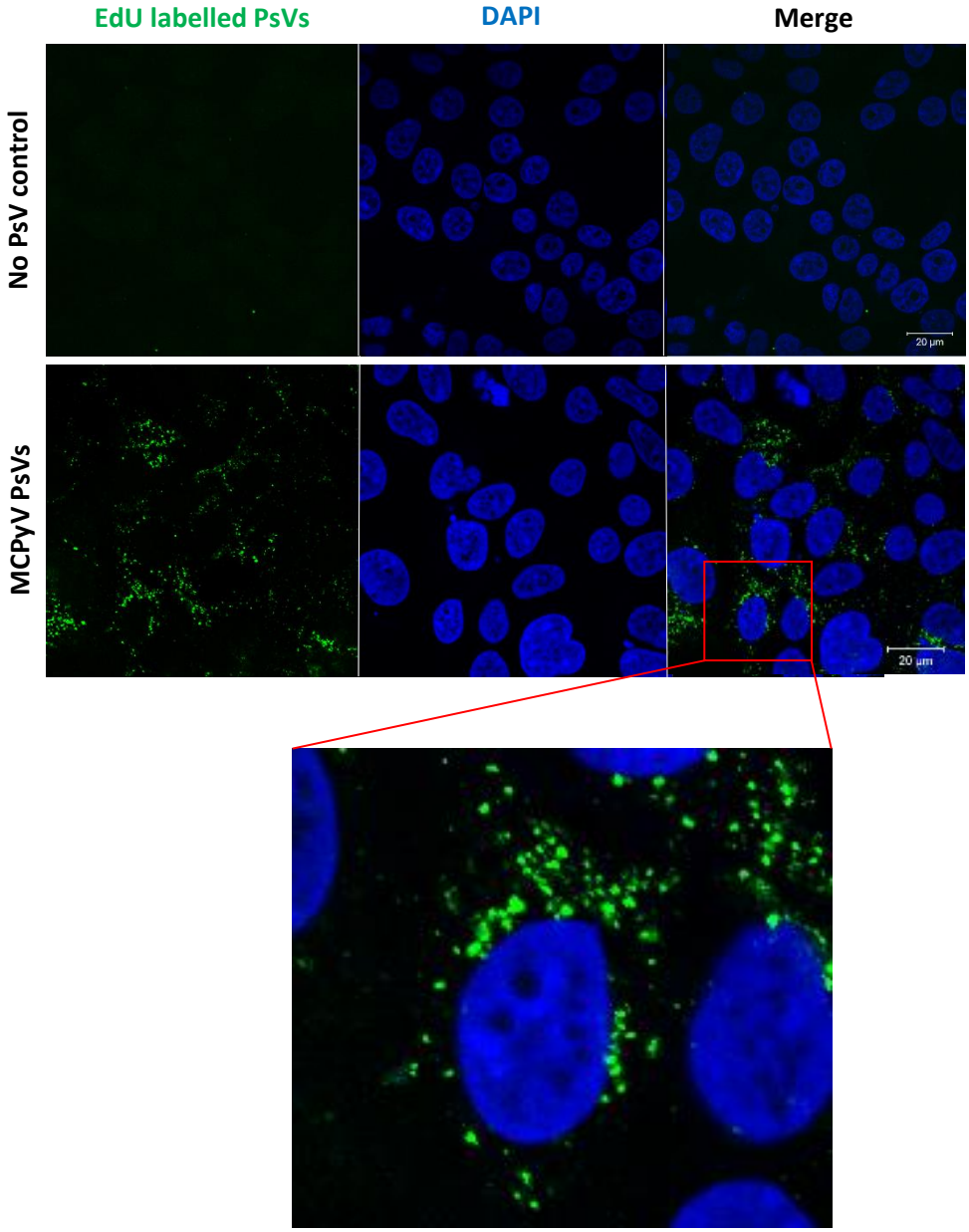

Figure 4.1: MCPyV PsVs localise to spherical structures. 293TT cells were transduced with EdU-labelled MCPyV PsVs with fixation after a 48-hour incubation. Cells were permeabilised before a click reaction was performed to label PsVs with Alexa Fluor 488. Cells were visualised using a ZEISS LSM880 upright confocal microscope and DAPI staining was used to identify nuclei. Scale bar 20 µm.

4.3 MCPyV traffics through the endosomal system

Following penetration, polyomavirus virions traffic through the endosomal network before arriving at the nucleus, where the genome is released (Geiger et al., 2011; Kuksin and L. C. Norkin, 2012b). Whilst this holds true for all tested polyomaviruses, whether this requirement would be conserved by MCPyV, given that the capsid is composed of only one minor capsid protein is unknown. Therefore, it was determined whether MCPyV PsVs localised to endosomal compartments. 293TT cells were transduced with EdU labelled PsVs, fixed at 48 hours and a click reaction performed. Late endosomes/lysosomes were visualised using antibody detection of the lysosomal-associated membrane protein 2 (LAMP2). Results showed that PsVs colocalised with LAMP2 coated vesicles (Figure 4.2). This was further supported by detection of PsVs primarily in regions with high amounts of LAMP2.

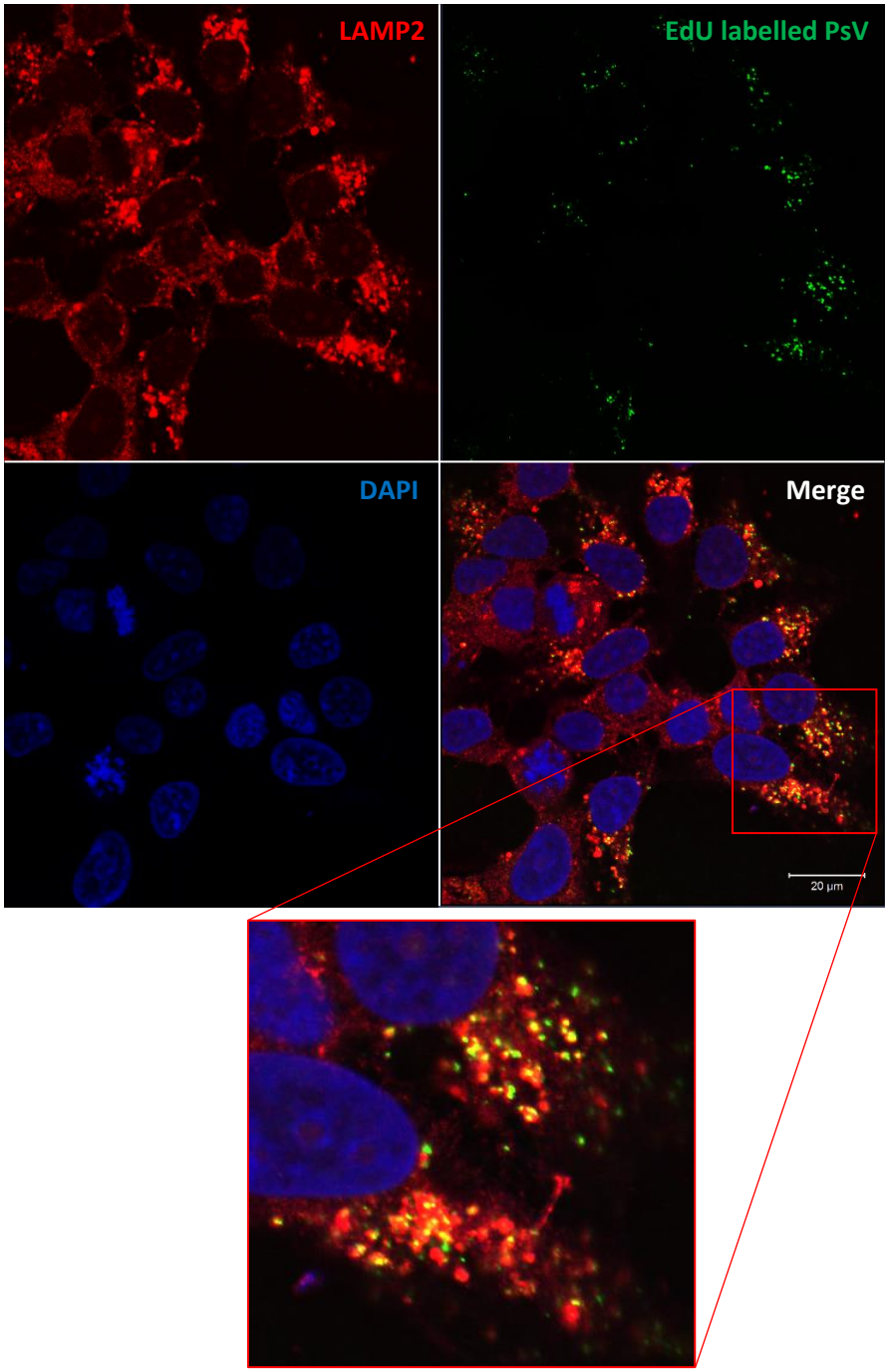

Figure 4.2: MCPyV PsVs colocalise to vesicles coated with LAMP2. 293TT cells were transduced with EdU-labelled MCPyV PsVs with fixation after a 48-hour incubation. Cells were permeabilised before a click reaction was performed to label PsVs with Alexa Fluor 488. Following the click reaction, endo/lysosomes were labelled through immunostaining using a LAMP2 antibody, with a secondary species-specific antibody conjugated to Alexa Fluor 546 used for visualisation. Cells were visualised using a ZEISS LSM880 upright confocal microscope and DAPI staining was used to identify nuclei. Scale bar 20 µm.

4.4 MCPyV requires an acidified environment during entry

Polyomaviruses require an acidic environment during entry (Gilbert and Benjamin, 2000). It is thought that acidification is required to initiate proteolytic rearrangements of the capsid, destabilising the integrity to allow conformational shifting before further processing and ultimately release of genomic contents. Although, this had not been confirmed for MCPyV.

To evaluate if acidification is required during MCPyV entry, 293TT cells were treated with ammonium chloride (NH_4Cl) in the presence of GFP-reporter containing MCPyV PsVs. NH_4Cl can passively enter cells before accumulating in compartments of the endosome-lysosome system, where it deprotonates to neutralise pH preventing the acidification of endosomes and lysosomes.

Results showed that treatment with NH_4Cl significantly impeded MCPyV transduction at both 5 mM and 10 mM, with 66% and 87% reduction in average number of GFP positive cells relative to untreated, respectively (Figure 4.3). This further suggested that MCPyV, like other polyomaviruses, shares a conserved requirement for acidification.

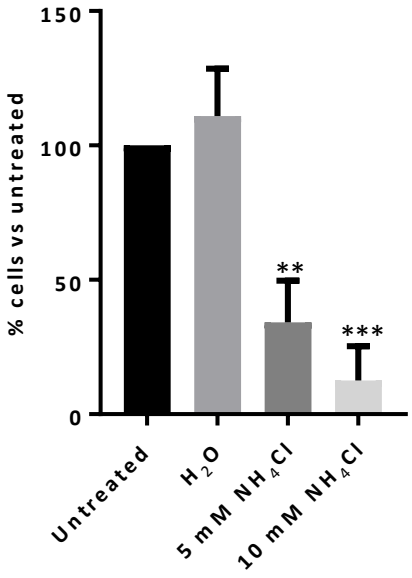

Figure 4.3: MCPyV transduction is dependent upon endosomal acidification. 293TT cells were pre-treated with drugs for 1 hour prior to a 2-hour incubation with MCPyV GFP PsVs in the presence of drug. Fresh medium was then added before incubation and visualisation of GFP-positive cells after 72 hours using an Incucyte ZOOM instrument. Predetermined analysis parameters were used to identify the number of GFP-positive cells for each sample before comparison to an untreated control.

To confirm that NH_4Cl treatment did not perturb penetration or GFP expression a range of control experiments were performed. Firstly, EdU-labelled PsVs were used to transduce cells in the presence of 10 mM NH_4Cl. Imaging showed that in the presence of drug, PsVs still penetrated cells and displaying a comparable distribution to control cells (Figure 4.4A). This confirmed that PsV penetration was unaffected by 10 mM NH_4Cl, suggesting that the effect was either upon trafficking or expression. To investigate whether 10 mM NH_4Cl had a detrimental effect upon the expression of GFP, cells were transfected with vector and treated with 10 mM NH_4Cl to determine whether any detrimental effect upon translation occurred. Results showed that treatment with 10 mM NH_4Cl had no effect upon expression of GFP (Figure 4.4B). As a further test, cells were again transfected with GFP before Incucyte imaging and analysis was performed. Using identical parameters of analysis that were defined for PsV assays, results showed that NH_4Cl treatment had no effect upon

the number of GFP positive cells (Figure 4.4C). Taken together these results showed that NH_4Cl affected MCPyV trafficking events and was not related to cellular penetration or GFP expression.

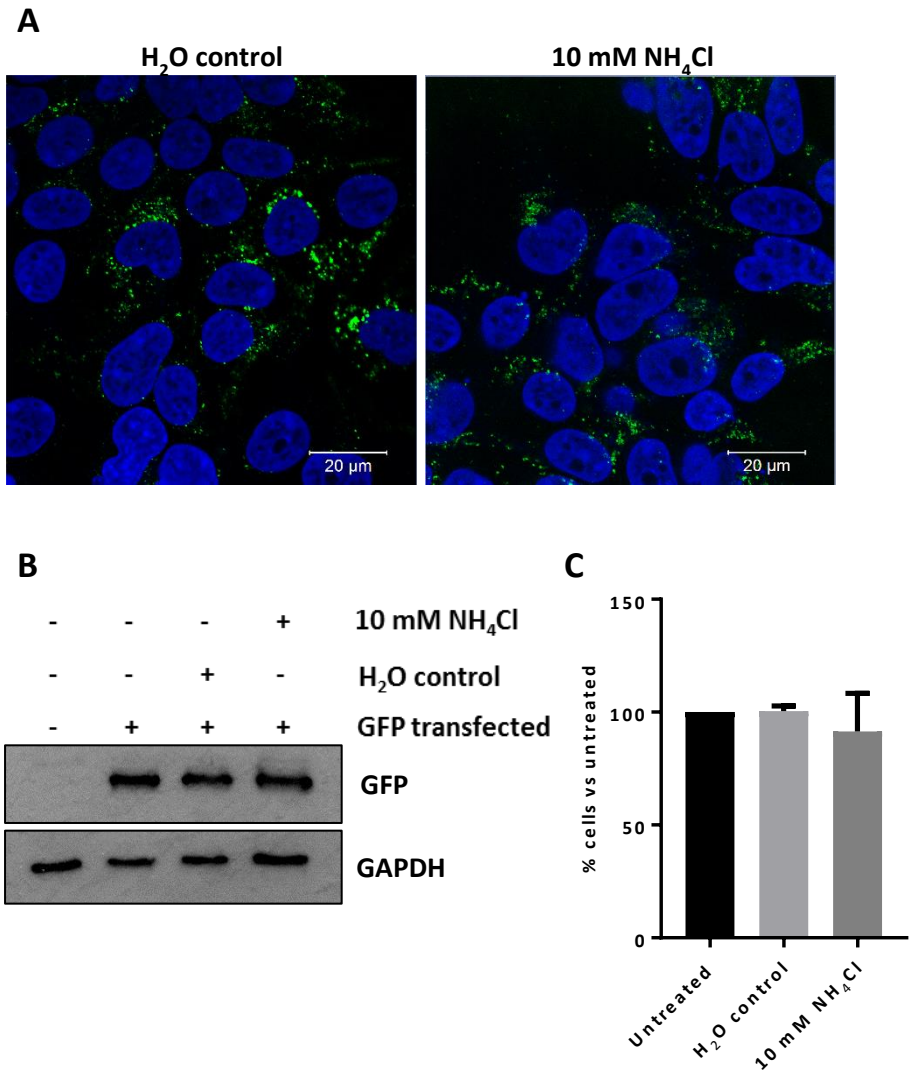

Figure 4.4: Treatment with NH_4Cl does not affect PsV penetration or GFP expression. (A) 293TT cells were transduced with EdU-labelled MCPyV PsVs with fixation after a 48-hour incubation. Cells were permeabilised before a click reaction was performed to label PsVs with Alexa Fluor 488. Cells were visualised using a ZEISS LSM880 upright confocal microscope and DAPI staining was used to identify nuclei. Scale bar 20 µm. (B+C) 293TT cells were incubated with GFP containing transfection complexes for 6 hours. Fresh growth medium containing drug was then added for a further 18 hours before lysis and Western blotting to detect the amount of GFP expressed (B) or evaluation of GFP-positive cells using an Incucyte with predetermined analysis parameters (C).

4.5 MCPyV PsVs enter acidified compartments

In addition to preventing acidification, NH_4Cl may have additional intracellular effects leading to vesicle swelling and reduced intralysosomal proteolysis. Alternative classical inhibitors of endosomal trafficking and acidification including wortmannin, monensin and chloroquine diphosphate were therefore tested. However, in all cases results showed that the inhibitors led to high rates of cell death at inhibitory concentrations and were therefore discarded (data not shown).

An alternative approach was therefore adopted using EGA. EGA is a drug that blocks a range of toxins from entering cells, including anthrax lethal toxin and diphtheria toxin (Gillespie et al., 2013; Schnell et al., 2016). Whilst EGA targets endosomal trafficking pathways, the mechanism of action is vastly different to that of NH_4Cl. EGA has no effect upon pH or acidification. However, when an endosome or lysosome becomes acidified, EGA prevents target membrane docking and release of cargo, instead leading to sequestration and accumulation of vesicles. Therefore, if MCPyV required and/or entered into acidified endo/lysosomes following penetration, virions would become trapped and unable to exit from the subsequently sequestered compartments.

Results showed that treatment with 10 μM and 25 μM EGA severely impaired transduction of 293TT cells, with an average reduction in GFP positive cells compared to untreated controls of 84% and 81%, respectively (Figure 4.5). This confirmed that MCPyV entered endosomes and remained contained within the vesicles during acidification.

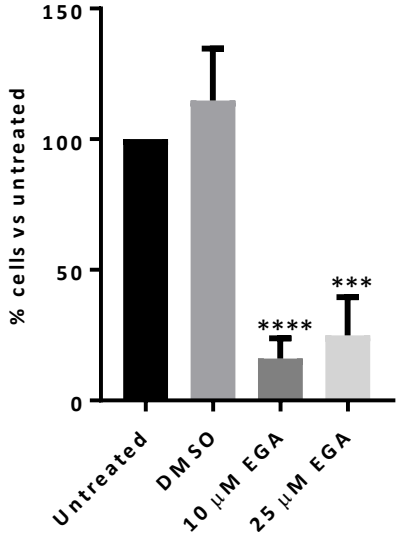

Figure 4.5: Treatment with EGA inhibits MCPyV entry. 293TT cells were pre-treated with drugs for 1 hour prior to a 2-hour incubation with MCPyV GFP PsVs in the presence of drug. Fresh medium was then added before incubation and visualisation of GFP-positive cells after 72 hours using an Incucyte ZOOM instrument. Predetermined analysis parameters were used to identify the number of GFP-positive cells for

Similarly to NH_4Cl, it was determined whether EGA had off-target effects upon penetration or GFP expression. Firstly, EdU-labelled PsVs were utilised to show that penetration of the cell occurred (Figure 4.6A). Interestingly, in the presence of EGA, EdU puncta appeared larger and less dispersed in comparison to the solvent control. This observed phenotype supported the hypothesis that EGA leads to accumulation of acidified compartments into which MCPyV virions were sequestered. Following transfection of GFP into cells, results showed that translation was not affected and no change in the detection of GFP positive cells was observed (Figure 4.6B and Figure 4.6C, respectively). This confirmed that MCPyV traffics through the endosomal network and that acidification is essential for efficient transduction of cells.

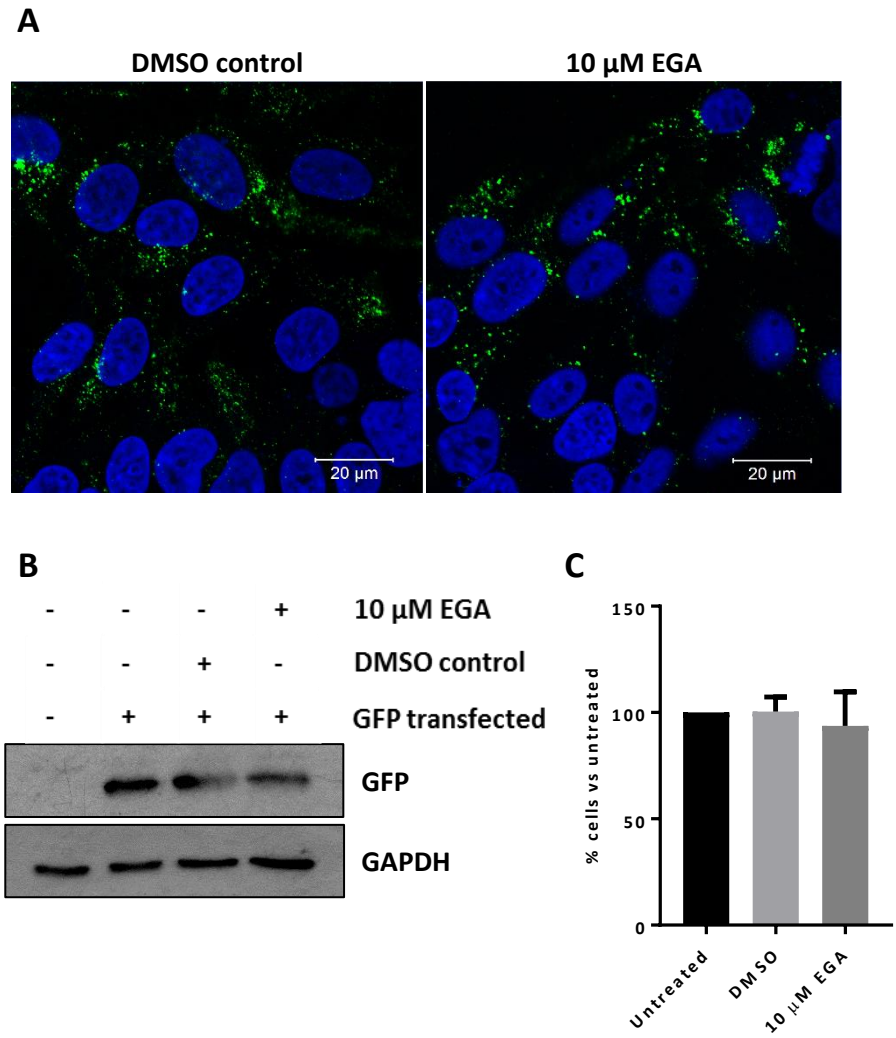

Figure 4.6: EGA does not affect MCPyV penetration or GFP expression. (A) 293TT cells were transduced with EdU-labelled MCPyV PsVs with fixation after a 48-hour incubation. Cells were permeabilised before a click reaction was performed to label PsVs with Alexa Fluor 488. Cells were visualised using a ZEISS LSM880 upright confocal microscope and DAPI staining was used to identify nuclei. Scale bar 20 µm. (B+C) 293TT cells were incubated with GFP containing transfection complexes for 6 hours. Fresh growth medium containing drug was then added for a further 18 hours before lysis and Western blotting to detect the amount of GFP expressed (B) or evaluation of GFP positive cells using an Incucyte with predetermined analysis parameters (C).

4.6 Manipulation of the endo/lysosomal network is time dependent

Post penetration, polyomaviruses traffic slowly through the cytoplasm to the nucleus. SV40 is the best characterised of the polyomaviruses and appears to be the most efficient in terms of entry and early protein production. However, the required partial disassembly and presentation of VP2/3 in the ER does not occur until 6 hours post infection and subsequent release into the cytoplasm to continue trafficking to the nucleus may potentially take up to 12 hours or longer (Kuksin and L. C. Norkin, 2012a). Previous results in Chapter 3 showed that MCPyV PsVs typically require a minimum incubation of 72 hours, whilst following SV40 infection, early proteins could be detected at 24 hours. Given that MCPyV appeared to traffic more slowly, a time-course using larger 24-hour intervals was therefore performed.

293TT cells were pre-treated for 1 hour with 10 mM NH_4Cl or 10 μM EGA before addition of MCPyV PsVs. Following removal of PsV containing medium, cells were incubated in either drug for a period of 24, 48 or 72 hours, with shorter time points washed with PBS and addition of medium without either drug for remaining time up to the 72-hour endpoint. Drugs were also introduced after 24 and 48 hours to evaluate any effects occurring later during entry. Results showed that inhibition of MCPyV transduction by both NH_4Cl and EGA was time-dependent (Figure 4.7).

Treatment with NH_4Cl for 48 and 72 hours led to significant inhibition of transduction, with 84% and 85% reduction in GFP positive cells, respectively (Figure 4.7A). Interestingly, when NH_4Cl was incubated with cells prior to addition of PsVs, a 166% increase in the number of GFP positive cells was observed, suggesting that shorter treatments may increase the efficiency of transduction. The reasons for this unexpected phenotype were unclear, however possible explanations could range from increased endocytosis in response to loss of endo/lysosomal acidification or a response mechanism that following drug removal led to quicker acidification and trafficking.

Treatment with NH_4Cl for 24 hours showed only a 14% and insignificant change in the number of GFP positive cells compared to the control. This suggested that either MCPyV does not require an acidified environment until later during the entry process

or that PsVs were held in vesicles awaiting acidification which following drug removal was permitted to proceed. In contrast, NH_4Cl treatment for 48 and 72 hours showed a comparable phenotype, with transduction greatly restricted. Addition of NH_4Cl 24 and 48 hours post PsV exposure showed a time-dependent response which returned to control levels of GFP positive cells (35% and 5% reduction, respectively). Given that 24-72-hour treatment led to a large increase in the number of GFP positive cells in comparison to treatment for the initial 48 hours, this suggested that the requirement of acidification for MCPyV occurs around 24 hours post penetration. Results also showed that 48-72-hour treatment had no detrimental effect upon transduction, which further indicated that the inhibitory effect of NH_4Cl was during earlier stages of entry, when virions would still be expected to be in endosomal compartments.

Results for EGA were comparable to that of NH_4Cl, showing clear evidence of time-dependency for drug effects (Figure 4.7B). Unlike NH_4Cl, EGA did not however cause an increase in transduction when incubated during initial attachment. Instead, treatment during attachment led to a 35% reduction in the number of GFP positive cells compared to the control. There is little data available regarding the mechanism of EGA and therefore why this reduction was observed was unclear but could potentially be due to irreversible inhibition, leading to reduced transduction as nascent components were not sufficiently produced during the incubation period. Incubation with EGA over longer periods led to a time-dependent decrease in the number of GFP positive cells, with a decrease in GFP positive cells of 55%, 81% and 88% for 24-, 48- and 72-hour drug incubation periods, respectively. Introduction of EGA at later time points led to recovery of transduction relative to cells treated for the full 72-hour period. When EGA was added from 24-72 hours post attachment a 49% decrease in the number of GFP positive cells relative to control was observed, which following addition of EGA from 48-72 hours displayed a phenotype comparable to control with 99% relative GFP positive cells. Taken together this suggested that NH_4Cl and EGA were inhibiting comparable stages of MCPyV entry and are most likely related to acidification. Given the reported mechanisms of action for both drugs, this provided strong evidence that MCPyV traffics through the

endo/lysosomal network and that acidification was an essential requirement for efficient transduction.

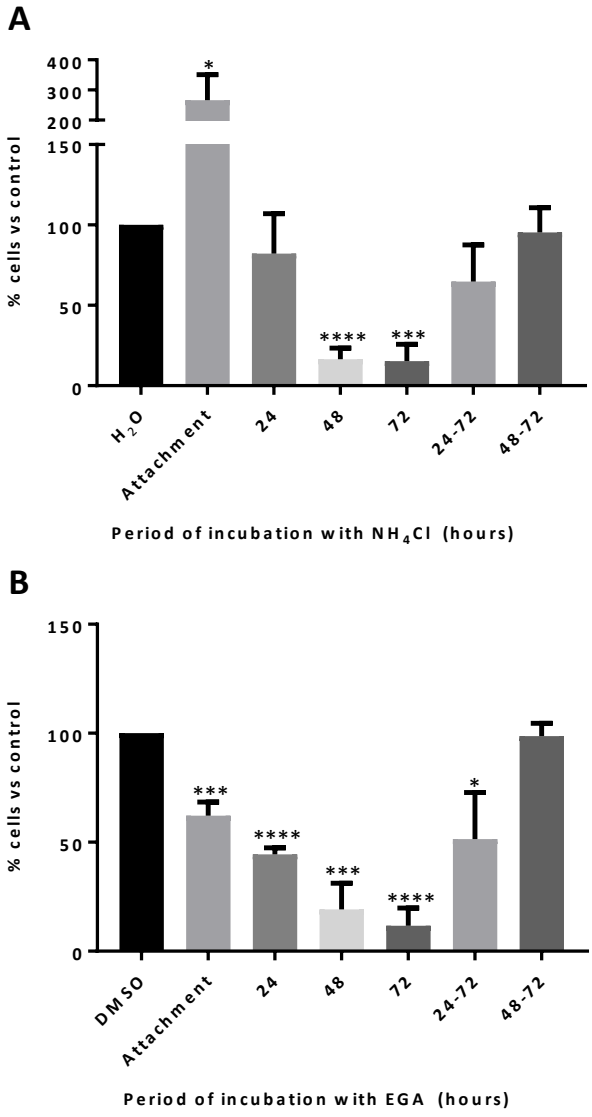

Figure 4.7: NH_4Cl and EGA effects upon MCPyV transduction are time dependent. 293TT cells were infected with MCPyV GFP PsVs in the presence of 10 mM NH_4Cl **(A)** or 10 µM EGA **(B)** for varying periods of time to determine whether infection was time dependent. Unless a time range is indicated (24-72 and 48-72 hours), 293TT cells were pre-treated with drugs for 1 hour prior to a 2-hour incubation with MCPyV GFP PsVs in the presence of drug if applicable. Fresh medium was then added before incubation for the indicated period of time, with introduction or removal of drugs performed in fresh growth medium as required. Visualisation of GFP-positive cells was performed after 72 hours using an Incucyte ZOOM instrument. Predetermined analysis parameters were used to identify the number of GFP-positive cells for each sample before comparison to a solvent control.

4.7 Endo/lysosomal network manipulation inhibits SV40 infection

It had previously been reported that NH_4Cl inhibits SV40 infection (Engel et al., 2011). However. no study has utilised EGA as an inhibitor and therefore it was investigated whether the observed inhibition of MCPyV was comparable to other members of the *Polyomaviridae*.

As previously described, Vero cells were infected with SV40 in the presence of either 10 mM NH_4Cl or 25 µM EGA, with fixation and immunostaining for LT performed 24-hours post infection. Results showed that treatment with NH_4Cl or EGA was detrimental to SV40 infection (Figure 4.8). Treatment with 10 mM NH_4Cl led to a 54% decrease in the number of LT positive cells (Figure 4.8A). 25 µM EGA treatment led to a greater decrease in the number of LT positive cells by 78%, suggesting that it was a more potent inhibitor of SV40 infection, in comparison to 10 mM NH_4Cl. Together these results supported that MCPyV traffics through the cell in a manner that is comparable to other polyomaviruses.

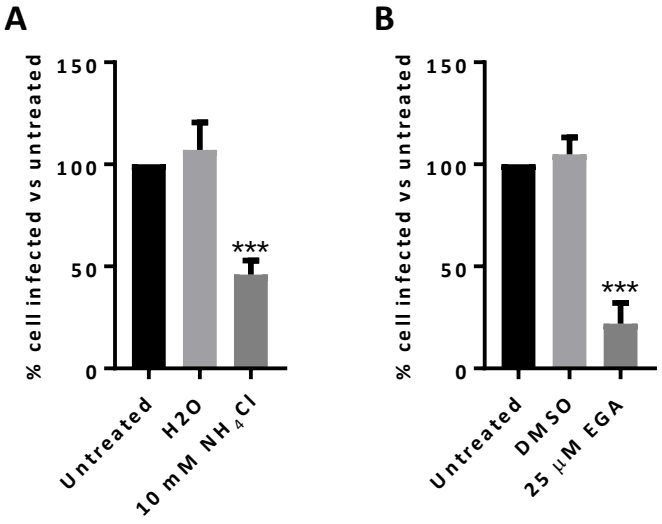

Figure 4.8: SV40 infection is perturbed by treatment with NH_4Cl (A) and EGA (B). Vero cells were pre-treated with drugs for 1 hour prior to a 2-hour incubation with SV40 at a MOI of 1, in the presence of drug. Fresh medium containing drug was then added before fixation following incubation for 24 hours. Cells were permeabilised and immunostained for LT, with a species-specific secondary antibody conjugated to Alexa Fluor 488 used for visualisation. Wells were then imaged using an Incucyte ZOOM instrument. Predetermined analysis parameters were used to identify the number of LT cells for each sample before comparison to an untreated control.

4.8 Broad spectrum ion channel inhibitor screen for MCPyV PsV transduction

The ability of cells to regulate the functions of a maturing endosome is not just dependent upon H^+, but also requires the flux of several ions including Cl^-, K^+, Na^+, and Ca^{2+}(Scott and Gruenberg, 2011).

To establish whether ion channel inhibition is detrimental to MCPyV transduction, PsVs containing the GFP-reporter vector were utilised alongside broad-spectrum ion channel inhibitors (Table 2.1). TEA mimics K^+ ions in order to block K^+ channels, verapamil inhibits both long lasting (L-type) and transient (T-type) Ca^{2+} channels, procainamide reversibly binds to and blocks voltage-gated Na^+ channels and NPPB blocks Cl^- channels via a currently unknown mechanism.

Results showed that treatment with 10 mM TEA and 10 µM verapamil led to a reduction in the number of GFP positive cells by 62% and 57%, respectively, whilst treatment with 50 µM procainamide and 10 µM NPPB had little effect (Figure 4.9). This suggested that K^+ and Ca^{2+} channels were potentially important during MCPyV transduction in contrast to Na^+ and Cl^- channels.

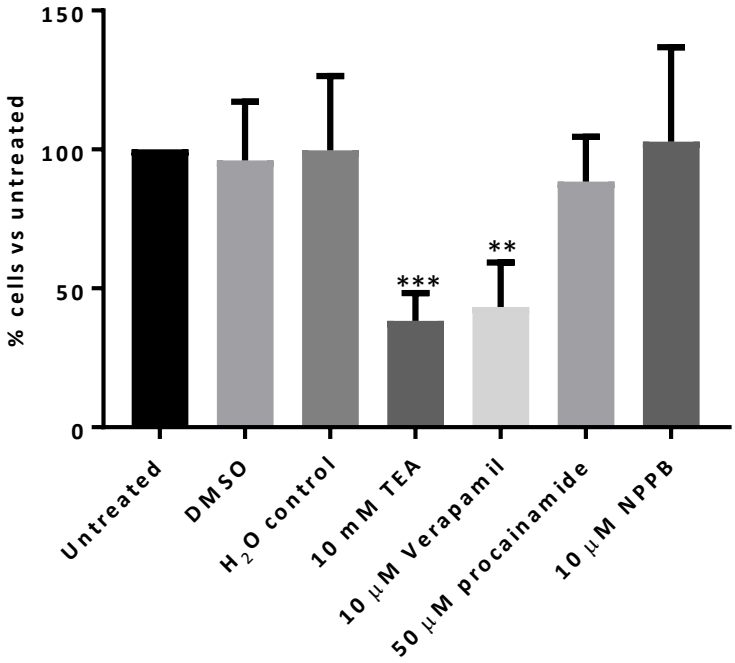

Figure 4.9: Effect of broad-spectrum ion channel inhibitors upon MCPyV transduction. 293TT cells were pre-treated with drugs for 1 hour prior to a 2-hour incubation with MCPyV GFP PsVs in the presence of drug. Fresh medium was then added before incubation and visualisation of GFP-positive cells after 72 hours using an Incucyte ZOOM instrument. Predetermined analysis parameters were used to identify the number of GFP-positive cells for each sample before comparison to an untreated control.

4.9 K^+ channel activity is important for MCPyV transduction

K^+ ion channel manipulation has previously been shown to be important during bunyamwera virus infection (Hover et al., 2016; Hover et al., 2018). Specifically, K^+ ion flux into endosomes during post-penetration trafficking was required and inhibition of K^+ channels led to a loss of infectivity.

Following identification that manipulation of endosomal acidification and treatment of cells with the broad-spectrum K^+ channel inhibitor TEA reduced MCPyV transduction, it was plausible that a similar mechanism is required during polyomavirus entry. MCPyV PsV assays were therefore performed using a larger panel of K^+ channel inhibitors to target a wider range of K^+ channels.

Results showed that 10 mM TEA, 50 mM KCl, 1 mM $BaCl_2$ and 1 mM 4AP reduced the number of GFP positive cells in comparison to untreated controls (Figure 4.10). Quinidine HCl was also used in these experiments, however due to cytotoxicity it was not included in results.

Treatment of cells with 10 mM KCl had no consistent effect upon transduction, whilst treatment with 50 mM led to a 55% reduction in GFP positive cells. K_2SO_4, used at 25 mM to introduce an equivalent number of K^+ ions as 50 mM KCl, had little effect, suggesting that the presence of K^+ ions alone was not sufficient to abrogate transduction and that KCl effects were potentially also reliant upon imbalances created through the additional presence of Cl^- ions or that KCl was specifically manipulating a cellular mechanism not affected by K_2SO_4.

4AP, which is a broad K_V channel inhibitor, reduced the number of GFP positive cells by 67% when used at 1 mM, suggesting that voltage-gated channels were potentially important during entry. Previous studies had identified that Kv1.3 channels are the most active in HEK293 cell lines, therefore margatoxin, which is a Kv1.3 specific inhibitor was used. Results showed that 20 nM margatoxin had no inhibitory effect, which suggested that MCPyV may potentially affect channels during entry or that basal channel activity with respect to Kv1.3 was not important during initial MCPyV entry.

Treatment with $BaCl_2$, which inhibits inward rectifier potassium channels (K_{IR}) through blockage by Ba^{2+} ions, led to an average reduction in GFP positive cells of 57%. There is evidence that some K_{IR} channels may be internalised with vesicles that enter the endocytic network, however whether these channels have functionality during endosomal acidification remains unknown (Zylbergold et al., 2010).

The mechanism of action of Qn has not yet been identified, in part due to promiscuous inhibition of K^+ channels and no clearly defined target family. The unrestrained inhibitory effects of Qn are further exemplified by its use as an anti-malarial drug which is believed to be toxic to the pathogen through effects upon the parasite's ability to metabolise haemoglobin. However, in relation to MCPyV, results showed that treatment with 100 µM Qn had no inhibitory effect.

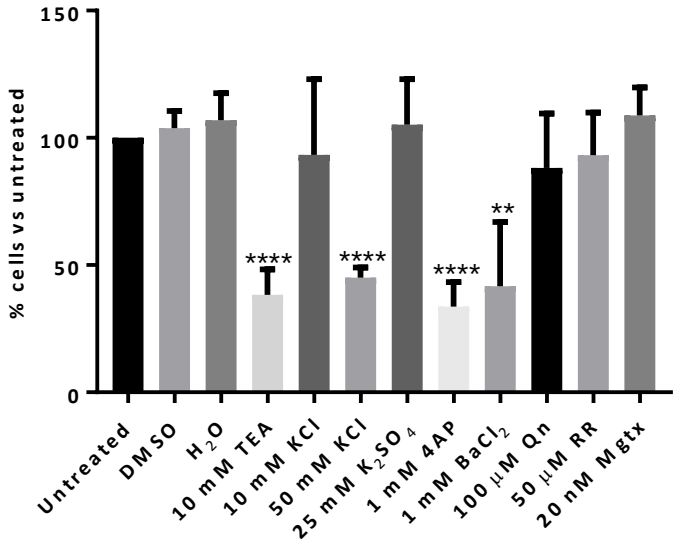

Figure 4.10: Effect of K^+ ion channel inhibitors upon MCPyV transduction. 293TT cells were pre-treated with drugs for 1 hour prior to a 2-hour incubation with MCPyV GFP PsVs in the presence of drug. Fresh medium was then added before incubation and visualisation of GFP-positive cells after 72 hours using an Incucyte ZOOM instrument. Predetermined analysis parameters were used to identify the number of GFP-positive cells for each sample before comparison to an untreated control.

TRP channels are typically localised at the plasma membrane, however there are also examples of channels that are present in endosomal membranes. Treatment of cells with 50 µM RR, a broad spectrum TRP channel inhibitor, had no detrimental effect upon MCPyV transduction, suggesting this channel family was not important during initial entry events.

To confirm that K^+ channel inhibitors were not directly affecting penetration, cells were treated with 10 mM TEA before transduction using EdU-labelled PsVs (Figure 4.11A). Results showed that MCPyV PsV were still able to penetrate into the cell, as seen by puncta forming around nuclei and that at least for TEA, drug treatment did not affect penetration. Drugs that had an inhibitory effect upon MCPyV transduction were also tested to confirm that GFP expression was not perturbed (Figure 4.11B). Treatment with 10 mM TEA, 1 mM 4AP and 50 mM KCl led to a non-significant reduction of 17%, 4% and 2% in comparison to an untreated control, respectively. Whilst a decrease of 17% for TEA treatment was greater than desired, this was

believed to be a product of a repeat that had a lower confluence in comparison to untreated cells and this subsequently skewed the data (not shown). Effects of 1 mM $BaCl_2$ upon GFP expression was not determined due to lack of reagent availability.

Due to time restrictions it was not possible to perform further experimentation to identify whether a specific K^+ channel or subset was important during MCPyV entry.

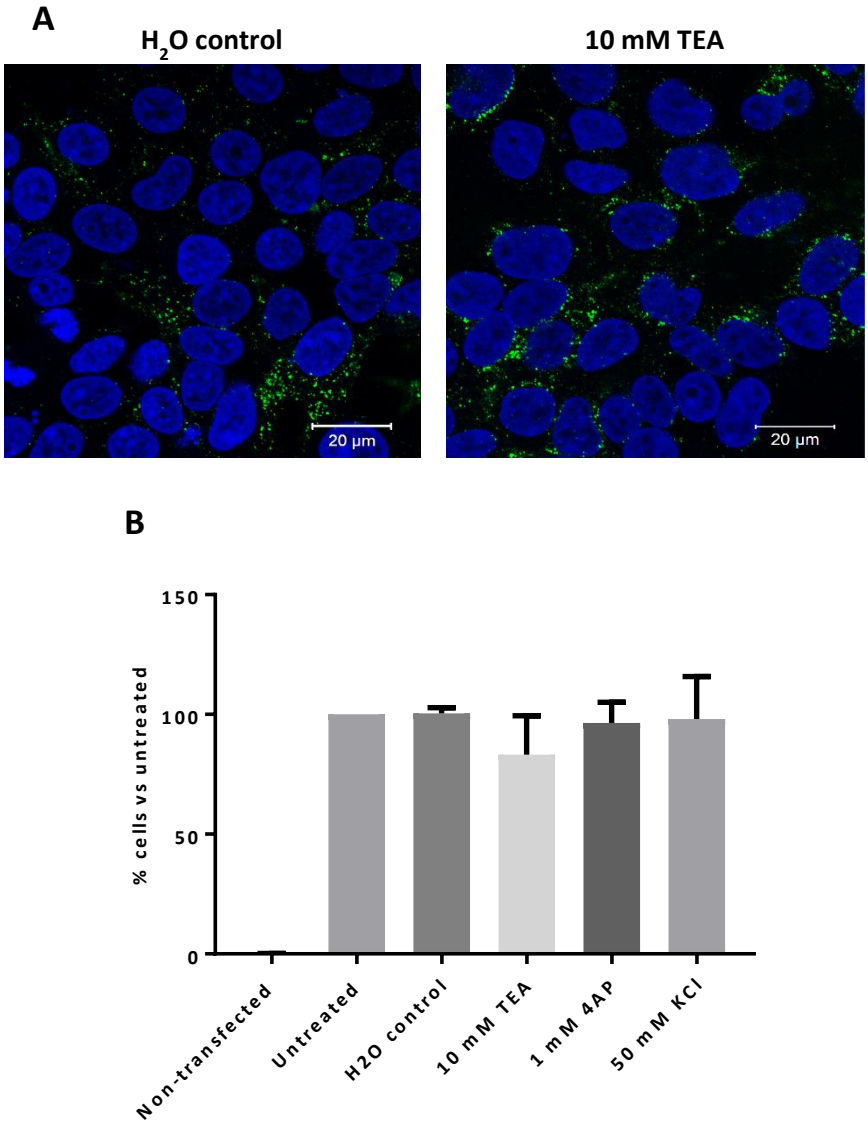

Figure 4.11: K^+ channel inhibitors do not affect penetration or expression of GFP. (A) 293TT cells were transduced with EdU-labelled MCPyV PsVs with fixation after a 48-hour incubation. Cells were permeabilised before a click reaction was performed to label PsVs with Alexa Fluor 488. Cells were visualised using a ZEISS LSM880 upright confocal microscope and DAPI staining was used to identify nuclei. Scale bar 20 µm. (B) 293TT cells were incubated with GFP containing transfection complexes for 6 hours. Fresh growth medium containing drug was then added for a further 18 hours before evaluation of GFP-positive cells using an Incucyte using predetermined analysis parameters.

4.10 Effects of broad-spectrum ion channel inhibitors upon early events during SV40 infection

To investigate whether ion channel inhibitor effects were conserved between different polyomavirus species, drugs were incubated with Vero cells during infection with SV40 (Figure 4.12). Results showed that similar to MCPyV, 50 µM procainamide had no inhibitory effect. 10 mM TEA also had no inhibitory effect which was in contrast to data obtained for MCPyV and suggested that K^+ channel activity may not be required during entry events for all polyomaviruses. Interestingly, treatment with 10 µM verapamil led to a 57% reduction in the number of LT-positive cells and therefore suggested that Ca^{2+} channel activity may represent a conserved requirement for polyomaviruses given that the same observation was made in relation to MCPyV. Due to reagent availability, NPPB, which had no inhibitory effect for MCPyV, was not included in the screen.

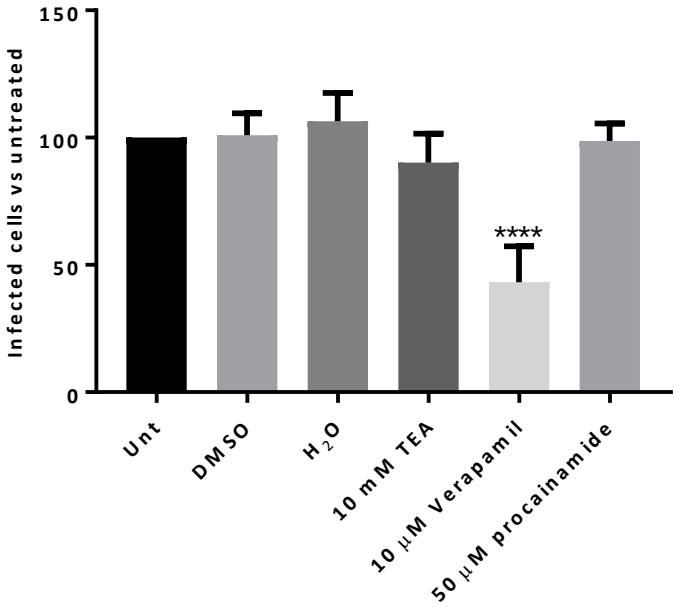

Figure 4.12: Effect of broad-spectrum ion channel inhibitors upon early events during SV40 infection. Vero cells were pre-treated with drugs for 1 hour prior to a 2-hour incubation with SV40 at a MOI of 1, in the presence of drug. Fresh medium containing drug was then added before fixation following incubation for 24 hours. Cells were permeabilised and immunostained for LT, with a species-specific secondary antibody conjugated to Alexa Fluor 488 used for visualisation. Wells were then imaged using an Incucyte ZOOM instrument. Predetermined analysis parameters were used to identify the number of LT cells for each sample before comparison to an untreated control.

4.11 K^+ channel inhibition does not impede SV40 infection

To establish whether K^+ channel requirements are conserved between a wide range of polyomaviruses, drugs in addition to TEA were used to test whether treatment would perturb SV40 infection of Vero cells.

Results showed that 10 mM TEA, 1 mM 4AP and 100 µM Qn had no inhibitory effect upon SV40 infection (Figure 4.13). Results for KCl and K_2SO_4 were discarded due to significant cytotoxicity for Vero cells at comparable concentrations to those used in 293TT cell based MCPyV experimentation. RR and $BaCl_2$ were not tested due to lack of reagent availability.

The fact that no inhibition of SV40 was observed could have been attributed to two alternative hypotheses. Firstly, it may have been that the requirement of K^+ channel activity was unique to MCPyV or that SV40 was a member of a group of polyomaviruses that does not require manipulation of K^+. Alternatively, the observed effects may have been cell-type specific. It may be that when using monkey cell lineages there are additional factors that could overcome inhibitors, which are not conserved with human lineages. Unfortunately, the limited range of cells that may be infected using MCPyV did not include Vero cells and therefore MCPyV PsVs could not be used to test drug effects in this cell line. Given that SV40 was more permissive to infection, it was more likely this virus could have been tested in 293TT cells. However, detection of T antigen following infection could not be applied to 293TT cells due to already expressing high amounts of both SV40 LT and ST. Due to time constraints potential alternative assays were not explored.

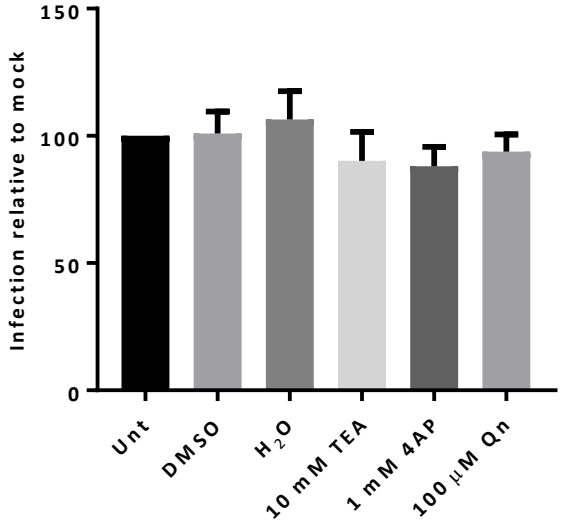

Figure 4.13: SV40 infection does not require K^+ ion channels. Vero cells were pre-treated with drugs for 1 hour prior to a 2-hour incubation with SV40 at a MOI of 1, in the presence of drug. Fresh medium containing drug was then added before fixation following incubation for 24 hours. Cells were permeabilised and immunostained for LT, with a species-specific secondary antibody conjugated to Alexa Fluor 488 used for visualisation. Wells were then imaged using an Incucyte ZOOM instrument. Predetermined analysis parameters were used to identify the number of LT cells for each sample before comparison to an untreated control.

4.12 L-type Ca^{2+} channel activity is not required for MCPyV transduction

Given that MCPyV and SV40 displayed conserved and comparable phenotype when treated with the broad spectrum Ca^{2+} inhibitor verapamil, it was explored whether a specific type of channel was required during entry. Verapamil has been shown to inhibit both L- and T-type Ca^{2+} channels. Available within the laboratory were Nif and Nit, both of which specifically inhibit L-type channels.

Results showed that treatment with 10 µM Nif and 10 µM Nit had no effect upon the number of GFP positive cells in comparison to the control, which suggested that L-type Ca^{2+} channels were not essential during MCPyV transduction (Figure 4.14). Large error bars were observed due to one repeat that had a very low number of positive cells for untreated, which in turn amplified errors, whilst results compared to DMSO remained consistently similar.

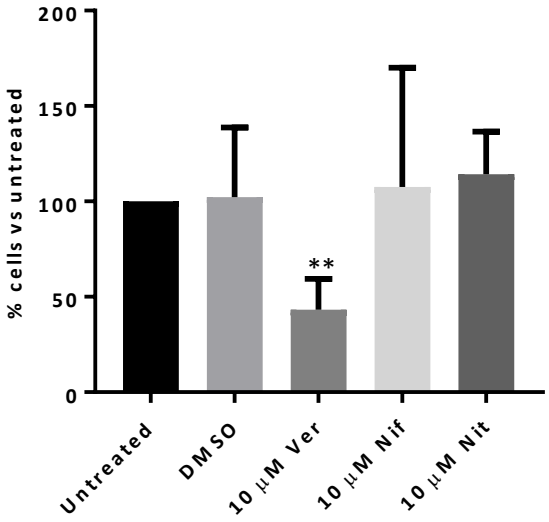

Figure 4.14: Effect of T-type Ca^{2+} channel inhibitors upon MCPyV transduction. 293TT cells were pre-treated with drugs for 1 hour prior to a 2-hour incubation with MCPyV GFP PsVs in the presence of drug. Fresh growth medium was then added before incubation and visualisation of GFP-positive cells after 72 hours using an Incucyte ZOOM instrument. Predetermined analysis parameters were used to identify the number of GFP positive cells for each sample before comparison to an untreated control.

4.13 L-type channel activity is not required for SV40 infection

Given that MCPyV did not require L-type channels it was expected that SV40 would follow the same trend since verapamil effects were similar. Nif and Nit were used to determine whether SV40 infection would be perturbed by the L-type Ca^{2+} channel inhibitors.

Comparably to MCPyV, results showed that 10 µM Nif and 10 µM Nit had no detrimental effect upon SV40 infection, with a reduction in LT positive cells of 8% and 16%, respectively (Figure 4.15). Taken together, results for MCPyV and SV40 showed that verapamil inhibited infection of both polyomaviruses, suggesting broad Ca^{2+} channel inhibition could potentially be detrimental to a variety, if not all, polyomaviruses. However, targeting of L-type channels had little inhibitory effect.

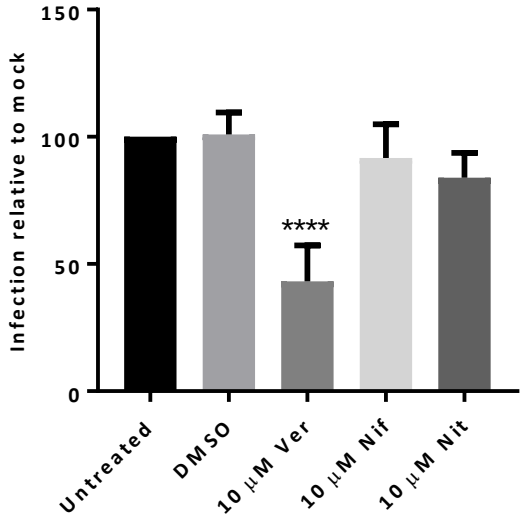

Figure 4.15: Effect of T-type Ca2+ channel inhibitors upon SV40 infection. Vero cells were pre-treated with drugs for 1 hour prior to a 2-hour incubation with SV40 at a MOI of 1, in the presence of drug. Fresh medium containing drug was then added before fixation following incubation for 24 hours. Cells were permeabilised and immunostained for LT, with a species-specific secondary antibody conjugated to Alexa Fluor 488 used for visualisation. Wells were then imaged using an Incucyte ZOOM instrument. Predetermined analysis parameters were used to identify the number of LT cells for each sample before comparison to an untreated control.

4.14 MCPyV but not SV40 infection is sensitive to T-type Ca^{2+} inhibitors

Given that two L-type channel inhibitors had no effect, this suggested that T-type channels were possibly required for efficient polyomavirus infection. Therefore the T-type specific inhibitors mibefradil and flunarizine were used in MCPyV transduction and SV40 infection assays. Both inhibitors displayed dose-dependent inhibition for MCPyV (Figure 4.16A) but had no significant effect upon SV40 infection (Figure 4.16B), suggesting that T-type Ca^{2+} activity was required for entry of MCPyV but not SV40. For SV40, 10 µM flunarizine was omitted due to cytotoxicity.

Treatment of 293TT cells with mibefradil during MCPyV transduction led to a reduction in GFP-positive cells of 26%, 41% and 99% at 2.5 µM, 5 µM and 10 µM, respectively. Flunarizine showed increased potency at lower concentrations with a

52% and 83% reduction in GFP positive cells when treated with 2 µM and 5 µM, respectively.

Interestingly this requirement was not conserved during SV40 infection, as treatment with 5 µM mibefradil and 5 µM flunarizine led to a reduction in LT positive cells of 16% and 22%, respectively. Treatment with 10 µM mibefradil, which completely abolished transduction of MCPyV, led to a 16% reduction in SV40 LT positive cells, further confirming that SV40 did not display the same sensitivity to T-type Ca^{2+} inhibitors as MCPyV.

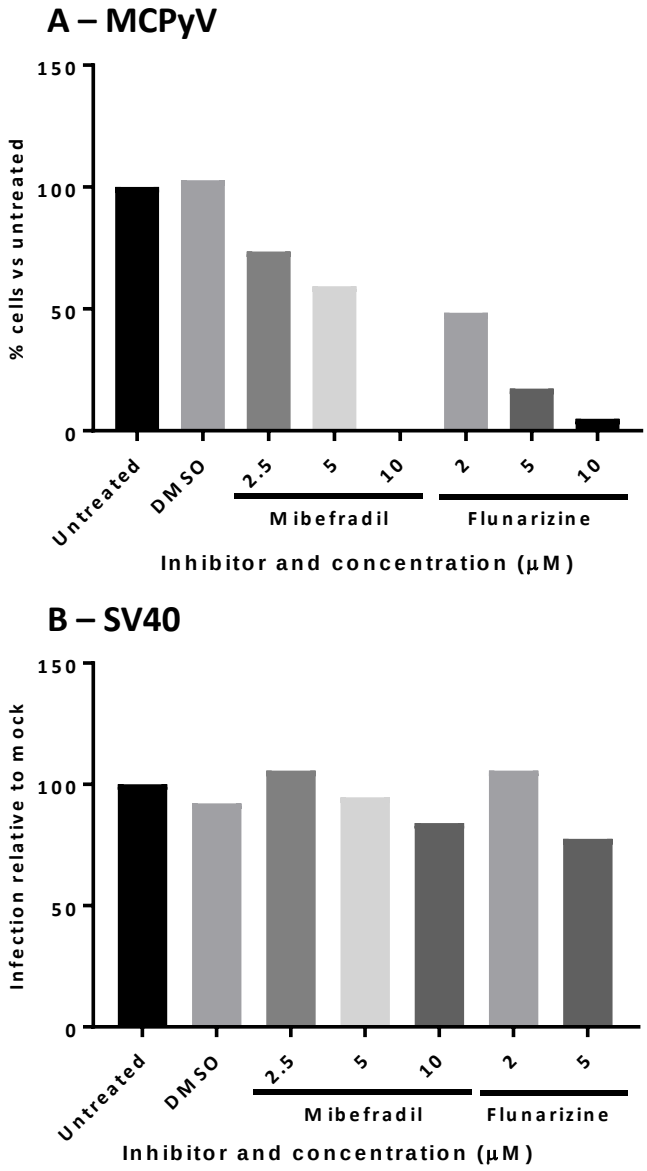

Figure 4.16: T-type Ca^{2+} channels are required for entry of MCPyV (A) but not SV40 (B). (A) 293TT cells were pre-treated with drugs for 1 hour prior to a 2-hour incubation with MCPyV GFP PsVs in the presence of drug. Fresh growth medium was then added before incubation and visualisation of GFP-positive cells after 72 hours using an Incucyte ZOOM instrument. Predetermined analysis parameters were used to identify the number of GFP positive cells for each sample before comparison to an untreated control. (B) Vero cells were pre-treated with drugs for 1 hour prior to a 2-hour incubation with SV40 at a MOI of 1, in the presence of drug. Fresh medium containing drug was then added before fixation following incubation for 24 hours. Cells were permeabilised and immunostained for LT, with a species-specific secondary antibody conjugated to Alexa Fluor 488 used for visualisation. Wells were then imaged using an Incucyte ZOOM instrument. Predetermined analysis parameters were used to identify the number of LT cells for each sample before comparison to an untreated control.

4.15 Discussion

To date there are limited studies available with regards to early events in the lifecycle of polyomaviruses. At the beginning of this study there had been no published data regarding MCPyV trafficking events, with confirmation that sequential binding of GAGs and sialylated glycans to permit entry, the extent of existing knowledge.

Given that other polyomaviruses traffic through the endo/lysosomal system and successful infection requires an acidified environment, it was firstly confirmed that this was the case for MCPyV. EdU labelled MCPyV PsVs showed discrete puncta within the cell which were confirmed to be within vesicles that were coated with the late endosomal and lysosomal associated protein LAMP2. Furthermore, treatment with 10 mM NH_4Cl, a drug that has been well established to deprotonate acidic environments within the cell, led to significant impairment of MCPyV transduction in a time dependent manner. Taken together these results confirmed that MCPyV like other polyomaviruses were present within the endo/lysosomal network and that acidification was required during entry. The requirement of acidification has also been independently verified by Becker *et al*., with their results comparably showing that NH_4Cl perturbed MCPyV transduction.

Whilst trafficking and acidification was not a novel discovery in relation to polyomaviruses, it has never been established as to how far into the endo/lysosomal network virions travel, with suggestions that observations of virions contained within lysosomes have potentially entered an environment that is too acidic for viable infection and merely represents an artefact with detection of virions that have missed a proposed window of opportunity for release from endosomes. EGA, a drug that leads to clustering of acidified lysosomes and in turn prevents cargo release, was therefore utilised during transduction and infection assays for MCPyV and SV40, respectively. Results showed that treatment with EGA severely perturbed both viruses, and that for SV40 it was more effective than NH_4Cl at the tested concentrations (78% vs 54%). This suggested that prior to ER fusion, SV40 virions enter lysosomes that are of a low pH and do not exit the endo/lysosomal network at an earlier and less acidic stage post penetration.

Acidification of endo/lysosomes requires the flux of ions in order to translocate H^+ ions across the membrane. This is achieved through the activity of ion channels, which whilst the field is still in its infancy, has been well characterised to require imbalances in several ions including K^+, Ca^{2+}, Na^+ and Cl^-. Following the use of broad-spectrum inhibitors against each of the aforementioned ion channels, results showed that treatment with TEA (K^+ channel inhibitor) was detrimental to MCPyV transduction and that treatment with verapamil (Ca^{2+} channel inhibitor) led to restriction of both MCPyV and SV40 infection.

In relation to MCPyV and K^+ channels, results showed that when a larger screen was performed KCl, 4AP and $BaCl_2$ all had inhibitory effects. Interestingly, inclusive of TEA, all four drugs led to comparable reduction and whilst this may be coincidental, there was also the possibility that targeting of the same inhibitory event may have occurred. TEA and 4AP both are primarily associated with the blockage of K_V channels, whereas $BaCl_2$ is an inhibitor of K_{IR} channels. Despite $BaCl_2$ deemed specific for K_{IR} channels, there were conflicting reports that suggested that outside of μM range the drug could also inhibit some K_V channels. Given that $BaCl_2$ was used at 1 mM there was therefore the potential that alongside TEA and 4AP, inhibition of MCPyV transduction by $BaCl_2$ was through blockage of K_V channels. To definitively confirm whether K_{IR} channel activity was required, assays that introduce caesium ions (Cs^+), another inhibitor of K_{IR} channels would be required.

The inhibition of MCPyV transduction associated with KCl treatment was less obvious. Results suggested that K^+ ion addition alone was not enough to cause inhibition, as treatment with 50 mM KCl would introduce an equivalent amount of K^+ ions as 25 mM K_2SO_4 which had no inhibitory effect. Therefore, this potentially suggested that Cl^- ions were solely responsible or required in addition to K^+ in order to perturb transduction. It was also plausible that treatment with 50 mM KCl disrupted ionic balances that were detrimental to an alternative viral requirement, as altering the overall concentration of K^+ and Cl^- ions would likely have consequences upon a larger range of ions and in turn pathways.

In contrast to MCPyV transduction assays, treatment of Vero cells during SV40 infection with K^+ channel inhibitors showed no effect upon the number of LT-positive

cells. This suggested that K^+ channels were either only required for MCPyV transduction or that it was a requirement for polyomavirus infection of human cell lines. In order to determine whether this was cell line specific, SV40 could be used to infect human cell lines. Given that 293TT cells stably express high amount of SV40 LT and ST it was not possible to use this cell line. Had more time been available, alternative assays to detect SV40 infection could have been performed to further identify whether this was cell line specific. Infection of HEK293 cells, that were not additionally transformed using SV40 T antigens were a viable option, as would have been moving into Renal Proximal Tubular Epithelial Cells (RPTECs). RPTECs are a primary human renal cell line that has been identified as the natural host cell reservoir during persistent human infection of BKPyV and is also permissive to SV40 infection. Alongside SV40 infection, BKPyV could have also been used to determine whether different human polyomaviruses are also sensitive to K^+ channel inhibition or whether observations were MCPyV specific.

Results showed that both MCPyV and SV40 were inhibited by treatment with verapamil, a clinically available L- and T-type Ca^{2+} inhibitor. Further screening showed that for both viruses the L-type inhibitors Nif and Nit had no inhibitory effect. This therefore suggested that T-type Ca^{2+}channel activity may be of importance to polyomavirus infection. Preliminary data suggested that this was the case for MCPyV but not SV40, with mibefradil and flunarizine treatment abolishing the ability of MCPyV to successfully enter the cell.

There was also the potential that effects observed following verapamil treatment, beyond T-type inhibition for MCPyV, could follow a similar mechanism of inhibition that has been shown for Ebola, whereby verapamil was shown to prevent TPC-mediated fusion of endosomes to the ER. SV40 has been shown to traffic through the ER on route to the nucleus. It is therefore plausible that polyomaviruses may employ a similar mechanism. If this is the case, or other polyomaviruses require T-type Ca^{2+} channel activity similarly to MCPyV, there is the potential that repurposing of clinically available drugs may represent a valid option in the therapeutic intervention of a range of polyomavirus-induced diseases, including BKPyV-mediated BKVAN and JCPyV-mediated PML.

Chapter 5

p38 MAPK drives ST-mediated cellular motility and migration

5.1 Introduction

MCPyV is known to be the causative agent in the majority of MCC cases (Feng et al., 2008). Clonal integration and mutation of the viral genome leads to truncation of LT resulting in a non-replicative virus. Full length LT is responsible for driving progression of later stages of the replicative cycle, such as genome replication and capsid protein production (Decaprio and Garcea, 2013). This is implemented by the formation of two opposed LT hexameric complexes which form a helicase, opening the viral genome for replication, providing RNA polymerase access to the late coding promoter and suppressing early gene expression. It is therefore unsurprising that in all studied cases of MCPyV-positive MCC, there is a loss of the helicase domain, which lies downstream of early stop codon mutations (Shuda et al., 2008). However, LT truncated forms arising in MCC always retain the ability to bind pRb. Despite the requirement for LT to bind pRb and the loss of the helicase domain in the progression of disease, ST has been implicated as the major oncogene. This is reinforced by depletion studies, where loss of ST expression leads to growth arrest in MCC cell lines (Shuda et al., 2014).

A hallmark of cancer is the ability to metastasise, and the highly migratory phenotypes associated with MCCs contributes in part to the aggressive nature of disease (Nieto et al., 2016). Metastasis is a complex multistep process and it has been well characterised that the MCPyV oncogene ST manipulates the host cell to enhance migratory phenotypes. In order for a cell to migrate, an essential step is the disruption of cell to cell junctions and breakdown of the surrounding extracellular matrix to enhance cellular dissociation (Knights et al., 2012). MCPyV ST induces the expression of A disintegrin and metalloproteinase (ADAM) proteins 10 and 17, which when inhibited ablate ST-mediated dissociation and motility (Nwogu et al., 2018). Differential expression of several proteins required for cytoskeletal rearrangements and microtubule destabilisation is also facilitated by ST (Knight et al., 2015). In particular, the microtubule-associated protein stathmin was highlighted as a key regulator in promoting motility and migration. Furthermore, ST has been identified to induce actin cytoskeleton rearrangements to enhance filopodia formation via the Rho-GTPases cdc42 and RhoA (Stakaitytė et al., 2017).

Impairment of MCPyV induced manipulation of both microtubule and actin cytoskeletons has been attributed to the protein phosphatase PP4, in particular the interaction of ST with its catalytic subunit, PP4C. By inhibiting the activity of PP4C or prevention of ST binding, ST-induced migratory phenotypes can be severely hindered. Given that PP4 is a phosphatase, it is not surprising that the ST interaction causes alteration in the phosphorylation status of proteins. Whilst ST mutants that lack the ability to bind to PP2A Aα or PP4C could both induce overexpression of stathmin, results showed that dephosphorylation of stathmin and subsequent deacetylation and destabilisation of tubulin required an interaction with PP4C. Similarly, the activation – through phosphorylation – of Rho-GTPases was shown to be dependent upon ST-mediated manipulation of PP4C.

Despite the knowledge that signalling cascades are likely to be important in the phosphorylation and subsequent alteration of protein activities following ST expression, there has been little investigation into how this occurs. This chapter describes an investigation into kinase pathways that are dysregulated by expression of MCPyV ST and subsequent evaluation to confirm that the p38 MAPK pathway is an essential mechanism required to promote the metastatic phenotypes synonymous with MCC.

5.2 Screening the phosphorylation status of MAPKs following MCPyV ST expression

In order to identify kinases that displayed altered phosphorylation status in the presence of MCPyV ST, a kinase immunoblot array assay was performed. HEK293 cells were transfected with GFP or ST-GFP and incubated for 24 hours. A 22-hour serum depletion was performed before a 2-hour boost with 10% (v/v) serum and subsequent lysis using a kit specific buffer. Lysed samples were standardised by BCA assay before incubation with membranes presenting immobilised phosphorylated MAPK proteins. Following washes, the amount of phosphorylated protein was determined by chemiluminescent detection and densitometry. A series of exposure times were taken so that each dot could be visualised whilst saturation was avoided, a representative image is shown in Figure 5.1A. Densitometry of each dot was

determined relative to mock and duplicates were averaged (Figure 5.1B). Results showed that most kinases displayed little to no increase in the amount of signal detected.

SV40 ST has previously been shown to bind to and inhibit PP2A, suppressing dephosphorylation of Akt which contributes to cellular transformation. In contrast, MCPyV ST does not activate Akt and it has further been shown that shRNA-mediated depletion of ST in the MCPyV-positive MCC cell line MKL-1 led to increased Akt phosphorylation and activation (Shuda et al., 2011). In the case of MCPyV ST, the loss of Akt activation is overcome by preventing hyperphosphorylated 4E-BP1 turnover, which contributes to cellular transformation by promoting cap-dependent protein translation. Similarly, the kinase screen suggested that no isoform of Akt showed substantially increased hyperphosphorylation following ST expression (Figure 5.1B).

The screen suggested that JNK2 displayed the largest increase in phosphorylation, whilst JNK1 and JNK3 remained unaffected. This was further supported by observation that a pan-JNK antibody also displayed increased phosphorylation and therefore implied that JNK2 could be activated by ST.

The p38 MAPK family also displayed increased phosphorylation of isoforms γ and δ, whilst α and β showed some but relatively lower levels of increase. This was somewhat unexpected, as what could be seen by eye suggested that all four isoforms highlighted in Figure 5.1A showed increased phosphorylation following ST expression. p38α is the most highly and ubiquitously expressed isoform of p38 throughout all human cells and results showed that the signal produced was significantly higher than the other isoforms in the array. Whilst variation in detection may be attributed to antibody binding kinetics, there was also the potential that high basal activation may have prevented the determination of differential phosphorylation. Whether p38 isoforms were phosphorylated by ST was therefore investigated.

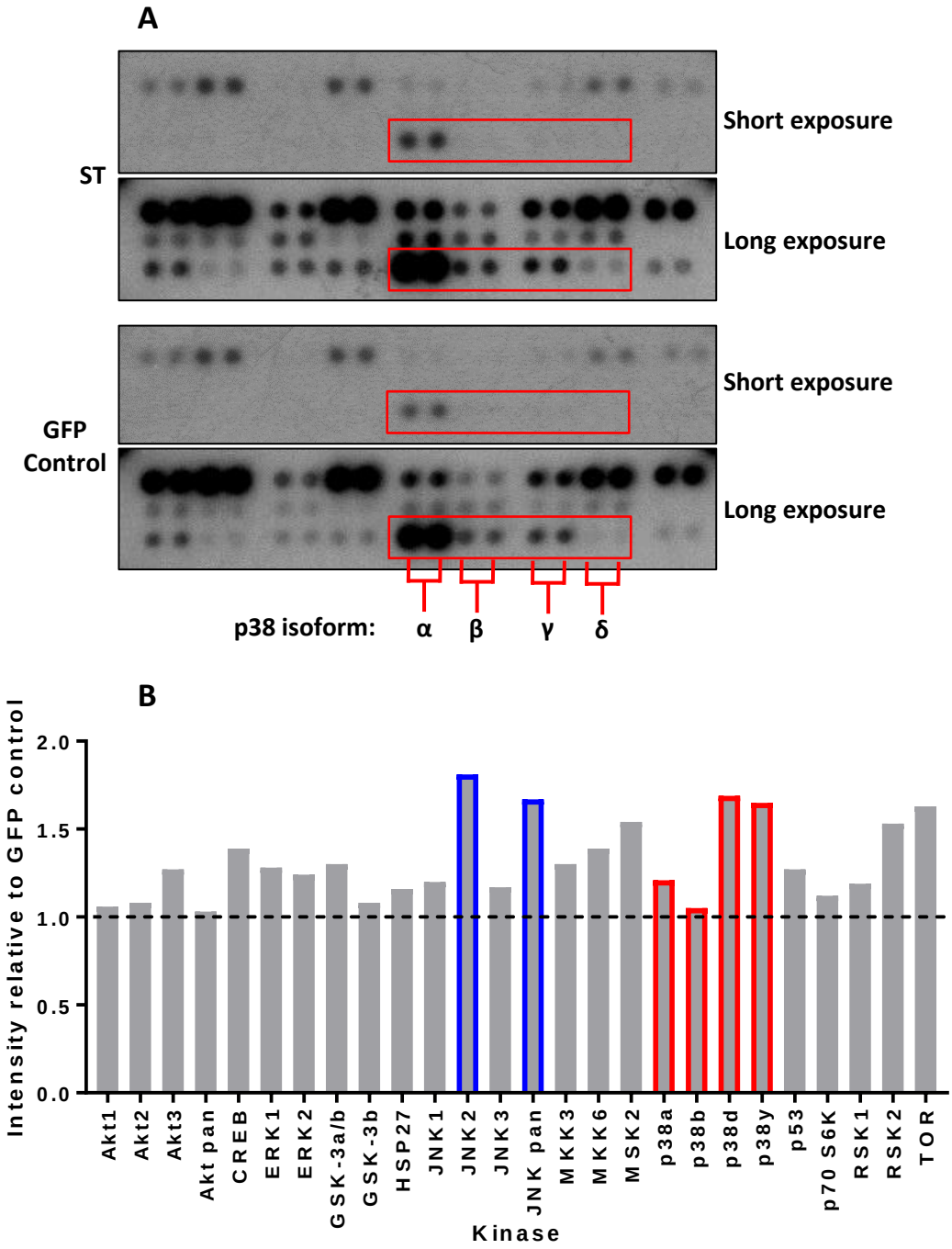

Figure 5.1: Evaluation of MAPK phosphorylation following the expression of MCPyV ST. HEK293 cells were transfected with GFP or ST-GFP and incubated for 22-hours in serum-free medium before a 2-hour serum addition. Lysis was performed using kinase array lysis buffer. BCA assays were performed to standardise protein concentrations before the kinase array assay was performed as per manufacturer specifications with detection using chemiluminescence detection and light sensitive film. (A) Short and long chemiluminescent exposures of ST-GFP and GFP (control) membranes. Red box highlights p38 MAPK isoforms. (B) Analysis of detection by densitometry of each kinase in ST-GFP expressing cells compared with GFP control. Highlighted in red are the four p38 isoforms and in blue JNK2 and JNK pan. Bars represent the average detection of two dots.

5.3 MCPyV ST expression leads to p38 hyperphosphorylation

Based upon initial kinase array data, it was investigated whether expression of ST led to p38 phosphorylation. HEK293 cells were transfected with empty vector or ST before lysis after 48-hours. Western blotting was then performed to determine the phosphorylation status of MAPKs.

Results showed that p38 was hyperphosphorylated in the presence of ST (Figure 5.2). Given that increased phosphorylation was observed, total p38 expression was also evaluated. Given that there was no change in the total amount of p38, this confirmed that ST expression induced hyperphosphorylation of p38 and that this was not an artefact of differential protein expression. Phosphorylation of ERK was also evaluated and Results showed that consistent with the kinase array data (Figure 5.1) there was no change in ERK phosphorylation status, which suggested that the observed effect may be p38 specific.

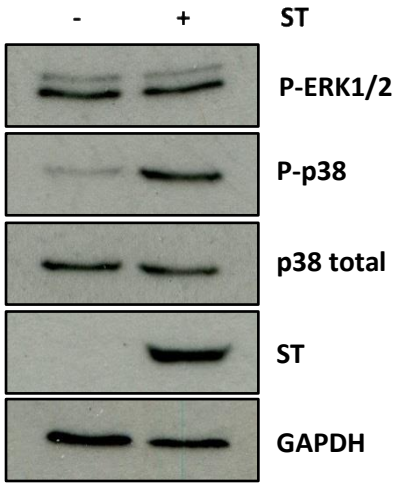

Figure 5.2: Expression of MCPyV ST induces hyperphosphorylation of p38. HEK293 cells were transfected with empty vector or ST with lysis using Leeds lysis buffer performed following a 48-hour incubation. Antibodies were used to detect phosphorylated ERK1/2 and p38 that corresponded to activated protein. p38 and GAPDH antibodies were used as loading controls and 2T2 hybridoma used to detect ST.

5.4 MCPyV ST induced p38 phosphorylation is due to activation

A current issue facing pharmaceutical production of therapeutics targeting p38 are negative feedback loops which activate upstream kinases in response to inhibition. Therefore, increased phosphorylation of p38 was not necessarily due to activation and could have instead been attributed to inhibition of the pathway. To determine whether p38 was activated, the phosphorylation status of downstream substrates was investigated.

To determine whether expression of ST induced p38 pathway activation, Western blotting was performed to detect three substrates of p38. MSK1 is a kinase downstream of p38 and ERK pathways that is responsible for further phosphorylation and activation of a range of transcription factors and may post-translationally modify histones and related proteins. ATF2 is a transcription factor that is activated by p38 and/or JNK, which is a member of the ATF/CREB family of leucine zipper proteins and primarily binds to both AP-1 and CRE DNA response elements. MK2 is a kinase that is solely activated by p38 and is responsible for a range of activities relating to TNFα biosynthesis, cytokine-induced mRNA stability and polymerisation of actin, the latter of which is mediated by phosphorylation and activation of HSP27.

Results showed that MK2, MSK1 and ATF2 all displayed increased phosphorylation following ST expression (Figure 5.3). This suggested that ST activated p38 and increased phosphorylation was not a consequence of negative feedback.

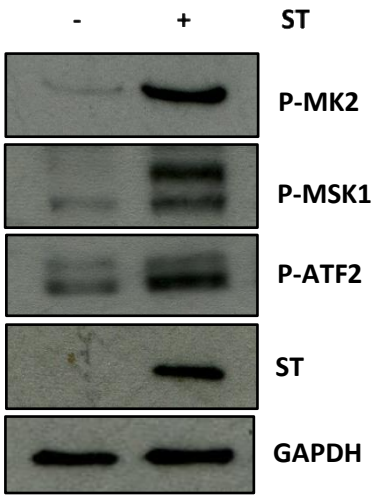

Figure 5.3: MCPyV ST leads to phosphorylation of p38 substrates. HEK293 cells were transfected with empty vector or ST with lysis using Leeds lysis buffer performed following a 48-hour incubation. Antibodies were used to detect phosphorylated MK2, MSK1 and ATF2 that corresponded to activated protein. GAPDH was used as a loading control and 2T2 hybridoma used to detect ST.

5.5 Inhibition of p38 ablates downstream target phosphorylation

To evaluate whether inhibition of p38 was sufficient to ablate ST-induced pathway activation, chemical inhibitors were utilised. Whilst the previously described kinase screen suggested that p38 isoforms γ and δ were the most upregulated, phosphorylation of MK2 is attributed solely to p38α activity. Despite the screen suggesting that p38α was not activated, the phosphorylation of MK2 and significant increase in pan-p38 phosphorylation most likely suggested that p38α was also activated. SB202190 is a potent, selective inhibitor of p38 isoforms α and β. SB202474, a structural analogue of SB202190 that has no inhibitory effect, was also used as a negative control. Before use, viability assays were performed to evaluate the toxicity of both compounds. The literature suggested that 10 μM SB202190 was sufficient to inhibit p38 α and β and both drugs were not toxic at this concentration (Figure 5.4) (Hirasawa et al., 2003; Schwartz et al., 2018). In both cases results showed that viability appeared to be increased following drug treatment compared to an untreated control, particularly at concentrations of 5 μM and 10 μM. The

concentrations used for the MTS assay confirmed that SB202190 and SB202474 were not toxic up to concentrations of 25 μM and 50 μM, respectively, which were both higher than the intended 10 μM to be used.

Given that the inhibitors did not have a detrimental effect upon cellular viability, HEK293 cells expressing ST were treated with SB202190 and SB202474 for 24 hours before lysis. Visualisation of MK2 phosphorylation showed that DMSO and 10 μM SB202474 negative controls had no influence upon phosphorylation of MK2 following ST expression (Figure 5.5). However, treatment with 10 μM SB202190, the p38 inhibitor, completely ablated MK2 phosphorylation. This therefore suggested that p38 activity was directly required for the phosphorylation of MK2.

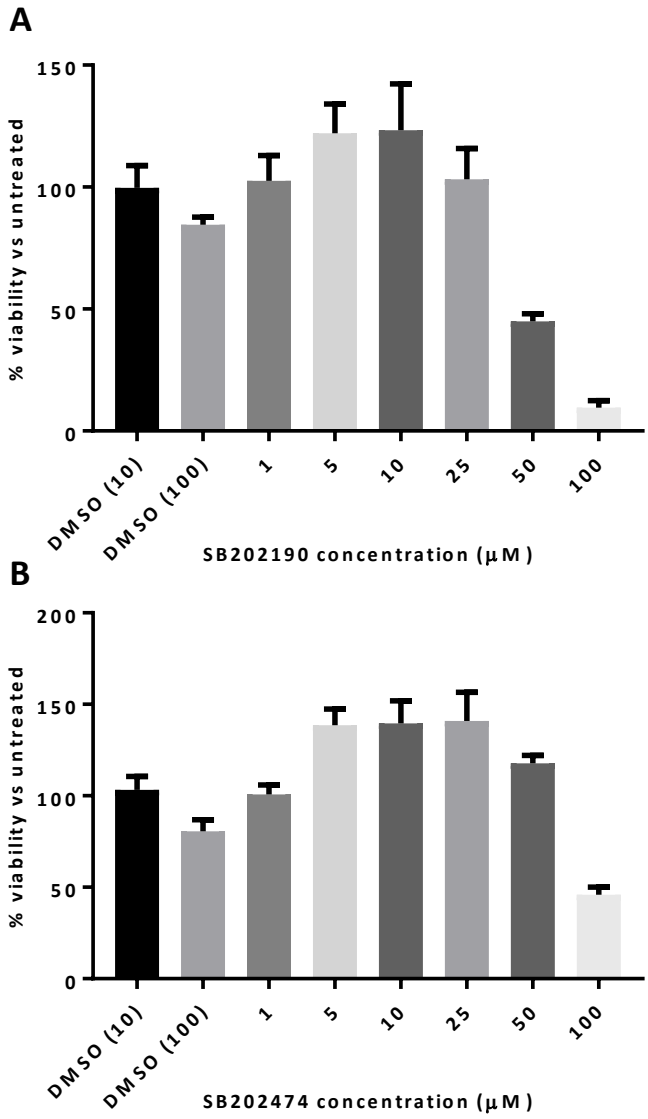

Figure 5.4: MTS viability assays to determine p38 compound toxicity in HEK293 cells. To determine whether SB202190 (A) or SB202474 (B) displayed cytotoxicity MTS assays were performed. $5x10^4$ HEK293 cells were seeded into wells of a 96-well plate. Following overnight incubation to allow cells to adhere 100 µL fresh growth medium containing a range of drug concentrations were applied to wells. Following a further 48-hour incubation 20 µL of MTS reagent was added to each well. Following a 1-hour incubation absorbance at 490 nm was determined using an automatic plate reader. Wells containing medium only were used to subtract background absorbance before comparison of each concentration to an untreated equivalent. Each condition was performed in triplicate.

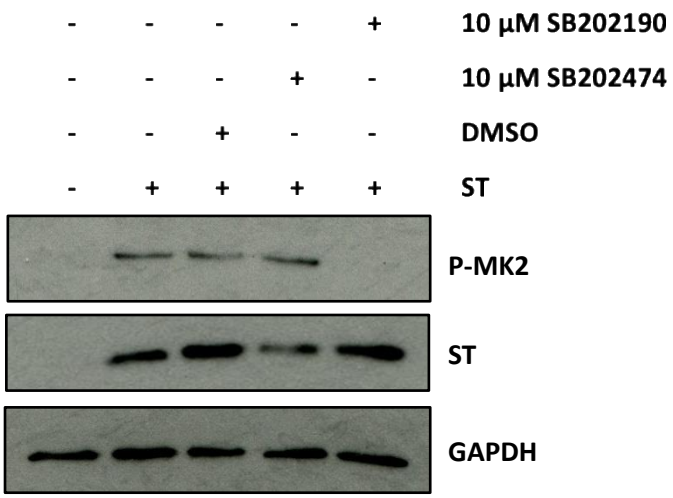

Figure 5.5: p38 activity is essential for ST induced MAPK pathway activation. HEK293 cells were transfected with empty vector or ST for 6 hours before aspiration of transfection complexes and replacement with fresh growth medium containing drug as described. Following a 48-hour incubation lysis using Leeds lysis buffer performed. An antibody was used to detect phosphorylated MK2, which corresponded to activated protein. GAPDH was used as a loading control and 2T2 hybridoma to detect ST.

5.6 ERK activity does not affect ST induced MSK1 activation

MK2 is phosphorylated only by p38, however other downstream targets, such as MSK1, may be activated by multiple kinases. It was therefore investigated whether MSK1 was solely activated by p38 or whether ERK could compensate for the inhibition.

Unlike p38 which may be targeted by MKK3/6 and MKK4, ERK1/2 are solely activated by MEK1/2, therefore the MEK1/2 inhibitor U0126 was used alongside the p38 inhibitor SB202190. To confirm that U0126 had no cytotoxic effects MTS assays were performed. Results indicated that at the working concentration of 20 µM, U0126 displayed no toxicity (Figure 5.6).

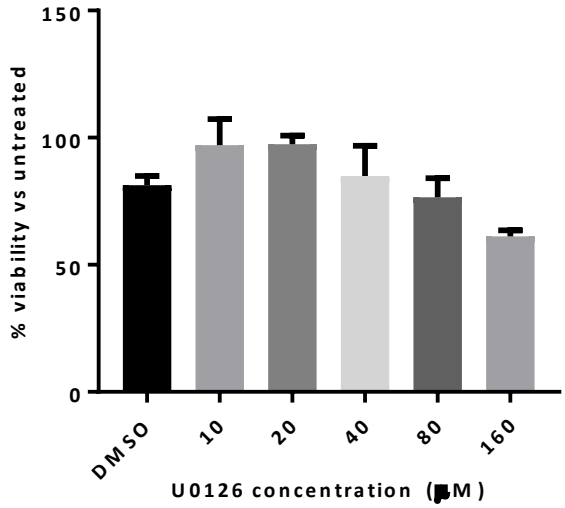

Figure 5.6: MTS viability assays to determine U0126 compound toxicity in HEK293 cells. To determine whether U0126 displayed cytotoxicity MTS assays were performed. $5x10^4$ HEK293 cells were seeded into wells of a 96-well plate. Following overnight incubation to allow cells to adhere 100 μL fresh growth medium containing a range of drug concentrations were applied to wells. Following a further 48-hour incubation 20 μL of MTS reagent was added to each well. Following a 1-hour incubation absorbance at 490 nm was determined using an automatic plate reader. Wells containing medium only were used to subtract background absorbance before

As previously described, inhibitors were added for the final 24 hours before lysis and Western blotting performed for MSK1 and MK2 phosphorylation (Figure 5.7). Treatment with the p38 inhibitor SB202190 led to a loss of MK2 phosphorylation as previously noted at 10 μM. As would be expected, given that MK2 is not a substrate of ERK, no decrease in phosphorylation was observed when cells were treated with 20 μM U0126. Results showed that MSK1 retained some phosphorylation when cells were treated with 20 μM U0126, whilst no signal was detected in the presence of 10 μM SB202190. This confirmed that substrates were activated by p38 and that ERK was dispensable.

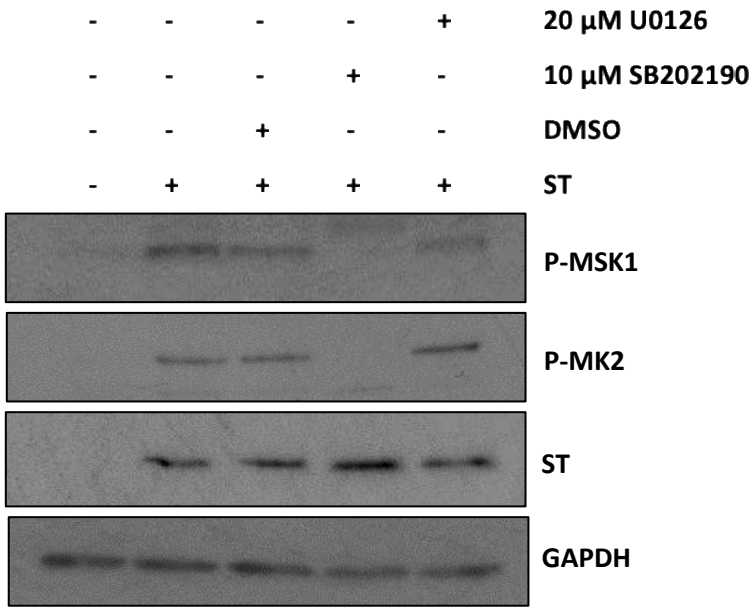

Figure 5.7: Inhibition of ERK activity does not affect MAPK substrate phosphorylation. HEK293 cells were transfected with empty vector or ST for 6 hours before aspiration of transfection complexes and replacement with fresh growth medium containing drug as described. Following a 48-hour incubation lysis using Leeds lysis buffer performed. Antibodies were used to detect phosphorylated MK2 and MSK1 that corresponded to activated protein. GAPDH was used as a loading control and 2T2 hybridoma to detect ST.

5.7 p38 inhibition abrogates ST-induced cellular motility

MCPyV ST manipulates the cellular cytoskeleton to enhance migration and motility. Research previously published by our laboratory showed that manipulation of cellular protein phosphorylation was essential for both microtubule destabilisation and actin polymerisation which led to enhanced filopodia formation. In both instances ST interaction with cellular protein phosphatases was required, however a mechanistic link between phosphatases and phenotypic alterations was never fully elucidated. It was therefore investigated whether p38 activity was important for cellular motility by performing a scratch assay utilising a monoclonal HEK293 FlpIn cell line with tetracycline-inducible ST expression. Scratches were performed 24-hours after ST-expression was induced by treatment with 2 μg/mL doxycycline hyclate. 10 μM SB202190 or appropriate control was incubated with cells for 1-hour

before scratching was performed and maintained for the duration of the time course. Images were taken 1- and 48-hours post-scratch to determine wound closure.

Results were similar to previous publications, with induction of ST expression significantly increasing the speed at which the wound closed (Figure 5.8A). Through comparison of the initial scratch (dashed blue line) with the distance closed (dashed red line), results showed that the induced sample was almost fully closed, whilst the uninduced cells displayed much less wound closure suggesting that ST promoted cellular motility. Interestingly, treatment with 10 μM SB202190 led to a reduction in the rate of wound closure that was comparable with uninduced cells.

Measurements of the width of each scratch were performed for each image to determine the speed at which wounds closed. Given that across all scratches there was not complete closure this was calculated as μm/hour. Results showed that cells not expressing ST displayed wound closure speeds of 5 μm/hour, whilst ST expressing cells displayed significantly increased closure of 12 μm/hour (Figure 5.8B). Treatment with SB202190 reduced wound closure to 5 μm/hour which was comparable with uninduced cells. This therefore suggested that inhibition of p38 was sufficient to prevent ST-induced wound closure following an initial scratch.

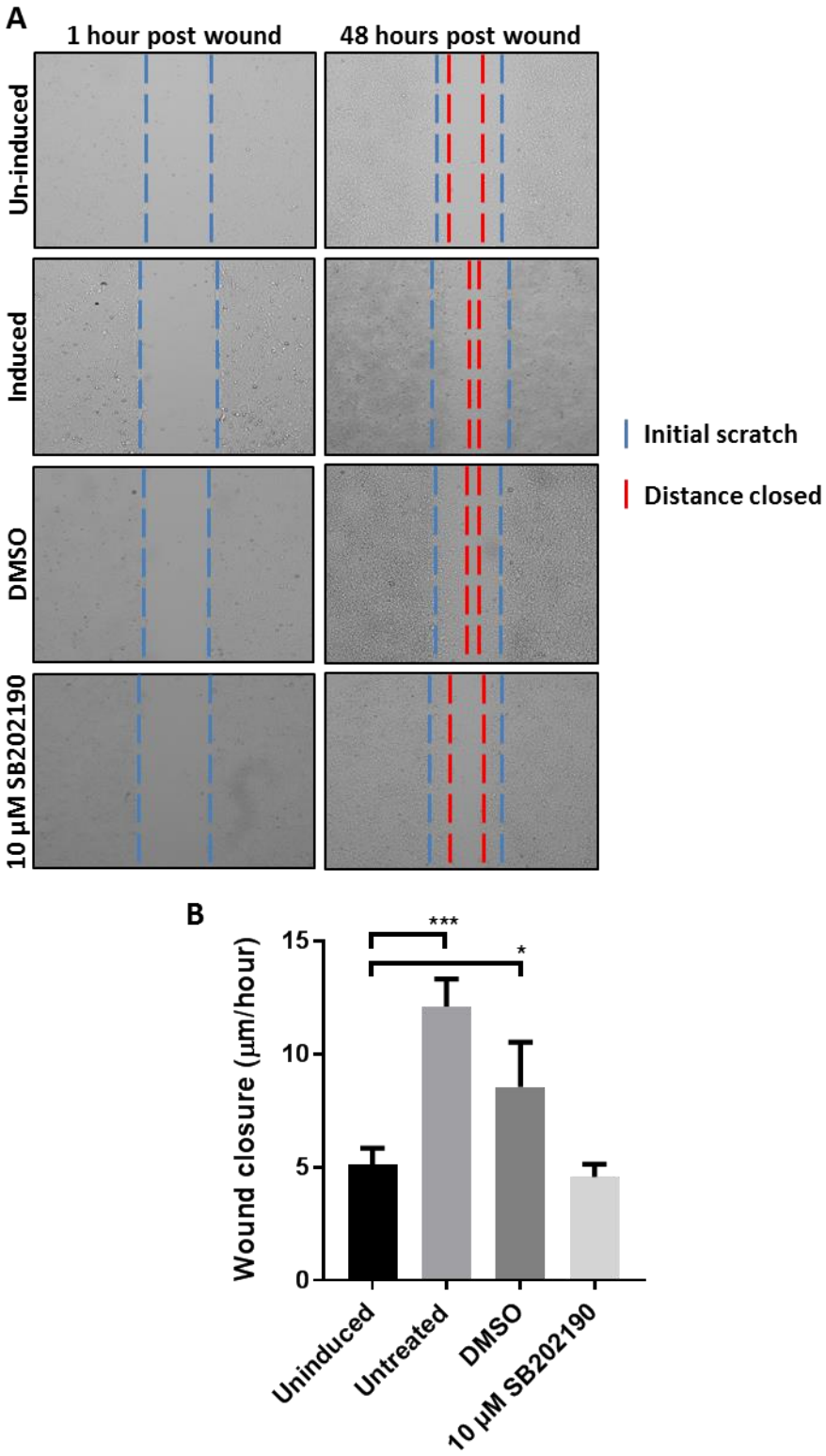

Figure 5.8: Scratch assay to determine the effect of p38 inhibition upon ST-induced cellular motility and migration. (A) Representative images of wound closure at 1- and 48-hours post scratch. (B) Analysis of wound closure of three biological repeats. ST-inducible HEK293 cells were seeded into wells of a 12-well poly-l-lysine treated plate. Growth medium +/- c 2 µg/mL doxycycline hyclate was added to wells and incubated for 24-hours to allow wells to reach 100% confluence. Growth medium was changed to fresh medium containing drug for 1-hour before a scratch was performed using a Thermo Fisher 100 µL ClipTip™. Cells were washed once with PBS to remove dislodged cells before addition of fresh growth medium containing drugs as applicable. Wells were then imaged 1- and 48-hours post scratch using an EVOS II FL Auto. Wound closure analysis was performed using ImageJ and blue and red dashed lines are indicative of initial and final boundaries, respectively.

5.8 p38 inhibition restricts migration of MCPyV-positive MCC

Given that results suggested that p38 inhibition prevented ST-induced cellular motility, it was investigated whether the same restriction would be observed in MCPyV-positive MCC cell lines.

The MCPyV-positive PeTa and WaGa cell lines were available within the laboratory. The effects of p38 inhibition upon the cell lines was determined by MTS assay (Figure 5.9). Results indicated that SB202190 and SB202474 had little effect upon cellular viability, suggesting that the drugs were not cytotoxic or displayed any effects upon cellular proliferation at concentrations of 1 and 10 μM.

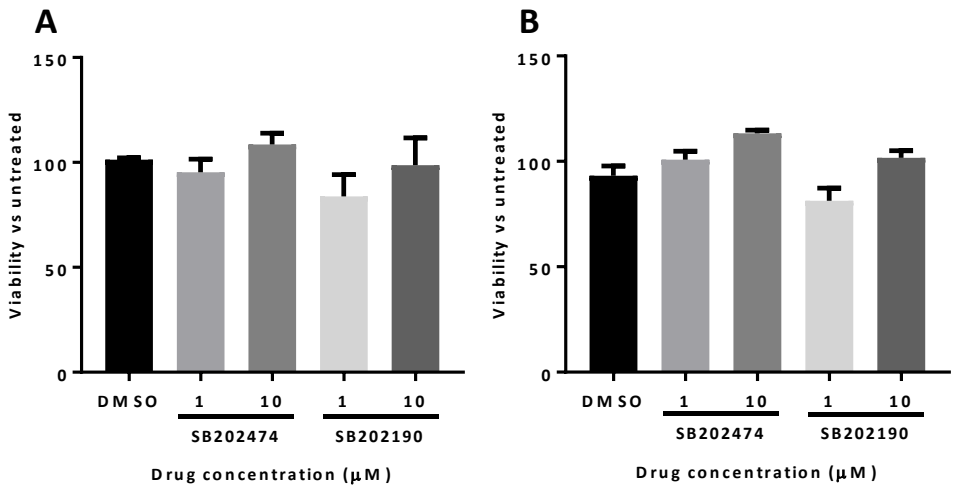

Figure 5.9: MTS assays to determine whether p38 inhibitors display cytotoxicity or affect proliferation of MCPyV-positive MCC cell lines PeTa (A) and WaGa (B). $2x10^5$ PeTa and WaGa cells were plated in wells of a 96-well plates containing 1 or 10 μM of SB202190 or SB202474. Following a 48-hour incubation 20 μL of MTS reagent was added to the wells before a further 1-hour incubation. Absorbance at 490 nm was determined using an automatic plate reader. Wells containing medium only were used to subtract background absorbance before comparison of each concentration to an untreated equivalent. Each condition was performed in triplicate.

Given that the available cell lines grew in suspension, it was not possible to perform scratch/wound healing assays. As an alternative, a transwell migration assay was performed using PeTa cells. Cells were incubated in reduced serum growth medium (containing 0.5% (v/v) FBS) and inhibitors where applicable for 24 hours. Cells were

transferred to the upper chamber of the transwell, with serum enriched growth medium (containing 20% (v/v) FBS) added into the lower chamber as a chemoattractant. Following a further 48-hour incubation the number of cells in the upper and lower chambers were counted and the percentage of cells migrated in each condition calculated, with untreated cells assumed to represent unrestricted migration (Figure 5.10). Results showed that the DMSO control and treatment with 10 μM SB202474 displayed no significant decrease in the number of migrated cells. In contrast, treatment with 10 μM SB202190 led to a significant loss of migration, with a 62% reduction in the number of migratory cells compared to untreated. This confirmed that p38 activity was essential to promote migratory phenotypes associated with MCC and that inhibition of p38 was sufficient to restrict the migration of the MCPyV-positive MCC PeTa cell line.

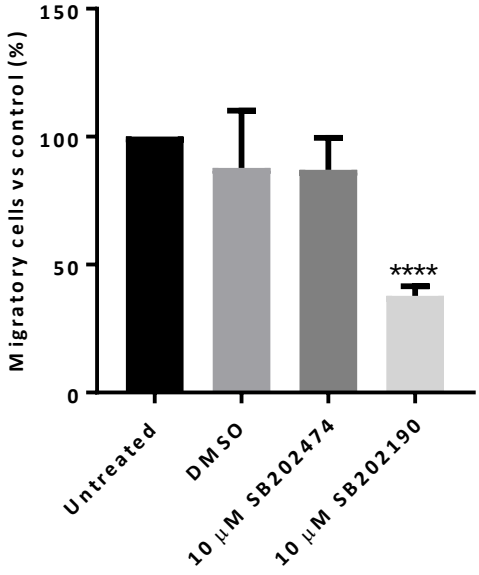

Figure 5.10: Effect of p38 inhibition upon the migration of MCPyV-positive MCC PeTa cells. $1x10^6$ PeTa cells were seeded in serum depleted medium (containing 0.5% (v/v) FBS) containing drug if applicable in wells of a 12-well plate. Following a 24-hour incubation 300 μL of serum depleted medium containing cells was added to the top chamber of a transwell. Serum enriched medium (containing 20% (v/v) FBS) was added to the bottom chamber before an incubation for 48-hours to allow cells to migrate. Medium was taken from both the top and bottom chambers and cell counts performed using a Countess II FL Automated cell counter. The percentage of migrated cells for each condition were calculated and then compared to an untreated control.

5.9 ST-mediated p38 activation is via MKK4 signalling not canonical MKK3/6

Activation of the MAPKs typically follow well characterised cascades in response to stress stimuli. In the case of p38, activation is typically initiated by the MAP2Ks, MKK3 and MKK6. The kinase screen previously performed in Figure 5.1 suggested that there was potentially upregulation of MKK3/6 phosphorylation.

To elucidate whether upstream kinases are activated or whether ST directly targets p38, ST was expressed in cells before Western blotting for phosphorylated MKK3/6. Results showed that following expression of ST, the phosphorylation status of MKK3/6 remained unchanged (Figure 5.11).

Whilst this result was surprising, given that MKK3/6 is attributed to p38 activation in most cases, a more debatable and alternative mechanism of activation relies upon phosphorylation of MKK4. Results showed that MKK4 showed significantly increased phosphorylation compared to mock transfected cells (Figure 5.11). This therefore suggested that ST-induced activation was via the non-canonical MKK4 cascade, potentially independently of MKK3/6. Observed differences in ST-induced MKK3/6 phosphorylation for the kinase screen were believed to be due to amplification of slight variance in basal levels of phosphorylation.

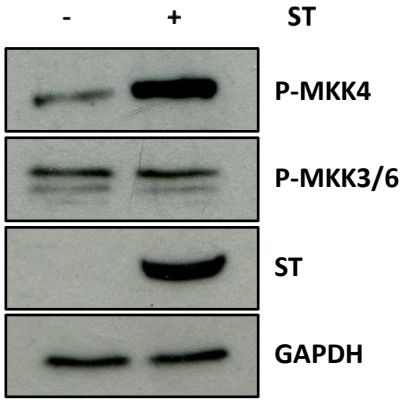

Figure 5.11: ST-mediated activation of p38 is via MKK4 signalling, independent of MKK3/6. HEK293 cells were transfected with empty vector or ST before a 48-hour incubation. Lysis using Leeds lysis buffer was performed. Antibodies were used to detect phosphorylated MKK4 and MKK3/6 that corresponded to activated protein. GAPDH was used as a loading control and 2T2 hybridoma to detect ST.

5.10 Activation of p38 is independent of extracellular stimuli

Activation of MAPKs is associated with extracellular stress stimuli. Due to the fact that ST activated the p38 pathway via a non-canonical MKK4 mechanism, it was investigated whether extracellular stimuli were required, or if activation was due to manipulation of cascades through protein-protein interactions, independent of stimuli.

HEK293 cells were transfected with ST before lysis after 48 hours. To evaluate the requirement of extracellular stimuli, medium was either unchanged or changed with fresh serum free-medium for the final two hours before lysis. As previously shown, results indicated that when the medium was not changed a small amount of basal MKK4 phosphorylation was observed in mock transfected cells, which was significantly increased upon ST expression (Figure 5.12). Following incubation with serum-free medium, basal phosphorylation of MKK4 was lost in cells that were mock transfected. In contrast, ST-expressing cells maintained phosphorylation of MKK4, which suggested that ST activated the p38 pathway independent of extracellular stimuli.

To determine whether p38 was active both with and without medium change, the phosphorylation status of MK2 was investigated. Results showed that in both conditions upregulated phosphorylation of MK2 was maintained upon ST expression. There was however detection of basal MK2 phosphorylation in mock transfected samples under both conditions. As such, further investigation would be required to determine whether this activation was due to basal MKK3/6 activation or whether the kinetics of p38 and/or MK2 dephosphorylation would require longer incubation to observe loss or will maintain basal phosphorylation in a range of conditions.

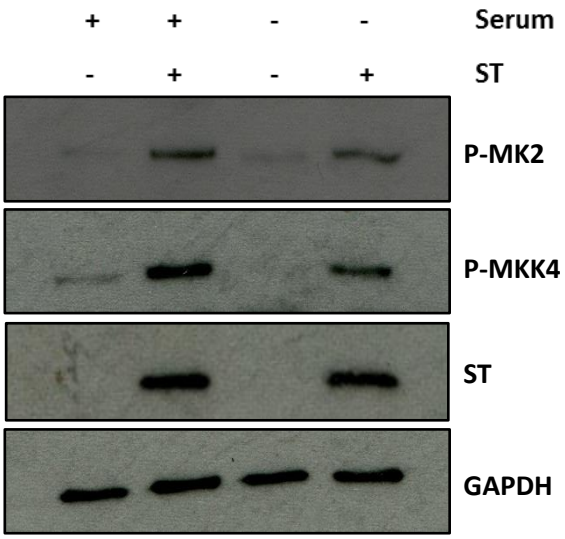

Figure 5.12: ST activates the p38 cascade independent of extracellular stimuli. HEK293 cells were transfected with empty vector or ST before a 46-hour incubation. Cells were then washed twice with PBS before replacement with fresh growth medium or medium containing no serum for 2 hours. Lysis using Leeds lysis buffer was then performed. Antibodies were used to detect phosphorylated MK2 and MKK4 that corresponded to activated protein. GAPDH was used as a loading control and 2T2 hybridoma to detect ST.

5.11 p38 cascade activation is dependent upon a ST-PP4C interaction

Due to continued MKK4 phosphorylation independent of extracellular stimuli, potential mechanisms through which ST could dysregulate the p38 signalling cascade were explored. ST has been shown to interact with protein phosphatases to manipulate the host cellular environment and due to the link between cellular phosphatases and protein phosphorylation, the possibility that ST interactions with phosphatases led to p38 dysregulation was investigated.

ST has previously been identified to interact with several protein phosphatase subunits including PP2A Aα, PP2A Aβ and PP4C. ST mutants have previously been generated to prevent interaction with different protein phosphatase subunits, which are summarised in Table 5.1. The Δ100-103 mutant, which cannot bind to any phosphatase subunit was produced through substitution to alanine at each residue. The R7A mutant provided loss of PP2A Aα binding and the R102A mutant led to loss

of PP4C binding. The F103A mutant led to loss of PP4C and PP2A Aβ binding and therefore if this mutant showed a change in phenotype whilst the R102A mutant retained wild-type phenotypes, this would have suggested that PP2A Aβ interaction was required for any phenotypic changes and that it was independent of PP4C binding.

Table 5.1: ST mutants and the loss of protein phosphatase subunit binding.

ST mutant	Maintains interaction with	Does not interact with
R7A	PP2A Aβ + PP4C	PP2A Aα
Δ100-103	None	PP2A Aα, PP2A Aβ + PP4C
R102A	PP2A Aα + PP2A Aβ	PP4C
F103A	PP2A Aα	PP2A Aβ + PP4C

The described mutants were available within the laboratory as GFP-tagged constructs, which were utilised in order to determine whether protein phosphatase interactions were important for manipulation of the p38 cascade. HEK293 cells were transfected with the ST-GFP mutants before Western blotting for phosphorylated MK2. Results showed that all constructs led to a similar amount of GFP-tagged mutant ST protein expression, which was confirmed by detection of GFP (Figure 5.13). The R7A mutant retained phosphorylation relative to WT, however all other mutants showed phosphorylation comparable to the GFP control. This suggested that PP4C was important for ST mediated p38 activation, given that all mutants that were unable to bind PP4C displayed loss of MK2 phosphorylation.

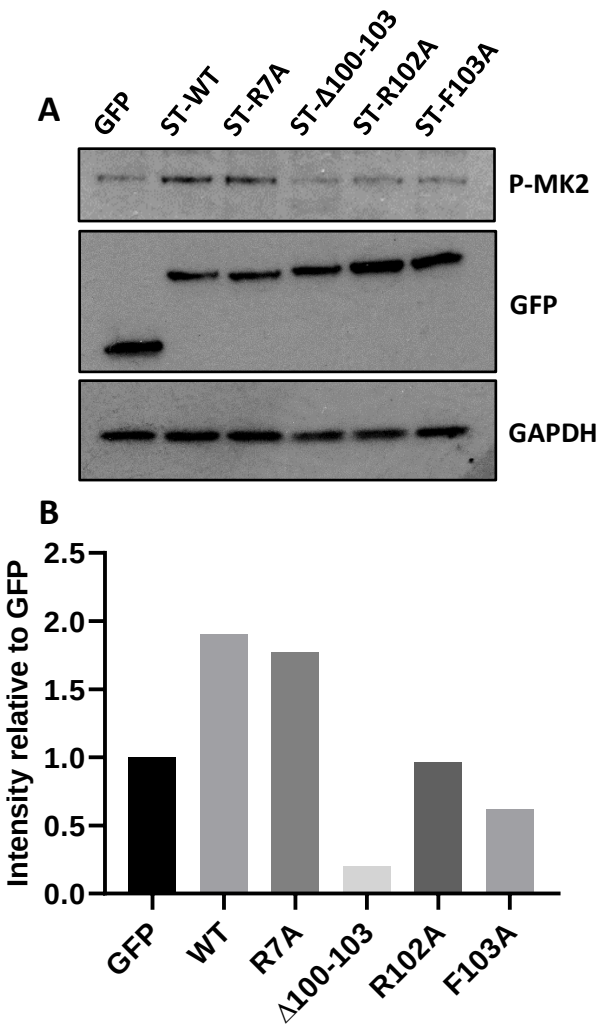

Figure 5.13: MK2 phosphorylation requires the interaction of ST with PP4C (A) and analysis by densitometry (B). HEK293 cells were transfected with GFP or an ST-GFP mutant before a 48-hour incubation. Lysis using Leeds lysis buffer was performed. An antibody was used to detect phosphorylated MK2, which corresponded to activated protein. GAPDH was used as a loading control and GFP to detect the expression of ST mutants. Densitometry was performed to determine MK2 phosphorylation using GAPDH as a control for expression to which values were normalised.

5.12 ST interacts with PP4C to perturb wild-type activities

Following identification that an interaction between ST and PP4C was essential for activation of the p38 pathway, the requirement of PP4C was further investigated. In order to determine whether the activity of PP4C was essential, WT and trans-dominant negative (TDN) PP4C constructs were co-transfected into HEK293 cells, in the presence of ST.

Results showed that expression of a TDN PP4C had no effect upon ST-induced hyperphosphorylation of MK2 (Figure 5.14A). Analysis by densitometry further confirmed that overexpression of the TDN PP4C had no phenotypic consequences in regard to MK2 phosphorylation, with results consistent to that of cells transfected with ST only (Figure 5.14B). Conversely, results indicated that co-transfection with WT PP4C led to reduced MK2 phosphorylation (Figure 5.14A+B). Overexpression of WT PP4C likely increased the total number of protein subunits compared to the normal cellular environment. Therefore, ST would be unable to bind all PP4C subunits to prevent the normal formation and functions of PP4, which could have a regulatory role upon ST-induced p38 activation. Taken together these results suggested that the interaction of ST with PP4C is required to perturb regulatory functions of PP4.

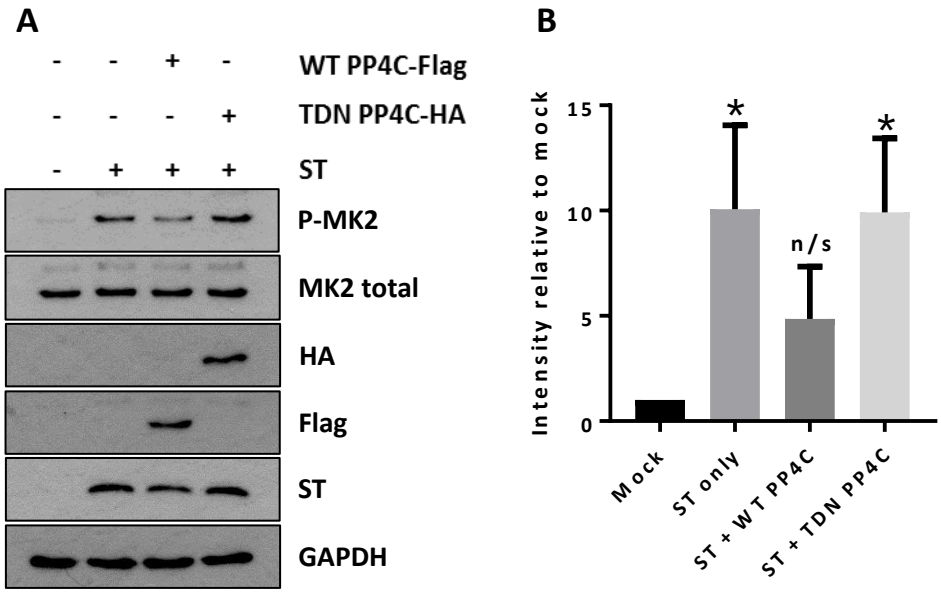

Figure 5.14: Dysregulation of PP4C is required for MCPyV ST induced hyperphosphorylation of MK2 (A) and analysis by densitometry (B). HEK293 cells were co-transfected with empty vector or ST +/- WT/TDN PP4C before a 48-hour incubation. Lysis using Leeds lysis buffer was performed. An antibody was used to detect phosphorylated MK2, which corresponded to activated protein. Flag and HA antibodies were used to detect WT and TDN PP4C, respectively. GAPDH and MK2 were used as a loading control and 2T2 hybridoma to detect ST. Densitometry was performed to determine MK2 phosphorylation using MK2 total as a control for expression to which values were normalised.

5.13 Discussion

Previous studies within our group have identified that MCPyV ST induces phenotypic alterations in a range of cytoskeletal proteins to enhance cellular motility. It has previously been demonstrated that the phosphorylation status of stathmin is manipulated by ST to promote microtubule destabilisation and ST-mediated Rho-GTPase activities are required to induce filopodia formation.

Despite clear evidence that phosphorylation-regulated protein activities are essential for ST-induced cellular motility, the mechanisms through which these phenotypes are brought about has not been fully elucidated. Given the requirement of

phosphorylation, coupled with the implication of protein phosphatase interactions in both studies, a kinase screen was performed to identify pathways that showed differential phosphorylation following ST expression. Results suggested that JNK2 and p38 isoforms displayed increased phosphorylation, which are members of the MAPK family. In this study a focus was placed upon the p38 pathway and ST-induced activation was confirmed using antibodies targeting p38 and activated downstream markers MK2, MSK1 and ATF2. Through the use of chemical inhibitors, it was further confirmed that MK2 and MSK1 were specifically phosphorylated by p38.

Scratch assays using ST-inducible HEK293 cells confirmed that p38 activity was required for ST-induced cellular motility. This was further confirmed using the MCPyV-positive MCC cell line PeTa in transwell assays, which again showed that p38 inhibition significantly restricted the migratory potential of cells.

Interestingly, results suggested that canonical MKK3/6 activation was not observed and that instead the lesser studied MKK4 potentially led to pathway activation. Results further indicated that p38 activation was independent of extracellular stimuli, as serum depletion did not prevent pathway activation. This suggested that ST-induced pathway activation was potentially mediated through pathway disruption within the cell.

ST has been well characterised to interact with and manipulate a range of protein phosphatases, therefore a panel of protein phosphatase binding mutants were utilised. Results suggested that interaction with PP4C was essential for p38 pathway activation and that PP2A Aα and PP2A Aβ interactions were dispensable. This was further confirmed using PP4C mutants, which showed that overexpression of WT PP4C reduced the ability of ST to phosphorylate MK2, whilst overexpression of a TDN PP4C has no consequences towards activation.

This study, in support of previously published data, has further highlighted that interaction of ST with PP4C is essential for enhancement of motility and migratory phenotypes that are associated with MCPyV-positive MCC. Here, a novel requirement of p38 pathway activity has been implicated in motility and investigation has found that inhibition can severely perturb migratory phenotypes.

Given that p38 phosphorylation can be directly linked to microtubule destabilisation via Tau mediated stathmin dephosphorylation, actin polymerisation through HSP27 phosphorylation, and vimentin stabilisation mediated by MK2 phosphorylation, there is the potential that p38 could represent a master regulator of ST-induced motility and migration.

Despite intense pharmaceutical interest in p38 as a therapeutic target, due to negative feedback and subsequent alternate pathway activation there are currently no suitable drugs that may be used for therapeutic intervention. Whilst there is still the potential that drugs may be developed in the future that specifically inhibit p38, given the currently low number of MCC cases in comparison to other diseases repurposing of available therapeutics may represent the most economic method of treatment. To this extent, complete mapping of how ST activates the p38 pathway may yield new proteins that could be targeted to restrict MCPyV-positive MCC.

In this study it was identified that ST-mediated activation is independent of extracellular stimuli and MKK3/6, which is not representative of classical p38 pathway activation. The identification of PP4C interaction as an essential mediator further highlights that ST manipulation is via intracellular mechanisms.

Previous data has recognised that ST interaction with PP4C is required for activation of the Rho-GTPases cdc42 and RhoA, which in turn induce filopodia formation and cell motility (Stakaitytė et al., 2017). Cdc42 and RhoA are typically associated with activation of MAPKs in response to TNFα to promote inflammatory responses via MKK4 activation of p38 and JNK. Whilst TNFα has been demonstrated to inhibit viral replication, there are several examples of viruses hijacking the response to enhance their lifecycles, such as during infection with BKPyV (Ribeiro et al., 2016). In the case of MCPyV it has previously been demonstrated that the LXCXE domain of LT can enhance expression of genes relating to cell cycle, DNA replication and cellular movement (Richards et al., 2015). The study reported that expression of several genes was enhanced when ST was co-expressed. Therefore ST-mediated activation of cdc42 and RhoA may increase gene expression or stabilise mRNAs through MAPK activation in addition to enhancing cellular motility.

Perturbing Rho-GTPase activity may therefore represent a potential target for inhibitors to prevent ST-mediated activation of p38 and ultimately restrict several metastatic phenotypes. Activity of cdc42 and RhoA depend upon (p21-activated kinases) PAKs to act as a scaffold and unpublished data from the laboratory demonstrated that siRNA mediated knock-out of PAK1 and PAK2 severely restricted migration and dissociation of ST-inducible cells. Disrupting PAK interaction with Rho-GTPases may possibly provide a novel approach in limiting MCPyV-positive MCC metastasis, however further investigation is currently required to link Rho-GTPases with p38 activation.

This study provides evidence that ST interaction with PP4C mediates p38 activation and by understanding the mechanisms, this may yield new potential targets in order to restrict the highly metastatic MCC and improve prognoses of patients.

Chapter 6

Final discussion

6.1 Introduction

The *Polyomaviridae* represents a diverse family of viruses that infect a wide range of mammals, birds and fish. Polyomaviruses ubiquitously infect the human population, maintaining a persistent asymptomatic infection in an immunocompetent host. BKPyV and JCPyV were identified as the causative agents of disease in immunocompromised humans in the early 1970s, however in contrast to the polyoma name, human polyomaviruses for a long time were not identified as the cause of cancer. This changed in 2008, when technological advances facilitated the identification of MCPyV as the causative agent of MCC (Feng et al., 2008).

The progression from MCPyV infection to MCC is the culmination of a series of events (Shuda et al., 2008; Schrama et al., 2019). Following expression of TAgs, UV-mediated mutation leads to rolling circle DNA replication of genomes containing a premature stop codon that truncates LT, resulting in loss of C-terminal activities including the helicase domain. With degradation over time of WT LT, the virus is unable to produce new progeny and complete its lifecycle. Instead, the mutated genome becomes integrated into the host, where expression of tLT, alongside the oncoprotein ST, promotes transformation of the host cell and ultimately MCC.

Despite obvious focus upon the association of MCPyV with MCC, the virus is also an example of a VP3-less polyomavirus. Most polyomaviruses can express and incorporate two minor capsid proteins, VP2 and VP3, into the capsid (Decaprio and Garcea, 2013). However, MCPyV lacks the ability to express a second minor capsid protein and therefore packages only one type of minor capsid protein (Schowalter and Buck, 2013). This uncommon feature makes MCPyV an attractive species to study, as comparison with other polyomaviruses could permit the identification of conserved requirements and development of therapeutics that are applicable to a range of diseases that are caused by continuous polyomavirus infection.

6.2 Creating systems to study polyomaviruses

A significant challenge to studying early events in human polyomavirus infection is a lack of cell systems in which the polyomavirus replicates. MCPyV is prime example, with a complex cocktail of inhibitors, enzymes and growth factors required to permit

productive infection of human dermal fibroblasts (Liu et al., 2016). To date there is little evidence of alternative cell lines that are permissive to MCPyV infection. Host range however, is not likely restricted by entry events, as other cell lines have been shown to permit transduction of PsVs containing reporter vectors, suggesting that a lack of replicative ability confines host range (Schowalter and Buck, 2013).

Due to the simplistic architecture of small non-enveloped DNA viruses, production of virus-like particles (VLPs) and PsVs is a plausible alternative to study polyoma and papillomaviruses (Pastrana et al., 2004; Buck and Thompson, 2007; Schowalter and Buck, 2013; Gee et al., 2013; Zhang et al., 2018; Becker et al., 2019) Whilst a VLP, which is an empty viral capsid, provides a useful tool to identify structural features of viruses, their application in functional studies is limited, due to lack of end-point analysis. An exploitable feature of polyoma and papillomaviruses is that they promiscuously package dsDNA. Therefore, reporter vectors that efficiently express proteins such as GFP or luciferase can be packaged into the capsid to mimic infection, with endpoint analysis of reporter features such as fluorescence and luminescence to determine early lifecycle events and requirements.

Despite protocols detailing the overall method to produce MCPyV PsVs being publicly available, at the start of this study there had been little investigation into early events in the lifecycle of MCPyV. The dual mechanism of how MCPyV binds to and enters the host cell had been characterised however, beyond this, information was limited (Schowalter et al., 2011). We therefore optimised the production of PsVs containing two different reporters. Firstly, PsVs were produced that contained either a GFP reporter or a secreted luciferase reporter in which EdU was incorporated to permit evaluation of successful trafficking and subcellular localisation, respectively. Previous use of GFP PsVs has relied upon flow cytometry to quantify the number of GFP-positive cells, which has presented challenges leading to limited studies. Therefore, the development of Incucyte-based detection provided a new, rapid and high-throughput method to study not only MCPyV or polyomaviruses, but any pseudovirus that will readily encapsidate vectors encoding fluorescent reporter proteins.

In contrast to MCPyV, SV40 infection is highly efficient and requires no artificial manipulation of the host cell. Therefore, rather than producing PsVs to provide comparison for any phenotypic changes seen during drug screening, infection with SV40 represents a more physiologically relevant system. Analysis of SV40 infection had previously been performed by Western blotting or flow cytometry using antibodies to detect the expression of viral proteins. Similar to systems that use PsVs, these methods have several limitations when factoring time and reagent consumption. We therefore investigated whether a 96-well plate format could be coupled with Incucyte analysis to reduce the amount of reagent required and processing time during SV40 experimentation.

Methods to quantify SV40 titres have seen little improvement since the optimisation of plaque assays in 1983 (Fendrick and Hallick, 1983). Whilst the plaque assay remains a routine and robust method of quantification, assays can take several weeks and can lack sensitivity. A more recent titration protocol coupled immunofluorescence with analysis by flow cytometry, reducing assay time to 2 days but increased the amount of reagents consumed (Drayman et al., 2010). Incucyte detection provided a new approach to the protocol used for flow cytometry, with a rapid and accurate method, which had the added benefit of using little virus stock or reagents to determine titre. Given that polyomaviruses have a relatively slow lifecycle and many do not exhibit lytic release required for plaque formation, quantification of other polyomavirus titres is typically performed by haemagglutination assay (Sinibaldi et al., 1987; Knowles et al., 1995; Hamilton et al., 2000; Knowles and Sasnauskas, 2003). As is found with PsVs, polyomaviruses may package non-viral DNA and there is a growing understanding that a significant proportion (approximately 30%) of virions may in fact package DNA that is not virus genomes (personal communications with Dr Christopher Buck). These viruses are likely to impact upon the reliability of titration by haemagglutination assay. Detection of infected cells by Incucyte analysis therefore could offer a more accurate and reliable method to determine virus titre.

6.3 Ion channels and polyomavirus infection, novel therapeutic targets?

Polyomaviruses are well established to traffic through the endo/lysosomal network following penetration and to require an acidified environment for initial proteolytic capsid rearrangements (Pelkmans et al., 2001; Querbes et al., 2006; Liebl et al., 2006; Jiang et al., 2009; Becker et al., 2019). Despite knowledge that polyomaviruses require an acidified environment, how far the virions enter the endo/lysosomal network had not been established. We therefore utilised EGA to determine whether virions were entering late endo/lysosomes or if there was a molecular cue to trigger earlier release from endosomes at a higher pH. Results indicated that MCPyV and SV40 could not infect the cell following treatment with EGA, confirming that polyomaviruses entered into acidified endosomes. The pH requirement for EGA action is currently unknown, therefore environmental acidity would have to be determined by another mechanism, such as using pH-sensitive dyes alongside infection with the viruses. Pre-treatment of virions in buffers with a range of pH prior to incubation with cells exposed to NH_4Cl could provide an alternative approach to determine pH requirements. However, experiments of this nature using BUNV showed that incubating the virus in a low pH buffer alone was not sufficient to enhance virus infectivity, with the presence of K^+ also essential (Hover et al., 2018). Results indicated that MCPyV required K^+ channel activity, with several channel inhibitors leading to a reduction in GFP-positive cells. This could provide evidence that a similar mechanism to BUNV is required for initial entry events, and it would be interesting to see whether similar treatment with low pH and high K^+ could enhance MCPyV transduction.

This mechanism would likely not be conserved for all polyomaviruses, since K^+ channel inhibition showed no effect upon the infection of SV40. While this was not consistent with the hypothesis of a universal requirement, there are several reasons that this may be the case. Firstly, experiments using SV40 were performed using a monkey cell line and MCPyV used a human line, therefore the requirement of K^+ channel activity may be specific to infection of human cells. Given that MCPyV can transduce only a small subset of cell lines, performing SV40 infections in human cell

lines may represent a better opportunity to further investigate whether effects are specific for host species. Alternatively it may be that K^+ channels constitute a requirement for infection of cells for human polyomaviruses and not simian polyomaviruses. Investigation as to whether viruses including BKPyV and JCPyV display similar requirements for K^+ channels could reveal if this is conserved or represents a unique condition for infection with a VP3-less polyomavirus. BKPyV is also able to infect Vero cells, therefore this virus represents an ideal candidate to further investigate polyomavirus requirements of K^+ channels (Eash et al., 2004).

Treatment using the T- and L-type Ca^{2+} channel inhibitor verapamil reduced MCPyV transduction and SV40 infection. Further investigation identified that L-type channel inhibition alone was not sufficient to inhibit infection by either virus. Whilst data was preliminary, treatment with the T-type Ca^{2+} channel inhibitors mibefradil and flunarizine showed dose-dependent results, with 10 μM of each compound abolishing MCPyV transduction. Neither drug however reduced SV40 infection, suggesting that T-type channel activity, similar to K^+ channels, may be cell line or polyomavirus species dependent and further investigation would be required to establish if that is the case.

It was however intriguing that SV40 infection could be inhibited by verapamil, but not by T- or L-type specific inhibitors. Whilst there was the potential that SV40 could activate both subfamilies of Ca^{2+} channel, given that polyomaviruses traffic through the endo/lysosomal network before fusion with the ER, it was also possible that a mechanism comparable to EBOV could have been inhibited. EBOV requires the activity of TPC1/2 to lower Ca^{2+} concentration within the endosomal compartment to facilitate fusion with endosomes, a process that can be prevented by verapamil-mediated NAADP signalling inhibition (Sakurai et al., 2015). Therefore, the inhibitory effect of verapamil upon SV40 infection may be due to loss of TPC activity and Ca^{2+} release. This requirement may be conserved between polyomaviruses and in the case of MCPyV is masked by an additional requirement of T-type channel activity. To further investigate whether TPC activity is required, the NAADP-signalling inhibitor tetrandrine or RNAi-mediated knock out of TPCs could be used. Given that EBOV has a very different virion structure to the polyomaviruses SV40 and MCPyV,

identification of comparable sensitivity to loss of TPC channel activity may reveal an essential check point for a wider range of viruses that traffic through the ER.

In this study, verapamil was shown to inhibit both SV40 infection and MCPyV transduction and may represent a potential therapeutic for the treatment of diseases related to polyomavirus infection, as the drug is already in clinical use and could therefore be repurposed without many of the stringent tests required prior to a drug reaching market. Similarly, mibefradil and flunarizine are available therapeutics and by identifying whether these inhibitors have an effect upon other human polyomaviruses, they may yield new avenues in the treatment, restriction and prevention of polyomavirus-associated disease.

In a wider context, this study has identified Ca^{2+} channels that are important in the sorting of a virus whilst transiting through the endo/lysosomal network. Whilst the roles of such ion channels remain elusive in the context of normal endo/lysosomal functions, this study highlights potential therapeutics that could be used for the treatment of channelopathies relating to Ca^{2+} channels in non-excitable cells.

6.4 p38 MAPK drives ST-mediated cellular motility and migration

MCC is a highly aggressive and metastatic form of skin cancer that originates from Merkel cells found around hair follicles and in the touch-sensitive basal layers of the epidermis (Morrison et al., 2009; Spurgeon and Lambert, 2013). In a minority of cases, UV exposure leads to extremely high mutational burden and non-viral MCC, however it is more common that clonal integration of a replication-defective MCPyV genome drives tumorigenesis, compensating for tens of thousands of somatic mutations (Starrett et al., 2017). Despite truncation of the LT. gene being an essential prerequisite for MCPyV-positive MCC, ST is the major oncogene. ST alone is sufficient to promote anchorage- and contact-independent growth of rodent fibroblasts and RNAi targeting of ST leads to growth arrest of MCPyV-positive MCCs (Shuda et al., 2011; Shuda et al., 2014).

Previous publications from the Whitehouse laboratory have identified that ST is responsible for driving cellular motility, migration and invasion, with cytoskeletal rearrangements requiring an essential interaction with the cellular protein

phosphatase, PP4C. This interaction facilitates dephosphorylation of stathmin to prevent acetylation as well as promoting destabilisation of microtubules and actin polymerisation through activation of the Rho family GTPases cdc42 and RhoA (Knight et al., 2015; Stakaitytė et al., 2017). Despite evidence that signalling pathways were modulated to promote migratory phenotypes, there had been little study into the molecular mechanisms by which ST facilitates such alterations. We therefore investigated whether signalling pathways were dysregulated by ST to promote migratory phenotypes.

Initial screening of kinases that were differentially phosphorylated at activation-associated residues following ST expression suggested that the level of p38 isoforms was upregulated. Subsequent analysis confirmed that p38 was hyperphosphorylated in its activation loop and three substrates, MK2, MSK1 and ATF2, all displayed increased phosphorylation. Further characterisation determined that p38 activation was essential for ST-induced enhanced migratory phenotypes in cells overexpressing ST and in MCC cell lines.

This study provides evidence that MCPyV-induced activation of p38 MAPK signalling is mediated by ST interaction with PP4C which dysregulates regulatory functions of phosphatase targeting, or upstream of, MKK4. This novel finding highlights how PP4C acts as a regulator of MAPK signalling and potentially implicates it as a target for modulation of diseases associated with p38 dysregulation.

Whilst ST expression enhances migratory phenotypes, further investigation is required to link p38 activity with microtubule destabilisation and actin filament formation. Heat shock protein 27 (HSP27) activity is directly related to the polymerisation of actin, accumulation of F-actin structures and promotion of cell migration (Mounier and Arrigo, 2002). p38 activation of the kinase MK2, which is hyperphosphorylated following ST expression, can in turn phosphorylate and activate HSP27 leading to actin polymerisation (Larsen et al., 1997; Guay et al., 1997; Sébastien et al., 2004). This may therefore represent the axis through which ST enhances F-actin, however a link between PP4C, RhoGTPases and p38 signalling is not currently known.

PP4C dephosphorylation of stathmin has not been shown to be a direct interaction. Therefore, ST may induce dephosphorylation through signalling pathways. Tau is a protein that is predominantly associated with Alzheimer's disease, however it also regulates microtubule stability, with hyperphosphorylation of Tau leading to dissociation from microtubule filaments to promote destabilisation (Kadavath et al., 2015). p38α activity is required for hyperphosphorylation of Tau, therefore p38 activation by ST may also contribute to the destabilisation of microtubules in addition to the effects of stathmin (Maphis et al., 2016). Unpublished data from the Whitehouse laboratory has also shown that, following ST expression, vimentin (a cytoskeletal intermediate filament protein and marker of EMT), is increased at the protein, but not at the RNA level (data not shown). Vimentin is a substrate of MK2 and therefore phosphorylation may lead to stabilisation, EMT and ultimately metastasis (Cheng et al., 2003; Powell et al., 2003; Wang et al., 2018).

Whilst immunotherapy targeting the PD1/PDL1 checkpoint is showing promise in the treatment of MCC, given the advanced age of patients and relatively low number of cases, it would be naïve to believe that pharmaceutical interest in MCC would be economically viable and management of disease to prolong life may represent a more viable option. With life expectancy increasing, incidence of such diseases is increasing, and it is therefore important to have a better understanding of the mechanisms by which viruses transform host cells and identify potential therapeutic targets. This chapter described a novel mechanism whereby ST interaction with PP4C mediates p38 pathway activation and promotion of phenotypes that are associated with metastasis. Whilst direct pharmaceutical interest in MCC is unlikely, the association of p38 activation with a range of diseases has led to a large body of investigation (Fisk et al., 2014; Xing, 2016; Patnaik et al., 2016; Scheltens et al., 2018). Issues with negative feedback causing unwanted side effects are a current stumbling block, however in the future it may be that modulation of p38 by targeting upstream factors can be used in clinic to restrict the metastatic potential of MCPyV-positive MCC and improve patient survival.

6.5 Concluding remarks

In summary, work described in this thesis provides two approaches that identify potential therapeutic targets for restriction of polyomavirus infections in general and metastasis of MCPyV-positive MCC.

Firstly, novel systems to study early events in the lifecycle of MCPyV and SV40 were described, with subsequent identification of the clinically available Ca^{2+} channel inhibitor verapamil that restricted the ability of both viruses to enter the cell. Furthermore, T-type Ca^{2+} channel and K^{+} channel inhibitors limited transduction of MCPyV. Continued investigation will find if MCPyV requirements are conserved among other human polyomaviruses. This study highlights the potential of repurposing clinically available drugs in the intervention and prevention of diseases related to polyomavirus infection.

Secondly, the highly metastatic phenotypes associated with MCPyV-positive MCC and expression of ST were shown to require activity of the p38 MAPK pathway. With intense pharmaceutical interest in this pathway, there is the potential that future identification of potent inhibitors could be used to restrict MCC metastasis and improve the prognosis of patients.

Taken together, the findings presented in this thesis advance the current understanding of entry requirements of polyomaviruses and pathways manipulated by MCPyV ST to promote metastasis. Elucidation of these events provides new insights into the molecular mechanisms for which polyomaviruses cause disease and emphasise the potential of repurposing available drugs to restrict disease and ultimately improve patient survival.

.

References

Abdul-Sada, H., Müller, M., Mehta, R., Toth, R., Arthur, J.S.C., Whitehouse, A. and Macdonald, A. 2017. The PP4R1 sub-unit of protein phosphatase PP4 is essential for inhibition of NF-κB by merkel polyomavirus small tumour antigen. *Oncotarget*. **8**(15), pp.25418–25432.

Abend, J.R., Joseph, A.E., Das, D., Campbell-Cecen, D.B. and Imperiale, M.J. 2009. A truncated T antigen expressed from an alternatively spliced BK virus early mRNA. *Journal of General Virology*. **90**(5), pp.1238–1245.

Akhbari, P., Tobin, D., Poterlowicz, K., Roberts, W. and Boyne, J.R. 2018. MCV-miR-M1 Targets the Host-Cell Immune Response Resulting in the Attenuation of Neutrophil Chemotaxis. *Journal of Investigative Dermatology*. **138**(11), pp.2343–2354.

Allander, T., Andreasson, K., Gupta, S., Bjerkner, A., Bogdanovic, G., Persson, M.A.A., Dalianis, T., Ramqvist, T. and Andersson, B. 2007. Identification of a Third Human Polyomavirus. *Journal of Virology*. **81**(8), pp.4130–4136.

Allen, P.J., Bowne, W.B., Jaques, D.P., Brennan, M.F., Busam, K. and Coit, D.G. 2005. Merkel cell carcinoma: Prognosis and treatment of patients from a single institution. *Journal of Clinical Oncology*. **23**(10), pp.2300–2309.

Alonso, G., Ambrosino, C., Jones, M. and Nebreda, A.R. 2000. Differential activation of p38 mitogen-activated protein kinase isoforms depending on signal strength. *Journal of Biological Chemistry*. **275**(51), pp.40641–40648.

Ambros, V. 2004. The functions of animal microRNAs. *Nature*. **431**(7006), pp.350–355.

An, P., Sáenz Robles, M.T. and Pipas, J.M. 2012. Large T Antigens of Polyomaviruses: Amazing Molecular Machines. *Annual Review of Microbiology*. **66**(1), pp.213–236.

Anderson, H.A., Chen, Y. and Norkin, L.C. 1998. MHC class I molecules are enriched in caveolae but do not enter with simian virus 40. *Journal of General Virology*.

79(6), pp.1469–1477.

Anon 2009. Chloride channels. *British Journal of Pharmacology*. **158**(Suppl 1), pp.S130–S134.

Baez, C.F., Brandão Varella, R., Villani, S. and Delbue, S. 2017. Human Polyomaviruses: The Battle of Large and Small Tumor Antigens. *Virology: Research and Treatment*. **8**, p.1178122X17744785.

Bagal, S.K., Brown, A.D., Cox, P.J., Omoto, K., Owen, R.M., Pryde, D.C., Sidders, B., Skerratt, S.E., Stevens, E.B., Storer, R.I. and Swain, N.A. 2013. Ion channels as therapeutic targets: A drug discovery perspective. *Journal of Medicinal Chemistry*. **56**(3), pp.593–624.

Bagrodia, S., Derijard, B., Davis, R.J. and Cerione, R.A. 1995. Cdc42 and PAK-mediated signaling leads to Jun kinase and p38 mitogen- activated protein kinase activation. *Journal of Biological Chemistry*. **270**(47), pp.27995–27998.

Barrantes, I.D.B. and Nebreda, A.R. 2012. Roles of p38 MAPKs in invasion and metastasis. *Biochemical Society Transactions*. **40**(1), pp.79–84.

Bates, E. 2015. Ion Channels in Development and Cancer. *Annual Review of Cell and Developmental Biology*. **31**(1), pp.231–247.

Baumgarten, C.M., Browe, D.M. and Ren, Z. 2005. *Swelling- and Stretch-activated Chloride Channels in the Heart: Regulation and Function* [Online]. Academia. [Accessed 27 March 2019]. Available from: http://www.ncbi.nlm.nih.gov/pubmed/21290764.

Becker, M., Dominguez, M., Greune, L., Soria-Martinez, L., Pfleiderer, M.M., Schowalter, R., Buck, C.B., Blaum, B.S., Schmidt, M.A. and Schelhaas, M. 2019. Infectious Entry of Merkel Cell Polyomavirus. *Journal of Virology*. **93**(6), JVI.02004-18.

Bennett, S.M., Broekema, N.M. and Imperiale, M.J. 2012. BK polyomavirus: Emerging pathogen. *Microbes and Infection*. **14**(9), pp.672–683.

Berger, L.C., Smith, D.B., Davidson, I., Hwang, J.J., Fanning, E. and Wildeman, A.G. 1996. Interaction between T antigen and TEA domain of the factor TEF-1

derepresses simian virus 40 late promoter in vitro: identification of T-antigen domains important for transcription control. *Journal of Virology*. **70**(2), pp.1203–12.

Berjanskii, M. V., Riley, M.I., Xie, A., Semenchenko, V., Folk, W.R. and Van Doren, S.R. 2000. NMR structure of the N-terminal J domain of murine polyomavirus T antigens: Implications for DnaJ-like domains and for mutations of T antigens. *Journal of Biological Chemistry*. **275**(46), pp.36094–36103.

Berridge, M.J., Bootman, M.D. and Lipp, P. 1998. Calcium - A life and death signal. *Nature*. **395**(6703), pp.645–648.

Bichakjian, C.K., Olencki, T., Aasi, S.Z., Alam, M., Andersen, J.S., Blitzblau, R., Bowen, G.M., Contreras, C.M., Daniels, G.A., Decker, R., Farma, J.M., Fisher, K., Gastman, B., Ghosh, K., Grekin, R.C., Grossman, K., Ho, A.L., Lewis, K.D., Loss, M., Lydiatt, D.D., Messina, J., Nehal, K.S., Nghiem, P., Puzanov, I., Schmults, C.D., Shaha, A.R., Thomas, V., Xu, Y.G., Zic, J.A., Hoffmann, K.G. and Engh, A.M. 2018. Merkel Cell Carcinoma. *JNCCN Journal of the National Comprehensive Cancer Network*. **16**(6), pp.742–774.

Blaikie, P.A., Fournier, E., Dilworth, S.M., Birnbaum, D., Borg, J.P. and Margolis, B. 1997. The role of the Shc phosphotyrosine interaction/phosphotyrosine binding domain and tyrosine phosphorylation sites in polyoma middle T antigen-mediated cell transformation. *Journal of Biological Chemistry*. **272**(33), pp.20671–20677.

Bochkareva, E., Martynowski, D., Seitova, A. and Bochkarev, A. 2006. Structure of the origin-binding domain of simian virus 40 large T antigen bound to DNA. *EMBO Journal*. **25**(24), pp.5961–5969.

Bollag, B., Hofstetter, C.A., Reviriego-Mendoza, M.M. and Frisque, R.J. 2010. JC virus small t antigen binds phosphatase PP2A and Rb family proteins and is required for efficient viral DNA replication activity. *PLoS ONE*. **5**(5), p.e10606.

Booth, I.R. 2003. Bacterial ion channels. *Genetic Engineering*. **25**(1), pp.91–111.

Borchert, S., Czech-Sioli, M., Neumann, F., Schmidt, C., Wimmer, P., Dobner, T.,

Grundhoff, A. and Fischer, N. 2014. High-Affinity Rb Binding, p53 Inhibition, Subcellular Localization, and Transformation by Wild-Type or Tumor-Derived Shortened Merkel Cell Polyomavirus Large T Antigens. *Journal of Virology*. **88**(6), pp.3144–3160.

Boxus, M. and Willems, L. 2009. Mechanisms of HTLV-1 persistence and transformation. *British Journal of Cancer*. **101**(9), pp.1497–1501.

Brancho, D., Tanaka, N., Jaeschke, A., Ventura, J.J., Kelkar, N., Tanaka, Y., Kyuuma, M., Takeshita, T., Flavell, R.A. and Davis, R.J. 2003. Mechanism of p38 MAP kinase activation in vivo. *Genes and Development*. **17**(16), pp.1969–1978.

Braun, A.P. 2012. Two-pore domain potassium channels: Variation on a structural theme. *Channels*. **6**(3), pp.139–140.

Bravo-Cordero, J.J., Magalhaes, M.A.O., Eddy, R.J., Hodgson, L. and Condeelis, J. 2013. Functions of cofilin in cell locomotion and invasion. *Nature Reviews Molecular Cell Biology*. **14**(7), pp.405–417.

Brechot, C., Pourcel, C., Louise, A., Rain, B. and Tiollais, P. 1980. Presence of integrated hepatitis B virus DNA sequences in cellular DNA of human hepatocellular carcinoma. *Nature*. **286**(5772), pp.533–535.

Buck, C.B. and Thompson, C.D. 2007. Production of Papillomavirus-Based Gene Transfer Vectors. *Current Protocols in Cell Biology*. **37**(1), 26.1.1-26.1.19.

Cang, C., Bekele, B. and Ren, D. 2014. The voltage-gated sodium channel TPC1 confers endolysosomal excitability. *Nature Chemical Biology*. **10**(6), pp.463–469.

Cang, C., Zhou, Y., Navarro, B., Seo, Y.J., Aranda, K., Shi, L., Battaglia-Hsu, S., Nissim, I., Clapham, D.E. and Ren, D. 2013. MTOR regulates lysosomal ATP-sensitive two-pore Na+ channels to adapt to metabolic state. *Cell*. **152**(4), pp.778–790.

Cantalupo, P.G., Buck, C.B. and Pipas, J.M. 2017. Complete genome sequence of a polyomavirus recovered from a pomona leaf-nosed bat (Hipposideros pomona) metagenome data set. *Genome Announcements*. **5**(3), pp.1053–1069.

Cargnello, M. and Roux, P.P. 2011. Activation and Function of the MAPKs and Their

Substrates, the MAPK-Activated Protein Kinases. *Microbiology and Molecular Biology Reviews*. **75**(1), pp.50–83.

Carrillo-Infante, C., Abbadessa, G., Bagella, L. and Giordano, A. 2007. Viral infections as a cause of cancer (review). *Int J Oncol*. **30**(6), pp.1521–1528.

Carter, J.J., Daugherty, M.D., Qi, X., Bheda-Malge, A., Wipf, G.C., Robinson, K., Roman, A., Malik, H.S. and Galloway, D.A. 2013. Identification of an overprinting gene in Merkel cell polyomavirus provides evolutionary insight into the birth of viral genes. *Proceedings of the National Academy of Sciences of the United States of America*. **110**(31), pp.12744–12749.

Catterall, W.A. 2000. From ionic currents to molecular mechanisms: The structure and function of voltage-gated sodium channels. *Neuron*. **26**(1), pp.13–25.

Chang, L. and Karin, M. 2001. Mammalian MAP kinase signalling cascades. *Nature*. **410**(6824), pp.37–40.

Chen, X.S., Stehle, T. and Harrison, S.C. 1998. Interaction of polyomavirus internal protein VP2 with the major capsid protein VP1 and implications for participation of VP2 in viral entry. *EMBO Journal*. **17**(12), pp.3233–3240.

Chen, Y., Wang, L., Jin, J., Luan, Y., Chen, C., Li, Y., Chu, H., Wang, X., Liao, G., Yu, Y., Teng, H., Wang, Y., Pan, W., Fang, L., Liao, L., Jiang, Z., Ge, X., Li, B. and Wang, P. 2017. p38 inhibition provides anti-DNA virus immunity by regulation of USP21 phosphorylation and STI NG activation. *Journal of Experimental Medicine*. **214**(4), pp.991–1010.

Chen, Y., Xu, Y., Bao, Q., Xing, Y., Li, Z., Lin, Z., Stock, J.B., Jeffrey, P.D. and Shi, Y. 2007. Structural and biochemical insights into the regulation of protein phosphatase 2A by small t antigen of SV40. *Nature Structural and Molecular Biology*. **14**(6), pp.527–534.

Cheng, J., Rozenblatt-Rosen, O., Paulson, K.G., Nghiem, P. and DeCaprio, J.A. 2013. Merkel Cell Polyomavirus Large T Antigen Has Growth-Promoting and Inhibitory Activities. *Journal of Virology*. **87**(11), pp.6118–6126.

Cheng, T.J., Tseng, Y.F., Chang, W. meih, Chang, M.D.T. and Lai, Y.K. 2003. Retaining

of the assembly capability of vimentin phosphorylated by mitogen-activated protein kinase-activated protein kinase-2. *Journal of Cellular Biochemistry*. **89**(3), pp.589–602.

Cheng, X., Shen, D., Samie, M. and Xu, H. 2010. Mucolipins: Intracellular TRPML1-3 channels. *FEBS Letters*. **584**(10), pp.2013–2021.

Chitty, J.L., Filipe, E.C., Lucas, M.C., Herrmann, D., Cox, T.R. and Timpson, P. 2018. Recent advances in understanding the complexities of metastasis. *F1000Research*. **7**, p.1169.

Cho, U.S. and Xu, W. 2007. Crystal structure of a protein phosphatase 2A heterotrimeric holoenzyme. *Nature*. **445**(7123), pp.53–57.

Choi, B., Fermin, C.D., Comardelle, A.M., Haislip, A.M., Voss, T.G. and Garry, R.F. 2008. Alterations in intracellular potassium concentration by HIV-1 and SIV Nef. *Virology Journal*. **5**.

Clayson, E.T., Brando, L. V and Compans, R.W. 1989. Release of simian virus 40 virions from epithelial cells is polarized and occurs without cell lysis. *Journal of Virology*. **63**(5), pp.2278–88.

Clever, J., Dean, D.A. and Kasamatsu, H. 1993. Identification of a DNA binding domain in simian virus 40 capsid proteins Vp2 and Vp3. *Journal of Biological Chemistry*. **268**(28), pp.20877–20883.

Coca-Prados, M., Yu, H.Y. and Hsu, M.T. 1982. Intracellular forms of simian virus 40 nucleoprotein complexes. IV. Micrococcal nuclease digestion. *Journal of virology*. **44**(2), pp.603–9.

Comerford, S.A., Schultz, N., Hinnant, E.A., Klapproth, S. and Hammer, R.E. 2012. Comparative analysis of SV40 17kT and LT function in vivo demonstrates that LTs C-terminus re-programs hepatic gene expression and is necessary for tumorigenesis in the liver. *Oncogenesis*. **1**(9), p.e28.

Cotsiki, M., Lock, R.L., Cheng, Y., Williams, G.L., Zhao, J., Perera, D., Freire, R., Entwistle, A., Golemis, E.A., Roberts, T.M., Jat, P.S. and Gjoerup, O. V. 2004. Simian virus 40 large T antigen targets the spindle assembly checkpoint protein

Bub1. *Proceedings of the National Academy of Sciences of the United States of America*. **101**(4), pp.947–952.

Cuadrado, A. and Nebreda, A.R. 2010. Mechanisms and functions of p38 MAPK signalling. *Biochemical Journal*. **429**(3), pp.403–417.

Cubitt, C.L. 2006. Molecular genetics of the BK virus *In*: *Advances in Experimental Medicine and Biology* [Online]. New York, NY: Springer New York, pp.85–95. [Accessed 15 March 2019]. Available from: http://www.ncbi.nlm.nih.gov/pubmed/16626029.

Daniels, R., Sadowicz, D. and Hebert, D.N. 2007. A very late viral protein triggers the lytic release of SV40. *PLoS Pathogens*. **3**(7), pp.0928–0938.

Dean, F.B. and Hurwitz, J. 1991. Simian virus 40 large T antigen untwists DNA at the origin of DNA replication. *Journal of Biological Chemistry*. **266**(8), pp.5062–5071.

Decaprio, J.A. and Garcea, R.L. 2013. A cornucopia of human polyomaviruses. *Nature Reviews Microbiology*. **11**(4), pp.264–276.

Dekeyser, M., François, H., Beaudreuil, S. and Durrbach, A. 2015. Polyomavirus-specific cellular immunity: From BK-virus-specific cellular immunity to BK-virus-associated nephropathy? *Frontiers in Immunology*. **6**(JUN).

Deryugina, E.I. and Quigley, J.P. 2006. Matrix metalloproteinases and tumor metastasis. *Cancer and Metastasis Reviews*. **25**(1), pp.9–34.

Diaz, J., Wang, X., Tsang, S.H., Jiao, J. and You, J. 2014. Phosphorylation of large T antigen regulates merkel cell polyomavirus replication. *Cancers*. **6**(3), pp.1464–1486.

Doench, J.G., Petersen, C.P. and Sharp, P.A. 2003. siRNAs can function as miRNAs. *Genes and Development*. **17**(4), pp.438–442.

Dolphin, A.C. 2016. Voltage-gated calcium channels and their auxiliary subunits: physiology and pathophysiology and pharmacology. *Journal of Physiology*. **594**(19), pp.5369–5390.

Doza, Y.N., Cuenda, A., Thomas, G.M., Cohen, P. and Nebreda, A.R. 1995. Activation of the MAP kinase homologue RK requires the phosphorylation of Thr-180 and

Tyr-182 and both residues are phosphorylated in chemically stressed KB cells. *FEBS Letters*. **364**(2), pp.223–228.

Drayman, N., Kler, S., Ben-nun-Shaul, O. and Oppenheim, A. 2010. Rapid method for SV40 titration. *Journal of Virological Methods*. **164**(1–2), pp.145–147.

Van Drogen, F. and Peter, M. 2002. MAP kinase cascades: Scaffolding signal specificity. *Current Biology*. **12**(2), pp.R53–R55.

Drusio, C., Becker, J.C., Schadendorf, D. and Ugurel, S. 2019. Merkel cell carcinoma. *Best Practice Onkologie*. **14**(7–8), pp.312–323.

Dubey, R.C., Mishra, N. and Gaur, R. 2019. G protein-coupled and ATP-sensitive inwardly rectifying potassium ion channels are essential for HIV entry. *Scientific Reports*. **9**(1), p.4113.

Dupin, N., Diss, T.L., Kellam, P., Tulliez, M., Du, M.Q., Sicard, D., Weiss, R.A., Isaacson, P.G. and Boshoff, C. 2000. HHV-8 is associated with a plasmablastic variant of Castleman disease that is linked to HHV-8-positive plasmablastic lymphoma. *Blood*. **95**(4), pp.1406–1412.

Dye, K.N., Welcker, M., Clurman, B.E., Roman, A. and Galloway, D.A. 2019. Merkel cell polyomavirus Tumor antigens expressed in Merkel cell carcinoma function independently of the ubiquitin ligases Fbw7 and β-TrCP M. J. Imperiale, ed. *PLoS Pathogens*. **15**(1), p.e1007543.

Eash, S., Querbes, W. and Atwood, W.J. 2004. Infection of Vero Cells by BK Virus Is Dependent on Caveolae. *Journal of Virology*. **78**(21), pp.11583–11590.

Eaton, D.C., Malik, B. and Ma, H.P. 2006. Hypertension and sodium channel turnover *In*: *Principles of Molecular Medicine* [Online]. Totowa, NJ: Humana Press, pp.613–621. [Accessed 19 March 2019]. Available from: http://link.springer.com/10.1007/978-1-59259-963-9_59.

Elphick, G.F., Querbes, W., Jordan, J.A., Gee, G. V., Eash, S., Manley, K., Dugan, A., Stanifer, M., Bhatnagar, A., Kroeze, W.K., Roth, B.L. and Atwood, W.J. 2004. The human polyomavirus, JCV, uses serotonin receptors to infect cells. *Science*. **306**(5700), pp.1380–1383.

Emerling, B.M., Platanias, L.C., Black, E., Nebreda, A.R., Davis, R.J. and Chandel, N.S. 2005. Mitochondrial Reactive Oxygen Species Activation of p38 Mitogen-Activated Protein Kinase Is Required for Hypoxia Signaling. *Molecular and Cellular Biology*. **25**(12), pp.4853–4862.

Engel, S., Heger, T., Mancini, R., Herzog, F., Kartenbeck, J., Hayer, A. and Helenius, A. 2011. Role of Endosomes in Simian Virus 40 Entry and Infection. *Journal of Virology*. **85**(9), pp.4198–4211.

Enslen, H., Raingeaud, J. and Davis, R.J. 1998. Selective activation of p38 mitogen-activated protein (MAP) kinase isoforms by the MAP kinase kinases MKK3 and MKK6. *Journal of Biological Chemistry*. **273**(3), pp.1741–1748.

Evans, G.L., Caller, L.G., Foster, V. and Crump, C.M. 2015. Anion homeostasis is important for non-lytic release of BK polyomavirus from infected cells. *Open Biology*. **5**(8), p.150041.

Fendrick, J.L. and Hallick, L.M. 1983. Optimal conditions for titration of SV40 by the plaque assay method. *Journal of Virological Methods*. **7**(2), pp.93–102.

Feng, H., Shuda, M., Chang, Y. and Moore, P.S. 2008. Clonal integration of a polyomavirus in human Merkel cell carcinoma. *Science*. **319**(5866), pp.1096–1100.

Ferenczy, M.W., Marshall, L.J., Nelson, C.D.S., Atwood, W.J., Nath, A., Khalili, K. and Majora, E.O. 2012. Molecular biology, epidemiology, and pathogenesis of progressive multifocal leukoencephalopathy, the JC virus-induced demyelinating disease of the human brain. *Clinical Microbiology Reviews*. **25**(3), pp.471–506.

Fine, D.A., Rozenblatt-Rosen, O., Padi, M., Korkhin, A., James, R.L., Adelmant, G., Yoon, R., Guo, L., Berrios, C., Zhang, Y., Calderwood, M.A., Velmurgan, S., Cheng, J., Marto, J.A., Hill, D.E., Cusick, M.E., Vidal, M., Florens, L., Washburn, M.P., Litovchick, L. and DeCaprio, J.A. 2012. Identification of FAM111A as an SV40 Host Range Restriction and Adenovirus Helper Factor. *PLoS Pathogens*. **8**(10).

Fisk, M., Gajendragadkar, P.R., Mäki-Petäjä, K.M., Wilkinson, I.B. and Cheriyan, J.

2014. Therapeutic potential of p38 MAP kinase inhibition in the management of cardiovascular disease. *American Journal of Cardiovascular Drugs*. **14**(3), pp.155–165.

Fitzgerald, T.L., Dennis, S., Kachare, S.D., Vohra, N.A., Wong, J.H. and Zervos, E.E. 2015. Dramatic Increase in the Incidence and Mortality from Merkel Cell Carcinoma in the United States. *The American surgeon*. **81**(8), pp.802–6.

Fluck, M.M. and Schaffhausen, B.S. 2009. Lessons in Signaling and Tumorigenesis from Polyomavirus Middle T Antigen. *Microbiology and Molecular Biology Reviews*. **73**(3), pp.542–563.

Forstová, J., Krauzewicz, N., Wallace, S., Street, A.J., Dilworth, S.M., Beard, S. and Griffin, B.E. 1993. Cooperation of structural proteins during late events in the life cycle of polyomavirus. *Journal of Virology*. **67**(3), pp.1405–13.

Foster, E.C. and Simmons, D.T. 2010. The SV40 large T-antigen origin binding domain directly participates in DNA unwinding. *Biochemistry*. **49**(10), pp.2087–2096.

Frost, J.A., Alberts, A.S., Sontag, E., Guan, K., Mumby, M.C. and Feramisco, J.R. 1994. Simian virus 40 small t antigen cooperates with mitogen-activated kinases to stimulate AP-1 activity. *Mol. Cell. Biol.*

Galione, A., Evans, A.M., Ma, J., Parrington, J., Arredouani, A., Cheng, X. and Zhu, M.X. 2009. The acid test: The discovery of two-pore channels (TPCs) as NAADP-gated endolysosomal Ca 2+ release channels. *Pflugers Archiv European Journal of Physiology*. **458**(5), pp.869–876.

Gardel, M.L., Schneider, I.C., Aratyn-Schaus, Y. and Waterman, C.M. 2010. Mechanical Integration of Actin and Adhesion Dynamics in Cell Migration. *Annual Review of Cell and Developmental Biology*. **26**(1), pp.315–333.

Gardner, S.D., Field, A.M., Coleman, D. V. and Hulme, B. 1971. New Human Papovavirus (B.K.) Isolated From Urine After Renal Transplantation. *The Lancet*. **297**(7712), pp.1253–1257.

Gee, G. V., O'Hara, B.A., Derdowski, A. and Atwood, W.J. 2013. Pseudovirus mimics cell entry and trafficking of the human polyomavirus JCPyV. *Virus Research*.

178(2), pp.281–286.

Gehring, G., Rohrmann, K., Atenchong, N., Mittler, E., Becker, S., Dahlmann, F., Pöhlmann, S., Vondran, F.W.R., David, S., Manns, M.P., Ciesek, S. and von Hahn, T. 2014. The clinically approved drugs amiodarone, dronedarone and verapamil inhibit filovirus cell entry. *Journal of Antimicrobial Chemotherapy*. **69**(8), pp.2123–2131.

Geiger, R., Andritschke, D., Friebe, S., Herzog, F., Luisoni, S., Heger, T. and Helenius, A. 2011. BAP31 and BiP are essential for dislocation of SV40 from the endoplasmic reticulum to the cytosol. *Nature Cell Biology*. **13**(11), pp.1305–1314.

Gheit, T., Dutta, S., Oliver, J., Robitaille, A., Hampras, S., Combes, J.D., McKay-Chopin, S., Le Calvez-Kelm, F., Fenske, N., Cherpelis, B., Giuliano, A.R., Franceschi, S., McKay, J., Rollison, D.E. and Tommasino, M. 2017. Isolation and characterization of a novel putative human polyomavirus. *Virology*. **506**, pp.45–54.

Van Ghelue, M., Khan, M.T.H., Ehlers, B. and Moens, U. 2012. Genome analysis of the new human polyomaviruses. *Reviews in Medical Virology*. **22**(6), pp.354–377.

Gilbert, J.M. and Benjamin, T.L. 2000. Early Steps of Polyomavirus Entry into Cells. *Journal of Virology*. **74**(18), pp.8582–8588.

Gillespie, E.J., Ho, C.L.C., Balaji, K., Clemens, D.L., Deng, G., Wang, Y.E., Elsaesser, H.J., Tamilselvam, B., Gargi, A., Dixon, S.D., France, B., Chamberlain, B.T., Blanke, S.R., Cheng, G., De La Torre, J.C., Brooks, D.G., Jung, M.E., Colicelli, J., Damoiseaux, R. and Bradley, K.A. 2013. Selective inhibitor of endosomal trafficking pathways exploited by multiple toxins and viruses. *Proceedings of the National Academy of Sciences of the United States of America*. **110**(50), pp.E4904–E4912.

Giraldo, N.A., Nguyen, P., Engle, E.L., Kaunitz, G.J., Cottrell, T.R., Berry, S., Green, B., Soni, A., Cuda, J.D., Stein, J.E., Sunshine, J.C., Succaria, F., Xu, H., Ogurtsova, A., Danilova, L., Church, C.D., Miller, N.J., Fling, S., Lundgren, L., Ramchurren, N., Yearley, J.H., Lipson, E.J., Cheever, M., Anders, R.A., Nghiem, P.T., Topalian, S.L. and Taube, J.M. 2018. Multidimensional, quantitative assessment of PD-1/PD-L1 expression in patients with Merkel cell carcinoma and association with

response to pembrolizumab 11 Medical and Health Sciences 1107 Immunology. *Journal for ImmunoTherapy of Cancer*. **6**(1), p.99.

Goedert, M., Cuenda, A., Craxton, M., Jakes, R. and Cohen, P. 1997. Activation of the novel stress-activated protein kinase SAPK4 by cytokines and cellular stresses is mediated by SKK3 (MKK6); Comparison of its substrate specificity with that of other SAP kinases. *EMBO Journal*. **16**(12), pp.3563–3571.

Goldsmith, Z.G. and Dhanasekaran, D.N. 2007. G Protein regulation of MAPK networks. *Oncogene*. **26**(22), pp.3122–3142.

Griffiths, D.A., Abdul-Sada, H., Knight, L.M., Jackson, B.R., Richards, K., Prescott, E.L., Peach, A.H.S., Blair, G.E., Macdonald, A. and Whitehouse, A. 2013. Merkel Cell Polyomavirus Small T Antigen Targets the NEMO Adaptor Protein To Disrupt Inflammatory Signaling. *Journal of Virology*. **87**(24), pp.13853–13867.

Grimm, C., Chen, C.C., Wahl-Schott, C. and Biel, M. 2017. Two-pore channels: Catalyzers of endolysosomal transport and function. *Frontiers in Pharmacology*. **8**(FEB), p.45.

Grizel, A. V., Glukhov, G.S. and Sokolova, O.S. 2014. Mechanisms of activation of voltage-gated potassium channels. *Acta Naturae*.

Gross, L. 1953. A filterable agent, recovered from Ak leukemic extracts, causing salivary gland carcinomas in C3H mice. *Proc Soc Exp Biol Med*. **83**(2), pp.414–421.

Gross, L. 1976. The fortuitous isolation and identification of the polyoma virus. *Cancer Research*. **36**(11 Pt 1), pp.4195–4196.

Guay, J., Lambert, H., Gingras-Breton, G., Lavoie, J.N., Huot, J. and Landry, J. 1997. Regulation of actin filament dynamics by p38 map kinase-mediated phosphorylation of heat shock protein 27. *Journal of Cell Science*. **110 (Pt 3**(3), pp.357–68.

Guéguinou, M., ChantÔme, A., Fromont, G., Bougnoux, P., Vandier, C. and Potier-Cartereau, M. 2014. KCa and Ca2+ channels: The complex thought. *Biochimica et Biophysica Acta - Molecular Cell Research*. **1843**(10), pp.2322–2333.

Gupta, S.G., Wang, L.C., Peñas, P.F., Gellenthin, M., Lee, S.J. and Nghiem, P. 2006. Sentinel lymph node biopsy for evaluation and treatment of patients with Merkel cell carcinoma: The Dana-Farber experience and meta-analysis of the literature. *Archives of Dermatology*. **142**(6), pp.685–690.

Hamilton, R.S., Gravell, M. and Major, E.O. 2000. Comparison of antibody titers determined by hemagglutination inhibition and enzyme immunoassay for JC virus and BK virus. *Journal of Clinical Microbiology*. **38**(1), pp.105–109.

Hanahan, D. and Weinberg, R.A. 2000. The hallmarks of cancer. *Cell*. **100**(1), pp.57–70.

Hara-Chikuma, M., Yang, B., Sonawane, N.D., Sasaki, S., Uchida, S. and Verkman, A.S. 2005. ClC-3 chloride channels facilitate endosomal acidification and chloride accumulation. *Journal of Biological Chemistry*. **280**(2), pp.1241–1247.

Harris, K.F., Christensen, J.B., Radany, E.H. and Imperiale, M.J. 1998. Novel Mechanisms of E2F Induction by BK Virus Large-T Antigen: Requirement of Both the pRb-Binding and the J Domains. *Molecular and Cellular Biology*. **18**(3), pp.1746–1756.

Harrison, C.J., Meinke, G., Kwun, H.J., Rogalin, H., Phelan, P.J., Bullock, P.A., Chang, Y., Moore, P.S. and Bohm, A. 2011. Asymmetric assembly of merkel cell polyomavirus large T-antigen origin binding domains at the viral origin. *Journal of Molecular Biology*. **409**(4), pp.529–542.

Hartmann, T., Xu, X., Kronast, M., Muehlich, S., Meyer, K., Zimmermann, W., Hurwitz, J., Pan, Z.Q., Engelhardt, S. and Sarikas, A. 2014. Inhibition of Cullin-RING E3 ubiquitin ligase 7 by simian virus 40 large T antigen. *Proceedings of the National Academy of Sciences of the United States of America*. **111**(9), pp.3371–3376.

Heath, M., Jaimes, N., Lemos, B., Mostaghimi, A., Wang, L.C., Peñas, P.F. and Nghiem, P. 2008. Clinical characteristics of Merkel cell carcinoma at diagnosis in 195 patients: the AEIOU features. *Journal of the American Academy of Dermatology*. **58**(3), pp.375–381.

Henriksen, S., Hansen, T., Bruun, J.-A. and Rinaldo, C.H. 2016. The Presumed

Polyomavirus Viroporin VP4 of Simian Virus 40 or Human BK Polyomavirus Is Not Required for Viral Progeny Release. *Journal of Virology*. **90**(22), pp.10398–10413.

Herrmann, M., Ruprecht, K., Sauter, M., Martinez, J., van Heteren, P., Glas, M., Best, B., Meyerhans, A., Roemer, K. and Mueller-Lantzsch, N. 2010. Interaction of human immunodeficiency virus gp120 with the voltage-gated potassium channel BEC1. *FEBS Letters*. **584**(16), pp.3513–3518.

Hibino, H., Inanobe, A., Furutani, K., Murakami, S., Findlay, I. and Kurachi, Y. 2010. Inwardly rectifying potassium channels: Their structure, function, and physiological roles. *Physiological Reviews*. **90**(1), pp.291–366.

Hilleman, M.R. 1998. Discovery of simian virus 40 (SV40) and its relationship to poliomyelitis virus vaccines. *Developments in Biological Standization*. **94**, pp.183–190.

Hipp, S., Berg, D., Ergin, B., Schuster, T., Hapfelmeier, A., Walch, A., Avril, S., Schmalfeldt, B., Höfler, H. and Becker, K.F. 2010. Interaction of Snail and p38 mitogen-activated protein kinase results in shorter overall survival of ovarian cancer patients. *Virchows Archiv*. **457**(6), pp.705–713.

Hirasawa, K., Kim, A., Han, H.-S., Han, J., Jun, H.-S. and Yoon, J.-W. 2003. Effect of p38 Mitogen-Activated Protein Kinase on the Replication of Encephalomyocarditis Virus. *Journal of Virology*. **77**(10), pp.5649–5656.

Hogan, T.F., Padgett, B.L., Walker, D.L., Borden, E.C. and McBain, J.A. 1980. Rapid detection and identification of JC virus and BK virus in human urine by using immunofluorescence microscopy. *Journal of Clinical Microbiology*. **11**(2), pp.178–183.

Hong, J., Zhou, J., Fu, J., He, T., Qin, J., Wang, L., Liao, L. and Xu, J. 2011. Phosphorylation of serine 68 of twist1 by MAPKs stabilizes twist1 protein and promotes breast cancer cell invasiveness. *Cancer Research*. **71**(11), pp.3980–3990.

Hover, S., Foster, B., Barr, J.N. and Mankouri, J. 2017. Viral dependence on cellular

ion channels – an emerging antiviral target? *Journal of General Virology*. **98**(3), pp.345–351.

Hover, S., Foster, B., Fontana, J., Kohl, A., Goldstein, S.A.N., Barr, J.N. and Mankouri, J. 2018. Bunyavirus requirement for endosomal K+reveals new roles of cellular ion channels during infection S. P. J. Whelan, ed. *PLoS Pathogens*. **14**(1), p.e1006845.

Hover, S., King, B., Hall, B., Loundras, E.A., Taqi, H., Daly, J., Dallas, M., Peers, C., Schnettler, E., Mckimmie, C., Kohl, A., Barr, J.N. and Mankouri, J. 2016. Modulation of potassium channels inhibits bunyavirus infection. *Journal of Biological Chemistry*. **291**(7), pp.3411–3422.

Hsieh, M.J., Chen, K.S., Chiou, H.L. and Hsieh, Y.S. 2010. Carbonic anhydrase XII promotes invasion and migration ability of MDA-MB-231 breast cancer cells through the p38 MAPK signaling pathway. *European Journal of Cell Biology*. **89**(8), pp.598–606.

Hu, Y.B., Dammer, E.B., Ren, R.J. and Wang, G. 2015. The endosomal-lysosomal system: From acidification and cargo sorting to neurodegeneration. *Translational Neurodegeneration*. **4**(1), p.18.

Igloi, Z., Mohl, B.-P., Lippiat, J.D., Harris, M. and Mankouri, J. 2015. Requirement for Chloride Channel Function during the Hepatitis C Virus Life Cycle. *Journal of Virology*. **89**(7), pp.4023–4029.

Imperiale, M.J. 2014. Polyomavirus miRNAs: The beginning. *Current Opinion in Virology*. **7**(1), pp.29–32.

Ishii, N., Nakanishi, A., Yamada, M., Macalalad, M.H. and Kasamatsu, H. 1994. Functional complementation of nuclear targeting-defective mutants of simian virus 40 structural proteins. *Journal of Virology*. **68**(12), pp.8209–16.

Iyer, J.G., Blom, A., Doumani, R., Lewis, C., Tarabadkar, E.S., Anderson, A., Ma, C., Bestick, A., Parvathaneni, U., Bhatia, S. and Nghiem, P. 2016. Response rates and durability of chemotherapy among 62 patients with metastatic Merkel cell carcinoma. *Cancer Medicine*. **5**(9), pp.2294–2301.

Janssens, V. and Goris, J. 2001. Protein phosphatase 2A: a highly regulated family of serine/threonine phosphatases implicated in cell growth and signalling. *Biochemical Journal*. **353**(3), pp.417–439.

Jentsch, T.J., Stein, V., Weinreich, F. and Zdebik, A.A. 2002. Molecular structure and physiological function of chloride channels. *Physiological Reviews*. **82**(2), pp.503–568.

Jiang, M., Abend, J.R., Tsai, B. and Imperiale, M.J. 2009. Early Events during BK Virus Entry and Disassembly. *Journal of Virology*. **83**(3), pp.1350–1358.

Jiang, Y., Chen, C., Li, Z., Guo, W., Gegner, J.A., Lin, S. and Han, J. 1996. Characterization of the structure and function of a new mitogen-activated protein kinase (p38beta). *The Journal of biological chemistry*. **271**(30), pp.17920–6.

Johansson, N., Ala-aho, R., Uitto, V.J., Grénman, R., Fusenig, N.E., López-Otín, C. and Kähäri, V.M. 2000. Expression of collagenase-3 (MMP-13) and collagenase-1 (MMP-1) by transformed keratinocytes is dependent on the activity of p38 mitogen-activated protein kinase. *Journal of Cell Science*. **113**(2), pp.227–235.

Johne, R., Buck, C.B., Allander, T., Atwood, W.J., Garcea, R.L., Imperiale, M.J., Major, E.O., Ramqvist, T. and Norkin, L.C. 2011. Taxonomical developments in the family Polyomaviridae. *Archives of Virology*. **156**(9), pp.1627–1634.

Joyce, J.A. and Pollard, J.W. 2009. Microenvironmental regulation of metastasis. *Nature Reviews Cancer*. **9**(4), pp.239–252.

Junttila, M.R., Ala-Aho, R., Jokilehto, T., Peltonen, J., Kallajoki, M., Grenman, R., Jaakkola, P., Westermarck, J. and Kähäri, V.M. 2007. P38A and P38Δ Mitogen-Activated Protein Kinase Isoforms Regulate Invasion and Growth of Head and Neck Squamous Carcinoma Cells. *Oncogene*. **26**(36), pp.5267–5279.

Kaae, J., Hansen, A. V., Biggar, R.J., Boyd, H.A., Moore, P.S., Wohlfahrt, J. and Melbye, M. 2010. Merkel cell carcinoma: Incidence, mortality, and risk of other cancers. *Journal of the National Cancer Institute*. **102**(11), pp.793–801.

Kadavath, H., Hofele, R. V., Biernat, J., Kumar, S., Tepper, K., Urlaub, H., Mandelkow,

E. and Zweckstetter, M. 2015. Tau stabilizes microtubules by binding at the interface between tubulin heterodimers. *Proceedings of the National Academy of Sciences of the United States of America*. **112**(24), pp.7501–7506.

Kalluri, R. and Weinberg, R.A. 2009. *The basics of epithelial-mesenchymal transition* [Online]. [Accessed 26 March 2019]. Available from: http://www.jci.org/articles/view/39104.

Kasianowicz, J.J. 2012. Introduction to ion channels and disease. *Chemical Reviews*. **112**(12), pp.6215–6217.

Kasper, J.S., Kuwabara, H., Arai, T., Ali, S.H. and DeCaprio, J.A. 2005. Simian Virus 40 Large T Antigen's Association with the CUL7 SCF Complex Contributes to Cellular Transformation. *Journal of Virology*. **79**(18), pp.11685–11692.

Kaufman, H.L., Russell, J., Hamid, O., Bhatia, S., Terheyden, P., D'Angelo, S.P., Shih, K.C., Lebbé, C., Linette, G.P., Milella, M., Brownell, I., Lewis, K.D., Lorch, J.H., Chin, K., Mahnke, L., von Heydebreck, A., Cuillerot, J.M. and Nghiem, P. 2016. Avelumab in patients with chemotherapy-refractory metastatic Merkel cell carcinoma: a multicentre, single-group, open-label, phase 2 trial. *The Lancet Oncology*. **17**(10), pp.1374–1385.

Khopde, S. and Simmons, D.T. 2008. Simian Virus 40 DNA Replication Is Dependent on an Interaction between Topoisomerase I and the C-Terminal End of T Antigen. *Journal of Virology*. **82**(3), pp.1136–1145.

Klein, E., Kis, L.L. and Klein, G. 2007. Epstein-Barr virus infection in humans: From harmless to life endangering virus-lymphocyte interactions. *Oncogene*. **26**(9), pp.1297–1305.

Klucky, B. and Wintersberger, E. 2007. Polyomavirus small T antigen transactivates genes by its ability to provoke the synthesis and the stabilization of MYC. *Oncogene*. **26**(43), pp.6356–6360.

Knight, L.M., Stakaityte, G., Wood, J.J., Abdul-Sada, H., Griffiths, D.A., Howell, G.J., Wheat, R., Blair, G.E., Steven, N.M., Macdonald, A., Blackbourn, D.J. and Whitehouse, A. 2015. Merkel Cell Polyomavirus Small T Antigen Mediates

Microtubule Destabilization To Promote Cell Motility and Migration. *Journal of Virology*. **89**(1), pp.35–47.

Knights, A.J., Funnell, A.P.W., Crossley, M. and Pearson, R.C.M. 2012. Holding Tight: Cell Junctions and Cancer Spread. *Trends in cancer research*. **8**, pp.61–69.

Knowles, W.A., Luxton, R.W., Hand, J.F., Gardner, S.D. and Brown, D.W.G. 1995. The JC virus antibody response in serum and cerebrospinal fluid in progressive multifocal leucoencephalopathy. *Clinical and Diagnostic Virology*. **4**(2), pp.183–194.

Knowles, W.A. and Sasnauskas, K. 2003. Comparison of cell culture-grown JC virus (primary human fetal glial cells and the JCI cell line) and recombinant JCV VP1 as antigen for the detection of anti-JCV antibody by haemagglutination inhibition. *Journal of Virological Methods*. **109**(1), pp.47–54.

Kobayashi, M., Nishita, M., Mishima, T., Ohashi, K. and Mizuno, K. 2006. MAPKAPK-2-mediated LIM-kinase activation is critical for VEGF-induced actin remodeling and cell migration. *EMBO Journal*. **25**(4), pp.713–726.

Krauzewicz, N., Streuli, C.H., Stuart-Smith, N., Jones, M.D., Wallace, S. and Griffin, B.E. 1990. Myristylated polyomavirus VP2: role in the life cycle of the virus. *Journal of Virology*. **64**(9), pp.4414–20.

Kuang, Q., Purhonen, P. and Hebert, H. 2015. Structure of potassium channels. *Cellular and Molecular Life Sciences*. **72**(19), pp.3677–3693.

Kuksin, D. and Norkin, L. C. 2012. Disassembly of Simian Virus 40 during Passage through the Endoplasmic Reticulum and in the Cytoplasm. *Journal of Virology*. **86**(3), pp.1555–1562.

Kuksin, D. and Norkin, Leonard C. 2012. Disassociation of the SV40 genome from capsid proteins prior to nuclear entry. *Virology Journal*. **9**.

Kumar, P., Yadav, A., Patel, S.N., Islam, M., Pan, Q., Merajver, S.D. and Teknos, T.N. 2010. Tetrathiomolybdate inhibits head and neck cancer metastasis by decreasing tumor cell motility, invasiveness and by promoting tumor cell anoikis. *Molecular Cancer*. **9**(1), p.206.

Kwun, H.J., Chang, Y. and Moore, P.S. 2017. Protein-mediated viral latency is a novel mechanism for Merkel cell polyomavirus persistence. *Proceedings of the National Academy of Sciences of the United States of America*. **114**(20), pp.E4040–E4047.

Kwun, H.J., Guastafierro, A., Shuda, M., Meinke, G., Bohm, A., Moore, P.S. and Chang, Y. 2009. The Minimum Replication Origin of Merkel Cell Polyomavirus Has a Unique Large T-Antigen Loading Architecture and Requires Small T-Antigen Expression for Optimal Replication. *Journal of Virology*. **83**(23), pp.12118–12128.

Kwun, H.J., Shuda, M., Camacho, C.J., Gamper, A.M., Thant, M., Chang, Y. and Moore, P.S. 2015. Restricted Protein Phosphatase 2A Targeting by Merkel Cell Polyomavirus Small T Antigen. *Journal of Virology*. **89**(8), pp.4191–4200.

Kwun, H.J., Shuda, M., Feng, H., Camacho, C.J., Moore, P.S. and Chang, Y. 2013. Merkel cell polyomavirus small T antigen controls viral replication and oncoprotein expression by targeting the cellular ubiquitin ligase SCFFbw7. *Cell Host Microbe*. **14**(2), pp.125–135.

Laferrière, J., Houle, F., Taher, M.M., Valerie, K. and Huot, J. 2001. Transendothelial Migration of Colon Carcinoma Cells Requires Expression of E-selectin by Endothelial Cells and Activation of Stress-activated Protein Kinase-2 (SAPK2/p38) in the Tumor Cells. *Journal of Biological Chemistry*. **276**(36), pp.33762–33772.

Lambert, A.W., Pattabiraman, D.R. and Weinberg, R.A. 2017. Emerging Biological Principles of Metastasis. *Cell*. **168**(4), pp.670–691.

Larsen, J.K., Yamboliev, I.A., Weber, L.A. and Gerthoffer, W.T. 1997. Phosphorylation of the 27-kDa heat shock protein via p38 MAP kinase and MAPKAP kinase in smooth muscle. *The American journal of physiology*.

Layer, R.T. and McIntosh, J.M. 2006. Conotoxins: Therapeutic potential and application. *Marine Drugs*. **4**(3), pp.119–142.

Lebbe, C., Becker, J.C., Grob, J.J., Malvehy, J., Del Marmol, V., Pehamberger, H., Peris,

K., Saiag, P., Middleton, M.R., Bastholt, L., Testori, A., Stratigos, A. and Garbe, C. 2015. Diagnosis and treatment of Merkel Cell Carcinoma. European consensus-based interdisciplinary guideline. *European Journal of Cancer*. **51**(16), pp.2396–2403.

Lei, X., Bai, Z., Ye, F., Xie, J., Kim, C.G., Huang, Y. and Gao, S.J. 2010. Regulation of NF-B inhibitor IBα and viral replication by a KSHV microRNA. *Nature Cell Biology*. **12**(2), pp.193–199.

Lemoine, D., Jiang, R., Taly, A., Chataigneau, T., Specht, A. and Grutter, T. 2012. Ligand-gated ion channels: New insights into neurological disorders and ligand recognition. *Chemical Reviews*. **112**(12), pp.6285–6318.

Lemos, B.D., Storer, B.E., Iyer, J.G., Phillips, J.L., Bichakjian, C.K., Fang, L.C., Johnson, T.M., Liegeois-Kwon, N.J., Otley, C.C., Paulson, K.G., Ross, M.I., Yu, S.S., Zeitouni, N.C., Byrd, D.R., Sondak, V.K., Gershenwald, J.E., Sober, A.J. and Nghiem, P. 2010. Pathologic nodal evaluation improves prognostic accuracy in Merkel cell carcinoma: Analysis of 5823 cases as the basis of the first consensus staging system. *Journal of the American Academy of Dermatology*. **63**(5), pp.751–761.

Li, J., Diaz, J., Wang, X., Tsang, S.H. and You, J. 2015. Phosphorylation of Merkel Cell Polyomavirus Large Tumor Antigen at Serine 816 by ATM Kinase Induces Apoptosis in Host Cells. *Journal of Biological Chemistry*. **290**(3), pp.1874–1884.

Li, P.P., Naknanishi, A., Tran, M.A., Ishizu, K.-I., Kawano, M., Phillips, M., Handa, H., Liddington, R.C. and Kasamatsu, H. 2003. Importance of Vp1 Calcium-Binding Residues in Assembly, Cell Entry, and Nuclear Entry of Simian Virus 40. *Journal of Virology*. **77**(13), pp.7527–7538.

Liao, J.B. 2006. Viruses and human cancer. *Yale J Biol Med*. **79**(3–4), pp.115–122.

Liddington, R.C., Yan, Y., Moulai, J., Sahli, R., Benjamin, T.L. and Harrison, S.C. 1991. Structure of simian virus 40 at 3.8-å resolution. *Nature*. **354**(6351), pp.278–284.

Liebl, D., Difato, F., Hornikova, L., Mannova, P., Stokrova, J. and Forstova, J. 2006. Mouse Polyomavirus Enters Early Endosomes, Requires Their Acidic pH for Productive Infection, and Meets Transferrin Cargo in Rab11-Positive

Endosomes. *Journal of Virology*. **80**(9), pp.4610–4622.

Lilyestrom, W., Klein, M.G., Zhang, R., Joachimiak, A. and Chen, X.S. 2006. Crystal structure of SV40 large T-antigen bound to p53: Interplay between a viral oncoprotein and a cellular tumor suppressor. *Genes and Development*. **20**(17), pp.2373–2382.

Lim, C.S., Whalley, D., Haydu, L.E., Murali, R., Tippett, J., Thompson, J.F., Hruby, G. and Scolyer, R.A. 2012. Increasing tumor thickness is associated with recurrence and poorer survival in patients with merkel cell carcinoma. *Annals of Surgical Oncology*. **19**(11), pp.3325–3334.

Lim, E.S., Reyes, A., Antonio, M., Saha, D., Ikumapayi, U.N., Adeyemi, M., Stine, O.C., Skelton, R., Brennan, D.C., Mkakosya, R.S., Manary, M.J., Gordon, J.I. and Wang, D. 2013. Discovery of STL polyomavirus, a polyomavirus of ancestral recombinant origin that encodes a unique T antigen by alternative splicing. *Virology*. **436**(2), pp.295–303.

Lin, Y., Mallen-St. Clair, J., Wang, G., Luo, J., Palma-Diaz, F., Lai, C., Elashoff, D.A., Sharma, S., Dubinett, S.M. and St. John, M. 2016. p38 MAPK mediates epithelial-mesenchymal transition by regulating p38IP and Snail in head and neck squamous cell carcinoma. *Oral Oncology*. **60**, pp.81–89.

Liu, W., Yang, R., Payne, A.S., Schowalter, R.M., Spurgeon, M.E., Lambert, P.F., Xu, X., Buck, C.B. and You, J. 2016. Identifying the Target Cells and Mechanisms of Merkel Cell Polyomavirus Infection. *Cell Host and Microbe*. **19**(6), pp.775–787.

Liu, X., Hein, J., Richardson, S.C.W., Basse, P.H., Toptan, T., Moore, P.S., Gjoerup, O. V. and Chang, Y. 2011. Merkel cell polyomavirus large T antigen disrupts lysosome clustering by translocating human Vam6p from the cytoplasm to the nucleus. *Journal of Biological Chemistry*. **286**(19), pp.17079–17090.

López-Nouoa, J.M. and Nieto, M.A. 2009. Inflammation and EMT: An alliance towards organ fibrosis and cancer progression. *EMBO Molecular Medicine*. **1**(6–7), pp.303–314.

Low, J.A., Magnuson, B., Tsai, B. and Imperiale, M.J. 2006. Identification of

Gangliosides GD1b and GT1b as Receptors for BK Virus. *Journal of Virology*. **80**(3), pp.1361–1366.

Lu, L., Zhang, Q., Wu, K., Chen, X., Zheng, Y., Zhu, C. and Wu, J. 2015. Hepatitis C virus NS3 protein enhances cancer cell invasion by activating matrix metalloproteinase-9 and cyclooxygenase-2 through ERK/p38/NF-κB signal cascade. *Cancer Letters*. **356**(2), pp.470–478.

Mahon, C., Liang, B., Tikhanovich, I., Abend, J.R., Imperiale, M.J., Nasheuer, H.P. and Folk, W.R. 2009. Restriction of Human Polyomavirus BK Virus DNA Replication in Murine Cells and Extracts. *Journal of Virology*. **83**(11), pp.5708–5717.

Mall, M.A. and Hartl, D. 2014. CFTR: Cystic fibrosis and beyond. *European Respiratory Journal*. **44**(4), pp.1042–1054.

Malladi, S., MacAlinao, D.G., Jin, X., He, L., Basnet, H., Zou, Y., De Stanchina, E. and Massagué, J. 2016. Metastatic Latency and Immune Evasion through Autocrine Inhibition of WNT. *Cell*. **165**(1), pp.45–60.

Mankouri, J., Dallas, M.L., Hughes, M.E., Griffin, S.D.C., Macdonald, A., Peers, C. and Harris, M. 2009. *Suppression of a pro-apoptotic K+ channel as a mechanism for hepatitis C virus persistence* [Online]. [Accessed 27 March 2019]. Available from: www.pnas.org/cgi/content/full/.

Maphis, N., Jiang, S., Xu, G., Kokiko-Cochran, O.N., Roy, S.M., Van Eldik, L.J., Watterson, D.M., Lamb, B.T. and Bhaskar, K. 2016. Selective suppression of the α isoform of p38 MAPK rescues late-stage tau pathology. *Alzheimer's Research and Therapy*. **8**(1), pp.1–15.

Del Marmol, V. and Lebbé, C. 2019. New perspectives in Merkel cell carcinoma. *Current opinion in oncology*. **31**(2), pp.72–83.

Martin, G.M., Chen, P.C., Devaraneni, P. and Shyng, S.L. 2013. Pharmacological rescue of trafficking-impaired ATP-sensitive potassium channels. *Frontiers in Physiology*. **4 DEC**, p.386.

Maru, S., Jin, G., Desai, D., Amin, S., Shwetank, Lauver, M.D. and Lukacher, A.E. 2017. Inhibition of Retrograde Transport Limits Polyomavirus Infection In Vivo .

mSphere. **2**(6).

Mattila, P.K. and Lappalainen, P. 2008. Filopodia: Molecular architecture and cellular functions. *Nature Reviews Molecular Cell Biology*. **9**(6), pp.446–454.

Mayberry, C.L., Soucy, A.N., Lajoie, C.R., DuShane, J.K. and Maginnis, M.S. 2019. JC Polyomavirus Entry by Clathrin-Mediated Endocytosis Is Driven by β-Arrestin. *Journal of Virology*. **93**(8), JVI.01948-18.

Mayo, M.A. 2005. Changes to virus taxonomy 2004. *Archives of Virology*. **150**(1), pp.189–198.

McGivern, J.G. 2007. Ziconotide: a review of its pharmacology and use in the treatment of pain. *Neuropsychiatric disease and treatment*. **3**(1), pp.69–85.

Meng, F., Zhang, H., Liu, G., Kreike, B., Chen, W., Sethi, S., Miller, F.R. and Wu, G. 2011. p38γ mitogen-activated protein kinase contributes to oncogenic properties maintenance and resistance to poly (ADP-ribose)-polymerase-1 inhibition in breast cancer. *Neoplasia (New York, N.Y.)*. **13**(5), pp.472–82.

Mercer, J., Schelhaas, M. and Helenius, A. 2010. Virus Entry by Endocytosis. *Annual Review of Biochemistry*. **79**(1), pp.803–833.

Mertens, S., Craxton, M. and Goedert, M. 1996. SAP kinase-3, a new member of the family of mammalian stress-activated protein kinases. *FEBS Letters*. **383**(3), pp.273–276.

Miller-Podraza, H., Bradley, R.M. and Fishman, P.H. 1982. Biosynthesis and Localization of Gangliosides in Cultured Cells. *Biochemistry*. **21**(14), pp.3260–3265.

Miller, N.J., Church, C.D., Fling, S.P., Kulikauskas, R., Ramchurren, N., Shinohara, M.M., Kluger, H.M., Bhatia, S., Lundgren, L., Cheever, M.A., Topalian, S.L. and Nghiem, P. 2018. Merkel cell polyomavirus-specific immune responses in patients with Merkel cell carcinoma receiving anti-PD-1 therapy. *Journal for ImmunoTherapy of Cancer*. **6**(1), p.131.

Mishra, N., Pereira, M., Rhodes, R.H., An, P., Pipas, J.M., Jain, K., Kapoor, A., Briese, T., Faust, P.L. and Ian Lipkin, W. 2014. Identification of a novel Polyomavirus in

a pancreatic transplant recipient with retinal blindness and Vasculitic Myopathy. *Journal of Infectious Diseases*. **210**(10), pp.1595–1599.

Mochizuki, S. and Okada, Y. 2007. ADAMs in cancer cell proliferation and progression. *Cancer Science*. **98**(5), pp.621–628.

Moens, U., Calvignac-Spencer, S., Lauber, C., Ramqvist, T., Feltkamp, M.C.W., Daugherty, M.D., Verschoor, E.J. and Ehlers, B. 2017. ICTV virus taxonomy profile: Polyomaviridae. *Journal of General Virology*. **98**(6), pp.1159–1160.

Moens, U., Rasheed, K., Abdulsalam, I. and Sveinbjørnsson, B. 2015. The role of Merkel cell polyomavirus and other human polyomaviruses in emerging hallmarks of cancer. *Viruses*. **7**(4), pp.1871–1901.

Moriyama, T., Marquez, J.P., Wakatsuki, T. and Sorokin, A. 2007. Caveolar Endocytosis Is Critical for BK Virus Infection of Human Renal Proximal Tubular Epithelial Cells. *Journal of Virology*. **81**(16), pp.8552–8562.

Morrison, D.K. and Davis, R.J. 2003. Regulation of MAP Kinase Signaling Modules by Scaffold Proteins in Mammals. *Annual Review of Cell and Developmental Biology*. **19**(1), pp.91–118.

Morrison, K.M., Miesegaes, G.R., Lumpkin, E.A. and Maricich, S.M. 2009. Mammalian Merkel cells are descended from the epidermal lineage. *Developmental Biology*. **336**(1), pp.76–83.

Mounier, N. and Arrigo, A.-P. 2002. Actin cytoskeleton and small heat shock proteins: how do they interact? *Cell stress & chaperones*. **7**(2), pp.167–76.

Nakamura, T., Sato, Y., Watanabe, D., Ito, H., Shimonohara, N., Tsuji, T., Nakajima, N., Suzuki, Y., Matsuo, K., Nakagawa, H., Sata, T. and Katano, H. 2010. Nuclear localization of Merkel cell polyomavirus large T antigen in Merkel cell carcinoma. *Virology*. **398**(2), pp.273–279.

Nakanishi, A., Chapellier, B., Maekawa, N., Hiramoto, M., Kuge, T., Takahashi, R. u., Handa, H. and Imai, T. 2008. SV40 vectors carrying minimal sequence of viral origin with exchangeable capsids. *Virology*. **379**(1), pp.110–117.

Nakanishi, A., Li, P.P., Qu, Q., Jafri, Q.H. and Kasamatsu, H. 2007. Molecular dissection

of nuclear entry-competent SV40 during infection. *Virus Research*. **124**(1–2), pp.226–230.

Nakanishi, A., Shum, D., Morioka, H., Otsuka, E. and Kasamatsu, H. 2002. Interaction of the Vp3 Nuclear Localization Signal with the Importin 2/ Heterodimer Directs Nuclear Entry of Infecting Simian Virus 40. *Journal of Virology*. **76**(18), pp.9368–9377.

Nelson, C.D.S., Ströh, L.J., Gee, G. V., O'Hara, B.A., Stehle, T. and Atwood, W.J. 2015. Modulation of a Pore in the Capsid of JC Polyomavirus Reduces Infectivity and Prevents Exposure of the Minor Capsid Proteins. *Journal of Virology*. **89**(7), pp.3910–3921.

Neu, U., Hengel, H., Blaum, B.S., Schowalter, R.M., Macejak, D., Gilbert, M., Wakarchuk, W.W., Imamura, A., Ando, H., Kiso, M., Arnberg, N., Garcea, R.L., Peters, T., Buck, C.B. and Stehle, T. 2012. Structures of merkel cell polyomavirus VP1 complexes define a sialic acid binding site required for infection. *PLoS Pathogens*. **8**(7), p.8.

Neu, U., Maginnis, M.S., Palma, A.S., Ströh, L.J., Nelson, C.D.S., Feizi, T., Atwood, W.J. and Stehle, T. 2010. Structure-function analysis of the human JC polyomavirus establishes the LSTc pentasaccharide as a functional receptor motif. *Cell Host and Microbe*. **8**(4), pp.309–319.

Neu, U., Stehle, T. and Atwood, W.J. 2009. The Polyomaviridae: Contributions of virus structure to our understanding of virus receptors and infectious entry. *Virology*. **384**(2), pp.389–399.

Nghiem, P., Kaufman, H.L., Bharmal, M., Mahnke, L., Phatak, H. and Becker, J.C. 2017. Systematic literature review of efficacy, safety and tolerability outcomes of chemotherapy regimens in patients with metastatic Merkel cell carcinoma. *Future Oncology*. **13**(14), pp.1263–1279.

Nghiem, P.T., Bhatia, S., Lipson, E.J., Kudchadkar, R.R., Miller, N.J., Annamalai, L., Berry, S., Chartash, E.K., Daud, A., Fling, S.P., Friedlander, P.A., Kluger, H.M., Kohrt, H.E., Lundgren, L., Margolin, K., Mitchell, A., Olencki, T., Pardoll, D.M., Reddy, S.A., Shantha, E.M., Sharfman, W.H., Sharon, E., Shemanski, L.R.,

Shinohara, M.M., Sunshine, J.C., Taube, J.M., Thompson, J.A., Townson, S.M., Yearley, J.H., Topalian, S.L. and Cheever, M.A. 2016. PD-1 blockade with pembrolizumab in advanced merkel-cell carcinoma. *New England Journal of Medicine*. **374**(26), pp.2542–2552.

Nichols, B. 2003. Caveosomes and endocytosis of lipid rafts. *Journal of Cell Science*. **116**(23), pp.4707–4714.

Nichols, C.G. and Lopatin, A.N. 1997. *Inward Rectifier Potassium Channels* [Online]. [Accessed 27 March 2019]. Available from: www.annualreviews.org.

Nieto, M.A., Huang, R.Y.Y.J., Jackson, R.A.A. and Thiery, J.P.P. 2016. Emt: 2016. *Cell*. **166**(1), pp.21–45.

Nishikawa, S.I., Fewell, S.W., Kato, Y., Brodsky, J.L. and Endo, T. 2001. Molecular chaperones in the yeast endoplasmic reticulum maintain the solubility of proteins for retrotranslocation and degradation. *Journal of Cell Biology*. **153**(5), pp.1061–1069.

Norkin, L.C. 1999. Simian virus 40 infection via MHC class I molecules and caveolae. *Immunological Reviews*. **168**, pp.13–22.

Norman, A. 1952. *On the origin of cancer foci* [Online]. [Accessed 26 March 2019]. Available from: https://www.ncbi.nlm.nih.gov/pmc/articles/PMC3597235/pdf/nihms-448949.pdf.

Norman, K.L., Hirasawa, K., Yang, A.D., Shields, M.A. and Lee, P.W.K. 2004. Reovirus oncolysis: The Ras/RalGEF/p38 pathway dictates host cell permissiveness to reovirus infection. *Proceedings of the National Academy of Sciences of the United States of America*. **101**(30), pp.11099–11104.

Norris, C.A., He, K., Springer, M.G., Hartnett, K.A., Horn, J.P. and Aizenman, E. 2012. Regulation of neuronal proapoptotic potassium currents by the hepatitis C virus nonstructural protein 5A. *Journal of Neuroscience*. **32**(26), pp.8865–8870.

Nukuzuma, S., Nakamichi, K., Kameoka, M., Sugiura, S., Nukuzuma, C., Tasaki, T. and Takegami, T. 2016. Suppressive effect of topoisomerase inhibitors on JC

polyomavirus propagation in human neuroblastoma cells. *Microbiology and Immunology*. **60**(4), pp.253–260.

Nwogu, N., Boyne, J.R., Dobson, S.J., Poterlowicz, K., Blair, G.E., Macdonald, A., Mankouri, J. and Whitehouse, A. 2018. Cellular sheddases are induced by Merkel cell polyomavirus small tumour antigen to mediate cell dissociation and invasiveness D. A. Galloway, ed. *PLoS Pathogens*. **14**(9), p.e1007276.

O'Connell, A.D., Morton, M.J. and Hunter, M. 2002. Two-pore domain K+ channels - Molecular sensors *In*: *Biochimica et Biophysica Acta - Biomembranes*., pp.152–161.

Okada, Y., Suzuki, T., Sunden, Y., Orba, Y., Kose, S., Imamoto, N., Takahashi, H., Tanaka, S., Hall, W.W., Nagashima, K. and Sawa, H. 2005. Dissociation of heterochromatin protein 1 from lamin B receptor induced by human polyomavirus agnoprotein: Role in nuclear egress of viral particles. *EMBO Reports*. **6**(5), pp.452–457.

Padgett, B.L., Zurhein, G.M., Walker, D.L., Eckroade, R.J. and Dessel, B.H. 1971. Cultivation of Papova-Like Virus From Human Brain With Progressive Multifocal Leucoencephalopathy. *The Lancet*. **297**(7712), pp.1257–1260.

Pallas, D.C., Shahrik, L.K., Martin, B.L., Jaspers, S., Miller, T.B., Brautigan, D.L. and Roberts, T.M. 1990. Polyoma small and middle T antigens and SV40 small t antigen form stable complexes with protein phosphatase 2A. *Cell*. **60**(1), pp.167–176.

Pallas, D.C., Weller, W., Jaspers, S., Miller, T.B., Lane, W.S. and Roberts, T.M. 1992. The third subunit of protein phosphatase 2A (PP2A), a 55-kilodalton protein which is apparently substituted for by T antigens in complexes with the 36- and 63-kilodalton PP2A subunits, bears little resemblance to T antigens. *Journal of Virology*. **66**(2), pp.886–893.

Panou, M.M., Prescott, E.L., Hurdiss, D.L., Swinscoe, G., Hollinshead, M., Caller, L.G., Morgan, E.L., Carlisle, L., Müller, M., Antoni, M., Kealy, D., Ranson, N.A., Crump, C.M. and Macdonald, A. 2018. Agnoprotein is an essential egress factor during BK Polyomavirus infection. *International Journal of Molecular Sciences*. **19**(3),

p.902.

Park, S.Y., Jeong, K.J., Panupinthu, N., Yu, S., Lee, J., Han, J.W., Kim, J.M., Lee, J.S., Kang, J., Park, C.G., Mills, G.B. and Lee, H.Y. 2011. Lysophosphatidic acid augments human hepatocellular carcinoma cell invasion through LPA1 receptor and MMP-9 expression. *Oncogene*. **30**(11), pp.1351–1359.

Parkin, D.M. 2006. The global health burden of infection-associated cancers in the year 2002. *International Journal of Cancer*. **118**(12), pp.3030–3044.

Parvani, J.G., Taylor, M.A. and Schiemann, W.P. 2011. Noncanonical TGF-β signaling during mammary tumorigenesis. *Journal of Mammary Gland Biology and Neoplasia*. **16**(2), pp.127–146.

PASSANO, L.M. 1963. Primitive Nervous Systems. *Proceedings of the National Academy of Sciences of the United States of*. **50**, pp.306–313.

Pastrana, D. V., Buck, C.B., Pang, Y.Y.S., Thompson, C.D., Castle, P.E., FitzGerald, P.C., Kjaer, S.K., Lowy, D.R. and Schiller, J.T. 2004. Reactivity of human sera in a sensitive, high-throughput pseudovirus-based papillomavirus neutralization assay for HPV16 and HPV18. *Virology*. **321**(2), pp.205–216.

Pastrana, D. V., Tolstov, Y.L., Becker, J.C., Moore, P.S., Chang, Y. and Buck, C.B. 2009. Quantitation of human seroresponsiveness to Merkel cell polyomavirus. *PLoS Pathogens*. **5**(9), p.e1000578.

Patnaik, A., Haluska, P., Tolcher, A.W., Erlichman, C., Papadopoulos, K.P., Lensing, J.L., Beeram, M., Molina, J.R., Rasco, D.W., Arcos, R.R., Kelly, C.S., Wijayawardana, S.R., Zhang, X., Stancato, L.F., Bell, R., Shi, P., Kulanthaivel, P., Pitou, C., Mulle, L.B., Farrington, D.L., Chan, E.M. and Goetz, M.P. 2016. A first-in-human phase i study of the oral p38 MAPK inhibitor, ralimetinib (LY2228820 Dimesylate), in patients with advanced cancer. *Clinical Cancer Research*. **22**(5), pp.1095–1102.

Peitsch, W.K. 2015. Associations between Merkel cell carcinoma and Merkel cell polyomavirus. *British Journal of Dermatology*. **173**(1), pp.7–8.

Pelkmans, L., Kartenbeck, J. and Helenius, A. 2001. Caveolar endocytosis of simian

virus 40 reveals a new two-step vesicular-transport pathway to the ER. *Nature Cell Biology*. **3**(5), pp.473–483.

Piechotta, P.L., Rapedius, M., Stansfeld, P.J., Bollepalli, M.K., Erhlich, G., Andres-Enguix, I., Fritzenschaft, H., Decher, N., Sansom, M.S.P., Tucker, S.J. and Baukrowitz, T. 2011. The pore structure and gating mechanism of K2P channels. *EMBO Journal*. **30**(17), pp.3607–3619.

Pipas, J.M. 1985. *Mutations near the carboxyl terminus of the simian virus 40 large tumor antigen alter viral host range.* [Online]. [Accessed 13 March 2019]. Available from: http://www.ncbi.nlm.nih.gov/pubmed/2985819%0Ahttp://www.pubmedcentral.nih.gov/articlerender.fcgi?artid=PMC254830.

Pollard, J.W. 2016. Defining metastatic cell latency. *New England Journal of Medicine*. **375**(3), pp.280–282.

Poulin, D.L., Kung, A.L. and DeCaprio, J.A. 2004. p53 Targets Simian Virus 40 Large T Antigen for Acetylation by CBP. *Journal of Virology*. **78**(15), pp.8245–8253.

Powell, D.W., Rane, M.J., Joughin, B.A., Kalmukova, R., Hong, J.-H., Tidor, B., Dean, W.L., Pierce, W.M., Klein, J.B., Yaffe, M.B. and McLeish, K.R. 2003. Proteomic Identification of 14-3-3 as a Mitogen-Activated Protein Kinase-Activated Protein Kinase 2 Substrate: Role in Dimer Formation and Ligand Binding. *Molecular and Cellular Biology*. **23**(15), pp.5376–5387.

Prevarskaya, N., Skryma, R. and Shuba, Y. 2010. Ion channels and the hallmarks of cancer. *Trends in Molecular Medicine*. **16**(3), pp.107–121.

Qian, M., Cai, D., Verhey, K.J. and Tsai, B. 2009. A lipid receptor sorts polyomavirus from the endolysosome to the endoplasmic reticulum to cause infection D. Galloway, ed. *PLoS Pathogens*. **5**(6), p.e1000465.

Querbes, W., Benmerah, A., Tosoni, D., Di Fiore, P.P. and Atwood, W.J. 2004. A JC Virus-Induced Signal Is Required for Infection of Glial Cells by a Clathrin- and eps15-Dependent Pathway. *Journal of Virology*. **78**(1), pp.250–256.

Querbes, W., O'Hara, B.A., Williams, G. and Atwood, W.J. 2006. Invasion of Host Cells

by JC Virus Identifies a Novel Role for Caveolae in Endosomal Sorting of Noncaveolar Ligands. *Journal of Virology*. **80**(19), pp.9402–9413.

Raghava, S., Giorda, K.M., Romano, F.B., Heuck, A.P. and Hebert, D.N. 2011. The SV40 late protein VP4 is a viroporin that forms pores to disrupt membranes for viral release C. Parrish, ed. *PLoS Pathogens*. **7**(6), p.e1002116.

Raman, M., Chen, W. and Cobb, M.H. 2007. Differential regulation and properties of MAPKs. *Oncogene*. **26**(22), pp.3100–3112.

Ribeiro, A., Merkle, M., Motamedi, N., Nitschko, H., Köppel, S. and Wörnle, M. 2016. BK virus infection activates the TNFα/TNF receptor system in Polyomavirus-associated nephropathy. *Molecular and Cellular Biochemistry*. **411**(1–2), pp.191–199.

Richards, K.F., Guastafierro, A., Shuda, M., Toptan, T., Moore, P.S. and Chang, Y. 2015. Merkel cell polyomavirus T antigens promote cell proliferation and inflammatory cytokine gene expression. *Journal of General Virology*. **96**(12), pp.3532–3544.

Riley, M.I., Yoo, W., Mda, N.Y. and Folk, W.R. 1997. Tiny T antigen: an autonomous polyomavirus T antigen amino-terminal domain. *Journal of Virology*. **71**(8), pp.6068–74.

Roger, S., Gillet, L., Le Guennec, J.Y. and Besson, P. 2015. Voltage-gated sodium channels and cancer: Is excitability their primary role? *Frontiers in Pharmacology*. **6**(JUL).

Royle, J., Dobson, S.J., Müller, M. and Macdonald, A. 2015. Emerging roles of viroporins encoded by DNA viruses: Novel targets for antivirals? *Viruses*. **7**(10), pp.5375–5387.

Rubin, H. 1994. Experimental control of neoplastic progression in cell populations: Foulds' rules revisited. *Proceedings of the National Academy of Sciences of the United States of America*. **91**(14), pp.6619–6623.

Ruvolo, P.P. 2016. The broken "Off" switch in cancer signaling: PP2A as a regulator of tumorigenesis, drug resistance, and immune surveillance. *BBA Clinical*. **6**,

pp.87–99.

Sablina, A.A. and Hahn, W.C. 2008. SV40 small T antigen and PP2A phosphatase in cell transformation. *Cancer and Metastasis Reviews*. **27**(2), pp.137–146.

Sakurai, Y., Kolokoltsov, A.A., Chen, C.C., Tidwell, M.W., Bauta, W.E., Klugbauer, N., Grimm, C., Wahl-Schott, C., Biel, M. and Davey, R.A. 2015. Two-pore channels control Ebola virus host cell entry and are drug targets for disease treatment. *Science*. **347**(6225), pp.995–998.

Satin, J., Kyle, J.W., Chen, M., Bell, P., Cribbs, L.L., Fozzard, H.A. and Rogart, R.B. 1992. A mutant of TTX-resistant cardiac sodium channels with TTX-sensitive properties. *Science*. **256**(5060), pp.1202–1205.

Schadendorf, D., Lebbé, C., zur Hausen, A., Avril, M.F., Hariharan, S., Bharmal, M. and Becker, J.C. 2017. Merkel cell carcinoma: Epidemiology, prognosis, therapy and unmet medical needs. *European Journal of Cancer*. **71**, pp.53–69.

Schaeffer, H.J. and Weber, M.J. 1999. Mitogen-activated protein kinases: specific messages from ubiquitous messengers. *Molecular and cellular biology*. **19**(4), pp.2435–44.

Schelhaas, M., Malmström, J., Pelkmans, L., Haugstetter, J., Ellgaard, L., Grünewald, K. and Helenius, A. 2007. Simian Virus 40 Depends on ER Protein Folding and Quality Control Factors for Entry into Host Cells. *Cell*. **131**(3), pp.516–529.

Scheltens, P., Prins, N., Lammertsma, A., Yaqub, M., Gouw, A., Wink, A.M., Chu, H.M., van Berckel, B.N.M. and Alam, J. 2018. An exploratory clinical study of p38α kinase inhibition in Alzheimer's disease. *Annals of Clinical and Translational Neurology*. **5**(4), pp.464–473.

Schiffman, M., Castle, P.E., Jeronimo, J., Rodriguez, A.C. and Wacholder, S. 2007. Human papillomavirus and cervical cancer. *Lancet*. **370**(9590), pp.890–907.

Schnell, L., Mittler, A.K., Mattarei, A., Tehran, D., Montecucco, C. and Barth, H. 2016. Semicarbazone EGA inhibits uptake of diphtheria toxin into human cells and protects cells article from intoxication. *Toxins*. **8**(7).

Schowalter, R.M. and Buck, C.B. 2013. The Merkel Cell Polyomavirus Minor Capsid

Protein. *PLoS Pathogens*. **9**(8), p.e1003558.

Schowalter, R.M., Pastrana, D. V. and Buck, C.B. 2011. Glycosaminoglycans and sialylated glycans sequentially facilitate merkel cell polyomavirus infectious entry. *PLoS Pathogens*. **7**(7), p.e1002161.

Schowalter, R.M., Reinhold, W.C. and Buck, C.B. 2012. Entry tropism of BK and Merkel cell polyomaviruses in cell culture. *PLoS ONE*. **7**(7), p.e42181.

Schrama, D., Sarosi, E.M., Adam, C., Ritter, C., Kaemmerer, U., Klopocki, E., König, E.M., Utikal, J., Becker, J.C. and Houben, R. 2019. Characterization of six Merkel cell polyomavirus-positive Merkel cell carcinoma cell lines: Integration pattern suggest that large T antigen truncating events occur before or during integration. *International Journal of Cancer*. **145**(4), pp.1020–1032.

Schrama, D., Ugurel, S. and Becker, J.C. 2012. Merkel cell carcinoma: Recent insights and new treatment options. *Current Opinion in Oncology*. **24**(2), pp.141–149.

Schüchner, S. and Wintersberger, E. 1999. Binding of polyomavirus small T antigen to protein phosphatase 2A is required for elimination of p27 and support of S-phase induction in concert with large T antigen. *Journal of virology*. **73**(11), pp.9266–73.

Schwartz, M., Böckmann, S., Borchert, P. and Hinz, B. 2018. SB202190 inhibits endothelial cell apoptosis via induction of autophagy and heme oxygenase-1. *Oncotarget*. **9**(33), pp.23149–23163.

Scott, C. and Griffin, S. 2015. Viroporins: Structure, function and potential as antiviral targets. *Journal of General Virology*. **96**(8), pp.2000–2027.

Scott, C.C. and Gruenberg, J. 2011. Ion flux and the function of endosomes and lysosomes: PH is just the start: The flux of ions across endosomal membranes influences endosome function not only through regulation of the luminal pH. *BioEssays*. **33**(2), pp.103–110.

Sébastien, P., Bryckaert, M. and Berrou, E. 2004. Control of actin dynamics by p38 MAP kinase - Hsp27 distribution in the lamellipodium of smooth muscle cells. *Journal of Cell Science*. **117**(12), pp.2569–2577.

Seo, G.J., Chen, C.J. and Sullivan, C.S. 2009. Merkel cell polyomavirus encodes a microRNA with the ability to autoregulate viral gene expression. *Virology*. **383**(2), pp.183–187.

Seshacharyulu, P., Pandey, P., Datta, K. and Batra, S.K. 2013. Phosphatase: PP2A structural importance, regulation and its aberrant expression in cancer. *Cancer Letters*. **335**(1), pp.9–18.

Shah, K. V. 2007. SV40 and human cancer: A review of recent data. *International Journal of Cancer*. **120**(2), pp.215–223.

Sheng, Q., Denis, D., Ratnofsky, M., Roberts, T.M., DeCaprio, J.A. and Schaffhausen, B. 1997. The DnaJ domain of polyomavirus large T antigen is required to regulate Rb family tumor suppressor function. *Journal of Virology*. **71**(12), pp.9410–6.

Shishido-Hara, Y., Hara, Y., Larson, T., Yasui, K., Nagashima, K. and Stoner, G.L. 2000. Analysis of Capsid Formation of Human Polyomavirus JC (Tokyo-1 Strain) by a Eukaryotic Expression System: Splicing of Late RNAs, Translation and Nuclear Transport of Major Capsid Protein VP1, and Capsid Assembly. *Journal of Virology*. **74**(4), pp.1840–1853.

Shuda, M., Chang, Y. and Moore, P.S. 2014. Merkel cell polyomavirus-positive merkel cell carcinoma requires viral small T-antigen for cell proliferation. *Journal of Investigative Dermatology*. **134**(5), pp.1479–1481.

Shuda, M., Feng, H., Kwun, H.J., Rosen, S.T., Gjoerup, O., Moore, P.S. and Chang, Y. 2008. T antigen mutations are a human tumor-specific signature for Merkel cell polyomavirus. *Proceedings of the National Academy of Sciences of the United States of America*. **105**(42), pp.16272–16277.

Shuda, M., Kwun, H.J., Feng, H., Chang, Y. and Moore, P.S. 2011. Human Merkel cell polyomavirus small T antigen is an oncoprotein targeting the 4E-BP1 translation regulator. *Journal of Clinical Investigation*. **121**(9), pp.3623–3634.

Siguier, M., Sellier, P. and Bergmann, J.F. 2012. BK-virus infections: A literature review. *Medecine et Maladies Infectieuses*. **42**(5), pp.181–187.

Sinibaldi, L., Viti, D., Goldoni, P., Cavallo, G., Caroni, C. and Orsi, N. 1987. Inhibition of

BK virus haemagglutination by gangliosides. *Journal of General Virology*. **68**(3), pp.879–883.

Sivilotti, L., Okuse, K., Akopian, A.N., Moss, S. and Wood, J.N. 1997. A single serine residue confers tetrodotoxin insensitivity on the rat sensory-neuron-specific sodium channel SNS. *FEBS Letters*. **409**(1), pp.49–52.

Skoczylas, C., Henglein, B. and Rundell, K. 2005. PP2A-dependent transactivation of the cyclin A promoter by SV40 ST is mediated by a cell cycle-regulated E2F site. *Virology*. **332**(2), pp.596–601.

Slack, J.M.W. 2013. *Molecular Biology of the Cell* [Online]. John Wiley & Sons, Ltd. [Accessed 18 March 2019]. Available from: http://doi.wiley.com/10.1002/bmb.2003.494031049999.

Snider, N.T. and Omary, M.B. 2014. Post-translational modifications of intermediate filament proteins: Mechanisms and functions. *Nature Reviews Molecular Cell Biology*. **15**(3), pp.163–177.

Sotillo, E., Garriga, J., Kurimchak, A. and Graña, X. 2008. Cyclin E and SV40 small t antigen cooperate to bypass quiescence and contribute to transformation by activating CDK2 in human fibroblasts. *Journal of Biological Chemistry*. **283**(17), pp.11280–11292.

Sowd, G.A. and Fanning, E. 2012. A Wolf in Sheep's Clothing: SV40 Co-opts Host Genome Maintenance Proteins to Replicate Viral DNA. *PLoS Pathogens*. **8**(11).

Spurgeon, M.E. and Lambert, P.F. 2013. Merkel cell polyomavirus: A newly discovered human virus with oncogenic potential. *Virology*. **435**(1), pp.118–130.

Stakaitytė, G., Nwogu, N., Dobson, S.J., Knight, L.M., Wasson, C.W., Salguero, F.J., Blackbourn, D.J., Blair, G.E., Mankouri, J., Macdonald, A. and Whitehouse, A. 2017. Merkel Cell Polyomavirus Small T Antigen Drives Cell Motility via Rho-GTPase-Induced Filopodium Formation. *Journal of Virology*. **92**(2).

Stakaityte, G., Nwogu, N., Lippiat, J.D., Blair, G.E., Poterlowicz, K., Boyne, J.R., MacDonald, A., Mankouri, J. and Whitehouse, A. 2018. The cellular chloride channels CLIC1 and CLIC4 contribute to virus-mediated cell motility. *Journal of*

Biological Chemistry. **293**(12), pp.4582–4590.

Stakaityte, G., Wood, J.J., Knight, L.M., Abdul-Sada, H., Adzahar, N.S., Nwogu, N., Macdonald, A. and Whitehouse, A. 2014. Merkel cell polyomavirus: Molecular insights into the most recently discovered human tumour virus. *Cancers*. **6**(3), pp.1267–1297.

Stang, E., Kartenbeck, J. and Parton, R.G. 1997. Major histocompatibility complex class I molecules mediate association of SV40 with caveolae. *Molecular Biology of the Cell*. **8**(1), pp.47–57.

Starrett, G.J., Marcelus, C., Cantalupo, P.G., Katz, J.P., Cheng, J., Akagi, K., Thakuria, M., Rabinowits, G., Wang, L.C., Symer, D.E., Pipas, J.M., Harris, R.S. and DeCaprio, J.A. 2017. Merkel cell polyomavirus exhibits dominant control of the tumor genome and transcriptome in virus-associated merkel cell carcinoma M. J. Imperiale, ed. *mBio*. **8**(1).

Stehle, T. and Harrison, S.C. 1997. High-resolution structure of a polyomavirus VP1-oligosaccharide complex: Implications for assembly and receptor binding. *EMBO Journal*. **16**(16), pp.5139–5148.

Steinberg, B.E., Huynh, K.K., Brodovitch, A., Jabs, S., Stauber, T., Jentsch, T.J. and Grinstein, S. 2010. A cation counterflux supports lysosomal acidification. *Journal of Cell Biology*. **189**(7), pp.1171–1186.

Strippoli, R., Benedicto, I., Foronda, M., Perez-Lozano, M.L., Sánchez-Perales, S., López-Cabrera, M. and Del Pozo, M.Á. 2010. p38 maintains E-cadherin expression by modulating TAK1-NF-κB during epithelial-to-mesenchymal transition. *Journal of Cell Science*. **123**(24), pp.4321–4331.

Stubdal, H., Zalvide, J., Campbell, K.S., Schweitzer, C., Roberts, T.M. and DeCaprio, J.A. 1997. Inactivation of pRB-related proteins p130 and p107 mediated by the J domain of simian virus 40 large T antigen. *Molecular and cellular biology*.

Sudo, T., Kawai, K., Matsuzaki, H. and Osada, H. 2005. p38 mitogen-activated protein kinase plays a key role in regulating MAPKAPK2 expression. *Biochemical and Biophysical Research Communications*. **337**(2), pp.415–421.

Suzuki, M., Morita, T. and Iwamoto, T. 2006. Diversity of Cl- channels. *Cellular and Molecular Life Sciences*. **63**(1), pp.12–24.

Suzuki, T., Orba, Y., Okada, Y., Sunden, Y., Kimura, T., Tanaka, S., Nagashima, K., Hall, W.W. and Sawa, H. 2010. The human polyoma JC virus agnoprotein acts as a viroporin. *PLoS Pathogens*. **6**(3).

Tan, K.B. 1977. Histones: metabolism in simian virus 40-infected cells and incorporation into virions. *Proceedings of the National Academy of Sciences of the United States of America*. **74**(7), pp.2805–9.

Tanoue, T. and Nishida, E. 2003. Molecular recognitions in the MAP kinase cascades. *Cellular Signalling*. **15**(5), pp.455–462.

Tarnita, R.M., Wilkie, A.R. and DeCaprio, J.A. 2018. Contribution of DNA Replication to the FAM111A-Mediated Simian Virus 40 Host Range Phenotype. *Journal of Virology*. **93**(1), pp.1330–1348.

Thiery, J.P. 2002. Epithelial–mesenchymal transitions in tumour progression. *Nature Reviews Cancer*. **2**(6), pp.442–454.

Toscano, M.G. and de Haan, P. 2018. How Simian Virus 40 Hijacks the intracellular protein trafficking pathway to Its Own Benefit ... and Ours. *Frontiers in Immunology*. **9**(MAY), p.1160.

Treisman, R., Novak, U., Favaloro, J. and Kamen, R. 1981. Transformation of rat cells by an altered polyoma virus genome expressing only the middle-T protein. *Nature*. **292**(5824), pp.595–600.

Trowbridge, P.W. and Frisque, R.J. 1995. Identification of three new JC virus proteins generated by alternative splicing of the early viral mRNA. *Journal of neurovirology*. **1**(2), pp.195–206.

Tsai, B., Gilbert, J.M., Stehle, T., Lencer, W., Benjamin, T.L. and Rapoport, T.A. 2003. Gangliosides are receptors for murine polyoma virus and SV40. *EMBO Journal*. **22**(17), pp.4346–4355.

Tsang, S.H., Wang, X., Li, J., Buck, C.B. and You, J. 2014. Host DNA Damage Response Factors Localize to Merkel Cell Polyomavirus DNA Replication Sites To Support

Efficient Viral DNA Replication. *Journal of Virology*. **88**(6), pp.3285–3297.

Tyson, J.R. and Snutch, T.P. 2013. Molecular nature of voltage-gated calcium channels: Structure and species comparison. *Wiley Interdisciplinary Reviews: Membrane Transport and Signaling*. **2**(5), pp.181–206.

Uhn, S.C., Morrone, S., Sablina, A.A., Arroyo, J.D., Hahn, W.C. and Xu, W. 2007. Structural basis of PP2A inhibition by small t antigen B. Sugden, ed. *PLoS Biology*. **5**(8), pp.1810–1819.

Utermark, T., Schaffhausen, B.S., Roberts, T.M. and Zhao, J.J. 2007. The p110 Isoform of Phosphatidylinositol 3-Kinase Is Essential for Polyomavirus Middle T Antigen-Mediated Transformation. *Journal of Virology*. **81**(13), pp.7069–7076.

Vargas-Rondón, N., Villegas, V.E. and Rondón-Lagos, M. 2018. The role of chromosomal instability in cancer and therapeutic responses. *Cancers*. **10**(1).

Vilchez, R.A. and Butel, J.S. 2004. Emergent human pathogen simian virus 40 and its role in cancer. *Clinical Microbiology Reviews*. **17**(3), pp.495–508.

Wang, W., Yi, M., Zhang, R., Li, J., Chen, S., Cai, J., Zeng, Z., Li, X., Xiong, W., Wang, L., Li, G. and Xiang, B. 2018. Vimentin is a crucial target for anti-metastasis therapy of nasopharyngeal carcinoma. *Molecular and Cellular Biochemistry*. **438**(1–2), pp.47–57.

Wang, X., Zhang, X., Dong, X.P., Samie, M., Li, X., Cheng, X., Goschka, A., Shen, D., Zhou, Y., Harlow, J., Zhu, M.X., Clapham, D.E., Ren, D. and Xu, H. 2012. TPC proteins are phosphoinositide- Activated sodium-selective ion channels in endosomes and lysosomes. *Cell*. **151**(2), pp.372–383.

Ward, J.M., Mäser, P. and Schroeder, J.I. 2009. Plant Ion Channels: Gene Families, Physiology, and Functional Genomics Analyses. *Annual Review of Physiology*. **71**(1), pp.59–82.

Wei, D., Huang, Z.H., Zhang, R.H., Wang, C.L., Xu, M.J., Liu, B.J., Wang, G.H. and Xu, T. 2014. Roles of p38 MAPK in the regulation of the inflammatory response to swine influenza virus-induced acute lung injury in mice. *Acta Virologica*. **58**(4), pp.374–379.

Weinberg, R.A. 1995. The retinoblastoma protein and cell cycle control. *Cell*. **81**(3), pp.323–330.

Welcker, M. and Clurman, B.E. 2005. The SV40 large T antigen contains a decoy phosphodegron that mediates its interactions with Fbw7/hCdc4. *Journal of Biological Chemistry*. **280**(9), pp.7654–7658.

Whalen, K.A., de Jesus, R., Kean, J.A. and Schaffhausen, B.S. 2005. Genetic Analysis of the Polyomavirus DnaJ Domain. *Journal of Virology*. **79**(15), pp.9982–9990.

Whitmarsh, A.J. and Davis, R.J. 1998. Structural organization of MAP-kinase signaling modules by scaffold proteins in yeast and mammals. *Trends in Biochemical Sciences*. **23**(12), pp.481–485.

Widmann, C., Gibson, S., Jarpe, M.B. and Johnson, G.L. 1999. Mitogen-activated protein kinase: Conservation of a three-kinase module from yeast to human. *Physiological Reviews*. **79**(1), pp.143–180.

Wu, J.H., Simonette, R.A., Nguyen, H.P., Rady, P.L. and Tyring, S.K. 2016. Small T-antigen of the TS-associated polyomavirus activates factors implicated in the MAPK pathway. *Journal of the European Academy of Dermatology and Venereology*. **30**(6), pp.1061–1062.

Xing, L. 2016. Clinical candidates of small molecule p38 MAPK inhibitors for inflammatory diseases. *MAP Kinase*. **4**(1).

Xu, L., Chen, S. and Bergan, R.C. 2006. MAPKAPK2 and HSP27 are downstream effectors of p38 MAP kinase-mediated matrix metalloproteinase type 2 activation and cell invasion in human prostate cancer. *Oncogene*. **25**(21), pp.2987–2998.

Yaciuk, P., Carter, M.C., Pipas, J.M. and Moran, E. 1991. Simian virus 40 large-T antigen expresses a biological activity complementary to the p300-associated transforming function of the adenovirus E1A gene products. *Molecular and Cellular Biology*. **11**(4), pp.2116–2124.

Yamada, M. and Kasamatsu, H. 1993. Role of nuclear pore complex in simian virus 40 nuclear targeting. *Journal of Virology*. **67**(1), pp.119–30.

Yamaguchi, H. and Condeelis, J. 2007. Regulation of the actin cytoskeleton in cancer cell migration and invasion. *Biochimica et Biophysica Acta - Molecular Cell Research*. **1773**(5), pp.642–652.

Yang, S.-H., Sharrocks, A.D. and Whitmarsh, A.J. 2003. Transcriptional regulation by the MAP kinase signaling cascades. *Gene*. **320**, pp.3–21.

Yardimci, H., Wang, X., Loveland, A.B., Tappin, I., Rudner, D.Z., Hurwitz, J., Van Oijen, A.M. and Walter, J.C. 2012. Bypass of a protein barrier by a replicative DNA helicase. *Nature*. **492**(7428), pp.205–209.

Yellen, G. 2002. The voltage-gated potassium channels and their relatives. *Nature*. **419**(6902), pp.35–42.

Yoon, S. and Seger, R. 2006. The extracellular signal-regulated kinase: Multiple substrates regulate diverse cellular functions. *Growth Factors*. **24**(1), pp.21–44.

Youlden, D.R., Soyer, H.P., Youl, P.H., Fritschi, L. and Baade, P.D. 2014. Incidence and survival for merkel cell carcinoma in Queensland, Australia, 1993-2010. *JAMA Dermatology*. **150**(8), pp.864–872.

Yu, F.H. and Catterall, W.A. 2003. Overview of the voltage-gated sodium channel family. *Genome biology*. **4**(3), p.207.

Yu, F.H., Yarov-Yarovoy, V., Gutman, G.A. and Catterall, W.A. 2005. Overview of molecular relationships in the voltage-gated ion channel superfamily. *Pharmacological Reviews*. **57**(4), pp.387–395.

Zaar, O., Gillstedt, M., Lindelöf, B., Wennberg-Larkö, A.M. and Paoli, J. 2016. Merkel cell carcinoma incidence is increasing in Sweden. *Journal of the European Academy of Dermatology and Venereology*. **30**(10), pp.1708–1713.

Zhang, P., Monteiro da Silva, G., Deatherage, C., Burd, C. and DiMaio, D. 2018. Cell-Penetrating Peptide Mediates Intracellular Membrane Passage of Human Papillomavirus L2 Protein to Trigger Retrograde Trafficking. *Cell*. **174**(6), pp.1465-1476.e13.

Zheng, K., Chen, M., Xiang, Y., Ma, K., Jin, F., Wang, Xiao, Wang, Xiaoyan, Wang, S. and Wang, Y. 2014. Inhibition of herpes simplex virus type 1 entry by chloride

channel inhibitors tamoxifen and NPPB. *Biochemical and Biophysical Research Communications*. **446**(4), pp.990–996.

Zhong, Y.S., Wang, J., Liu, W.M. and Zhu, Y.H. 2013. Potassium ion channels in retinal ganglion cells (Review). *Molecular Medicine Reports*. **8**(2), pp.311–319.

Zhou, A.Y., Ichaso, N., Adamarek, A., Zila, V., Forstova, J., Dibb, N.J. and Dilworth, S.M. 2011. Polyomavirus Middle T-Antigen Is a Transmembrane Protein That Binds Signaling Proteins in Discrete Subcellular Membrane Sites. *Journal of Virology*. **85**(7), pp.3046–3054.

Zhou, J., Pham, H.T., Ruediger, R. and Walter, G. 2003. Characterization of the Aalpha and Abeta subunit isoforms of protein phosphatase 2A: differences in expression, subunit interaction, and evolution. *The Biochemical journal*. **369**(Pt 2), pp.387–98.

Zhu, M.X., Ma, J., Parrington, J., Calcraft, P.J., Galione, A. and Evans, A.M. 2010. Calcium signaling via two-pore channels: Local or global, that is the question. *American Journal of Physiology - Cell Physiology*. **298**(3), pp.C430–C441.

Zylbergold, P., Ramakrishnan, N. and Hébert, T.E. 2010. The role of G proteins in assembly and function of Kir3 inwardly rectifying potassium channels. *Channels*. **4**(5), p.411.